NUREG/IA-0251

International Agreement Report

Improvement of RELAP5/MOD3.3 Reflood Model Based on the Assessments against FLECHT-SEASET Tests

Prepared by:
Tong-Soo Choi, Chang-Hwan Ban
KEPCO Nuclear Fuel
Daejeon, Korea

Dong-Gu Kang, Seung-Hoon Ahn
Korea Institute of Nuclear Safety
Daejeon, Korea

A. Calvo, NRC Project Manager

Office of Nuclear Regulatory Research
U.S. Nuclear Regulatory Commission
Washington, DC 20555-0001

February 2011

Prepared as part of
The Agreement on Research Participation and Technical Exchange
Under the International Code Assessment and Maintenance Program (CAMP)

Published by
U.S. Nuclear Regulatory Commission

AVAILABILITY OF REFERENCE MATERIALS IN NRC PUBLICATIONS

NRC Reference Material

As of November 1999, you may electronically access NUREG-series publications and other NRC records at NRC's Public Electronic Reading Room at http://www.nrc.gov/reading-rm.html. Publicly released records include, to name a few, NUREG-series publications; *Federal Register* notices; applicant, licensee, and vendor documents and correspondence; NRC correspondence and internal memoranda; bulletins and information notices; inspection and investigative reports; licensee event reports; and Commission papers and their attachments.

NRC publications in the NUREG series, NRC regulations, and *Title 10, Energy*, in the Code of *Federal Regulations* may also be purchased from one of these two sources.

1. The Superintendent of Documents
   U.S. Government Printing Office
   Mail Stop SSOP
   Washington, DC 20402-0001
   Internet: bookstore.gpo.gov
   Telephone: 202-512-1800
   Fax: 202-512-2250
2. The National Technical Information Service
   Springfield, VA 22161-0002
   www.ntis.gov
   1-800-553-6847 or, locally, 703-605-6000

A single copy of each NRC draft report for comment is available free, to the extent of supply, upon written request as follows:

Address: U.S. Nuclear Regulatory Commission
Office of Administration
Publications Branch
Washington, DC 20555-0001
E-mail: DISTRIBUTION.RESOURCE@NRC.GOV
Facsimile: 301-415-2289

Some publications in the NUREG series that are posted at NRC's Web site address http://www.nrc.gov/reading-rm/doc-collections/nuregs are updated periodically and may differ from the last printed version. Although references to material found on a Web site bear the date the material was accessed, the material available on the date cited may subsequently be removed from the site.

Non-NRC Reference Material

Documents available from public and special technical libraries include all open literature items, such as books, journal articles, and transactions, *Federal Register* notices, Federal and State legislation, and congressional reports. Such documents as theses, dissertations, foreign reports and translations, and non-NRC conference proceedings may be purchased from their sponsoring organization.

Copies of industry codes and standards used in a substantive manner in the NRC regulatory process are maintained at—

The NRC Technical Library
Two White Flint North
11545 Rockville Pike
Rockville, MD 20852-2738

These standards are available in the library for reference use by the public. Codes and standards are usually copyrighted and may be purchased from the originating organization or, if they are American National Standards, from—

American National Standards Institute
11 West 42nd Street
New York, NY 10036-8002
www.ansi.org
212-642-4900

Legally binding regulatory requirements are stated only in laws; NRC regulations; licenses, including technical specifications; or orders, not in NUREG-series publications. The views expressed in contractor-prepared publications in this series are not necessarily those of the NRC.

The NUREG series comprises (1) technical and administrative reports and books prepared by the staff (NUREG-XXXX) or agency contractors (NUREG/CR-XXXX), (2) proceedings of conferences (NUREG/CP-XXXX), (3) reports resulting from international agreements (NUREG/IA-XXXX), (4) brochures (NUREG/BR-XXXX), and (5) compilations of legal decisions and orders of the Commission and Atomic and Safety Licensing Boards and of Directors' decisions under Section 2.206 of NRC's regulations (NUREG-0750).

NUREG/IA-0251

International Agreement Report

Improvement of RELAP5/MOD3.3 Reflood Model Based on the Assessments against FLECHT-SEASET Tests

Prepared by:
Tong-Soo Choi, Chang-Hwan Ban
KEPCO Nuclear Fuel
Daejeon, Korea

Dong-Gu Kang, Seung-Hoon Ahn
Korea Institute of Nuclear Safety
Daejeon, Korea

A. Calvo, NRC Project Manager

Office of Nuclear Regulatory Research
U.S. Nuclear Regulatory Commission
Washington, DC 20555-0001

February 2011

Prepared as part of
The Agreement on Research Participation and Technical Exchange
Under the International Code Assessment and Maintenance Program (CAMP)

Published by
U.S. Nuclear Regulatory Commission

ABSTRACT

The reflood model of RELAP5/MOD3.3 was assessed against eight selected FLECHT-SEASET tests. Comparisons of predicted and measured peak cladding temperatures and quench times indicated that the code predicts peak cladding temperatures relatively well. However, rod quenches were predicted to occur too early. To improve the predictability for quench times, we carefully reviewed and modified the wall-to-fluid heat transfer models for the film boiling regime. After the modifications, the same set of eight FLECHT-SEASET tests was simulated again to show that the modifications made in this study improve the code's predictability not only for quench times but also for peak clad temperatures. The modifications reduced the RMS error in the prediction of peak clad temperatures and quench times from 48.3 to 36.7 K and 85.9 to 32.1 seconds, respectively.

FOREWORD

RELAP5 is one of the best-estimate safety codes to date. It was developed by United States Nuclear Regulatory Commission (USNRC) and RELAP5/MOD3.3 (patch 03), released in 2006, is its latest version. Though USNRC has been moving most of their developmental efforts from RELAP5 to TRACE, the code has been widely applied to analyze system transients of Pressurized Water Reactors (PWRs), including the postulated large break loss-of-coolant accident (LBLOCA).

A few years ago, three Korean organizations, Korea Atomic Energy Research Institute (KAERI), Korea Electric Power Research Institute (KEPRI), and Korea Nuclear Fuel (KNF), succeeded to co-develop a best-estimate LBLOCA evaluation model using a modified version of RELAP5/MOD3.1. And now, KNF is trying to extend the best-estimate evaluation model by adopting RELAP5/MOD3.3 because it has several new models or improvements to existing models, and user conveniences compared to (a modified version of) RELAP5/MOD3.1.

To develop a best estimate evaluation model for LBLOCA analyses using a code, we have to show how accurately the code predicts important phenomena occurring in that accident by comparing the code predictions to various separate effect test data and that is why we tried to assess the reflood model of RELAP5/MOD3.3 against FLECHT-SEASET tests.

This report was prepared basically to record the results that we obtained from the RELAP5/MOD3.3 assessment using the FLECHT-SEASET test data. By the way, we had to modify the code because the code was appraised to have some deficiencies in the reflood wall-to-fluid heat transfer models. So, this report explains also the code modifications we made and their effect on the code's predictive capability.

The code modifications suggested in this report makes the code predict much better the peak clad temperatures and quench times of FLECHT-SEASET tests. However, the reflood model of RELAP5/MOD3.3 should be further improved because the code does not show good predictive capability for some test conditions even with the modifications. Thus, this study needs to be followed by such improvements as the addition of a spacer grid heat transfer model.

CONTENTS

LIST OF FIGURES

LIST OF TABLES

ACKNOWLEDGEMENTS

This study utilized the experimental data which was processed during the KNF-USNRC co-work for assessing the reflood model of TRACE. The authors are grateful to the participants of that co-work (J. H. Jeong of KNF and G. Rhee of USNRC). The authors also acknowledge the financial support of the National Research Foundation under the national mid-and-long-term nuclear research and development program of the Ministry of Education, Science and Technology of the Rebublic of Korea.

EXECUTIVE SUMMARY

To assess the reflood model of RELAP5/MOD3.3, simulations of eight FLECHT-SEASET tests were conducted. The selected FLECHT-SEASET tests have various initial and boundary conditions such as the flooding rate varying from 2.1 to 15.5 cm/s, the upper plenum pressure varying from 0.13 to 0.41 MPa, and the coolant temperature varying from 306 to 408 K. A more detailed axial noding for the bundle test section was used in this assessment compared to other previous ones. Predictions for several significant parameters including peak clad temperatures, quench times, and heat transfer coefficients at various elevations were compared to the measurement data. From the comparison, the following findings were obtained.

- The code predicts the measured peak clad temperatures within ±10% deviation.
- The code predicts rod quenches to occur much earlier than the measurement data.
- The code has a tendency of under-predicting peak vapor temperatures at 2 different elevations, especially those of low flooding rate tests.
- The code has a tendency of over-predicting the overall pressure drop for the entire bundle (or collapsed level in the core).

Based on these findings, the wall-to-fluid heat transfer models which are activated during the reflood calculations were modified to improve the code's predictability mainly for quench times. The modifications can be summarized as follows:

- The film boiling heat transfer regime was divided into three different sub-regimes (inverted annular film boiling regime, inverted slug film boiling regime, and dispersed flow film boiling regime).
- Appropriate heat transfer correlations were selected to predict wall-to-vapor or wall-to-liquid heat transfers in each sub-regime.
- Minor coding errors in the subroutines computing the post-CHF droplet diameter and the transition boiling heat transfer coefficient, respectively were fixed.
- The radiation heat transfer model was slightly modified to assume more reasonable and consistent values for emissivity and droplet diameter.

All the modifications were embodied into a modified version and the same set of eight FLECHT-SEASET tests were simulated again with the modified version. From the comparisons of the predictions using the modified version to the predictions using the original version as well as the measurement data, the following conclusions were derived.

- The RMS error in overall PCT predictions can be reduced from 48.3 to 36.7 K by the modifications.
- The RMS error in overall quench time predictions can be reduced from 85.9 to 32.1 seconds by the modifications.
- The film boiling heat transfer coefficients predicted using the modified version shows better agreement with the measurement data compared to those predicted using the original version.
- Wall-to-vapor heat transfers are increased by the modifications so that the predicted vapor

temperatures are higher than those predicted by the original version.

- Even with the modifications, the code still has a tendency of over-predicting the overall pressure drop for the entire core (or collapsed liquid level in the core). Thus, further efforts to improve the reflood model of RELAP5/MOD3.3 should be made to the wall or interfacial drag models.

ABBREVIATIONS

HTC	Heat Transfer Coefficient
KAERI	Korea Atomic Energy Research Institute
KEPRI	Korea Electric Power Research Institute
KNF	Korea Nuclear Fuel
LBLOCA	Large Break Loss-Of-Coolant-Accident
PCT	Peak Clad Temperature
PWR	Pressurized Water Reactor
RMS	Root-Mean-Square
USNRC	United States Nuclear Regulatory Commission

NOMENCLAUTURE

a_f	liquid absorption coefficient
a_{gf}	interfacial area per unit volume
C_D	droplet drag coefficient
D_h	hydraulic diameter
d	average droplet diameter
d_{max}	maximum droplet diameter defined by Eq.(5)
$d_{We=1.5}$	droplet diameter when Weber number = 1.5
$d_{We=7.5}$	droplet diameter when Weber number = 7.5
F_{lt}	Linear function depending on the gas Reynolds number
F_{wf}	wall-to-liquid grey body factor
f_w	wall friction factor
G_f	liquid mass flux
g	gravitational acceleration
h_{Br}	HTC calculated with the Bromley correlation
h_{CT}	HTC calculated with the CATHARE correlation
h_{Ditt}	HTC calculated with a call to the subroutine DITTUS
h_{fg}	latent heat of vaporization
h_{FR}	HTC calculated with the Forslund-Rohsenow correlation
h_{lam}	laminar convective HTC
h_{max}	HTC defined by Eq.(26)
h_{MBr}	HTC calculated with the modified Bromley Correlation
h_{tur}	turbulent convective HTC
h_{wf}	wall-to-liquid HTC
$h_{wf,DF}$	wall-to-vapor HTC for the DFFB regime
$h_{wf,IA}$	wall-to-liquid HTC for the IAFB regime
h_{wg}	wall-to-vapor HTC
$h_{wg,DF}$	wall-to-vapor HTC for the DFFB regime
$h_{wg,IA}$	wall-to-vapor HTC for the IAFB regime
K_{BY}	Reynolds number dependent coefficient defined by Eq.(13)
k_g	vapor conductivity
P/D_R	pitch-to-diameter ratio
q''_{CHF}	critical heat flux
R_1, R_2, R_3	R terms in radiation heat transfer model used to calculate the grey body factor
Re_d	droplet Reynolds number

Re_g	vapor Reynolds number
T_{sat}	saturation temperature
T_w	wall temperature
$T_{w,CHF}$	wall temperature at the CHF point
v_g	vapor velocity
v_r	relative velocity
x, y	weighting functions defined by Eq.(10)
Z_{Qmin}	distance from the point in question to the bottom quench front

Greeks

α_f	liquid volume fraction
α_g	vapor volume fraction
ΔT_{CHF}	difference between the wall temperature at the CHF point and the saturation temperature
δ	vapor film thickness
ε_f	liquid emissivity
ε_w	wall emissivity
μ_g	vapor viscosity
ρ_f	liquid density
ρ_g	vapor density
σ	surface tension
τ_i	friction force per unit volume due to interfacial drag
τ_w	fiction force per unit volume due to wall drag
Φ_{2p}	two-phase enhancement factor
Φ_{tur}	turbulent flow multiplier for a vertical bundle geometry

Subscripts

IA	inverted annular film boiling
DF	dispersed flow film boiling
f	liquid
g	vapor
wf	wall-to-liquid
wg	wall-to-vapor
sat	saturation
lam	laminar
tur	turbulent

1. INTRODUCTION

In the analyses of a Pressurized Water Reactor (PWR) Large Break Loss-Of-Coolant Accident (LBLOCA), one of the most important tasks is to predict accurately the thermal-hydraulic phenomena occurring in the core during the reflood phase. This phase typically starts with a nearly empty core under adiabatic conditions. Subcooled water is then injected from the bottom of core. The injected water interacts with hot fuel rods and produces large amounts of steam which binds the flooding rate via increasing upper plenum pressure. During the phase, various heat transfer regimes (or modes) such as single-phase vapor convection, nucleate boiling, transition boiling, film boiling, and single-phase liquid convection exist in the core, sometimes all at once.

To accurately predict complicated thermal-hydraulic phenomena in the core during reflood, RELAP5/MOD3.3 (patch 03) has a special heat transfer package that is activated during that phase only. Most of this package had been originally developed by Analytis [1] and was slightly modified in its official release.

Few activities, with the exception of developmental assessment by Analytis, have been made to assess the reflood model of RELAP5/MOD3.3. To the best of our knowledge, the most recent assessment of RELAP5 reflood model was conducted by Koszela [2] using an interim version (RELAP5/MOD3.2.2 Gamma). He simulated the ABB Atom 3×3-Rod Bundle Reflooding Tests using the default model options and concluded that the code still had several deficiencies in the reflood model. In his work, the cladding temperature peaks and final quenches were predicted to occur too early.

One of the purposes of this report is to assess the RELAP5/MOD3.3 reflood model using selected FLECHT-SEASET tests. Compared to previous similar assessments [3], [4], a more detailed axial noding for the bundle test section and more accurate initial and boundary conditions were used in this assessment.

Based on our assessment, we carefully reviewed and modified the wall-to-fluid heat transfer models. Note that these modifications introduced nearly no new heat transfer correlations. The correlations used in the original version were restructured to result in better predictions.

To investigate the effect of our modifications, assessment calculations were conducted again using the modified version against the same set of FLECHT-SEASET tests. Various significant parameters including peak clad temperatures (PCTs), quench times, and heat transfer coefficients (HTCs) were compared to both values predicted using the original version and measurements.

The assessment of the original RELAP5/MOD3.3 reflood model against eight FLECHT-SEASET tests is described in Chapter 2. A brief description for the FLECHT-SESET facility and the selected tests is also made in this chapter. Chapter 3 describes the reflood model of RELAP5/MOD3.3 briefly and explains how we modified the code to improve the wall-to-fluid heat transfer models. The effect of code modifications is also analyzed in this Chapter. Final conclusions of this study are presented in Chapter 4.

2. ASSESSMENT OF ORIGINAL REFLOOD MODEL

2.1 FLECHT-SEASET Tests

The FLECHT-SEASET tests have been regarded as representative reflood experiments because the test facility was large and relatively well instrumented. The test facility was constructed by modifying the FLECHT facility mainly to accept a new heater rod bundle of which dimensions were typical of the Westinghouse 17x17 fuel bundle. It consisted of a cylindrical test section, a coolant accumulator, an entrained liquid separation tank, an external pipe downcomer for the gravity reflood tests, a steam boiler for back-pressure regulation, and the required piping and valves. As the facility is described in detail in a FLECHT-SEASET data report [5], only the major components are briefed here. The overall facility layout is presented in Figure 1.

A cylindrical test section was composed of a lower plenum, a low mass housing, and an upper plenum. The low-mass housing contained the heater rod bundle consisting of 161 heater rods and 16 thimble rods which were placed with a square lattice array similar to the 17x17 Westinghouse fuel bundle design. It was a cylindrical vessel with a 19.37 cm (7.625 in) inside diameter by 0.477 cm (0.188 in) wall, constructed of SA-312, type 304 stainless steel. The minimum wall thickness was chosen so that the housing would absorb or release the minimum amount of heat to the rod bundle. The length of the heated part was 3.66 m (12 ft).

The cross-sectional view of the heater rod bundle is shown in Figure 2 with the corresponding instrumentation groups. The bundle comprised 161 heater rods (68 instrumented), 4 instrumented thimbles, 12 steam probes, 8 solid triangular fillers, and 8 spacer grids. A Kanthal heater coil imbedded in boron nitride was used to heat the rods which had stainless steel cladding. The outside diameter and the wall thickness of the heater rod were 9.5 mm (0.374 in) and 0.64 mm (0.025 in), respectively. Rod clad temperatures were measured by Type K thermocouples which were welded at the inner surface of the stainless steel cladding. The rod-to-rod pitch was 12.6 mm (0.496 in) and each rod had a cosine axial power profile shown in Figure 3. The triangular fillers were welded to the grids to maintain the proper grid locations. The fillers served also to reduce the amount of excess flow area.

The low mass housing was joined to the upper and lower plenums by flange connections. There were an upper and a lower extension in the upper and lower plenums. The entrained liquid collected in the upper plenum was prevented from falling back into the bundle by the upper extension. The lower extension had a role of distributing the injected coolant uniformly.

After passing through the upper plenum baffle pipe which helped improve liquid carryout separation, the exhaust vapor was directed to the entrainment separator through the exhaust line piping. The entrainment separator was a standard liquid-vapor separator having a large volume to minimize the housing pressure oscillations.

Before a test was conducted, auxiliary components such as the carryover vessel, entrainment separator, separator drain tank, test section upper plenum, and test section outlet piping were heated to slightly above the saturation temperature by clamp-on strip heaters. The test section, carryover vessel, and exhaust line components were pressurized to the desired pressure by a steam boiler. When the coolant supplied by the gas-pressurized accumulator reached the bottom of the heated part of the heater rod bundle, it was circulated to assure the water in the lower plenum were at the specified temperature. Power was then supplied to the test bundle

and the rods were heated up. When the bundle temperature from any two designated thermocouples reached the preset value, flooding and power decay were initiated automatically.

The instrumentation of the FLECHT-SEASET facility was quite extensive, including 205 heater rod thermocouples, 12 differential pressure cells positioned 0.3048 m (1 ft) apart along the axial direction of the heated section, 12 steam probes, and inlet and outlet flow meters.

Among the numerous tests performed at the FLECHT-SEASET test facility, 8 forced reflood tests were selected for RELAP5/MOD3.3 assessment. Their test conditions are presented in Table 1. These tests were also used for the assessment of TRACE [6]. Flooding rates varied from 2.1 to 15.5 cm/s (0.81 to 6.10 in/sec) with the upper plenum pressure varying from 0.13 to 0.41 MPa (19 to 60 psia) and the coolant temperature varying from 306 to 408 K (91 to 257 °F). All 8 tests had the same initial rod power of 2.3 kW/m (0.7 kW/ft) at the peak location and they had a uniform radial power distribution. Note that the test conditions listed in Table 1 are nominal values and the actual values varied to some extent with time.

2.2 RELAP5 Model

For the RELAP5 simulations, only the bundle test section was modeled in a detailed manner. Other parts of the test facility, such as the coolant injection system and the bundle flow exhaust system, were greatly simplified. The facility was represented by four fluid components (Figure 4). Two time-dependent volume (TMDPVOL) components represent the coolant injection system and the flow exhaust system. One single-volume (SNGLVOL) component represents the inlet pipe and one pipe (PIPE) component does the heated section of the cylindrical housing. The heated section was modeled using 49 equal length (7.62 cm (3.0 in)) axial nodes. Note that the top and bottom elevations of the PIPE component were extended to 3.81 cm (1.5 in) above and below the heated section to make the center of the first and last nodes meet with the measurement locations. With this noding, it was possible to give the form losses at the spacer grids to the locations close to the real bottom elevations of spacer grids. It was also possible to obtain the heater rod clad temperatures at the exact locations of measurement. The form losses at the spacer grids were modeled by specifying the pressure loss coefficient to 1.20. The same loss coefficient was used also in the assessment of TRACE [6].

Five heat structures were located in the PIPE component to model the active heater rods, the housing wall, the thimbles, the filler rods, and the failed heater rods. The number of failed heater rods was 4 for Test 31302 and 2 for the others. The length of the first and last axial nodes is one half of other ones so that the center of all other axial nodes matched with the center of the hydraulic nodes in the PIPE component. Heater rods were divided into 7 radial nodes to model the Kanthal heater coil insulated with boron nitride that is encased with stainless steel cladding.

The electrical power was provided as a time-dependent table. The coolant inlet velocity as a function of time was given to a time-dependent junction (TMDPJUN) component. The inlet coolant temperature and the upper plenum pressure were given to the TMDPVOL components representing the coolant injection system and the flow exhaust system, respectively. The initial temperatures of heater rods and the housing wall at various axial locations were determined from a linear interpolation of measurement data. The initial temperature of the failed rods and fillers were assumed to be equal to that of the housing wall.

The calculations were initiated at the time of flooding. The user's guidelines in [7] were followed tightly to select appropriate inputs for the time step control, the volume-related options, and junction-related options. The maximum time step was set to 0.1 s in all calculations though the

time step was reduced automatically to satisfy the Courant limit or avoid water property failures.

We believe the modeling approach described above has several arguable features that should be discussed more.

First, compared to other previous FLECHT-SEASET calculations, a more detailed axial noding for the bundle test section was used in this study. At first, we tried to use 20 equal length nodes for the test section just like other previous assessments [3], [4], but the predicted bottom quench front in that case showed stepwise increases during the entire transient (Figure 5). In addition, with 20 equal length nodes, we can not compare predicted temperatures directly to measurements directly, as mentioned earlier.

Second, the entire test section was modeled as a single channel. Even though the tests we selected for this assessment had a uniform radial power distribution, the clad temperature measurements at an elevation have some distribution. Per Westinghouse [8], the distribution can be attributed to the individual heater rod resistance differences, manufacturing tolerances on materials, dimension variations, initial temperature differences, the radial location of a heater rod relative to the unheated guide thimbles, and sub-channel-to-sub-channel flow variations. It is nearly impossible to correctly take all these factors into account in a RELAP5 calculation because the code is basically a one-dimensional code. Certainly, some previous RELAP5 calculations used a two channel modeling for the test section, but we believe it may introduce another kind of uncertainties related to the use of cross-flow junctions. A single channel modeling for the test section has an effect of averaging the radial distribution of clad temperatures. Thus, the arithmetic average values of measured PCTs and quench times were used in the quantitative comparison to predictions in this study.

Third, we did not take into account the radiation heat transfer between the housing wall and peripheral rods. According to Westinghouse [8], the radiation heat transfer from the housing can be restricted to the outer-most rods. Thus, no readings from those thermocouples located in the outer-most row of rods were used in the quantitative comparison to predictions.

Appendix to this report presents the input deck for Test 31805 and only the inputs for test specific initial and boundary conditions can vary test by test.

2.3 Assessment Results

FLECHT-SEASET test simulations using RELAP5/MOD3.3 (patch 03) were started at the time of reflood corresponding to the initial injection of cold water into the test section. To assess the predictive capability of the code, detailed comparisons between measurement data and RELAP5 calculations were made for each test. The compared parameters are as follows:

- Heater rod clad temperatures at 8 different elevations; 0.610 m (2 ft), 1.219 m (4 ft), 1.829 m (6 ft), 1.981 m (6.5 ft), 2.438 m (8 ft), 3.048 m (10 ft), 3.353 m (11 ft), and 3.505 m (11.5 ft)
- Vapor temperatures at 1.829 m (6 ft) and 3.048 m (10 ft) elevations
- Quench front elevation as a function of time
- Differential pressure for the entire 3.658 m (12 ft) core
- Differential pressure between 1.829 m (6 ft) and 2.134 m (7 ft) elevations
- Differential pressure between 3.048 m (10 ft) and 3.353 m (11 ft) elevations
- HTCs at 5 different elevations; 1.219 m (4 ft), 1.829 m (6 ft), 1.981 m (6.5 ft), 2.438 m (8 ft), and 3.048 m

FLECHT-SEASET had more than one rod temperature measurements at an elevation. For example, at 1.8 m (6 ft) elevation, there existed 21 thermocouples for the rod clad temperatures. In the comparison to the predicted one, all the valid measurement data were used.

Not only the measured but also the predicted quench front elevation was evaluated from the heater rod clad temperatures. If the rod clad temperature drop during a time step (or the measurement interval) at an elevation was lower than a specified value, the elevation was regarded as quenched. In other words, the rod clad temperature should satisfy the following relation at the quench time.

$$\left.\frac{dT}{dt}\right|_{t=\text{Quench Time}} = \frac{T_{t+3\cdot\Delta t} - T_{t+2\cdot\Delta t}}{t_{t+3\cdot\Delta t} - t_{t+2\cdot\Delta t}} < -X \qquad (1)$$

where T and t are the rod clad temperature and time, respectively and Δt is the time step or the measurement interval. For X, 27.8 K/s (50 °F/sec) was tried first, but in a few cases having a very gradual temperature decrease, 16.7 K/s (30 °F/sec) was used also. The measured quench time at an elevation was obtained by averaging the quench times which were determined using all the valid thermocouple readings at that elevation.

Both the measured and the predicted HTCs are defined as the heat flux divided by the difference between the clad and the saturation temperatures. The measured HTCs were already derived by the USNRC [6]. They used a program called IHCP1D with the 9 second average option to remove high oscillations. For consistency, the same time averaging process was also applied to get the predicted HTCs. For the measured HTCs, three HTCs (minimum, maximum, and average) derived from multiple rod clad temperature measurements are presented. The average one was computed as the arithmetic average of HTCs from all instrumented rods having valid clad temperature measurements at a given elevation.

Comparisons of predicted results to the measurement data are made in Figure 6 through Figure 157. The figures contain also the results using a modified version, but only the results with the original version are discussed in this chapter. The results with a modified version will be discussed in Chapter 3 emphasizing the effect of modifications.

2.3.1 Test 31805

Test 31805 was a 2.1 cm/s (0.81 in/sec) reflood test at 0.28 MPa (40 psia). Inlet liquid temperature was 324 K (124 °F). Of all the tests simulated in this study, this test had the lowest flooding rate.

Heater rod clad temperatures predicted by RELAP5 at various elevations are compared to the measured data in Figure 6 through Figure 13. The maximum predicted PCT is 1359 K at 1.981 m (6.5 ft) elevation while the measured PCTs at the same elevation are in the range of 1353~1509 K. Though the prediction locates between the maximum and minimum measured values, the code is believed to under-predict the PCT because the prediction is 92 K lower than the arithmetic average of measurements. The tendency of under-predicting PCTs becomes stronger at higher elevations. The predicted PCTs at 2.438 m (8 ft), 3.048 m (10 ft), and 3.353 m (11 ft) elevations are even lower than the lowest measured PCT at each elevation. The percent differences between the predicted PCTs and the measurements at 3.353 m (11 ft) and 3.505 m (11.5 ft) elevations are smaller than those at 2.438 m (8 ft) or 3.048 m (10 ft) elevations.

Vapor temperatures predicted are compared to the measured data in Figure 14 and Figure 15. The vapor temperature at 1.829 m (6 ft) was under-predicted much compared to the measurements. The rapid increase before ~30 seconds and the re-heating after ~60 seconds were not simulated well. The predicted vapor temperature at 3.048 m (10 ft) increased too fast as soon as the transient began and the peak temperature was predicted to occur too early.

The predicted and measured quench fronts are compared in Figure 16. The final quenches were predicted to occur much earlier than the measurements at all elevations except a bottom region (at and below 1.219 m (4 ft)). The difference between the predicted quench time and the arithmetic average of measured quench times (predicted – measured) varies from -177 to -7 seconds and the maximum absolute deviation occurred at 3.505 m (11.5 ft).

The predicted and measured differential pressures for the entire core region, a mid-level (1.829 to 2.134 m (6 to 7 ft)), and a top region (3.048 to 3.353 m (10 to 11 ft)) are compared in Figure 17, Figure 18, and Figure 19, respectively. The predicted value for the entire core is higher than the measurement data from the beginning of transient and the deviation is about 2~3 kPa (0.29~0.44 psi) after ~100 seconds. It means that the lower part of the test section was filled up with liquid too fast and the difference of collapsed liquid level was maintained until the end of transient as the differential pressure is essentially equivalent to the hydrostatic head. The predicted differential pressure for the mid-level becomes higher than the measurement at ~250 seconds. For the top region, the differential pressure was predicted relatively well until a quantitative comparison becomes doubtful due to large oscillations in the prediction.

The predicted and measured HTCs at five different elevations are compared in Figure 20 through Figure 24. Excluding the early steam cooling only period, the HTCs at all elevations were significantly over-predicted until the quench time. Generally speaking, the reflood HTCs increases abruptly as the transition boiling regime begins. Thus, the figures indicate that the code over-predicted much the HTCs in the film boiling regime.

2.3.2 Test 31504

Test 31504 was a 2.4 cm/s (0.97 in/sec) reflood test at 0.28 MPa (40 psia). Inlet liquid temperature was 324 K (124 °F). The test had very similar initial and boundary conditions to those of Test 31805 but the flooding rate was slightly higher than that of Test 31805.

Heater rod clad temperatures predicted by RELAP5 at various elevations are compared to the measured data in Figure 25 through Figure 32. The maximum PCT predicted by the code is 1319 K at 1.981 m (6.5 ft) elevation while the measured PCTs at the same elevation are in the range of 1322-1423 K. The predicted maximum PCT is 42 K lower than the arithmetic average of measurements. The tendency of under-predicting PCTs becomes stronger at higher elevations. The predicted PCTs at 1.981 m (6.5 ft), 2.438 m (8 ft), and 3.048 m (10 ft) elevations are even lower than the lowest measured PCT at each elevation. The percent differences between the predicted PCTs and the measurements at 3.353 m (11 ft) and 3.505 m (11.5 ft) elevations are much smaller than at 2.438 m (8 ft) or 3.048 m (10 ft) elevations.

Vapor temperatures predicted are compared to the measured data in Figure 33 and Figure 34. The vapor temperature at 1.829 m (6 ft) was under-predicted much compared to the measurements. The rapid increase before ~20 seconds and the re-heating after ~50 seconds were not simulated well. The predicted vapor temperature at 3.048 m (10 ft) increased too fast as soon as the transient began and the peak temperature was predicted to occur too early.

The predicted and measured quench fronts are compared in Figure 35. The final quenches were predicted to occur much earlier than the measurements at all elevations except a bottom region (at and below 1.219 m (4 ft)). The difference between the predicted quench time and the arithmetic average of measured quench times (predicted – measured) varies from -149 to -5 seconds and the maximum absolute deviation occurred at 3.353 m (11 ft).

The predicted and measured differential pressures for the entire core region, a mid-level (1.829 to 2.134 m (6 to 7 ft)), and a top region (3.048 to 3.353 m (10 to 11 ft)) are compared in Figure 36, Figure 37, and Figure 38, respectively. The predicted value for the entire core is higher than the measurement data from the beginning of transient and the deviation is about 4~5 kPa (0.58~0.73 psi) after ~60 seconds. It means that the lower part of the test section was filled up with liquid too fast and the difference of collapsed liquid level was maintained until the end of transient. The predicted differential pressure for the mid-level becomes higher than the measurement after ~200 seconds. For the top region, the differential pressure was over-predicted early in the transient, but the deviation does not look large.

The predicted and measured HTCs at five different elevations are compared in Figure 39 through Figure 43. Excluding the early steam cooling only period, the HTCs at all elevations were significantly over-predicted until the quench time, which means that the code over-predicted much the HTCs in the film boiling regime.

2.3.3 Test 31203

Test 31203 was a 3.8 cm/s (1.51 in/sec) reflood test at 0.28 MPa (40 psia). Inlet liquid temperature was 52 K (126 °F). The test has very similar initial and boundary conditions to those of Test 31805 or Test 31504 but the flooding rate was a little higher than that of Test 31504.

Heater rod clad temperatures predicted by RELAP5 at various elevations are compared to the measured data in Figure 44 through Figure 51. The maximum PCT predicted by the code is 1224 K at 1.829 m (6.0 ft) elevation while the measured PCTs at the same elevation are in the range of 1206-1297 K. Note that the highest average of the measured PCTs was obtained at 1.981 m (6.5 ft) elevation. The predicted maximum PCT is 45 K lower than the arithmetic average of measurements at that elevation. The predicted PCTs at 1.981 m (6.5 ft) and 2.438 m (8 ft) are even lower than the lowest measured PCT at each elevation. On the contrary, the predicted PCTs at 3.353 m (11 ft) and 3.505 m (11.5 ft) are higher than the arithmetic average of measurements at each elevation.

Vapor temperatures predicted are compared to the measured data in Figure 52 and Figure 53. The vapor temperature at 1.829 m (6 ft) was under-predicted much compared to the measurements. The rapid increase before ~10 seconds and the re-heating after ~30 seconds were not simulated well. The predicted vapor temperature at 3.048 m (10 ft) increased too fast as soon as the transient began and the peak temperature was predicted to occur too early.

The predicted and measured quench fronts are compared in Figure 54. The final quenches were predicted to occur much earlier than the measurements at all elevations except the lowest elevation (0.610 m (2 ft)). The difference between the predicted quench time and the arithmetic average of measured quench times (predicted – measured) varies from -148 to -6 seconds and the maximum absolute deviation occurred at 3.048 m (10 ft).

The predicted and measured differential pressures for the entire core region, a mid-level (1.829 to 2.134 m (6 to 7 ft)), and a top region (3.048 to 3.353 m (10 to 11 ft)) are compared in Figure 55, Figure 56, and Figure 57, respectively. The predicted value for the entire core is about 3~4 kPa (0.44~0.58 psi) higher than the data after ~20 seconds. The predicted differential pressure for the mid-level becomes higher than the measurement after ~130 seconds. For the top region, the differential pressure was over-predicted early in the transient.

The predicted and measured HTCs at five different elevations are compared in Figure 58 through Figure 62. Excluding the early steam cooling only period, the HTCs at all elevations were significantly over-predicted until the quench time, which means that the code over-predicted much the HTCs in the film boiling regime.

2.3.4 Test 31302

Test 31302 was a 7.7 cm/s (3.01 in/sec) reflood test at 0.28 MPa (40 psia). Inlet liquid temperature was 325 K (126 °F). The test has very similar initial and boundary conditions to those of Test 31203 but the flooding rate was about two times higher than that of Test 31203.

Heater rod clad temperatures predicted by RELAP5 at various elevations are compared to the measured data in Figure 63 through Figure 70. The maximum PCT predicted by the code is 1159 K at 1.829 m (6.0 ft) elevation while the measured PCTs at the same elevation are in the range of 1120~1191 K. The predicted maximum PCT is only 2 K lower than the arithmetic average of measurements at the same elevation. Only the PCTs at 3.353 m (11 ft) were definitely over-predicted.

Vapor temperatures predicted are compared to the measured data in Figure 71 and Figure 72. The vapor temperature at 1.829 m (6 ft) was predicted relatively well though the maximum temperature occurred a little earlier than the measurements. The vapor temperatures at 3.048 m (10 ft) were 100~200 K over-predicted.

The predicted and measured quench fronts are compared in Figure 73. The final quenches were predicted to occur much earlier than the measurements at all elevations. The difference between the predicted quench time and the arithmetic average of measured quench times (predicted – measured) varies from -120 to -7 seconds and the maximum absolute deviation occurred at 3.048 m (10 ft).

The predicted and measured differential pressures for the entire core region, a mid-level (1.829 to 2.134 m (6 to 7 ft)), and a top region (3.048 to 3.353 m (10 to 11 ft)) are compared in Figure 74, Figure 75, and Figure 76, respectively. The differential pressure for the entire core region was predicted relatively well before ~100 seconds, but it was over-predicted by 2~4 kPa (0.29~0.58 psi) after that time. The predicted differential pressure for the mid-level becomes higher than the measurement after ~70 seconds. For the top region, the predicted differential pressure looks higher than the measurement after ~120 seconds when the prediction starts to oscillate severely. The times when the predicted differential pressures for the mid-level and a top region become higher than the measurements are close to the times when the predicted rod clad temperatures at those elevations start to drop fast (Figure 65 and Figure 68). Thus, we believe the over-predicted differential pressure (or collapsed liquid level) is one of the reasons why the quench times of this test were predicted to occur much earlier than the experiment.

The predicted and measured HTCs at five different elevations are compared in Figure 77 through Figure 81. The HTCs in the film boiling regime were a little over-predicted at all

elevations, but the deviations are not as large as in the cases of lower flooding rate tests (Test 31805, Test 31504, and Test 31203).

2.3.5 Test 31701

Test 31701 was a 15.5 cm/s (6.10 in/sec) reflood test at 0.28 MPa (40 psia). Inlet liquid temperature was 326 K (127 °F). Of all the tests simulated in this study, this test had the highest flooding rate.

Heater rod clad temperatures predicted by RELAP5 at various elevations are compared to the measured data in Figure 82 through Figure 89. The maximum PCT predicted by the code is 1135 K at 1.829 m (6.0 ft) elevation while the measured PCTs at the same elevation are in the range of 1114~1175 K. The predicted maximum PCT is 17 K lower than the arithmetic average of measurements at the same elevation. Just like Test 31302, the PCT predictions are relatively excellent compared to lower flooding rate tests (Test 31805, 31504, and 31203).

Vapor temperatures predicted are compared to the measured data in Figure 90 and Figure 91. The vapor temperature at 1.829 m (6 ft) was predicted relatively well though the heat up early in the transient was predicted to stop a few seconds earlier than the measurements. The vapor temperature at 3.048 m (10 ft) was over-predicted by 50~150 K.

The predicted and measured quench fronts are compared in Figure 92. The final quenches were predicted to occur a little earlier than the measurements at all elevations. The difference between the predicted quench time and the arithmetic average of measured quench times (predicted – measured) varies from -41 to -3 seconds and the maximum absolute deviation occurred at 3.048 m (10 ft). Note that the measured quench times show a wide distribution in a top region at and above 3.048 m (10 ft).

The predicted and measured differential pressures for the entire core region, a mid-level (1.829 to 2.134 m (6 to 7 ft)), and a top region (3.048 to 3.353 m (10 to 11 ft)) are compared in Figure 93, Figure 94, and Figure 95, respectively. The predicted value for the entire core is higher than the measurement data from the beginning of transient and the deviation is about 3~5 kPa (0.44~0.73 psi) after ~10 seconds. The predicted differential pressure for the mid-level becomes higher than the measurement after ~25 seconds. The top region was also predicted to be filled with liquid earlier than the measurement.

The predicted and measured HTCs at five different elevations are compared in Figure 96 through Figure 100. The code tends to over-predict the HTCs, especially in a lower part of the core. We believe that the rapid filling of the core with liquid, which is observed in Figure 93, Figure 94, or Figure 95, is one of the main reasons for the over-prediction of HTCs.

2.3.6 Test 31108

Test 31108 was a 7.9 cm/s (3.11 in/sec) reflood test at 0.13 MPa (40 psia). Inlet liquid temperature was 306 K (91 °F). The test has similar initial and boundary conditions to those of Test 31302 but the upper plenum pressure is about one half of that of Test 31302.

Heater rod clad temperatures predicted by RELAP5 at various elevations are compared to the measured data in Figure 101 through Figure 108. The maximum PCT predicted by the code is 1145 K at 1.829 m (6.0 ft) elevation while the measured PCTs at the same elevation are in the range of 1126~1200 K. The predicted maximum PCT is 23 K lower than the arithmetic average

of measurements at the same elevation. The predicted PCTs are slightly lower than the arithmetic average of measurements at all elevations except 3.048 m (10 ft) and 3.353 m (11 ft) where PCTs were definitely over-predicted.

Vapor temperatures predicted are compared to the measured data in Figure 109 and Figure 110. The vapor temperature at 1.829 m (6 ft) was predicted relatively well though the maximum temperature occurred a little earlier than the measurements. The vapor temperatures at 3.048 m (10 ft) were 100~200 K over-predicted.

The predicted and measured quench fronts are compared in Figure 111. The final quenches were predicted to occur much earlier than the measurements at all elevations except 3.505 m (11.5 ft) elevation. The difference between the predicted quench time and the arithmetic average of measured quench times (predicted – measured) varies from -162 to +13 seconds and the maximum absolute deviation occurred at 3.048 m (10 ft).

The predicted and measured differential pressures for the entire core region, a mid-level (1.829 to 2.134 m (6 to 7 ft)), and a top region (3.048 to 3.353 m (10 to 11 ft)) are compared in Figure 112, Figure 113, and Figure 114, respectively. The differential pressure for the entire core region is higher than the measurement data from the beginning of transient and the deviation is 3~7 kPa (0.44~1.02 psi) after ~10 seconds. The predicted differential pressure for the mid-level becomes higher than the measurement after ~90 seconds. For the top region, the predicted differential pressure is maintained a little higher than the measurement for ~150 seconds and oscillates highly after that time. The times when the predicted differential pressures for the mid-level and the top region become higher than the measurements are close to the times when the predicted rod clad temperatures at those elevations start to drop fast (Figure 103 and Figure 106). Thus, we believe the over-predicted differential pressure (or collapsed liquid level) is one of the reasons why the quench times of this test were predicted to occur much earlier than the experiment.

The predicted and measured HTCs at five different elevations are compared in Figure 115 through Figure 119. The film boiling HTCs were a little over-predicted in a lower part of the core while they were a little under-predicted in a top region.

2.3.7 Test 32013

Test 32013 was a 2.6 cm/s (1.04 in/sec) reflood test at 0.41 MPa (60 psia). Inlet liquid temperature was 339 K (150 °F). The test has similar initial and boundary conditions to those of Test 31504 but the upper plenum pressure is 0.14 MPa (20 psi) higher that of Test 31504.

Heater rod clad temperatures predicted by RELAP5 at various elevations are compared to the measured data in Figure 120 through Figure 127. The maximum PCT predicted by the code is 1326 K at 1.981 m (6.5 ft) elevation while the measured PCTs at the same elevation are in the range of 1306~1431 K. The predicted maximum PCT is 55 K lower than the arithmetic average of measurements. The tendency of under-predicting PCTs becomes stronger at higher elevations. The predicted PCTs at 2.438 m (8 ft) and 3.048 m (10 ft) elevations are even lower than the lowest measured PCT at each elevation. The percent differences between the predicted PCTs and the measurements at 3.353 m (11 ft) and 3.505 m (11.5 ft) elevations are smaller than at 2.438 m (8 ft) and 3.048 m (10 ft) elevations.

Vapor temperatures predicted are compared to the measured data in Figure 128 and Figure 129. The vapor temperature at 1.829 m (6 ft) was under-predicted much compared to the

measurements. The rapid increase before ~20 seconds and the re-heating after ~50 seconds were not simulated well. The predicted vapor temperature at 3.048 m (10 ft) increased too fast as soon as the transient began and the peak temperature was predicted to occur too early.

The predicted and measured quench fronts are compared in Figure 130. The final quenches were predicted to occur much earlier than the measurements at all elevations except a bottom region (at and below 1.219 m (4 ft)). The difference between the predicted quench time and the arithmetic average of measured quench times (predicted – measured) varies from -101 to -2 seconds and the maximum absolute deviation occurred at 3.505 m (11.5 ft).

The predicted and measured differential pressures for the entire core region, a mid-level (1.829 to 2.134 m (6 to 7 ft)), and a top region (3.048 to 3.353 m (10 to 11 ft)) are compared in Figure 131, Figure 132, and Figure 133, respectively. The predicted value for the entire core was predicted quite well. However, the predicted differential pressure for the mid-level becomes higher than the measurement after ~180 seconds. For the top region, the differential pressure was over-predicted early in the transient, but the difference does not look large.

The predicted and measured HTCs at five different elevations are compared in Figure 134 through Figure 138. Excluding the early steam cooling only period, the HTCs at all elevations were over-predicted much until the quench time, which means that the code over-predicted the HTCs in the film boiling regime.

2.3.8 Test 32114

Test 32114 was a 2.5~3.1 cm/s (1.00~1.22 in/sec) reflood test at 0.28 MPa (40 psia). Inlet liquid temperature was 408 K (257 °F). Of all the tests simulated in this study, this test had the smallest inlet subcooling of 5 K (10 °F). Other seven tests had similar inlet subcooling of 74~79 K (134~143 °F).

Heater rod clad temperatures predicted by RELAP5 at various elevations are compared to the measured data in Figure 139 through Figure 146. The maximum PCT predicted by the code is 1320 K at 1.981 m (6.5 ft) elevation while the measured PCTs at the same elevation are in the range of 1292~1443 K. The predicted maximum PCT is 67 K lower than the arithmetic average of measurements. Compared to the arithmetic average of measurement at each elevation, The PCTs at 0.610~3.048 m (2~10 ft) were under-predicted while those at higher elevations were over-predicted.

Vapor temperatures predicted are compared to the measured data in Figure 147 and Figure 148. The vapor temperature at 1.829 m (6 ft) was significantly under-predicted compared to the measurements. The predicted vapor temperature at 3.048 m (10 ft) increased too fast while the peak temperature predicted is not much different from the measured values.

The predicted and measured quench fronts are compared in Figure 149. The final quenches were predicted to occur much earlier than the measurements at all elevations, even at the elevations where PCTs were over-predicted. The difference between the predicted quench time and the arithmetic average of measured quench times (predicted – measured) varies from -113 to -15 seconds and the maximum absolute deviation occurred at 1.981 m (6.5 ft).

The predicted and measured differential pressures for the entire core region, a mid-level (1.829 to 2.134 m (6 to 7 ft)), and a top region (3.048 to 3.353 m (10 to 11 ft)) are compared in Figure 150, Figure 151, and Figure 152, respectively. The predicted value for the entire core is higher

than the measurement from the beginning of transient and the deviation is 3~4 kPa (0.44~0.58 psi) after ~40 seconds. The predicted differential pressures for the mid-level and top region were predicted relatively well until large oscillations were observed.

The predicted and measured HTCs at five different elevations are compared in Figure 153 through Figure 157. Excluding the early steam cooling only period, the film boiling HTCs at all elevations were over-predicted.

2.3.9 All 8 Tests

The percent deviation between RELAP5/MOD3.3 predicted PCTs and measurements at 8 different elevations are compared for all 8 tests in Figure 158. As shown in the figure, RELAP5/MOD3.3 predicted the measured PCTs within ±10% deviation. The code was well able to predict PCTs at lower elevations (up to 1.219 m (4 ft)) while it under-predicted those at middle elevations (1.829~2.438 m (6~8 ft)). The PCTs were less under-predicted at upper elevations at or above 3.048 m (10 ft), and even over-predicted for a few tests. This is understandable because RELAP5 does not have a spacer grid model. In other words, the under-prediction of PCTs at higher elevations was compensated to some extent by the lack of a spacer grid model. The under-prediction of PCTs at middle elevations was more severe for the tests having relatively lower flooding rates (≤ 3.8 cm/s (1.51 in/sec)) and less severe for the tests having higher flooding rates (≥ 7.7 cm/s (3.01 in/sec)). The predictive capability did not show any consistent or significant variance depending on other test conditions such as upper plenum pressure or coolant inlet subcooling. The RMS error in PCT predictions corresponding to Figure 158 is 48.3 K.

The code under-predicted the peak vapor temperatures at 1.829 m (6 ft) for most tests. The code over-predicted the peak vapor temperature at this elevation for only two tests (Test 31302 and Test 31108) which had flooding rates of 7.7 cm/s (3.01 in/sec) and 7.9 cm/s (3.11 in/sec), respectively. The largest deviation was 186 K under-prediction in Test 31504. The code had a tendency of under-predicting the peak vapor temperature at 3.048 m (10 ft) for the test having relatively lower flooding rates (Test 31805, 31504, 32013, and 32114), but the code over-predicted it for the tests having higher flooding rates (Test 31302, Test 31701, and Test 31108). The largest deviation was 165 K over-prediction for Test 31108. Note that this quantitative analysis for the vapor temperature predictions can not be regarded as sufficiently accurate since there only a few measurements are available at a specified elevation.

Though the code predicted PCTs relatively well, it could not do quench times. The differences between the predicted and measured quench times at 8 different elevations are compared for all 8 tests in Figure 159. As shown in the figure, rod quenches were predicted to occur too early for almost all elevations. In most tests, the differences between the predicted and measured quench times increased with elevations, reaching their maximum at around 3.048 m (10 ft) elevation. The differences were smaller in a test having a higher flooding rate, but we should also consider that the differences may be bigger when the real quench times are longer. Comparing Test 31108 to Test 31302 or Test 32013 to Test 31504, it can be seen that the code tends to predict better the quench times of a test having a higher upper plenum pressure. No clear conclusions can be made for the effect of inlet subcooling on the predictive capability for quench times. The RMS error in quench time predictions deduced from Figure 159 is 85.9 seconds.

The code over-predicted the overall pressure drop for the entire bundle in most tests. The differences between the predicted and measured pressure drops were well below the

measurement uncertainty of 2.66 kPa (0.39 psi) only for Test 32013. In other cases, the deviation varied from 3~7 kPa (0.44~1.02 psi) though it was also a function of time. The pressure drop for a mid-level region (1.829 to 2.134 m (6 to 7 ft)) was also over-predicted for most tests after some time when the bottom quench front approached close to the region. The same tendency was observed for the prediction of the pressure drop for a top region (3.048 to 3.353 m (10 to 11 ft)).

The code tended to over-predict the HTCs at all elevation for all tests after a well predicted, short period of vapor only cooling. The over-prediction of HTCs in a top region is smaller than that in a middle region due to the lack of a spacer grid model.

In summary, RELAP5/MOD3.3 predicted the PCTs of the selected FLECHT-SEASET tests relatively well, within ±10% deviation. However, the code predicted quench times to occur much earlier than the measurement data. As the code over-predicted significantly the film boiling HTCs in most cases, the wall-to-fluid heat transfer models in that heat transfer regime should be investigated intensively. The overall tendency of over-predicting differential pressure for the entire core (or collapsed liquid level) indicates that the interfacial or wall drag models of the code may also have some deficiencies. By the way, the predicted differential pressures can alter if the wall-to-fluid heat transfer models are changed. Thus, we focus on the wall-to-fluid heat transfer models first to improve the predictive capability for quench times. An intensive review and improvements of drag models is regarded as a future work.

3. MODIFICATION OF FILM BOILING WALL-TO-FLUID HEAT TRANSFER MODELS

To improve the predictive capability mainly for quench times, the film boiling wall-to-fluid heat transfer models of RELAP5/MOD3.3, which are activated when the reflood option is invoked, were modified. The current models of RELAP5/MOD3.3 are discussed in brief first, and the modified models are described thereafter.

3.1 Brief of Current Models

Differently from other best-estimate codes like TRACE [9], COBRA/TRAC [10], or COBRA-TF [8], RELAP5/MOD3.3 does not draw a line between the inverted annular film boiling (IAFB) heat transfer regime and the dispersed flow film boiling (DFFB) heat transfer regime. It uses the same wall-to-fluid heat transfer models for the entire film boiling regime.

The code takes the maximum of HTCs calculated by three different correlations as the film boiling HTC to liquid.

$$h_{wf} = \max(h_{Br}, h_{CT}, h_{FR}) \tag{2}$$

where h_{Br}, h_{CT}, and h_{Fr} are the HTCs calculated using the Bromley correlation, an empirical CATHARE correlation, and the Forslund-Rohsenow correlation, respectively.

The film boiling wall-to-vapor HTC is returned from the DITTUS subroutine. Here, in the default model, h_{Ditt} is obtained by taking the maximum of a turbulent convective HTC calculated using the Dittus-Boelter correlation, a HTC corresponding to a constant laminar convective Nusselt number of 4.36, and a natural convective HTC calculated using the Churchill-Chu correlation. Note that the mass flux in the Dittus-Boelter correlation contains not only the vapor mass flux but also a portion of the liquid mass flux ($G_f \cdot \rho_f / \rho_g$) in two-phase flow cases. Then, h_{Ditt} is void fraction ramped so that it goes to zero as the void fraction goes to zero.

$$h_{wg} = h_{Ditt} \cdot \alpha_g \tag{3}$$

RELAP5/MOD3.3 takes into account the wall-to-liquid radiation heat transfer in the film boiling regime and adds it to the wall-to-liquid convective heat transfer. The radiation heat transfer model of the code is based on that developed by Sun [11]. In this model, the radiation heat flux is proportional to the wall-to-liquid grey body factor given by

$$F_{wf} = \frac{1}{R_2\left(1 + \frac{R_3}{R_1} + \frac{R_3}{R_2}\right)} \tag{4}$$

where R terms are given as a function of the emissivity of wall, vapor, and liquid. Constant values of 0.02 and 0.9 are assumed for the vapor emissivity and the wall emissivity, respectively. The liquid emissivity depends on the liquid absorption coefficient, a_f which is defined as

$$a_f = \frac{1.11 \cdot \alpha_f}{d} \tag{5}$$

where α_f is the liquid volume fraction and d is the liquid droplet diameter which is given as the minimum of the following two expressions.

$$d_{max} = \sqrt{1 - \alpha_g} \cdot D_h \tag{6}$$

$$d_{We=7.5} = \frac{7.5 \cdot \sigma}{\rho_g \cdot v_r^2} \tag{7}$$

More detailed information on the film boiling wall-to-fluid heat transfer models used in RELAP5/MOD3.3 can be found in the code manual [7].

3.2 Modified Models

In the modified version, the film boiling heat transfer regime is divided into three separate regimes. The IAFB and DFFB regimes are assumed to exist if void fractions are under 0.6 and over 0.9, respectively. Appropriate wall-to-fluid heat transfer correlations, described later, are used for each regime, and the HTCs in the region having void fractions between 0.6 and 0.9 are obtained by spline interpolation of the IAFB and DFFB HTCs:

$$h_{wf} = y \cdot h_{wf,IA} + (1 - y) \cdot h_{wf,DF} \tag{8}$$

$$h_{wg} = y \cdot h_{wg,IA} + (1 - y) \cdot h_{wg,DF} \tag{9}$$

where the weighting function, y is calculated from

$$y = x \cdot (2 - x) \quad \text{with} \quad x = \frac{0.9 - \alpha_g}{0.9 - 0.6} \tag{10}$$

Note that the void fraction limits defining each film boiling regime and the interpolation method are the same as used in TRACE [9].

For the IAFB wall-to-liquid HTC, the CATHARE correlation was selected among the three correlations in Eq.(2).

$$h_{wf,IA} = [1400 - 1880 \cdot \min(0.05, Z_{Qmin})] \cdot \min(0.999 - \alpha_g, 0.5) + h_{MBr} \cdot (1 - \alpha_g)^{0.5} \tag{11}$$

where h_{MBr} is calculated from a modified Bromley correlation.

$$h_{MBr} = 0.62 \cdot \left\{ \frac{g \cdot \rho_g \cdot \Delta\rho \cdot k_g^3 \left[h_{fg} + 0.5 \cdot (T_w - T_{spt}) \right]}{\max(0.005, Z_{Qmin}) \cdot \mu_g \cdot (T_w - T_{spt})} \right\}^{0.25} \tag{12}$$

Here, Z_{Qmin} is the distance from the point in question to the bottom quench front. It replaces the wave length in the normal Bromley correlation.

For the DFFB wall-to-liquid HTC, a modified Forslund-Rohsenow correlation was applied.

$$h_{wf,DF} = K_{BY} \cdot 0.25\pi \cdot \left[\frac{6 \cdot (0.999 - \alpha_g)}{\pi}\right]^{2/3} \cdot \left\{\frac{g \cdot \rho_g \cdot \rho_f \cdot h_{fg} \cdot k^3}{\left[(T_w - T_{spt}) \cdot \mu_g \cdot d\left(\frac{\pi}{6}\right)^{1/3}\right]}\right\}^{0.25} \tag{13}$$

where K_{BY} is a function of the gas Reynolds number given as

$$K_{BY} = \left(\frac{Re_g - 4000}{100000}\right)^{0.6} \tag{14}$$

Eq.(13) is identical to the Forslund-Rohsenow correlation used to find h_{FR} in Eq.(2) except that it has a Reynolds number dependent coefficient, K_{BY} proposed by Bajorek and Young [12].

The IAFB wall-to-vapor HTC is given as a value corresponding to the conduction-only heat transfer:

$$h_{wg,IA} = 2 \cdot k_g / \delta \tag{15}$$

where k_g is the vapor conductivity and δ is the vapor film thickness in the rod bundle geometry obtained from geometrical consideration:

$$\delta = 0.5 \cdot D_h \cdot \left\{\left[1 + \alpha_g \cdot [(4/\pi) \cdot (P/D_R)^2 - 1]\right]^{0.5} - 1\right\} \tag{16}$$

Note that we followed the same approach as used in TRACE for calculating the IAFB wall-to-vapor HTC.

The DFFB wall-to-vapor HTC in the modified version is determined from

$$h_{wg,DF} = \Phi_{2p} \cdot [F_{lt} \cdot h_{lam} + (1 - F_{lt}) \cdot \Phi_{tur} \cdot h_{tur}] \tag{17}$$

where h_{tur} is the single-phase turbulent convective HTC calculated using the Dittus-Boelter correlation. In this case only the vapor mass flux is used to find the Reynolds number. Φ_{tur} is a turbulent flow multiplier applied to a vertical bundle geometry and it is equal to the rod pitch to diameter ratio [7]. This multiplier can be used as an option in a calculation using the original version but it is not a part of the default model. h_{lam} is the maximum of a single-phase laminar convective HTC corresponding to a constant Nusselt number of 10.0 and a single-phase natural convective HTC calculated using the Churchill-Chu correlation. Note that the laminar convective Nusselt number was increased from 4.36 to 10.0 because the former has been regarded as a value appropriate only for internal flows. The same laminar convective Nusselt number of 10.0

has been used in COBRA/TRAC [10]. F_{lt} is a linear function of the gas Reynolds number. It has a value of 1.0 at Re_g = 3000 and a value of 0.0 at Re_g = 10000 as proposed by Bajorek and Young [12]. Φ_{2p} is a two-phase enhancement factor to account for increases in convective heat transfer due to the relative motion of vapor and droplets. A similar factor has been used not only in TRACE [9] but also in COBRA-TF [8]. The factor can be derived using a rough wall analogy [13]:

$$\Phi_{2p} = \sqrt{\frac{\tau_i + \tau_w}{\tau_w}} \tag{18}$$

where τ_i and τ_w are friction forces per unit volume due to interfacial and wall drags, respectively and they are given in RELAP5/MOD3.3 as

$$\tau_w = \frac{1}{2} \cdot \rho_g \cdot f_w \cdot v_g^2 / D_h \tag{19}$$

$$\tau_i = \frac{1}{8} \cdot \rho_g \cdot a_{gf} \cdot C_D \cdot v_r^2 \tag{20}$$

where the interfacial area per unit volume, a_{gf}, and the droplet drag coefficient, C_D are in turn given as

$$a_{gf} = \frac{3.6 \cdot \alpha_f}{d} \tag{21}$$

$$C_D = \frac{24 \cdot (1 + 0.1 \cdot Re_d^{0.75})}{Re_d} \tag{22}$$

For the wall friction factor, f_w in Eq.(19), a constant value corresponding to its fully developed one for a smooth pipe, 0.02 is assumed as in TRACE [9].

Four minor modifications were made to the radiation heat transfer model. First, the vapor emissivity is now obtained from the EMISS subroutine instead of using a constant value. The same subroutine is also used in TRACE to solve for the emissivity of liquid and vapor. Second, the wall emissivity was reduced to 0.7 to make the code agree with its manual. Third, the droplet diameter is now determined using the same method in subroutines FIDISV and FIDIS2, where the interfacial area is determined for bubbles and droplets. Note that the droplet diameter calculation method in these subroutines had a minor error which was corrected as described in Section 3.3. Fourth, a simpler approximation, that overrides Eq.(4), was introduced to find the wall-to-liquid grey body factor for the IAFB regime.

$$F_{wf} = \frac{1}{\frac{1}{\varepsilon_f \cdot \sqrt{\alpha_f}} + \left(\frac{1}{\varepsilon_w} - 1 \right)} \tag{23}$$

The radiation heat transfers using the grey body factors in Eq.(4) and Eq.(23) are lumped into the wall-to-liquid heat transfer components for the DFFB and IAFB regimes, respectively.

3.3 Coding Error Corrections

As mentioned in the previous section, the subroutines calculating the interfacial area for bubbles and droplets contain a coding error. In subroutines FIDISV and FIDIS2, the average droplet diameter during reflood is given as

$$d = \min(D_h, \text{dcon2}, \text{diam}) \tag{24}$$

where dcon2 = 0.0015 m for the post-CHF droplets and diam is defined as

$$\text{diam} = \max(\text{dmin}, d_{We=1.5}) \tag{25}$$

where dmin = 0.0015 m if pressure is sufficiently low.

Equation (24) should be corrected because dcon2 is not a maximum but a minimum average droplet diameter as per Analytis [1]. The correct expression should read

$$d = \min(D_h, \text{diam}) \tag{26}$$

Another coding error exists in the Weismann transition boiling wall-to-liquid HTC correlation. The correlation includes h_{max} which is defined as

$$h_{max} = \frac{0.5 \cdot q''_{CHF}}{\Delta T_{CHF}} \tag{27}$$

where ΔT_{CHF} is the difference between the wall temperature at the CHF point and the saturation temperature according to Analytis [1]. However, it is coded as if it were the difference between the current wall temperature and the saturation temperature:

$$\Delta T_{CHF} = \max[3,\min(40,T_w - T_{sat})] \tag{28}$$

The correct form of this parameter should be

$$\Delta T_{CHF} = \max[3,\min(40,T_{w,CHF} - T_{sat})] \tag{29}$$

From test calculations employing only these error corrections, it was revealed that they do not have a significant effect on the calculations for FLECHT-SEASET tests. Thus, the errors can be regarded as minor.

3.4 Effect of Modifications

To test the modifications, calculations for all the tests listed in Table 1 were conducted again using the modified version. The results are compared not only to those predicted by the original version but also to the measurement data in this section.

3.4.1 Test 31805

The predicted heater rod clad temperatures using the modified version at various elevations are presented in Figure 6 through Figure 13. The maximum predicted PCT is 1383 K at 1.981 m (6.5 ft) elevation while it was 1359 K at the same elevation with the original version. The predicted PCTs at all elevations are higher than those predicted using the original version and they locate between the maximum and minimum measured values at all elevations.

The predicted vapor temperatures at 1.829 m (6 ft) and 3.048 m (10 ft) elevations are presented in Figure 14 and Figure 15, respectively. The predicted vapor temperatures at both elevations are higher than those predicted using the original version and closer to the measurements.

The predicted quench front is presented in Figure 16. The predictive capability for quench times was greatly improved by the modifications. The difference between the predicted quench time and the arithmetic average of measured quench times (predicted – measured) varies from -32 to +2 seconds and the maximum absolute deviation occurred at 1.981 m (6.5 ft). The difference varied from -177 to -7 seconds when the original version was used.

The predicted and measured differential pressures for the entire core region, a mid-level (1.829 to 2.134 m (6 to 7 ft)), and a top region (3.048 to 3.353 m (10 to 11 ft)) are presented in Figure 17, Figure 18, and Figure 19, respectively. The predicted value for the entire core is still higher than the measurement data, but the deviation was slightly reduced by the modifications. The time when the predicted differential pressure for the mid-level becomes higher than the measurement was ~30 seconds delayed compared to the prediction using the original version. The predicted differential pressure for the top region was not altered much by the modifications except that the time of large oscillations were ~150 seconds delayed compared to the prediction using the original version. It means the liquid fraction in a top region was predicted to increase more slowly with the modified version than with the original version.

The predicted and measured HTCs at five different elevations are presented in Figure 20 through Figure 24. The predicted film boiling HTCs are still higher than the measured ones at most elevations, but the deviations were reduced compared to the predictions using the original version. The HTC at 3.048 m (10 ft) elevation agrees with the measured data very well.

3.4.2 Test 31504

The predicted heater rod clad temperatures using the modified version at various elevations are presented in Figure 25 through Figure 32. The maximum PCT predicted by the code is 1370 K at 1.981 m (6.5 ft) elevation while it was 1319 K at the same elevation with the original version. The predicted PCTs are higher than those predicted using the original version and they locate between the maximum and minimum measured values at most elevations. Only the predicted PCT at 3.505 m (11.5 ft) is 41 K lower than that predicted using the original version.

The predicted vapor temperatures at 1.829 m (6 ft) and 3.048 m (10 ft) elevations are presented in Figure 33 and Figure 34, respectively. The predicted vapor temperatures at both elevations are higher than those predicted using the original version and closer to the measurements.

The predicted quench front is presented in Figure 35. The predictive capability for quench times was greatly improved by the modifications. Only the quench times at and below 1.219 m (4 ft) were slightly under-predicted and the difference between the predicted quench time and the arithmetic average of measured quench times (predicted – measured) varies from -15 to +14

seconds and the maximum absolute deviation occurred at 1.219 m (4 ft). The difference varied from -149 to -5 seconds when the original version was used.

The predicted and measured differential pressures for the entire core region, a mid-level (1.829 to 2.134 m (6 to 7 ft)), and a top region (3.048 to 3.353 m (10 to 11 ft)) are presented in Figure 36, Figure 37, and Figure 38, respectively. The predicted value for the entire core is still higher than the measurement data, but the deviation was slightly reduced by the modifications. The time when the predicted differential pressure for the mid-level becomes higher than the measurement was ~50 seconds delayed compared to the prediction using the original version. The predicted differential pressure for the top region was not altered much by the modifications except that the time of large oscillations were ~100 seconds delayed compared to the prediction using the original version.

The predicted and measured HTCs at five different elevations are presented in Figure 39 through Figure 43. The predicted film boiling HTCs are still higher than the measured ones at most elevations, but the deviations were reduced compared to the predictions using the original version. The HTCs at 2.438 m (8 ft) and 3.048 m (10 ft) elevations agree with the measured data fairly well.

3.4.3 Test 31203

The predicted heater rod clad temperatures using the modified version at various elevations are presented in Figure 44 through Figure 51. The maximum predicted PCT is 1265 K at 1.981 m (6.5 ft) elevation while it was 1224 K at 1.829 m (6.0 ft) elevation with the original version. The predicted PCTs are higher than those predicted using the original version and they locate between the maximum and minimum measured values at most elevations. Only the predicted PCT at 3.505 m (11.5 ft) is 11 K lower than that predicted using the original version.

The predicted vapor temperatures at 1.829 m (6 ft) and 3.048 m (10 ft) elevations are presented in Figure 52 and Figure 53, respectively. The predicted vapor temperatures at both elevations are higher than those predicted using the original version and closer to the measurements.

The predicted quench front is presented in Figure 54. The predictive capability for quench times was greatly improved by the modifications. However, the final quenches were still predicted to occur a little earlier than the measurements at most elevations. The difference between the predicted quench time and the arithmetic average of measured quench times (predicted – measured) varies from -35 to +1 seconds and the maximum absolute deviation occurred at 3.048 m (10 ft). The difference varied from -148 to -6 seconds when the original version was used.

The predicted and measured differential pressures for the entire core region, a mid-level (1.829 to 2.134 m (6 to 7 ft)), and a top region (3.048 to 3.353 m (10 to 11 ft)) are presented in Figure 55, Figure 56, and Figure 57, respectively. The predicted value for the entire core is still higher than the measurement data, but the deviation was slightly reduced by the modifications. The time when the predicted differential pressure for the mid-level becomes higher than the measurement was ~30 seconds delayed compared to the prediction using the original version. The predicted differential pressure for the top region was not altered much by the modifications except the time of large oscillations were ~100 seconds delayed compared to the prediction using the original version.

The predicted and measured HTCs at five different elevations are presented in Figure 58 through Figure 62. Though the film boiling HTCs were predicted relatively well, the transition boiling was predicted to occur earlier than the measurements.

3.4.4 Test 31302

The predicted heater rod clad temperatures using the modified version at various elevations are presented in Figure 63 through Figure 70. The maximum predicted PCT is 1166 K at 1.829 m (6.0 ft) elevation while it was 1159 K at the same elevation with the original version. The predicted PCTs are higher than those predicted using the original version and they locate between the maximum and minimum measured values at most elevations. The predicted PCT at 3.353 m (11 ft) is higher than the measurements just like that predicted using the original version.

The predicted vapor temperatures at 1.829 m (6 ft) and 3.048 m (10 ft) elevations are presented in Figure 71 and Figure 72, respectively. The predicted vapor temperatures at both elevations are slightly higher than those predicted using the original version. Time when the vapor loses superheating was delayed by the modifications at both elevations.

The predicted quench front is presented in Figure 73. The predictive capability for quench times was greatly improved by the modifications. However, the final quenches were still predicted to occur earlier than the measurements at most elevations. The difference between the predicted quench time and the arithmetic average of measured quench times (predicted – measured) varies from -57 to +38 seconds and the maximum absolute deviation occurred at 3.048 m (10 ft). The difference varied from -120 to -7 seconds when the original version was used. Though the difference was reduced much by the modifications, the effect of modifications is rather limited compared to that observed for lower flooding rate tests (Test 31805, Test 31504, and Test 31203).

The predicted and measured differential pressures for the entire core region, a mid-level (1.829 to 2.134 m (6 to 7 ft)), and a top region (3.048 to 3.353 m (10 to 11 ft)) are presented in Figure 74, Figure 75, and Figure 76, respectively. The modified version predicted better the differential pressure for the entire core than the original version, especially after ~100 seconds. The time when the predicted differential pressure for the mid-level becomes higher than the measurement was ~30 seconds delayed compared to the prediction using the original version. The predicted differential pressure for the top region was not altered much by the modifications except that the time of large oscillations were ~60 seconds delayed compared to the prediction using the original version.

The predicted and measured HTCs at five different elevations are presented in Figure 77 through Figure 81. Though the film boiling HTCs were predicted relatively well, the transition boiling was predicted to start earlier than the measurements.

3.4.5 Test 31701

The predicted heater rod clad temperatures using the modified version at various elevations are presented in Figure 82 through Figure 89. The maximum predicted PCT is 1136 K at 1.829 m (6.0 ft) elevation while it was 1135 K at the same elevation with the original version. The predicted PCTs are slightly higher than those predicted using the original version at all elevations. They locate between the maximum and minimum measured values at all elevations except 3.353 m (11 ft) elevation.

The predicted vapor temperatures at 1.829 m (6 ft) and 3.048 m (10 ft) elevations are presented in Figure 90 and Figure 91, respectively. The peak vapor temperatures predicted at both elevations are not different much from those predicted using the original version. Only the time when the vapor loses superheating was delayed by the modifications.

The predicted quench front is presented in Figure 92. The predictive capability for quench times was a little improved by the modifications. However, the final quenches were still predicted to occur earlier than the measurements at most elevations. The difference between the predicted quench time and the arithmetic average of measured quench times (predicted – measured) varies from -30 to -1 seconds and the maximum absolute deviation occurred at 3.048 m (10 ft). The difference varied from -41 to -3 seconds when the original version was used. Though the difference was reduced a little by the modifications, the effect of modifications is rather limited compared to that observed for the tests having relatively low flooding rates (Test 31805, Test 31504, and Test 31203).

The predicted and measured differential pressures for the entire core region, a mid-level (1.829 to 2.134 m (6 to 7 ft)), and a top region (3.048 to 3.353 m (10 to 11 ft)) are presented in Figure 93, Figure 94, and Figure 95, respectively. The predicted value for the entire core is still higher than the measurement data, but the difference from the measurement was slightly reduced by the modifications. The time when the predicted differential pressure for the mid-level becomes higher than the measurement was ~15 seconds delayed compared to the prediction using the original version. The predicted differential pressure for the top region was not altered much by the modifications except the time of large oscillations were ~30 seconds delayed compared to the prediction using the original version.

The predicted and measured HTCs at five different elevations are presented in Figure 96 through Figure 100. The predicted HTC at 1.219 m (4 ft) was not altered much by the modifications. The predictions for HTCs at other locations were improved a little, but the transition boiling was predicted to occur earlier than the measurements.

3.4.6 Test 31108

The predicted heater rod clad temperatures using the modified version at various elevations are presented in Figure 101 through Figure 108. The maximum PCT predicted by the code is 1167 K at 1.981 m (6.5 ft) elevation while it was 1145 K at 1.829 m (6.0 ft) elevation with the original version. The predicted PCTs are higher than those predicted using the original version. The PCTs at and above 2.438 m (8 ft) were definitely over-predicted by the modified version. PCTs were predicted to occur later in time compared to not only the measurements but also the predictions using the original version.

The predicted vapor temperatures at 1.829 m (6 ft) and 3.048 m (10 ft) elevations are presented in Figure 109 and Figure 110. The predicted vapor temperatures at both elevations are nearly equal to or slightly higher than those predicted using the original version. The times when the vapor loses superheating were delayed by the modifications at both elevations.

The predicted quench front is presented in Figure 111. The predictive capability for quench times was much improved by the modifications. However, the final quenches were still predicted to occur earlier than the measurements at all elevations but 3.353 m (11 ft) and 3.505 m (11.5 ft) elevations. The difference between the predicted quench time and the arithmetic average of measured quench times (predicted – measured) varies from -77 to +130 seconds and the

maximum absolute deviation occurred at 3.505 m (11.5 ft). The difference varied from -162 to +13 seconds when the original version was used. Though the predicted quench front went closer to the measurement with the modifications, the top-down quenchings at a top region were not predicted well.

The predicted and measured differential pressures for the entire core region, a mid-level (1.829 to 2.134 m (6 to 7 ft)), and a top region (3.048 to 3.353 m (10 to 11 ft)) are presented in Figure 112, Figure 113, and Figure 114, respectively. The predicted value for the entire core is still higher than the measurement data, but the deviation was slightly reduced by the modifications. The time when the predicted differential pressure for the mid-level becomes higher than the measurement was ~40 seconds delayed compared to the prediction using the original version. The predicted differential pressure for the top region was not altered much by the modifications, but the large oscillations from ~150 seconds with the original version were replaced with a sudden increase at ~265 seconds.

The predicted and measured HTCs at five different elevations are presented in Figure 115 through Figure 119. Though the film boiling HTCs were reduced compared those predicted using the original version, the transition boiling was still predicted to start earlier than measurements.

3.4.7 Test 32013

The predicted heater rod clad temperatures using the modified version at various elevations are presented in Figure 120 through Figure 127. The maximum predicted PCT is 1353 K at 1.981 m (6.5 ft) elevation while it was 1326 K at the same elevation with the original version. The predicted PCTs are higher than those predicted using the original version and they locate between the maximum and minimum measured values at all elevations.

The predicted vapor temperatures at 1.829 m (6 ft) and 3.048 m (10 ft) elevations are presented in Figure 128 and Figure 129, respectively. The vapor temperatures increased for a longer time compared to the predictions with the original version. The time when the vapor loses superheating was delayed by the modifications at both elevations.

The predicted quench front is presented in Figure 130. The predictive capability for quench times was greatly improved by the modifications. Only the quench times at 0.610 m (2 ft), 1.219 m (4 ft), and 3.048 m (10 ft) elevations were slightly under-predicted and the difference between the predicted quench time and the arithmetic average of measured quench times (predicted – measured) varies from -7 to +12 seconds and the maximum absolute deviation occurred at 3.353 m (11 ft). The difference varied from -101 to -2 seconds when the original version was used.

The predicted and measured differential pressures for the entire core region, a mid-level (1.829 to 2.134 m (6 to 7 ft)), and a top region (3.048 to 3.353 m (10 to 11 ft)) are presented in Figure 131, Figure 132, and Figure 133, respectively. The predicted value for the entire core agrees with the measurement excellently. Even the small over-prediction by the original version was removed by the modifications. The prediction of the differential pressure for the mid-level was significantly improved by the modifications. The over-prediction with the original version which was observed after ~180 seconds was reduced to an acceptable level. The predicted differential pressure for the top region was not altered much by the modifications except that the time of large oscillations was ~100 seconds delayed compared to the prediction using the original version.

The predicted and measured HTCs at five different elevations are presented in Figure 134 through Figure 138. The film boiling HTCs were predicted very well especially at or over 2.438 m (8 ft) elevation. HTCs at other elevations were slightly over-predicted compared to the measurement data.

3.4.8 Test 32114

The predicted heater rod clad temperatures using the modified version at various elevations are presented in 139 through Figure 146. The maximum predicted PCT is 1356 K at 1.981 m (6.5 ft) elevation while it was 1320 K at the same elevation with the original version. The predicted PCTs are higher than those predicted using the original version and they locate between the maximum and minimum measured values at most elevations. The predicted PCT at 3.505 m (11.5 ft) is lower than that predicted with the original version while the predicted PCTs at 3.048 m (10 ft) and 3.353 m (11 ft) are higher than the measurements.

The predicted vapor temperatures at 1.829 m (6 ft) and 3.048 m (10 ft) elevations are presented in Figure 147 and Figure 148, respectively. The predicted vapor temperatures at both elevations are slightly higher than those predicted using the original version. The time when the vapor loses superheating was delayed by the modifications at both elevations.

The predicted quench front is presented in Figure 149. The predictive capability for quench times was greatly improved by the modifications. However, the final quenches of 1.981 m (6.5 ft) elevation and lower elevations were predicted to occur slightly earlier than the measurements while the quenches over 1.981 m (6.5 ft) elevation were predicted to occur later than the measurements. The difference between the predicted quench time and the arithmetic average of measured quench times (predicted – measured) varies from -26 to +64 seconds and the maximum absolute deviation occurred at 3.048 m (10 ft). The difference varied from -113 to -15 seconds when the original version was used.

The predicted and measured differential pressures for the entire core region, a mid-level (1.829 to 2.134 m (6 to 7 ft)), and a top region (3.048 to 3.353 m (10 to 11 ft)) are presented in Figure 150, Figure 151, and Figure 152, respectively. The predicted value for the entire core is still higher than the measurement data, but the deviation was slightly reduced by the modifications. For the predicted differential pressure for the mid-level, the time when large oscillations occur was ~100 seconds delayed by the modifications. A similar effect of code modifications can be observed in the prediction for the differential pressure for the top region.

The predicted and measured HTCs at five different elevations are presented in Figure 153 through Figure 157. Though the film boiling HTCs were reduced with the modifications, the HTCs at or below 1.981 m (6.5 ft) were predicted to increase to the magnitude of HTCs in the transition boiling earlier than the measurements.

3.4.9 All 8 Tests

Similar to Figure 158, the deviations of the predicted PCTs from the measurements are presented in Figure 160. The predictability for PCTs was not improved significantly but the RMS error in overall PCT predictions dropped from 48.3 to 36.7 K. Comparisons of the maxima and minima curves from Figures 158 and 160 in Figure 161 show more clearly the effect of the modifications. The largest PCT under-prediction dropped from 9.4 to 5.9%. Though the largest PCT over-prediction increased from 10.4 to 14.5% after the modifications, we believe that the

results with the modified version is more reasonable because the code has no model to take into account the heat transfer enhancement by spacer grids, which is dominant at upper elevations. The improved predictability for PCTs can be assured by Figure 162 where all the predicted PCTs are plotted versus the measured ones. Least-square fitting curves before and after the modifications are also compared in this figure.

A similar but more significant effect of the modifications can be seen in terms of quench times. The differences between measurements and predictions with the modified version are presented in Figure 163, and the maxima and minima curves of Figure 163 are compared to those of Figure 159 in Figure 164. These figures indicate that quench times are better predicted with the modified version. The improved predictability for quench times can be seen more clearly in Figure 165 which presents the predicted quench times as a function of the measured ones. The RMS error in overall quench time predictions dropped from 85.9 to 32.1 seconds.

As shown in Eq.(2), the original code takes the maximum HTCs calculated by three different correlations as the film boiling HTC to liquid. That model may provide a good approximation for the IAFB HTC to liquid. However, it must over-predict the DFFB HTC to liquid because the HTC calculated with the CATHARE correlation is usually higher than that calculated with the Forslund-Rohsenow correlation. As we modified the code to use a modified Forslund-Rohsenow correlation for the DFFB HTC to liquid, the heat transfer to liquid must have been reduced.

On the contrary, the DFFB HTC to vapor was increased by the modifications. We introduced not only a turbulent flow multiplier but also a two-phase enhancement factor to the DFFB HTC to vapor, as shown in Eq.(17). These factors, as their names imply, have an effect of enhancing the wall-to-vapor heat transfer. As a result, the predicted vapor temperatures increased with the modifications. Though it is hard to say quantitatively since only two or three vapor temperature measurements are available at an elevation, the figures containing the vapor temperature predictions indicate that the DFFB HTC to vapor was modified to the right direction.

Note that even the modified version still over-predicts HTCs at lower or middle elevations. HTCs at higher elevations were predicted relatively well. However, if we had introduced a spacer grid model, it would have over-predicted also HTCs at higher elevations.

The code tends to over-predict the overall pressure drop for the entire bundle for most tests even with the modifications. Though predictions were improved a little by the modifications, the differences between the predicted and measured pressure drops are greater than the measurement uncertainty for all tests except Test 32013. In addition, the pressure drop was over-predicted from the beginning of the transient. Thus, we suspect that this over-predicted pressure drop for the entire bundle (or collapsed liquid level) is one of the reasons for the over-prediction of HTCs at lower and middle elevations.

4. CONCLUSIONS

The reflood model of RELAP5/MOD3.3 was assessed using eight FLECHT-SEASET tests. From the assessment, the following findings were obtained.

- The code predicts the measured PCTs within ±10% deviation.
- The code predicts rod quenches to occur significantly earlier than the measurement data.
- The code has a tendency of under-predicting peak vapor temperatures at 2 different elevations, especially those of low flooding rate tests.
- The code has a tendency of over-predicting the overall pressure drop for the entire bundle.

Based on these findings, the wall-to-fluid heat transfer models which are activated during the reflood calculations were modified to improve the code's predictability mainly for quench times. We divided the film boiling heat transfer regime into three different sub-regimes and selected appropriate heat transfer correlations for each sub-regime. In addition, we fixed minor coding errors in a few subroutines and modified slightly the radiation heat transfer model to assume more reasonable and consistent emissivity and droplet diameter.

Another set of calculations for the same FLECHT-SEASET tests were conducted with the modifications. From the comparisons of the predictions not only to the measurement data but also to the predictions using the original version, the following conclusions were derived.

- The RMS error in overall PCT predictions is reduced from 48.3 to 36.7 K by the modifications.
- The RMS error in overall quench time predictions is reduced from 85.9 to 32.1 s by the modifications.
- The film boiling HTCs predicted using the modified version shows better agreement with the measurement data compared to those predicted using the original version.
- Wall-to-vapor heat transfers were increased by the modifications so that the predicted vapor temperatures are higher than those predicted by the original version.
- Even with the modifications, the code still has a tendency of over-predicting the overall pressure drop for the entire core (or collapsed liquid level in the core). Thus, further efforts to improve the reflood model of RELAP5/MOD3.3 should be made to the wall or interfacial drag models.

5. REFERENCES

[1]. Analytis, G. Th., Developmental Assessment of RELAP5/MOD3.1 with Separate Effect and Integral Test Experiments: Model Changes and Options. Nuclear Engineering and Design, 163, p.125-148, 1996.

[2]. Koszela, Z., Assessment of RELAP5/MOD3.2.2 Gamma against ABB Atom 3×3-Rod Bundle Reflooding Tests. Nuclear Engineering and Design, 223, p.49-73, 2003.

[3]. Chung, B. D. et al., Improvements to the RELAP5/MOD3 Reflood Model Assessment. Journal of Korean Nuclear Society, 26, p.265-276, 1994.

[4]. Baek, J. S. et al., Assessment of FLECHT SEASET Unblocked Forced Reflood Tests Using RELAP5/MOD3. Journal of Korean Nuclear Society, 24, p.297-310, 1992.

[5]. Loftus, M. J. et al., PWR FLECHT-SEASET Unblocked Bundle, Force and Gravity Reflood Task Data Report, NUREG/CR-1532, 1980.

[6]. USNRC, TRACE V5.0 Assessment Manual, 2007.

[7]. USNRC, RELAP5/MOD3.3 Code Manual. NUREG/CR-5535/Rev 1, 2001.

[8]. Westinghouse, Analysis of FLECHT SEASET 163-Rod Blocked Bundle Data Using COBRA-TF. NUREG/CR-4166, 1985.

[9]. USNRC, TRACE V5.0 Theory Manual, 2007.

[10]. Thurgood, M. J. et al., COBRA/TRAC-A Thermal Hydraulic Code for Transient Analysis of Nuclear Reactor Vessels and Primary Coolant Systems. NUREG/CR-3046, 1983.

[11]. Sun, K. H., Gonzales-Santalo, J. M., and Tien, C.L., Calculations of Combined Radiation and Convection Heat Transfer in Rod Bundles Under Emergency Cooling Conditions. Journal of Heat Transfer, 98:3, p.414-420, 1976.

[12]. Bajorek, S. M. and Young, M. Y., Direct-Contact Heat Transfer Model for Dispersed-Flow Film Boiling. Nuclear Technology, 132, p.375-388, 2000.

[13]. Kays, W., Convective Heat and Mass Transfer. McGraw-Hill, p.348-349, 1993.

Table 1. FLECHT-SEASET Tests for RELAP5 Assessment

No.	Test No.	Flooding Rate	Upper Plenum Pressure	Coolant Inlet Temperature	Inlet subcooling
		cm/s (in/sec)	MPa (psia)	K (°F)	K (°F)
1	31805	2.10 (0.81)	0.28 (40)	324 (124)	79 (143)
2	31504	2.40 (0.97)	0.28 (40)	324 (124)	79 (143)
3	31203	3.84 (1.51)	0.28 (40)	325 (126)	78 (141)
4	31302	7.65 (3.01)	0.28 (40)	325 (126)	78 (141)
5	31701	15.50 (6.10)	0.28 (40)	326 (127)	77 (140)
6	31108	7.90 (3.11)	0.13 (19)	306 (91)	74 (134)
7	32013	2.64 (1.04)	0.41 (60)	339 (150)	79 (143)
8	32114	2.5~3.1 (1.0~1.22)	0.28 (40)	408 (257)	5 (10)

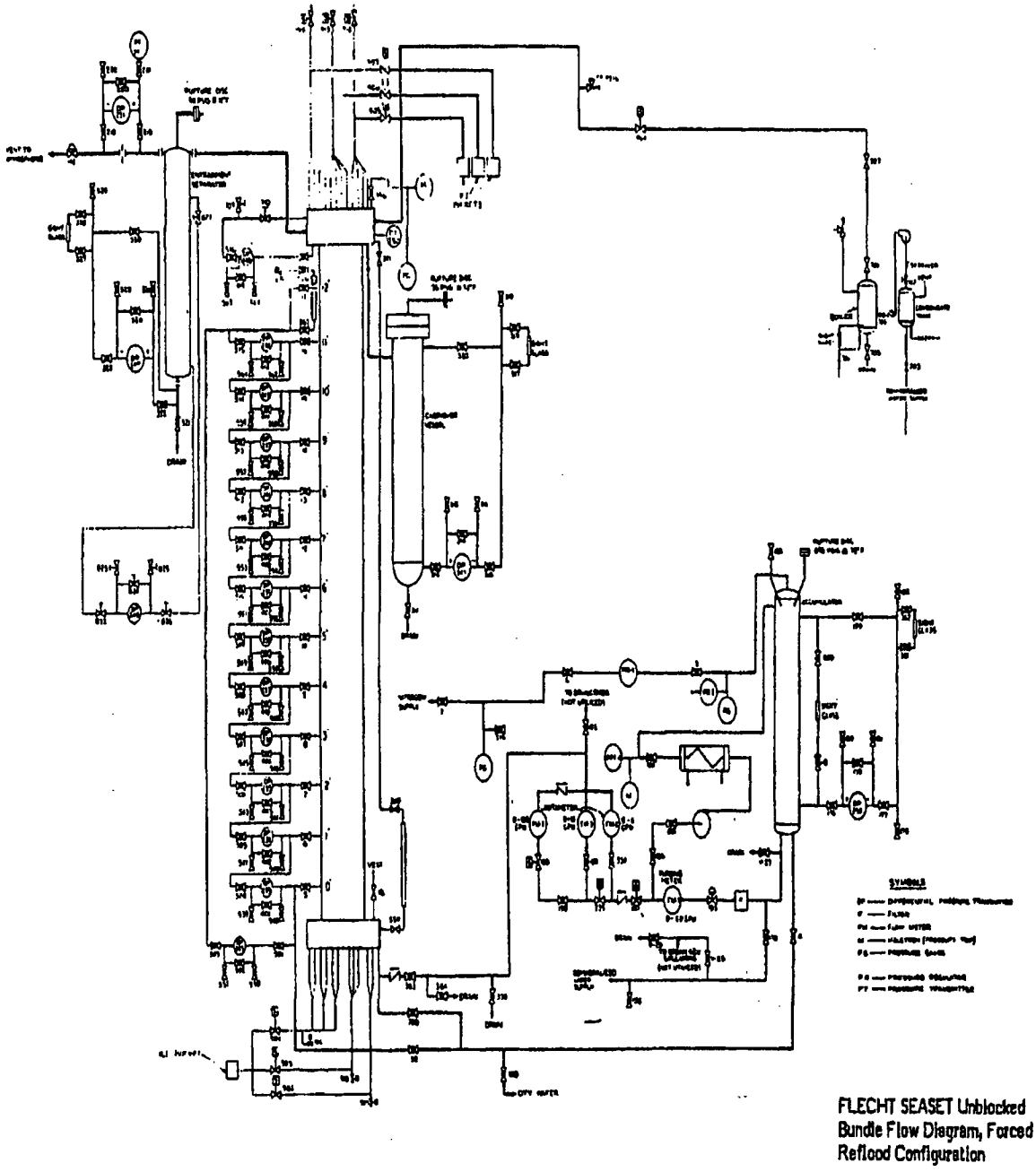

Figure 1. Facility Flow Diagram for Forced Reflood Tests

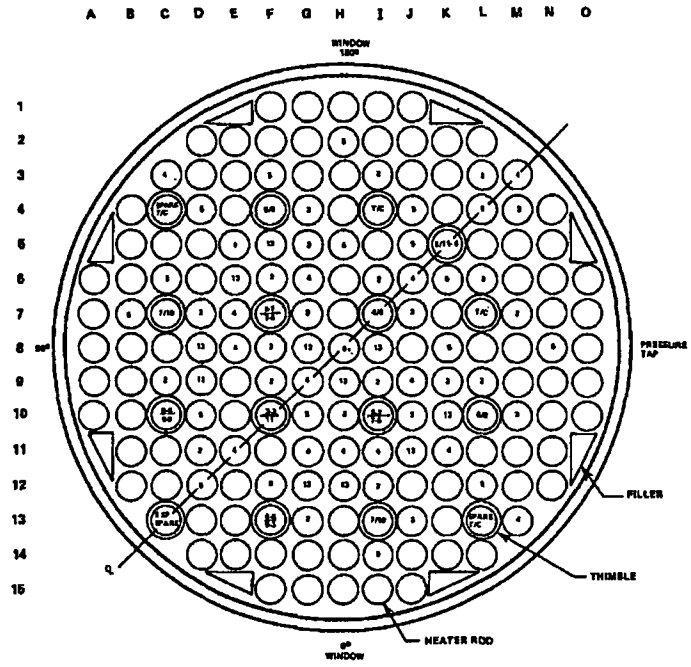

Figure 2. Cross-sectional View of Bundle Heated Section

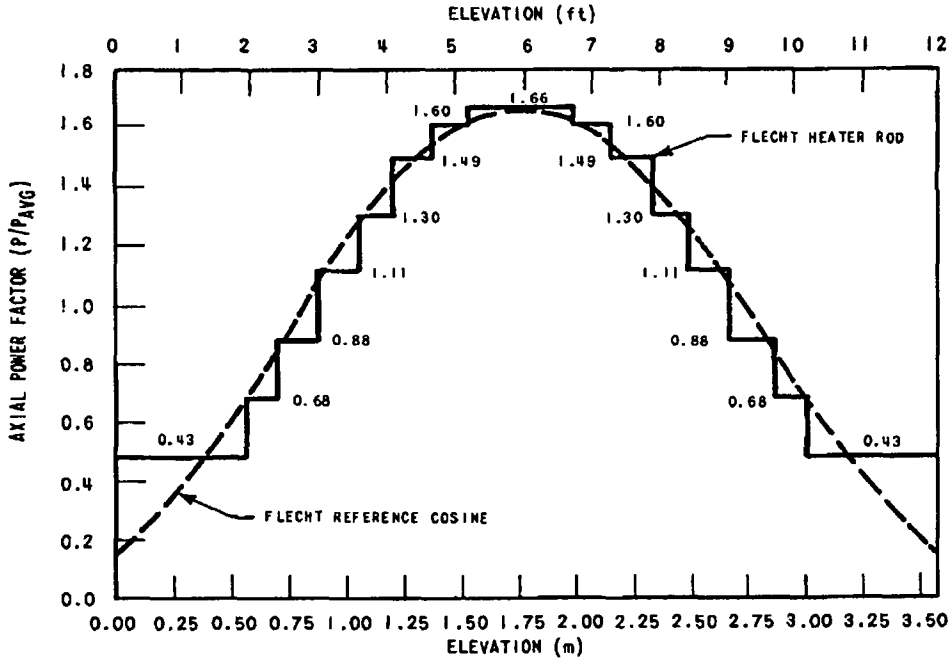

Figure 3. Axial Power Profile of Heater Rods

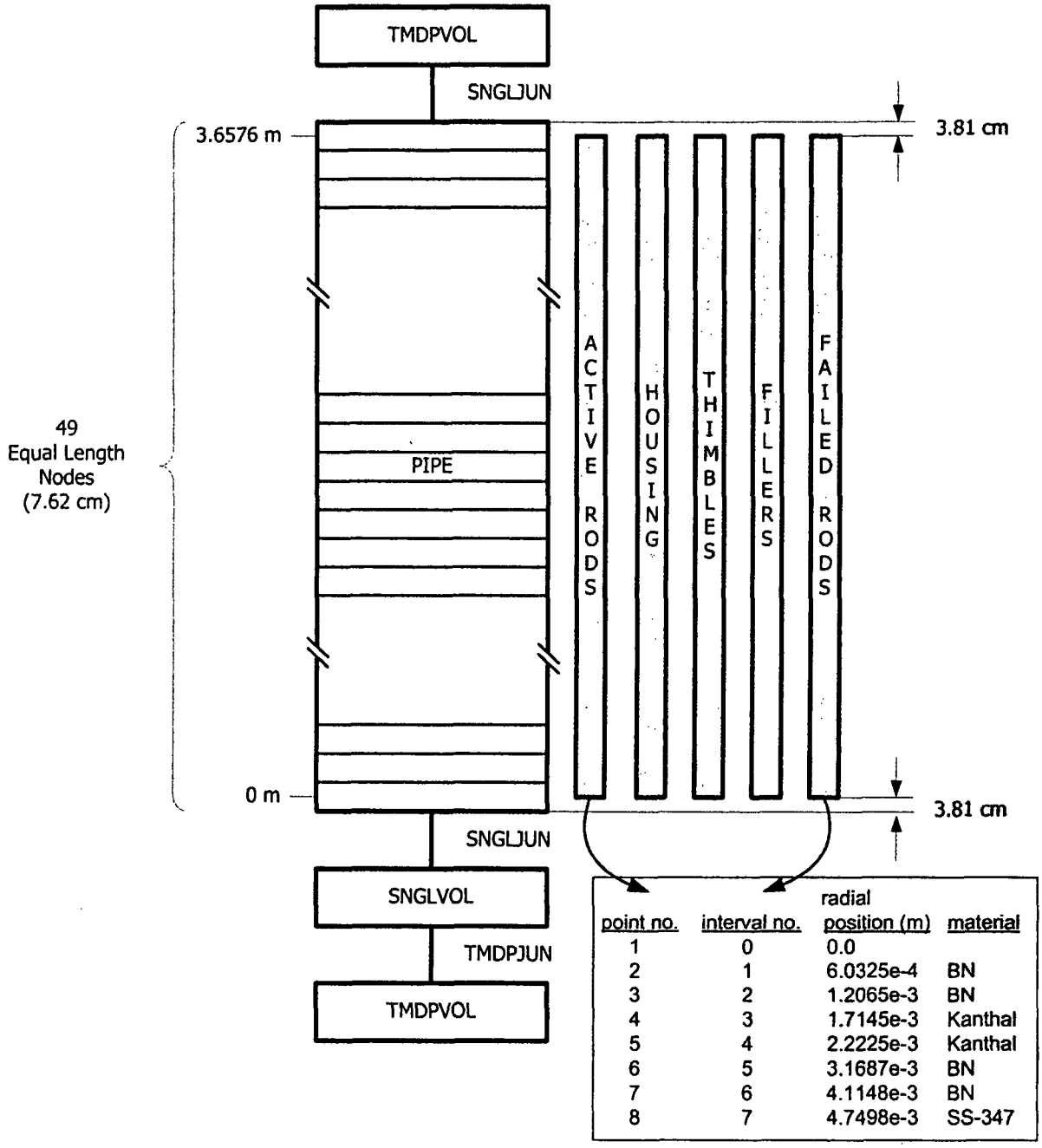

point no.	interval no.	radial position (m)	material
1	0	0.0	
2	1	6.0325e-4	BN
3	2	1.2065e-3	BN
4	3	1.7145e-3	Kanthal
5	4	2.2225e-3	Kanthal
6	5	3.1687e-3	BN
7	6	4.1148e-3	BN
8	7	4.7498e-3	SS-347

Figure 4. FLECHT-SEASET RELAP5 Noding Diagram

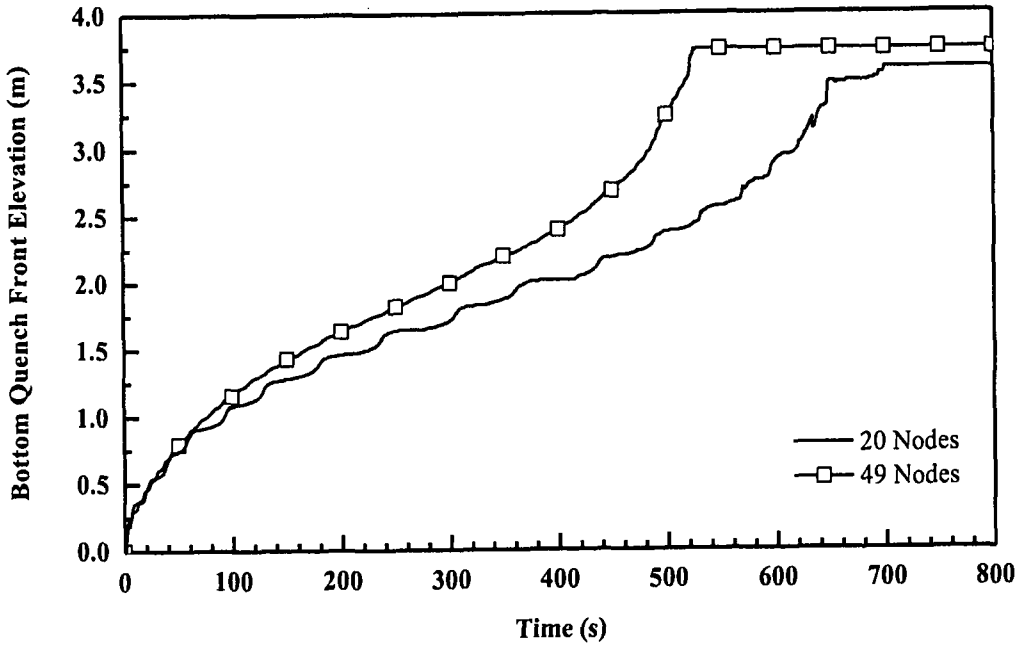

Figure 5. Effect of Axial Noding on Quench Front Elevation

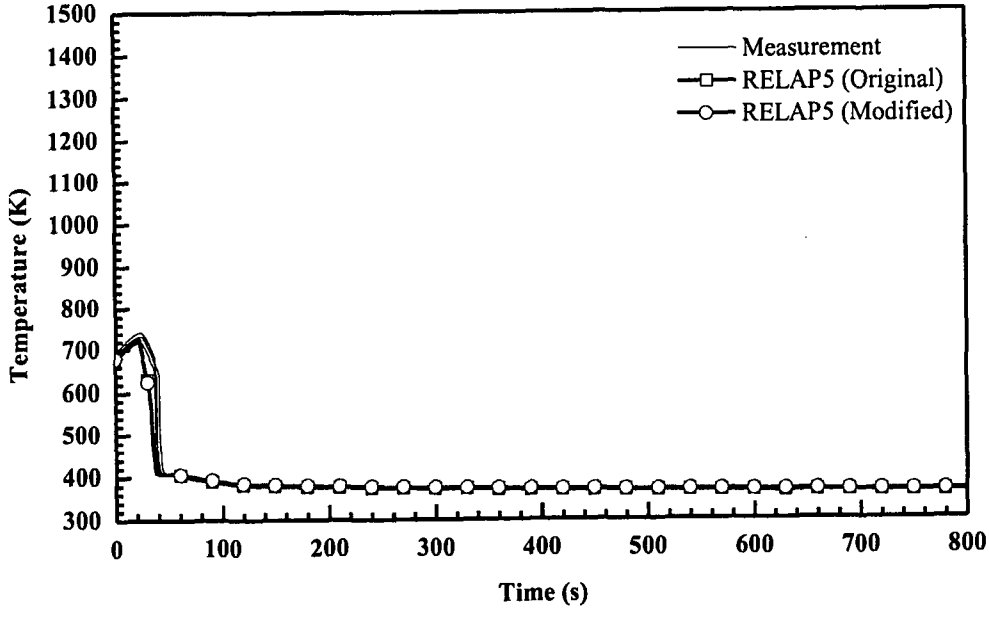

Figure 6. Rod Clad Temperatures at 2 ft from Heated Bottom for Test 31805

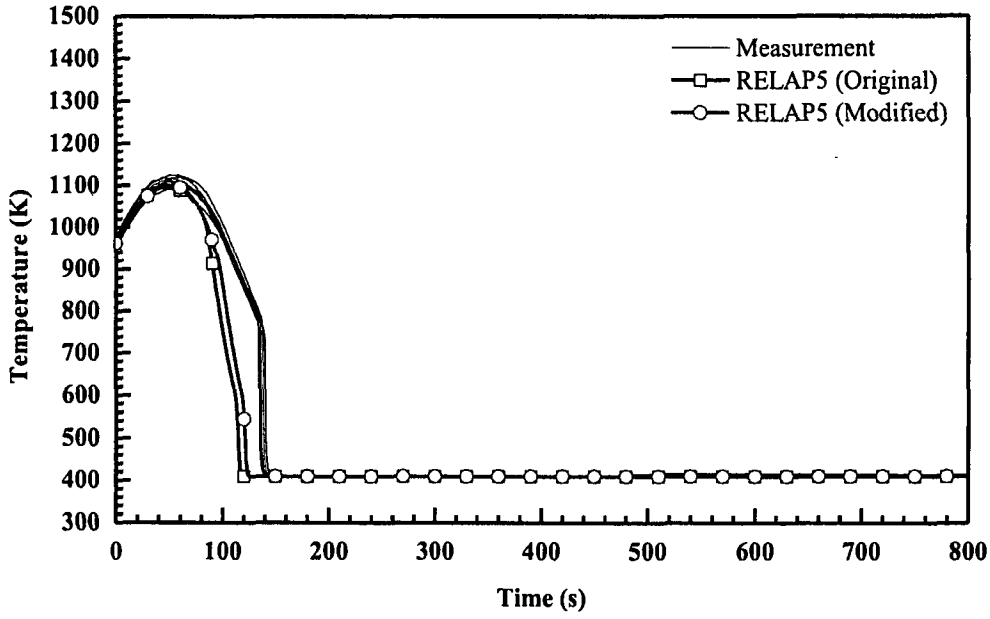

Figure 7. Rod Clad Temperatures at 4 ft from Heated Bottom for Test 31805

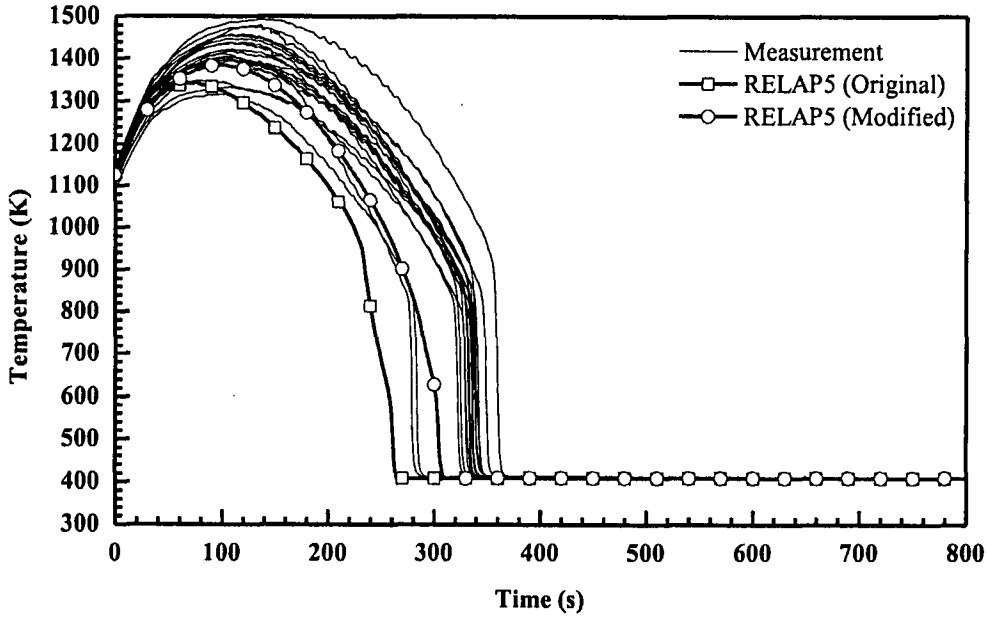

Figure 8. Rod Clad Temperatures at 6 ft from Heated Bottom for Test 31805

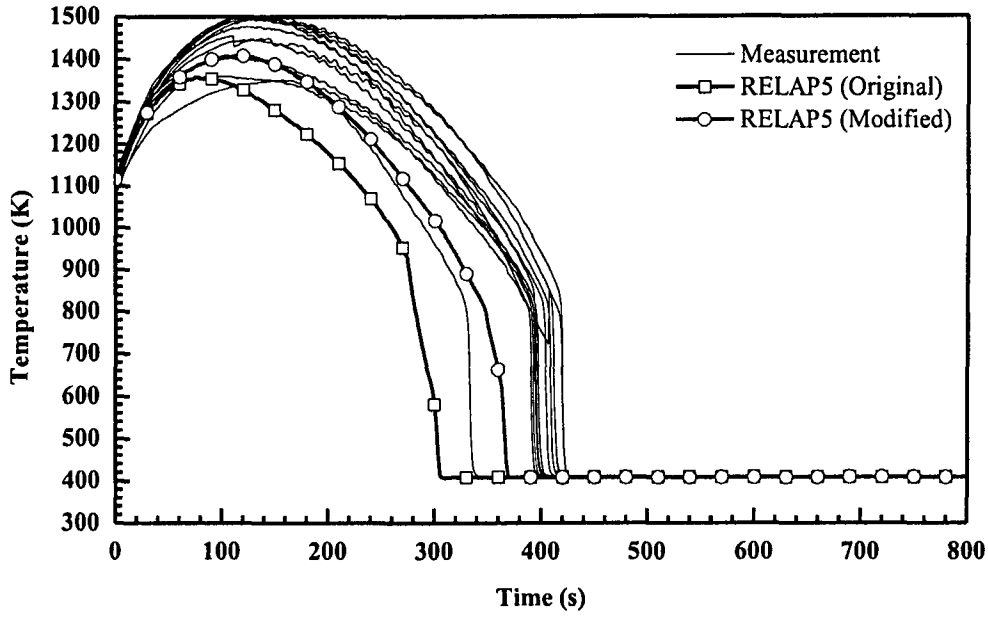

Figure 9. Rod Clad Temperatures at 6.5 ft from Heated Bottom for Test 31805

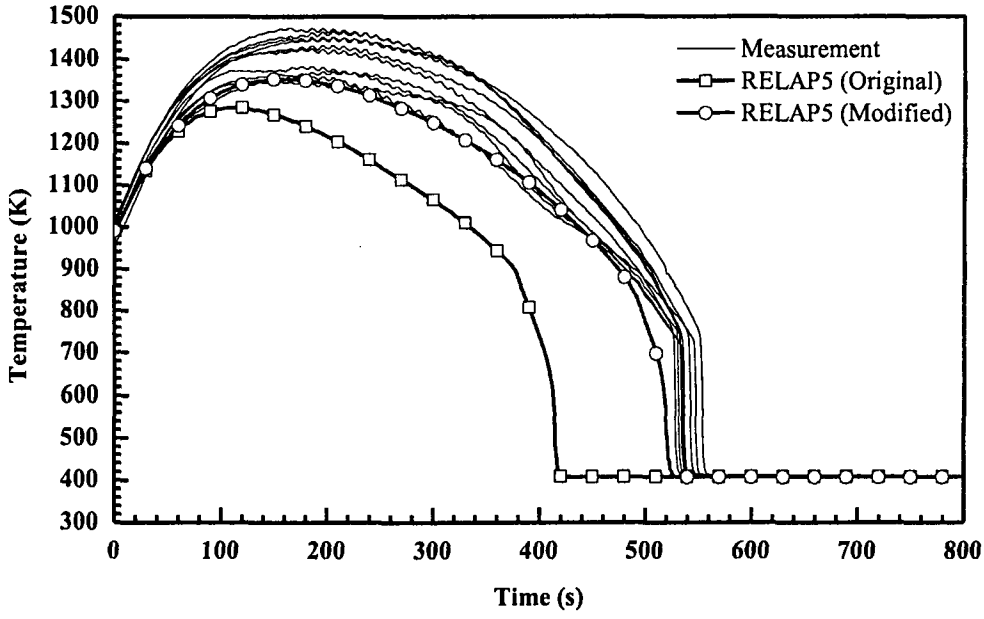

Figure 10. Rod Clad Temperatures at 8 ft from Heated Bottom for Test 31805

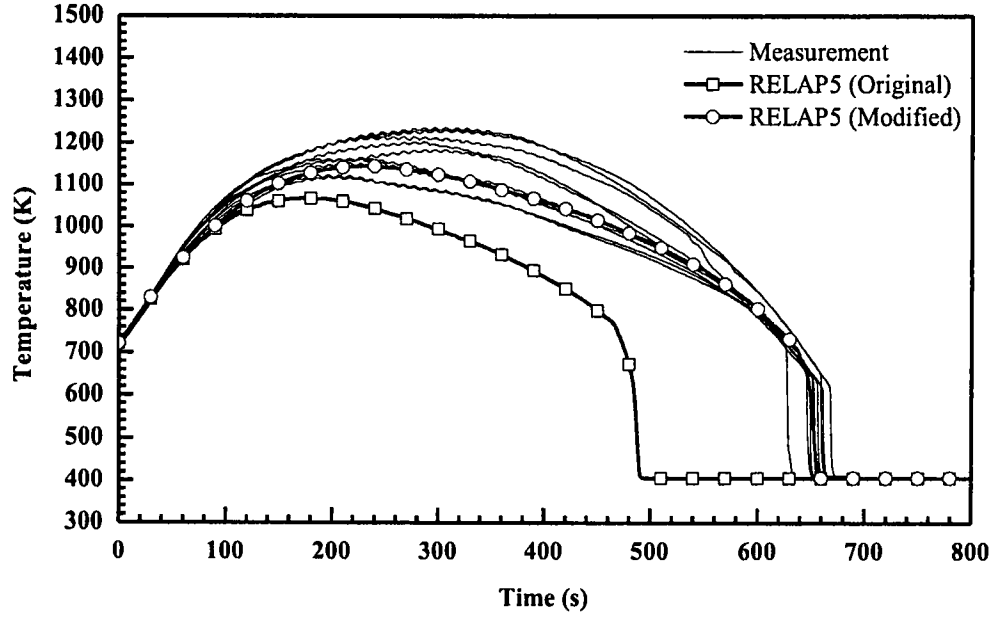

Figure 11. Rod Clad Temperatures at 10 ft from Heated Bottom for Test 31805

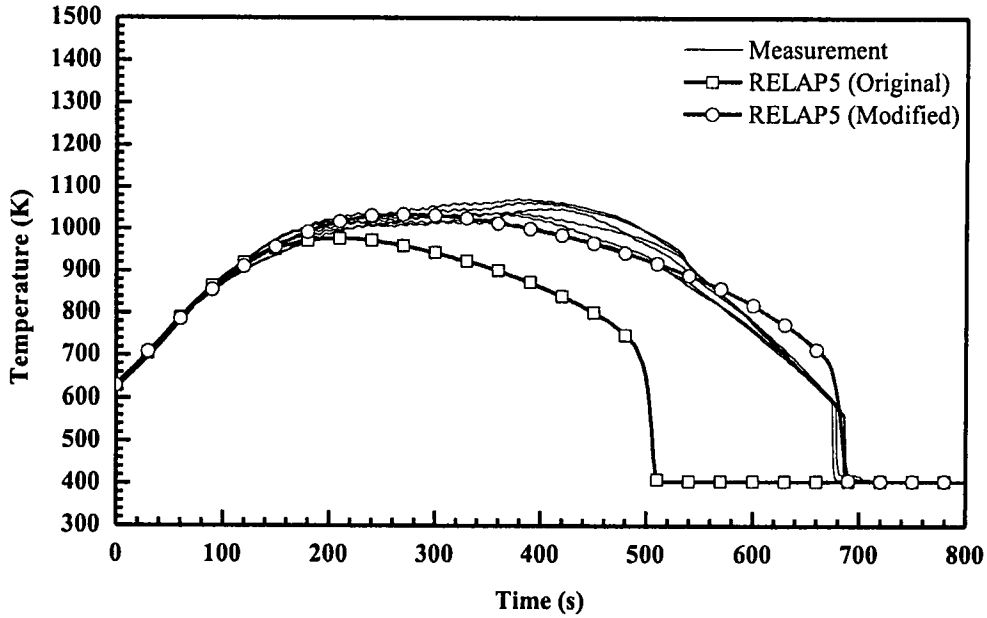

Figure 12. Rod Clad Temperatures at 11 ft from Heated Bottom for Test 31805

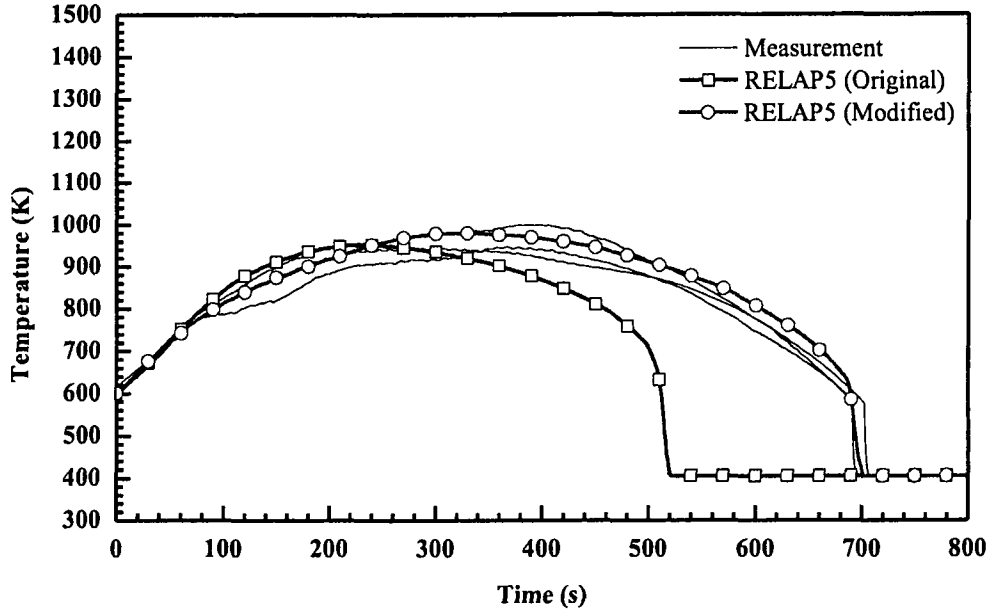

Figure 13. Rod Clad Temperatures at 11.5 ft from Heated Bottom for Test 31805

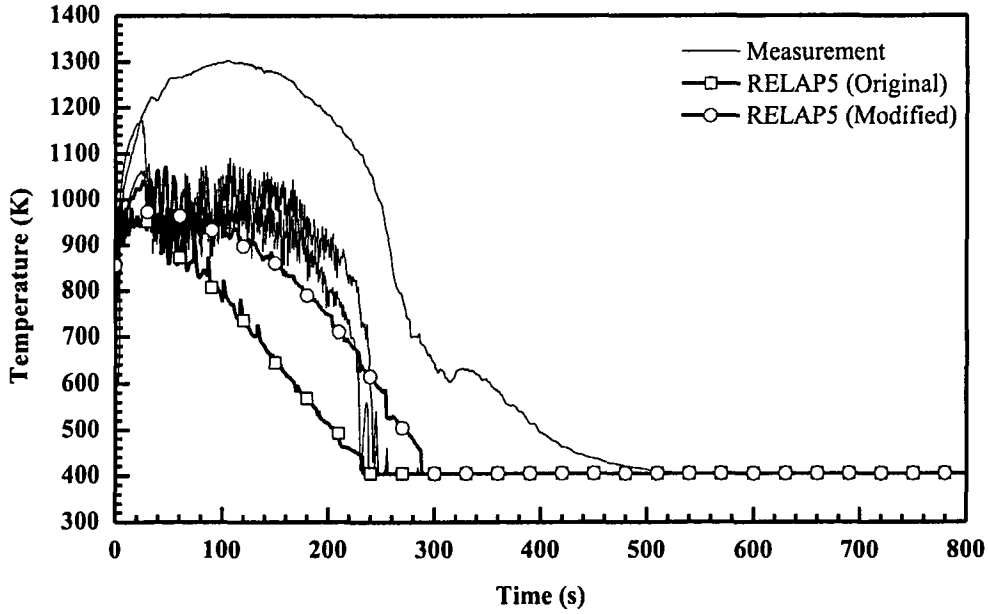

Figure 14. Vapor Temperatures at 6 ft from Heated Bottom for Test 31805

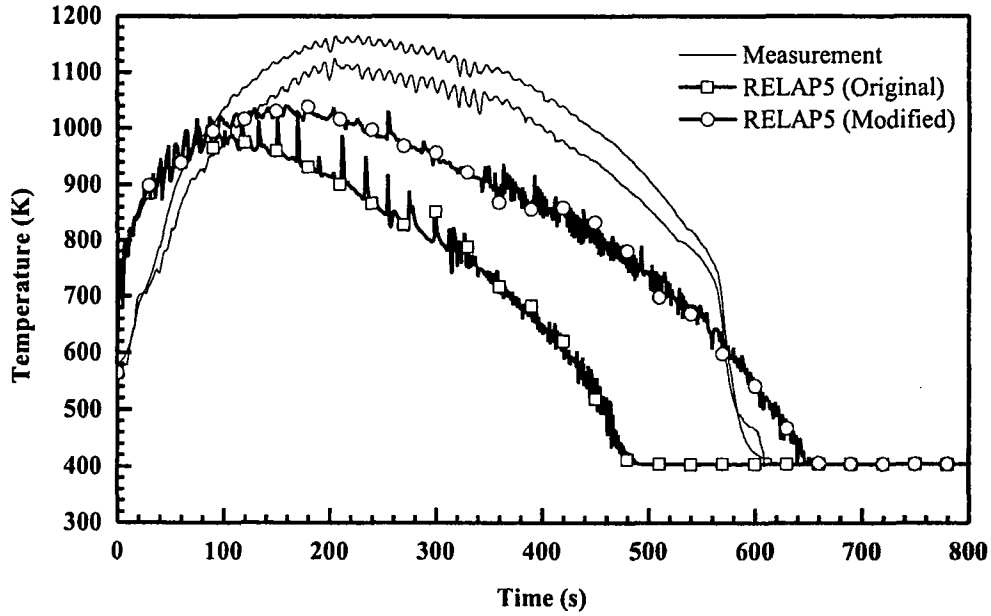

Figure 15. Vapor Temperatures at 10 ft from Heated Bottom for Test 31805

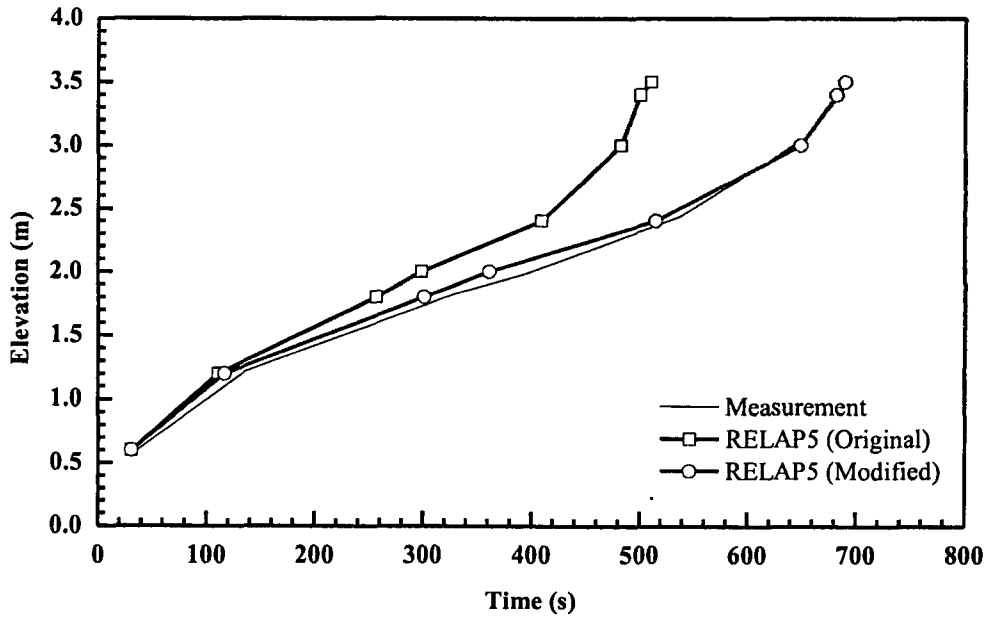

Figure 16. Quench Profile as a Function of Time for Test 31805

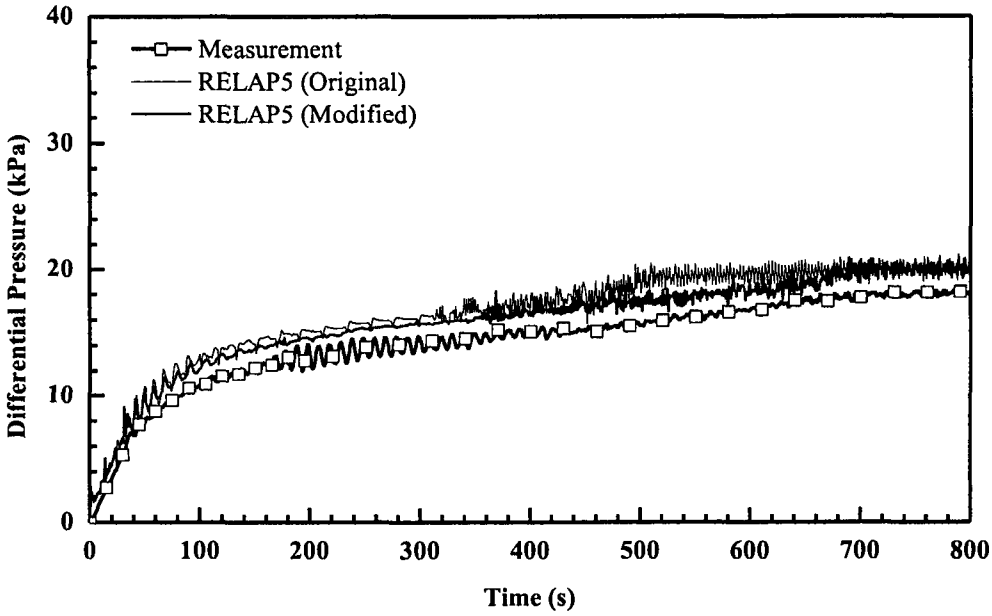

Figure 17. Differential Pressure for the Entire 12 ft Core for Test 31805

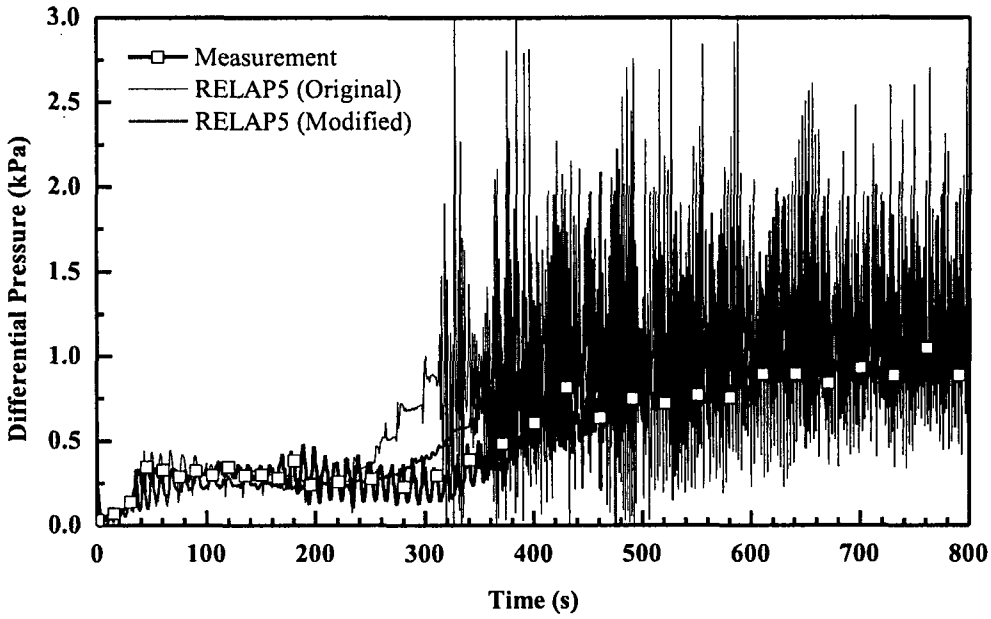

Figure 18. Differential Pressure at 6~7 ft Elevation for Test 31805

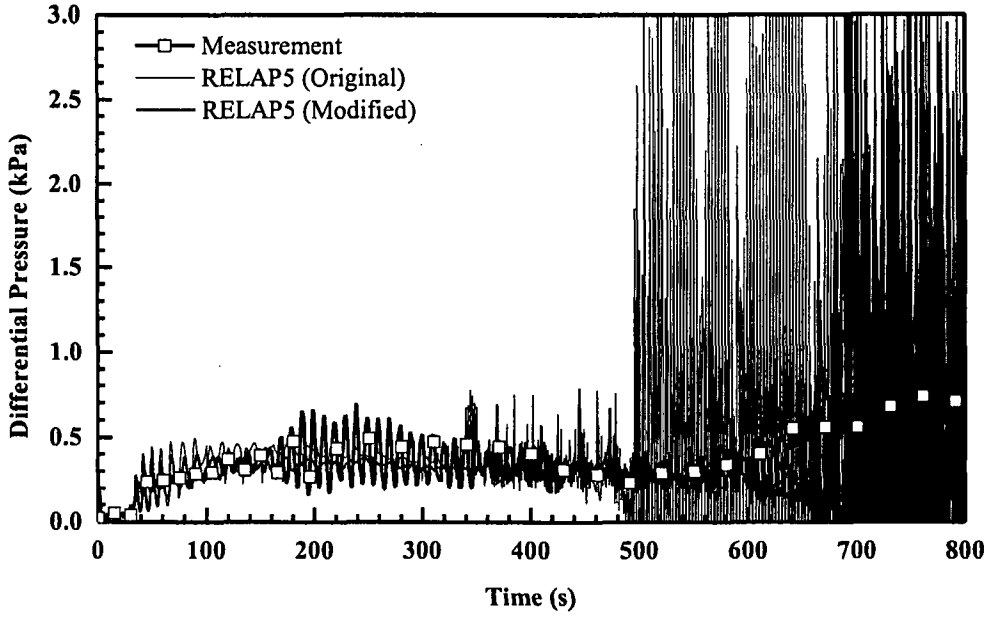

Figure 19. Differential Pressure at 10~11 ft Elevation for Test 31805

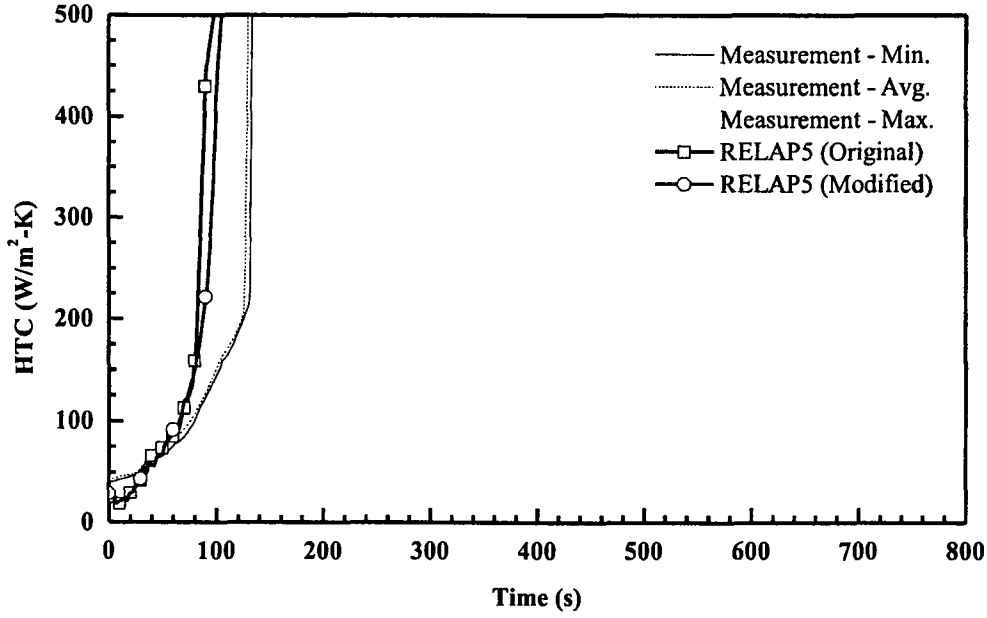

Figure 20. Heat Transfer Coefficient at 4 ft from Heated Bottom for Test 31805

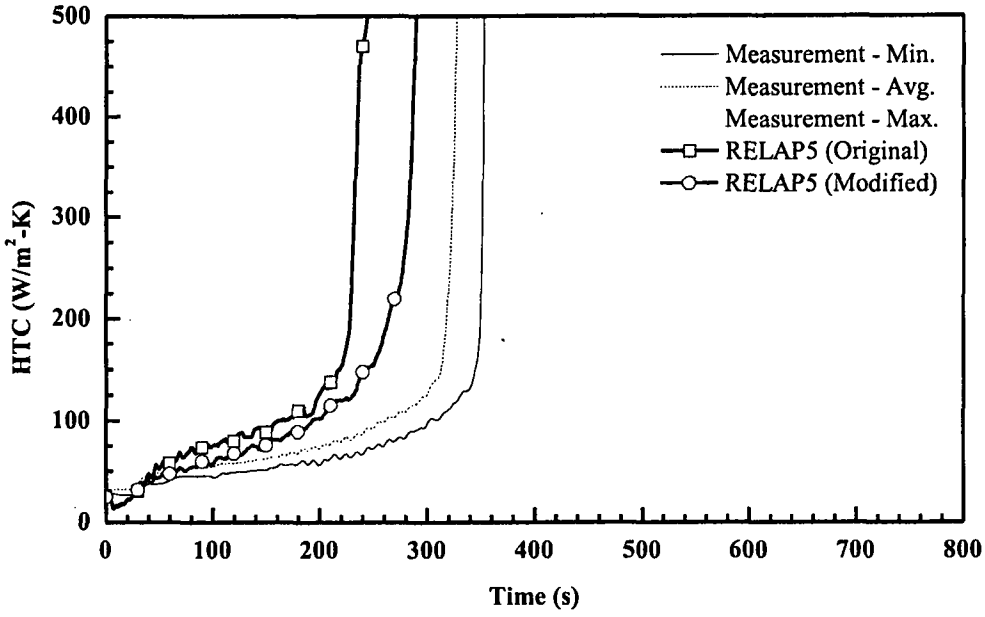

Figure 21. Heat Transfer Coefficient at 6 ft from Heated Bottom for Test 31805

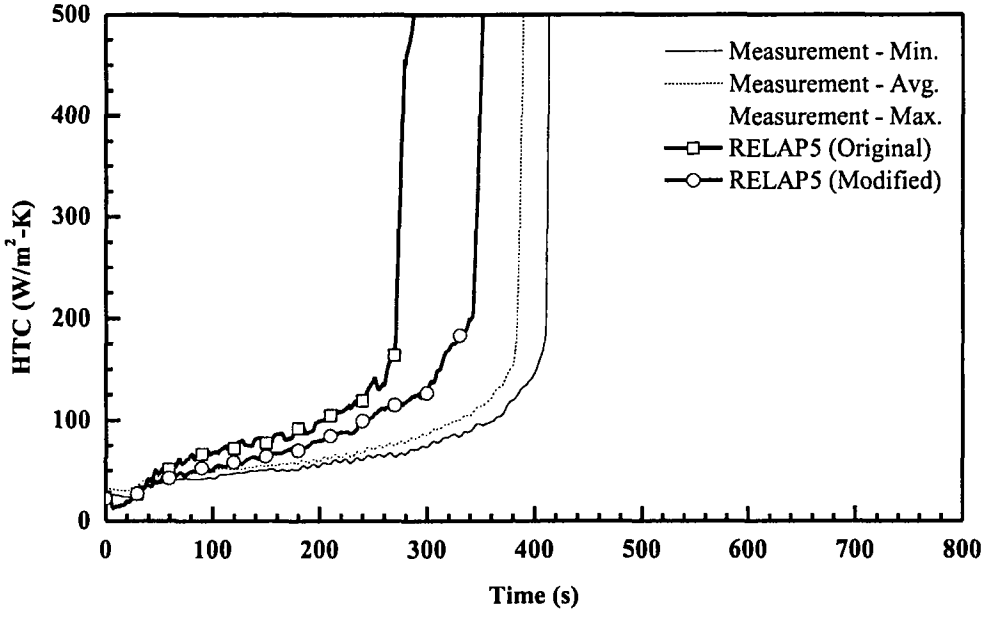

Figure 22. Heat Transfer Coefficient at 6.5 ft from Heated Bottom for Test 31805

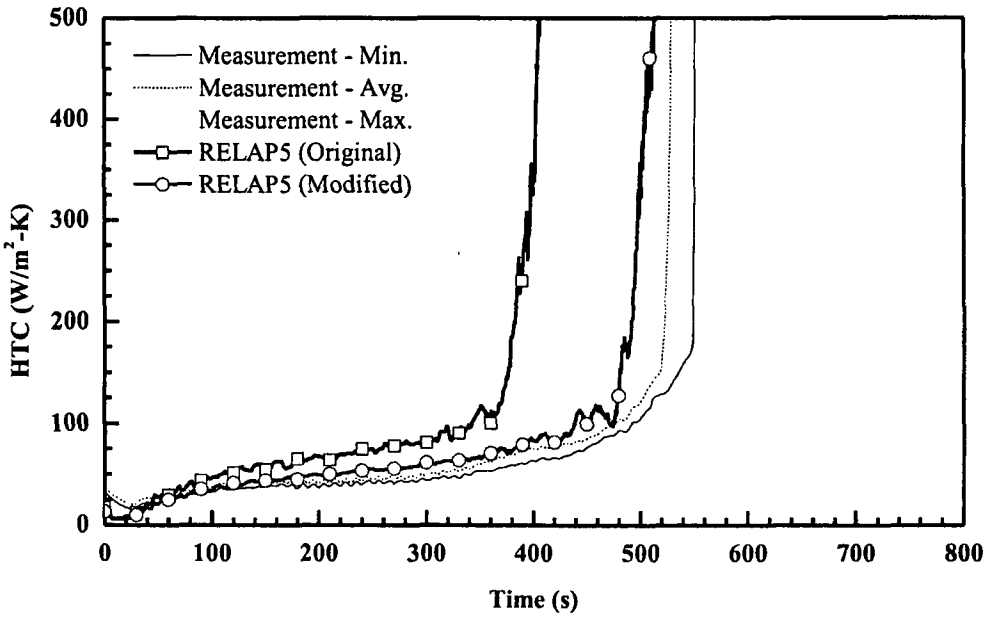

Figure 23. Heat Transfer Coefficient at 8 ft from Heated Bottom for Test 31805

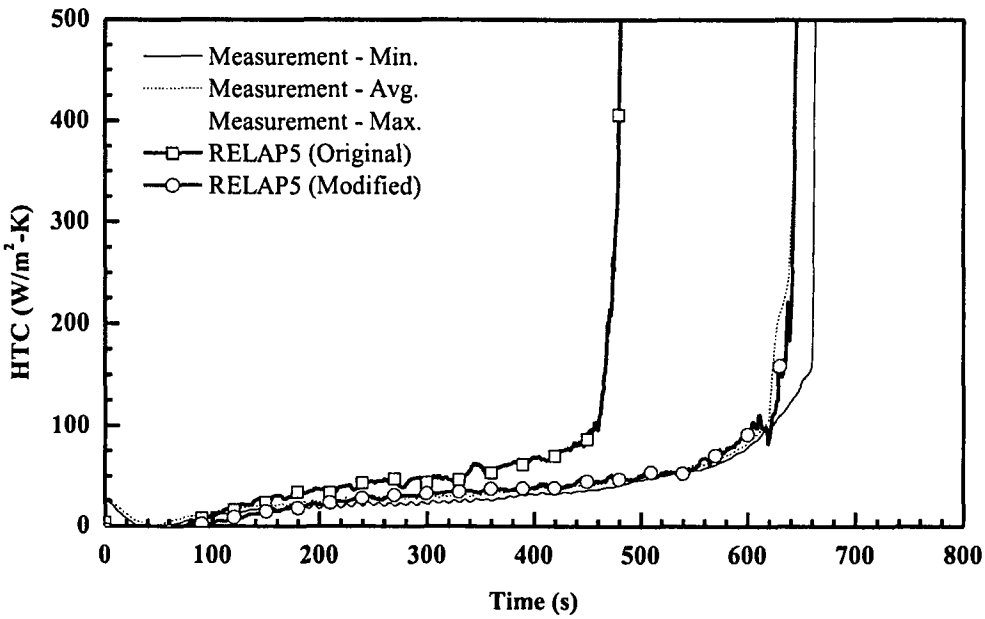

Figure 24. Heat Transfer Coefficient at 10 ft from Heated Bottom for Test 31805

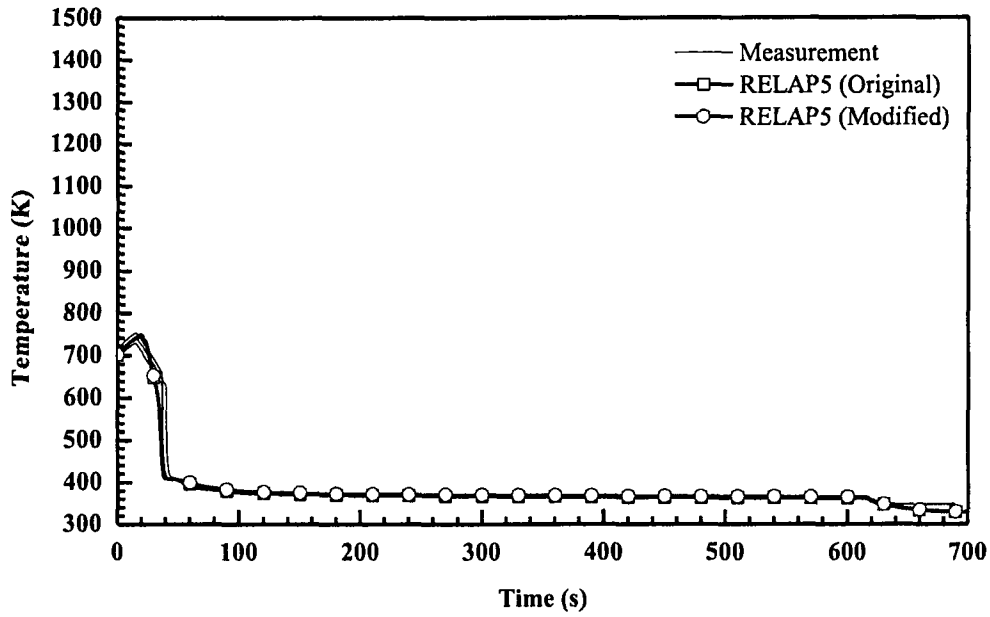

Figure 25. Rod Clad Temperatures at 2 ft from Heated Bottom for Test 31504

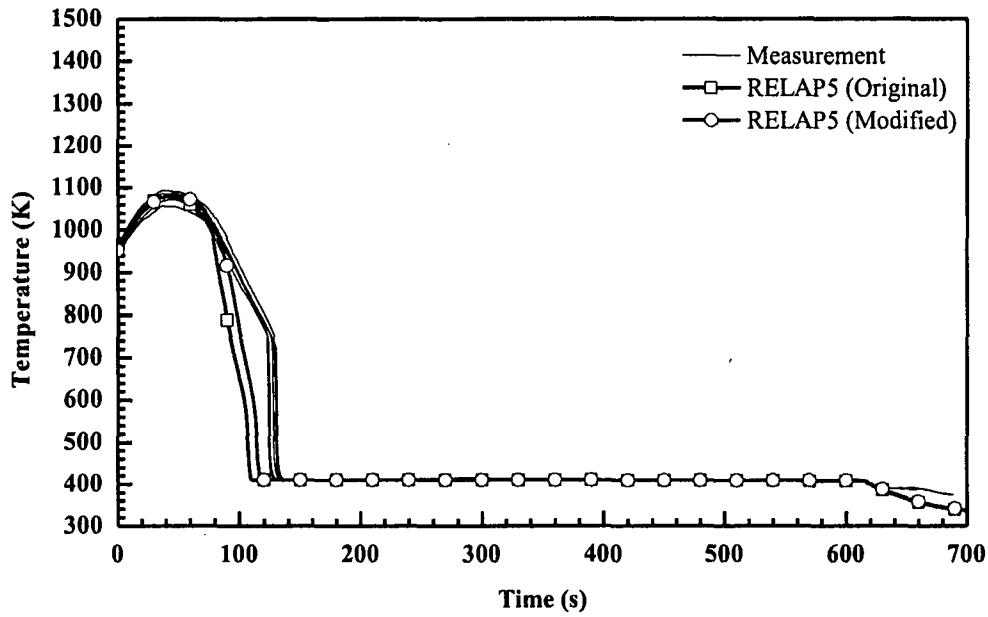

Figure 26. Rod Clad Temperatures at 4 ft from Heated Bottom for Test 31504

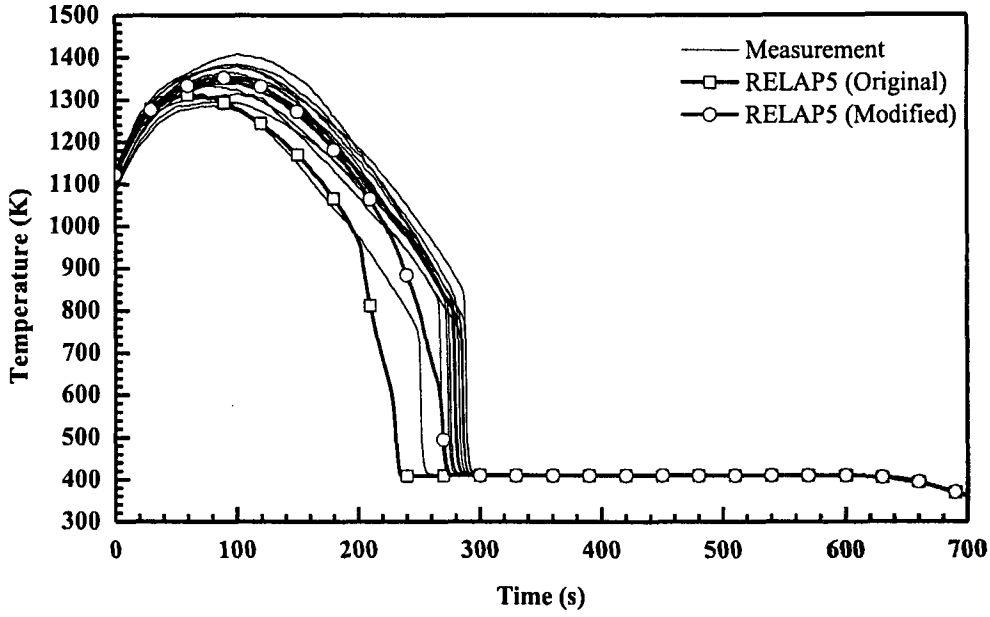

Figure 27. Rod Clad Temperatures at 6 ft from Heated Bottom for Test 31504

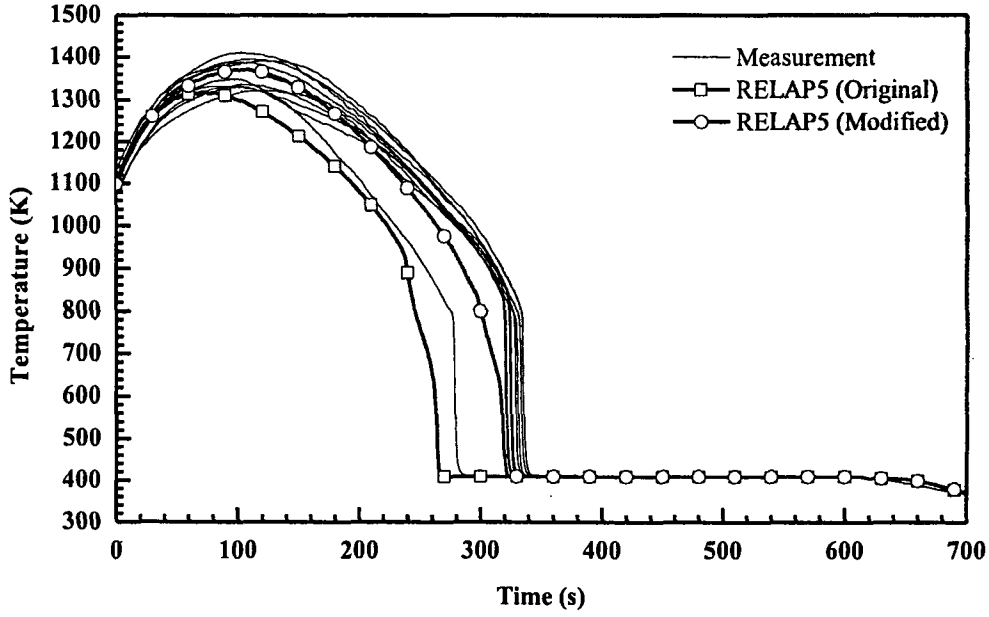

Figure 28. Rod Clad Temperatures at 6.5 ft from Heated Bottom for Test 31504

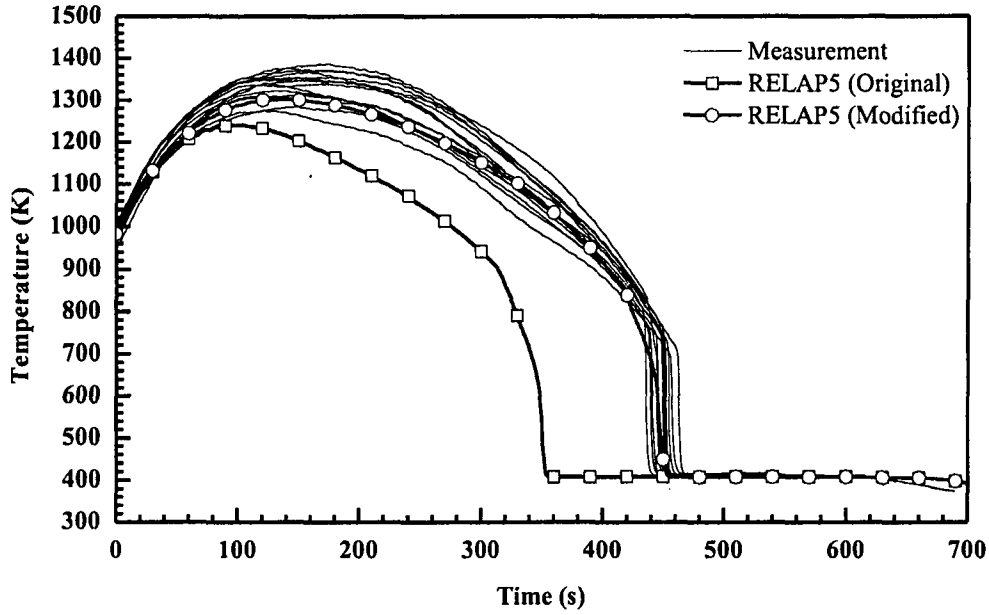

Figure 29. Rod Clad Temperatures at 8 ft from Heated Bottom for Test 31504

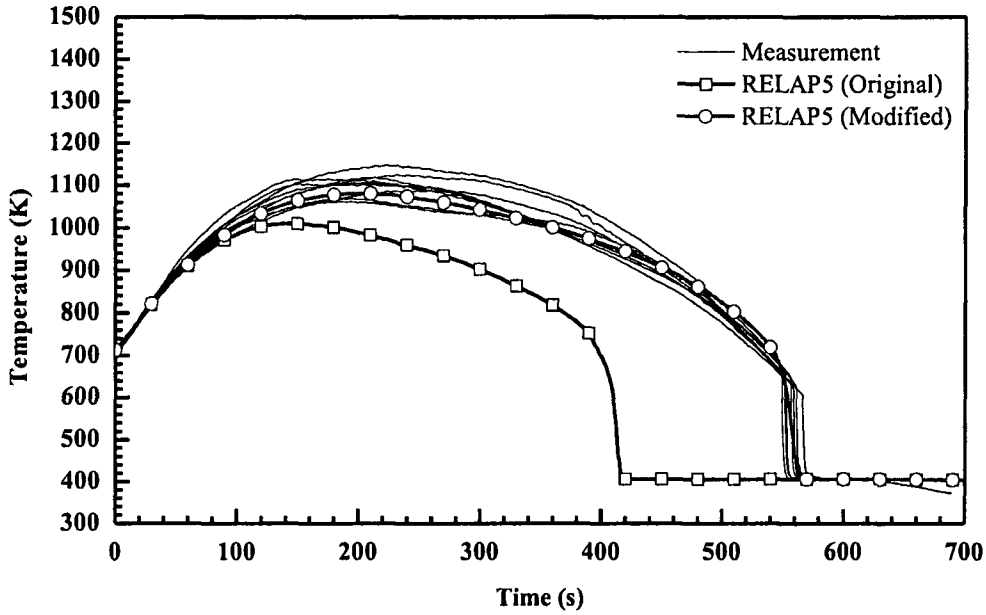

Figure 30. Rod Clad Temperatures at 10 ft from Heated Bottom for Test 31504

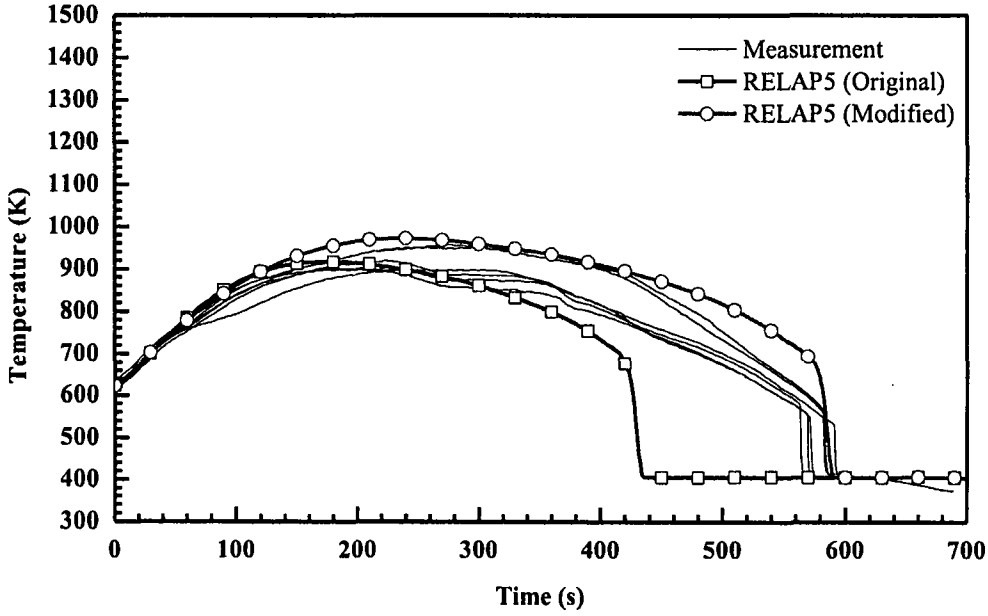

Figure 31. Rod Clad Temperatures at 11 ft from Heated Bottom for Test 31504

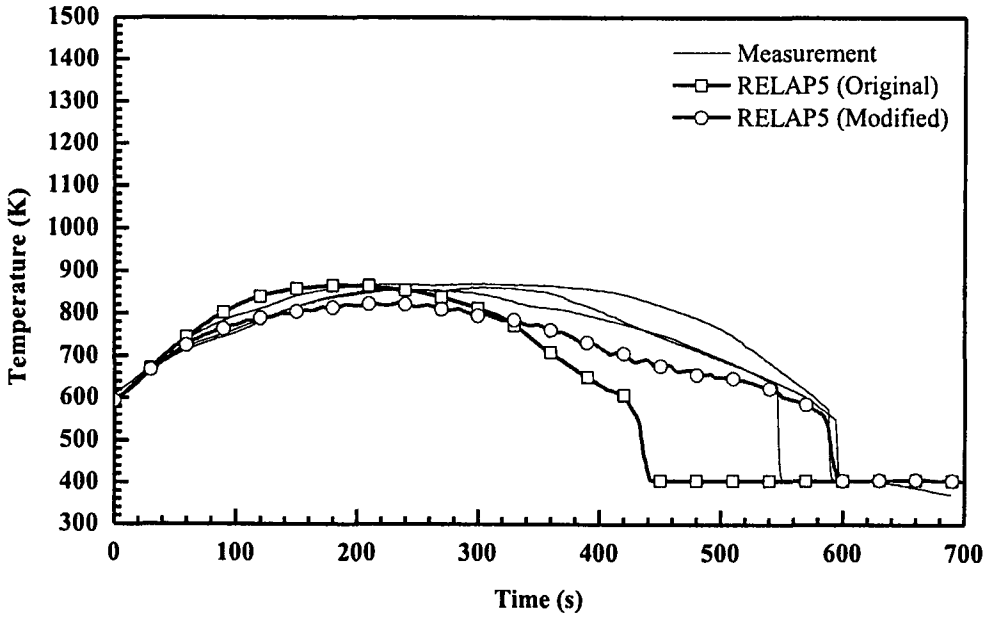

Figure 32. Rod Clad Temperatures at 11.5 ft from Heated Bottom for Test 31504

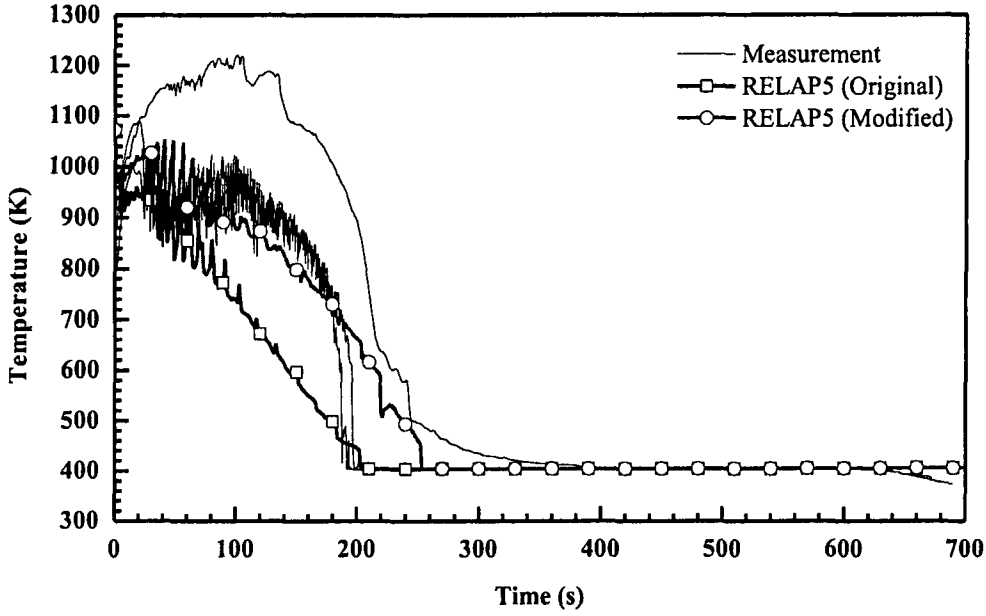

Figure 33. Vapor Temperatures at 6 ft from Heated Bottom for Test 31504

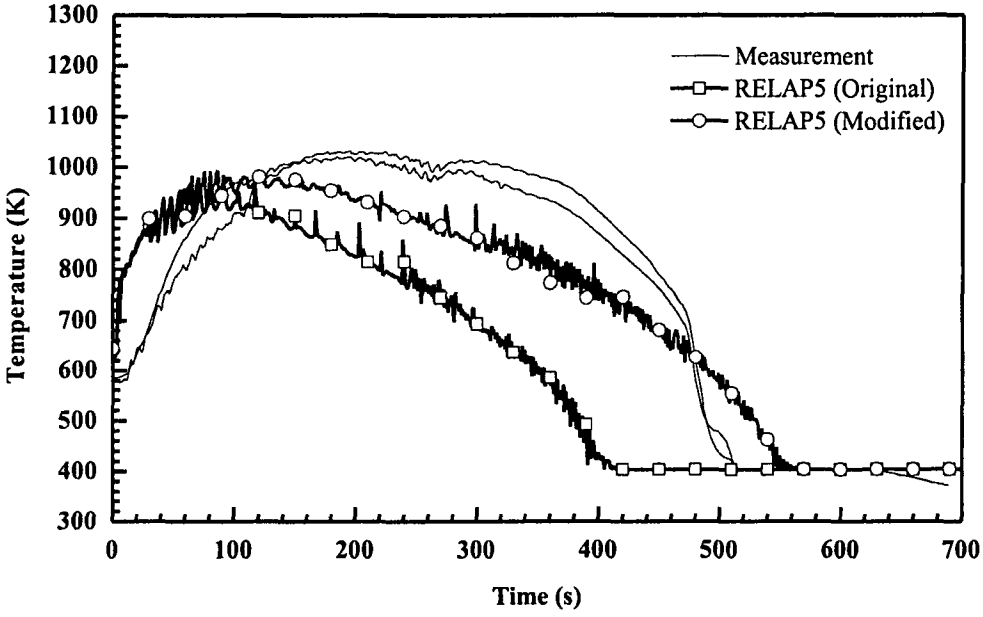

Figure 34. Vapor Temperatures at 10 ft from Heated Bottom for Test 31504

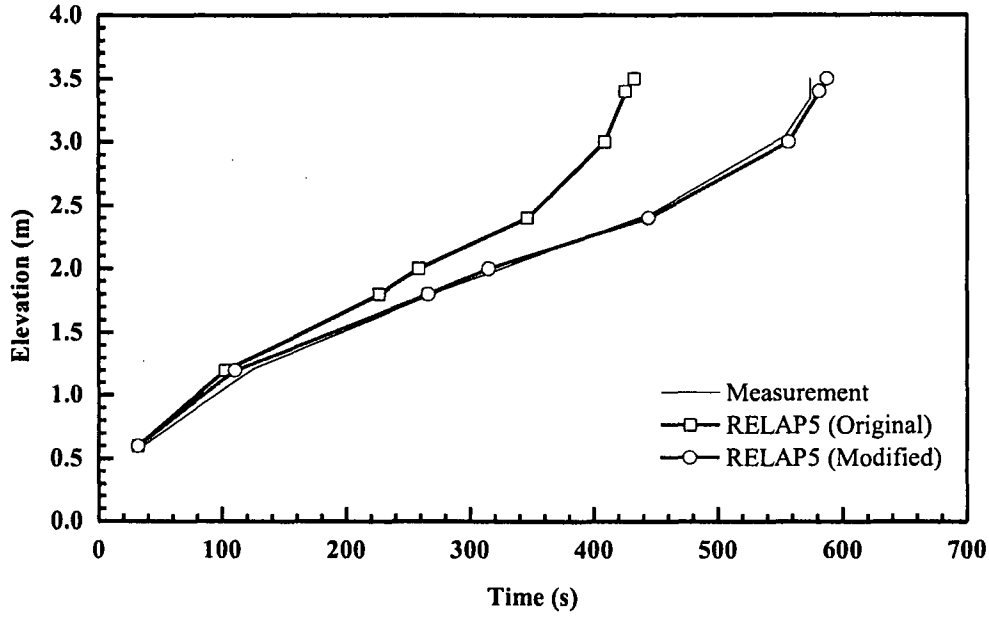

Figure 35. Quench Profile as a Function of Time for Test 31504

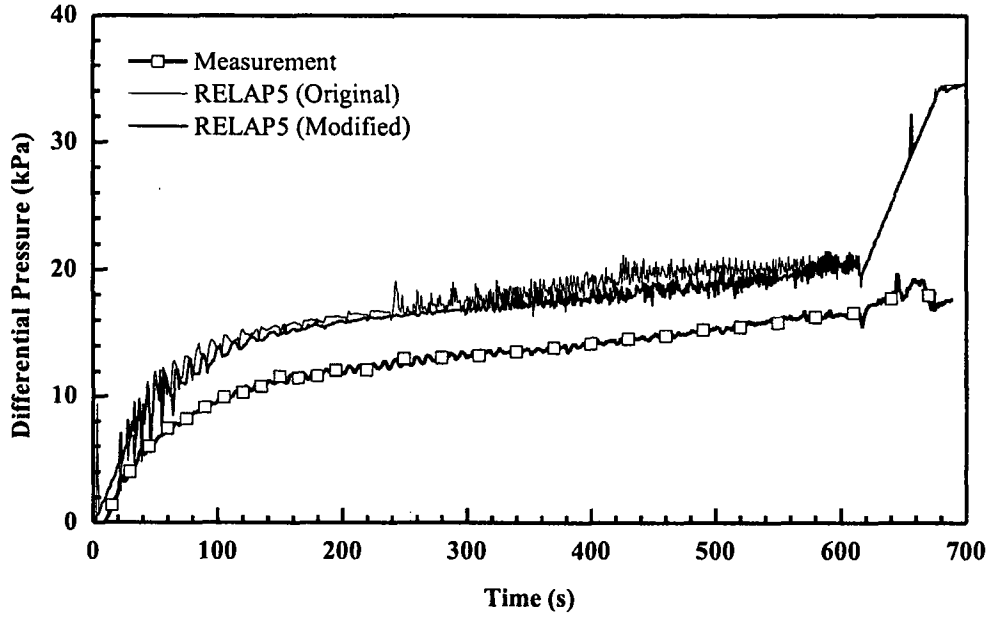

Figure 36. Differential Pressure for the Entire 12 ft Core for Test 31504

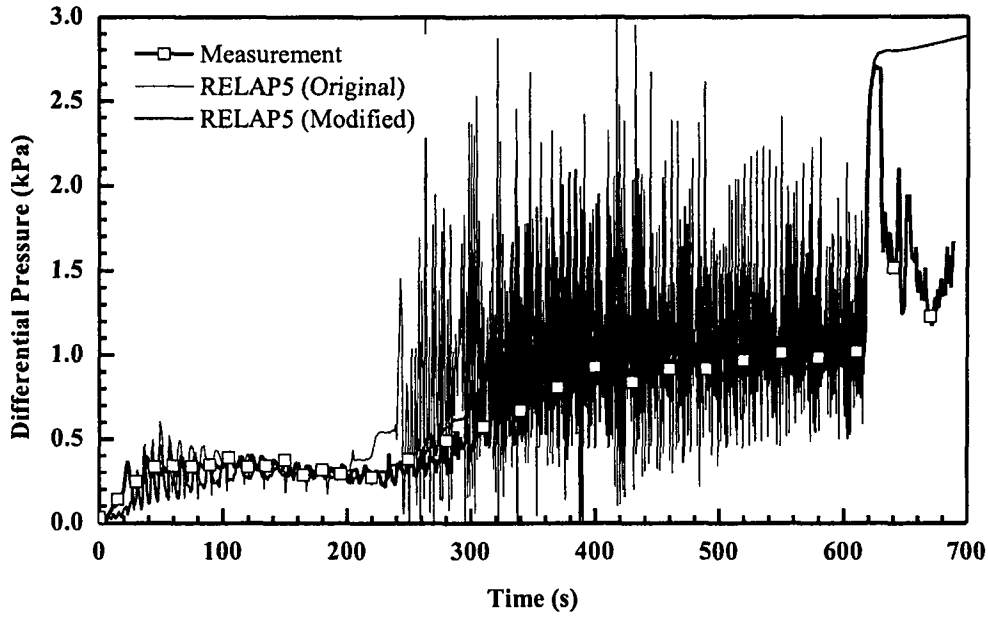

Figure 37. Differential Pressure at 6~7 ft Elevation for Test 31504

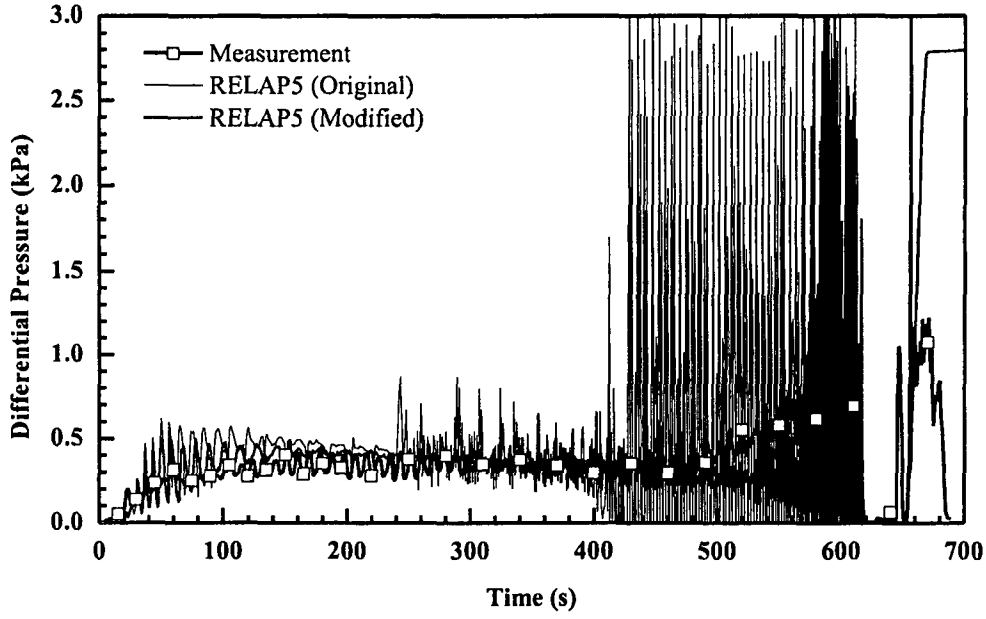

Figure 38. Differential Pressure at 10~11 ft Elevation for Test 31504

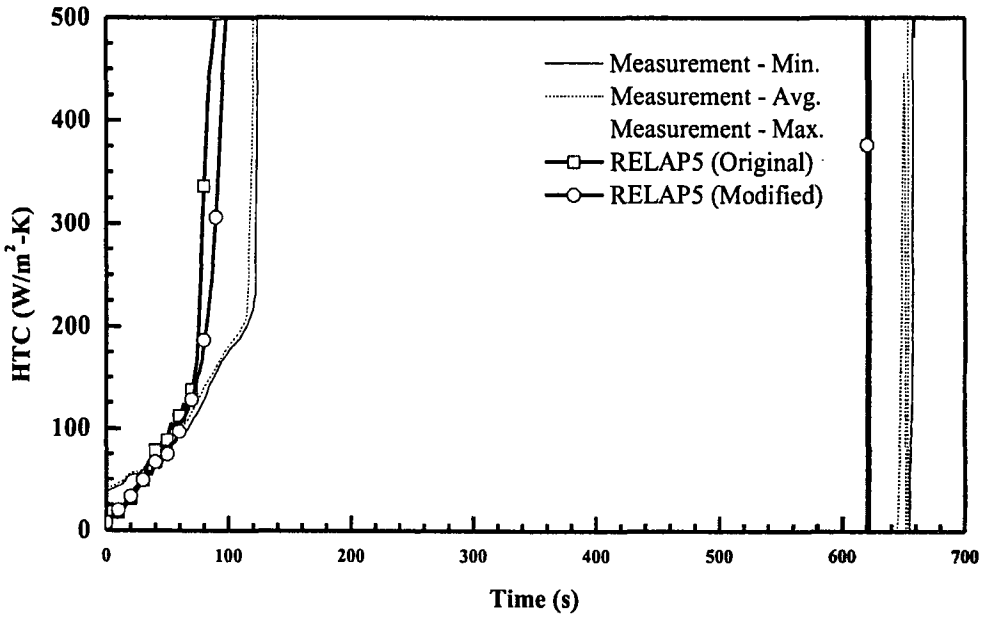

Figure 39. Heat Transfer Coefficient at 4 ft from Heated Bottom for Test 31504

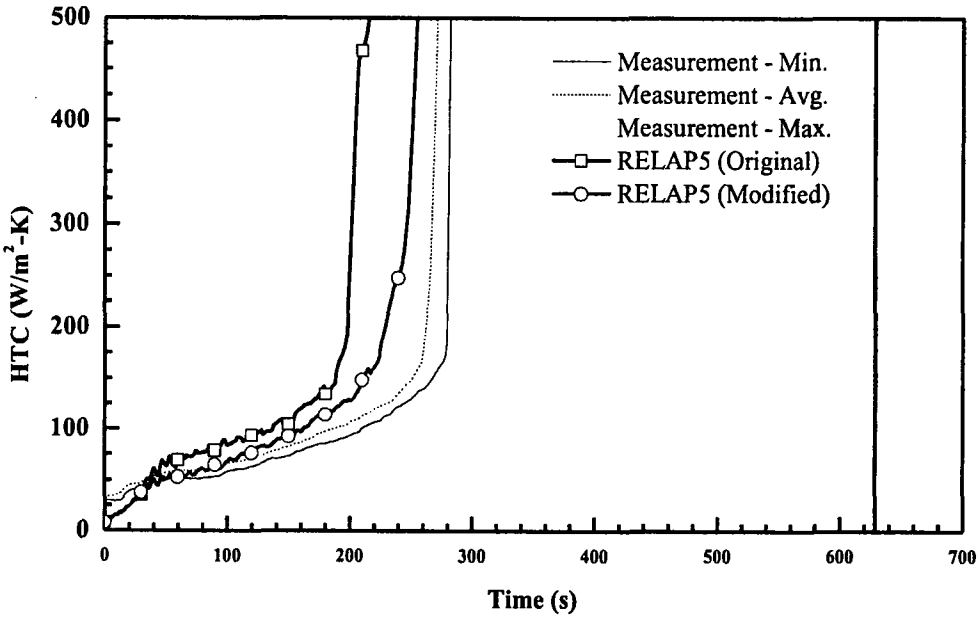

Figure 40. Heat Transfer Coefficient at 6 ft from Heated Bottom for Test 31504

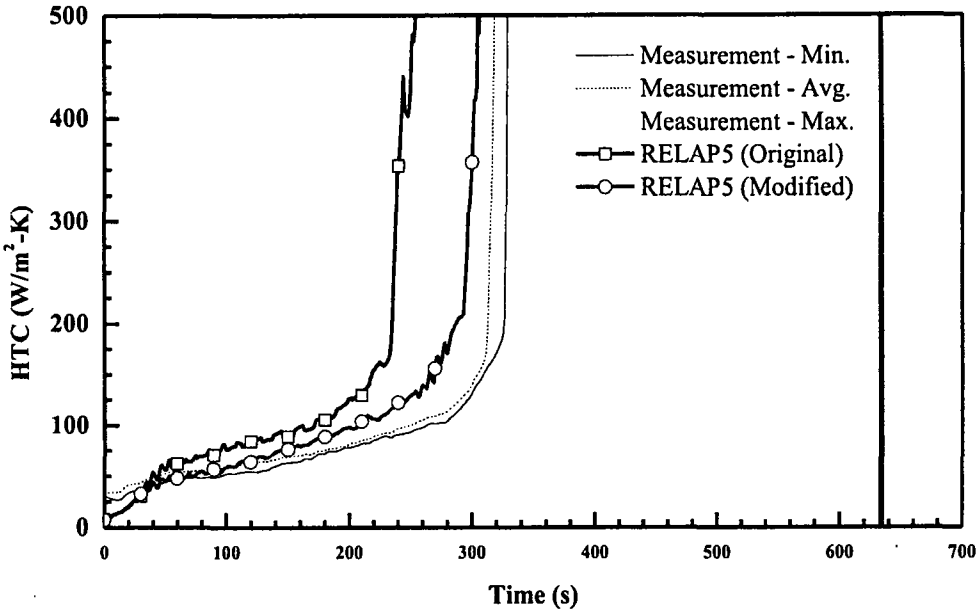

Figure 41. Heat Transfer Coefficient at 6.5 ft from Heated Bottom for Test 31504

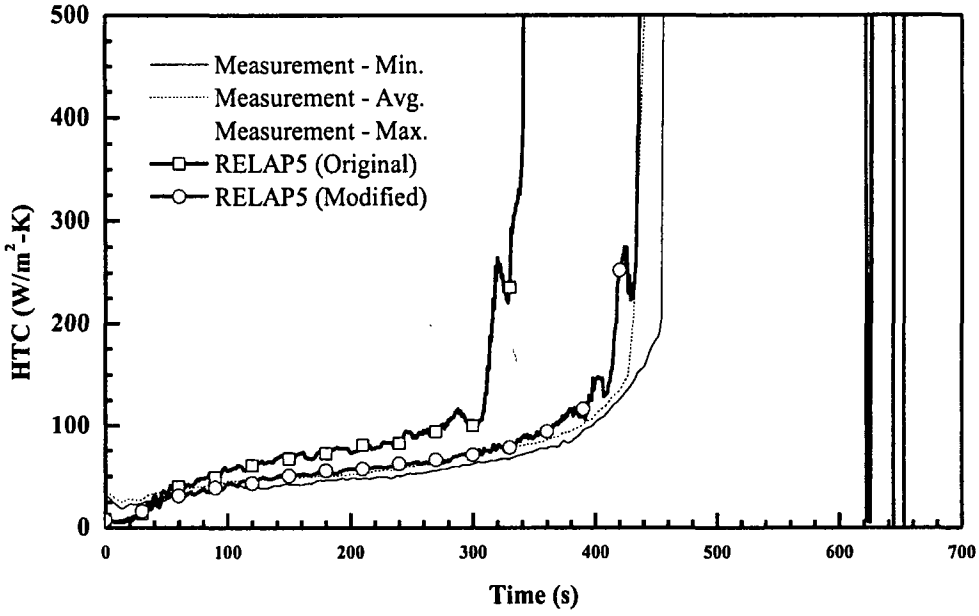

Figure 42. Heat Transfer Coefficient at 8 ft from Heated Bottom for Test 31504

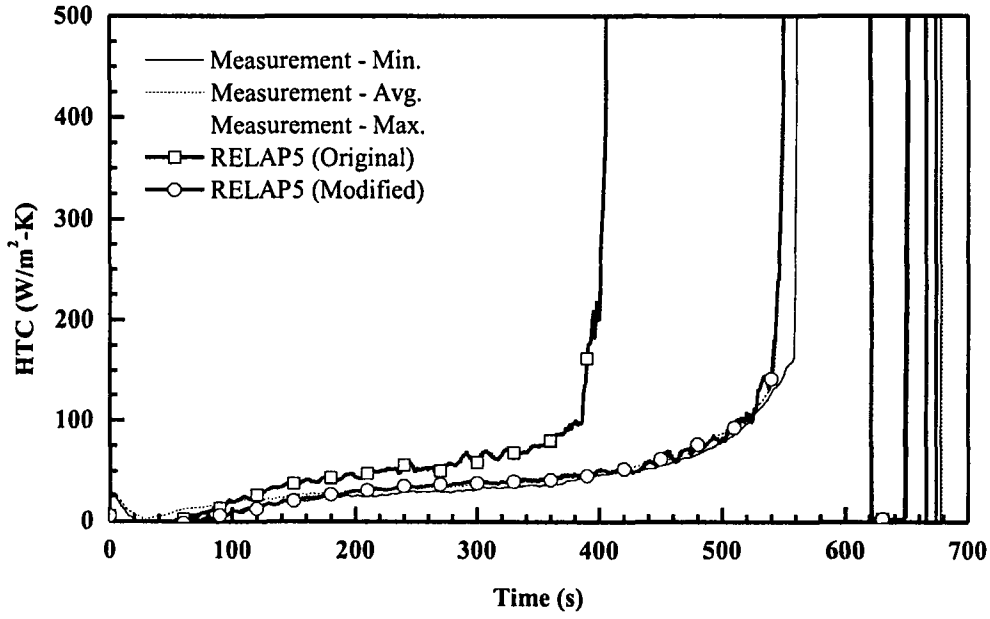

Figure 43. Heat Transfer Coefficient at 10 ft from Heated Bottom for Test 31504

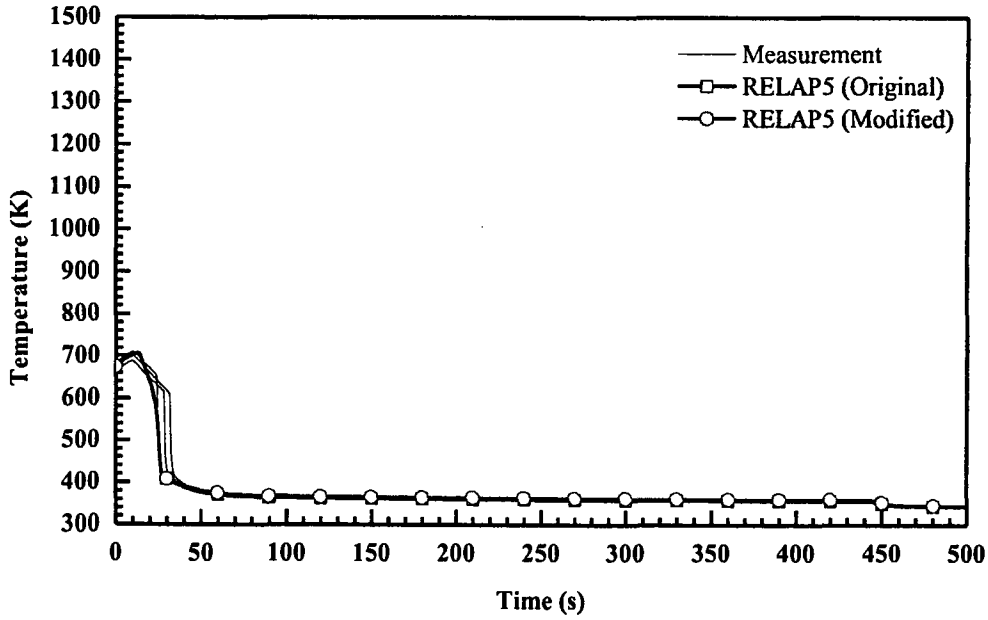

Figure 44. Rod Clad Temperatures at 2 ft from Heated Bottom for Test 31203

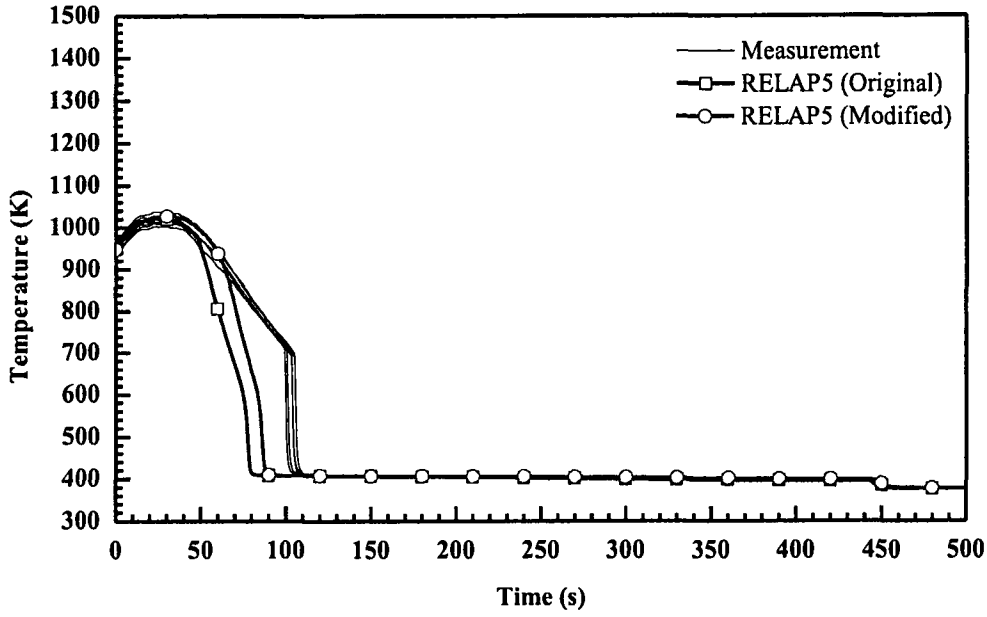

Figure 45. Rod Clad Temperatures at 4 ft from Heated Bottom for Test 31203

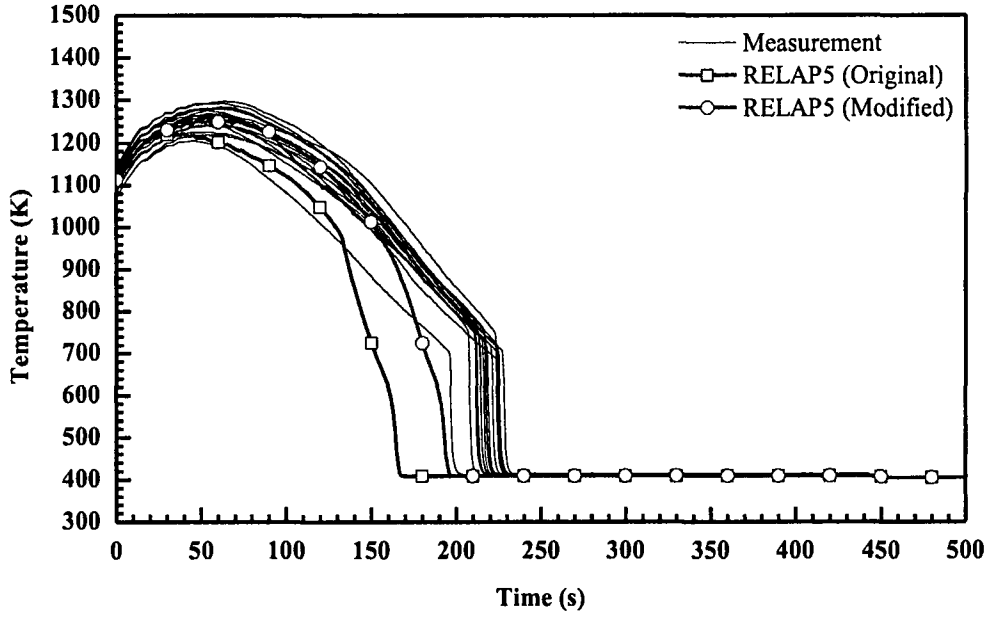

Figure 46. Rod Clad Temperatures at 6 ft from Heated Bottom for Test 31203

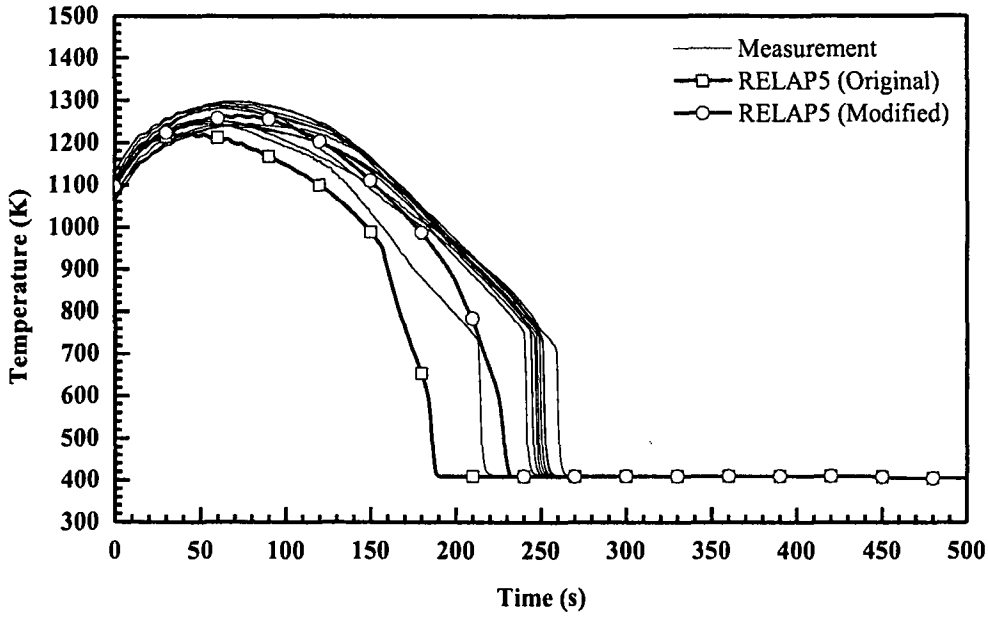

Figure 47. Rod Clad Temperatures at 6.5 ft from Heated Bottom for Test 31203

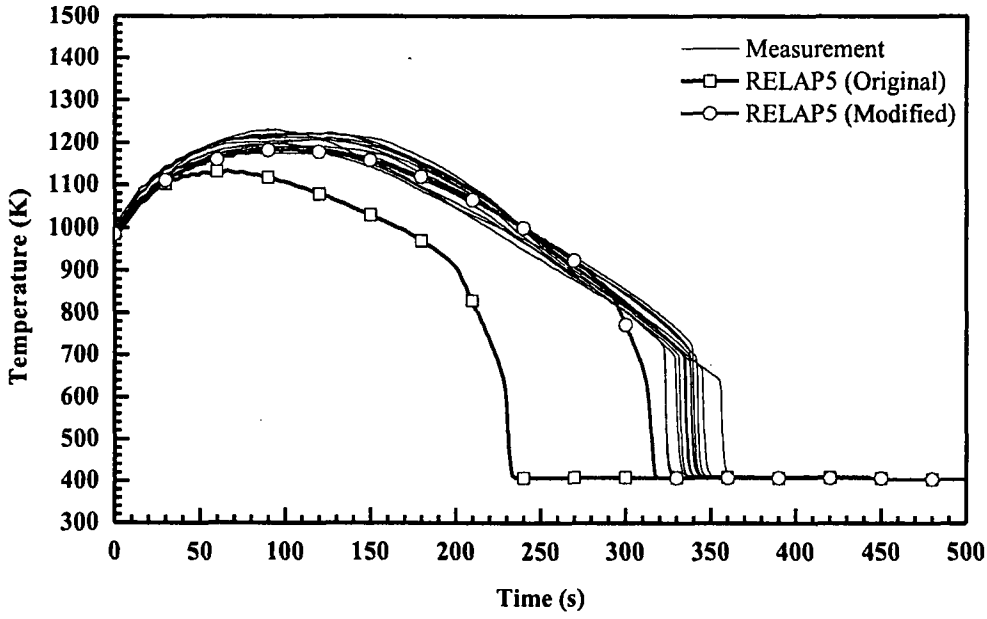

Figure 48. Rod Clad Temperatures at 8 ft from Heated Bottom for Test 31203

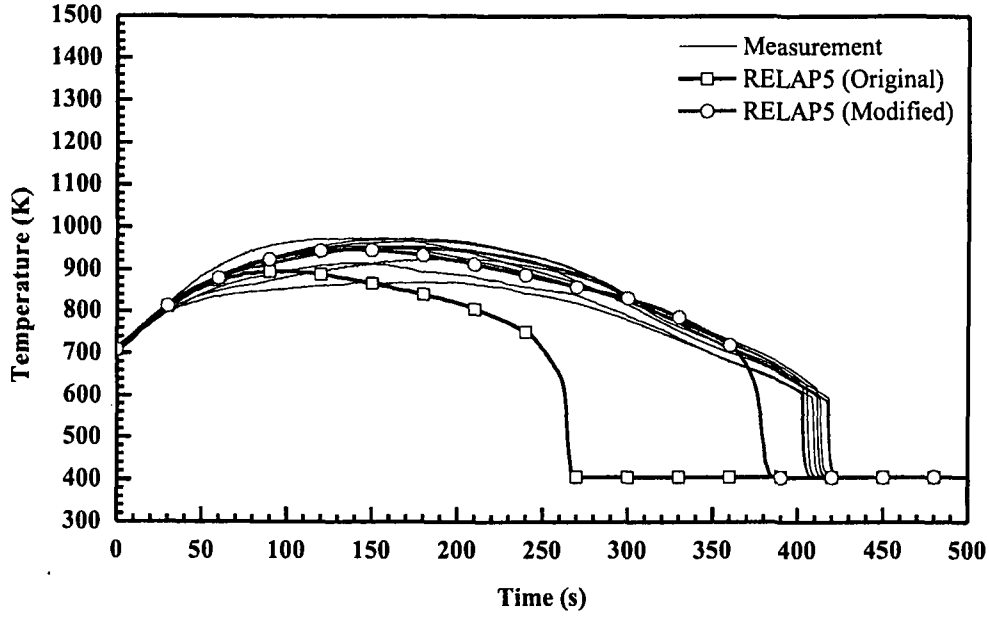

Figure 49. Rod Clad Temperatures at 10 ft from Heated Bottom for Test 31203

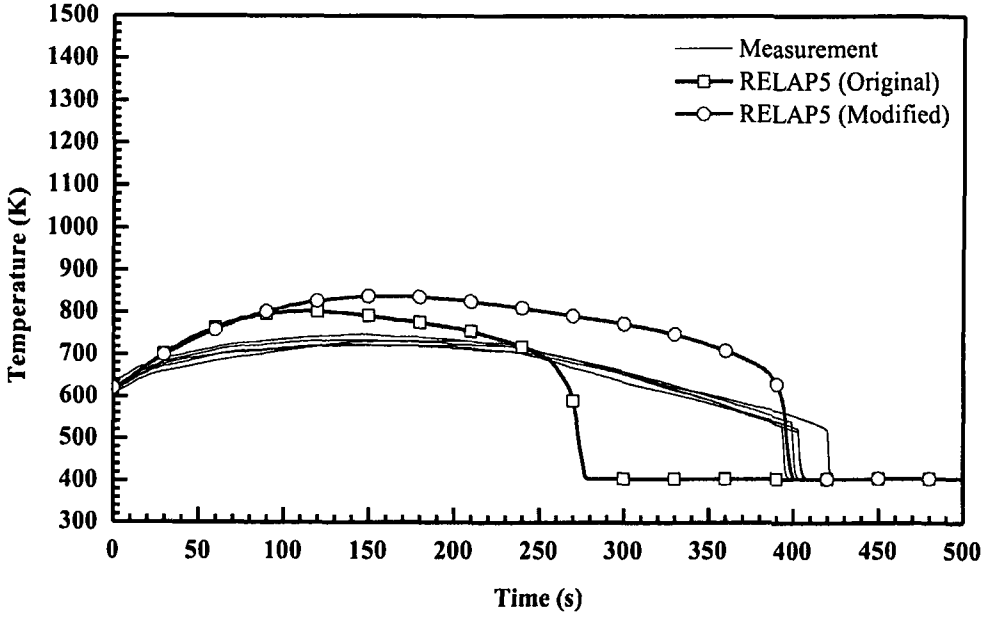

Figure 50. Rod Clad Temperatures at 11 ft from Heated Bottom for Test 31203

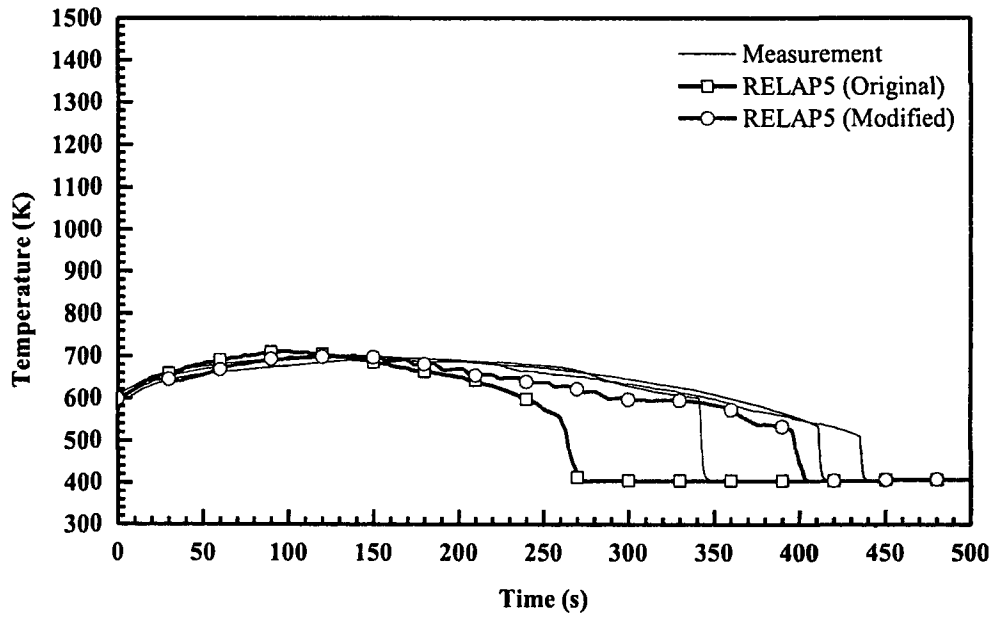

Figure 51. Rod Clad Temperatures at 11.5 ft from Heated Bottom for Test 31203

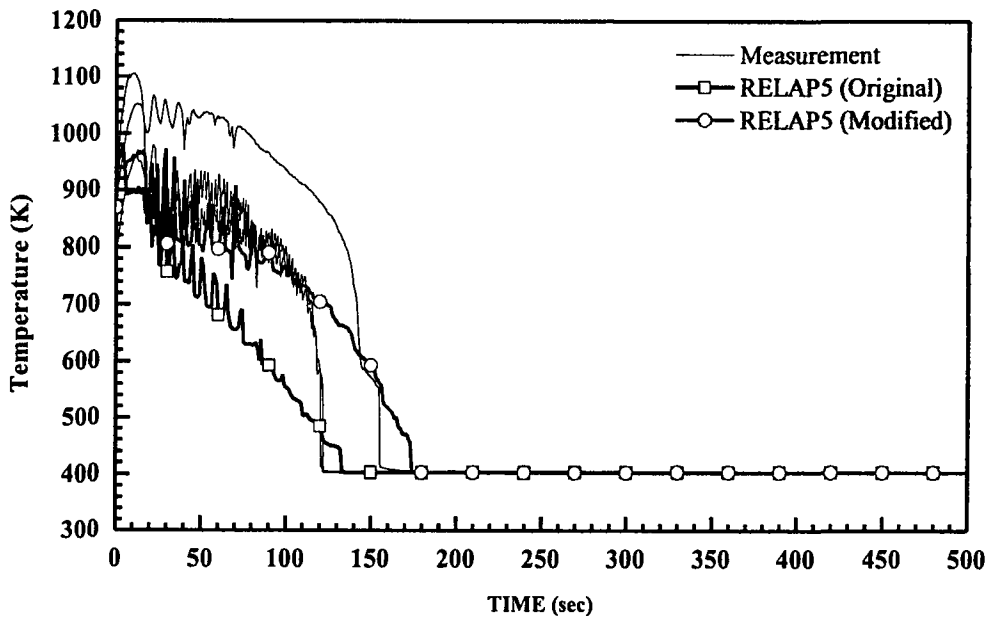

Figure 52. Vapor Temperatures at 6 ft from Heated Bottom for Test 31203

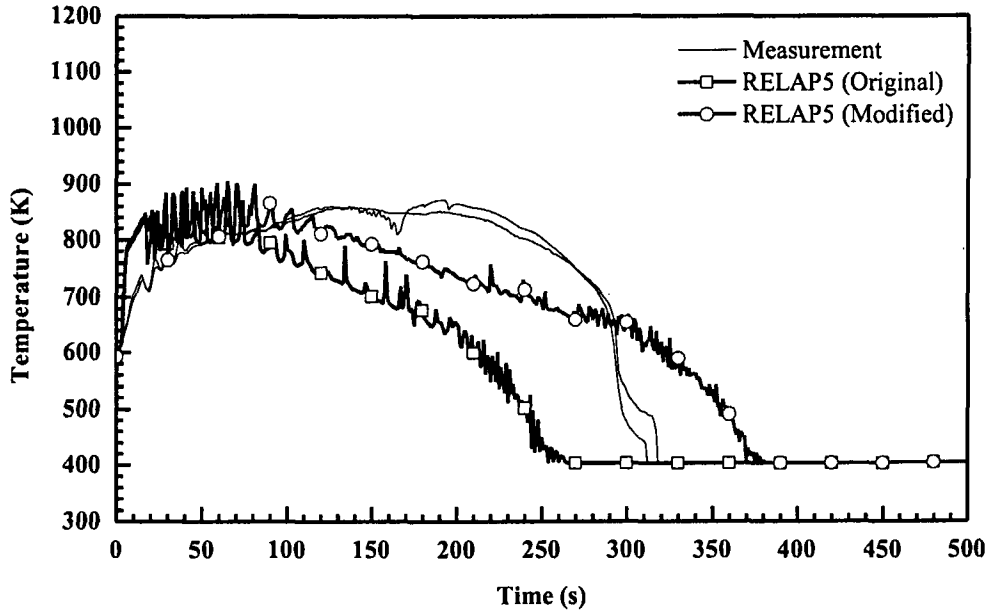

Figure 53. Vapor Temperatures at 10 ft from Heated Bottom for Test 31203

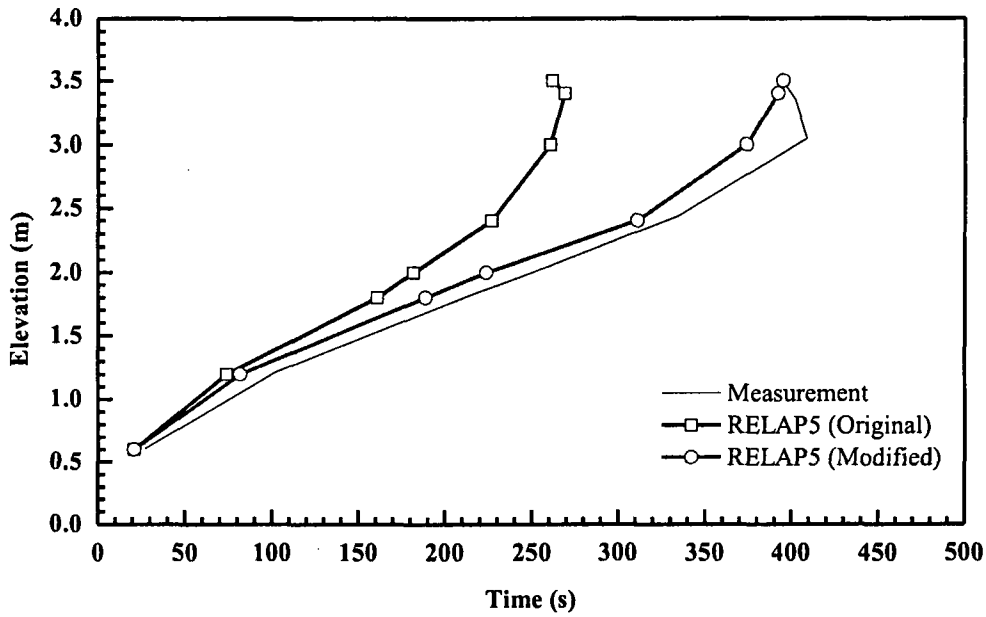

Figure 54. Quench Profile as a Function of Time for Test 31203

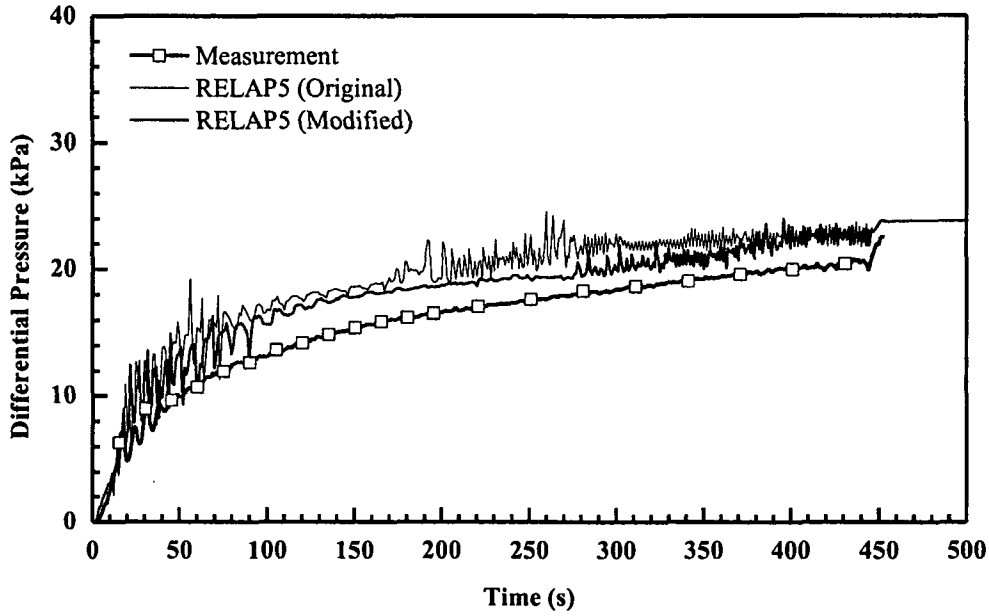

Figure 55. Differential Pressure for the Entire 12 ft Core for Test 31203

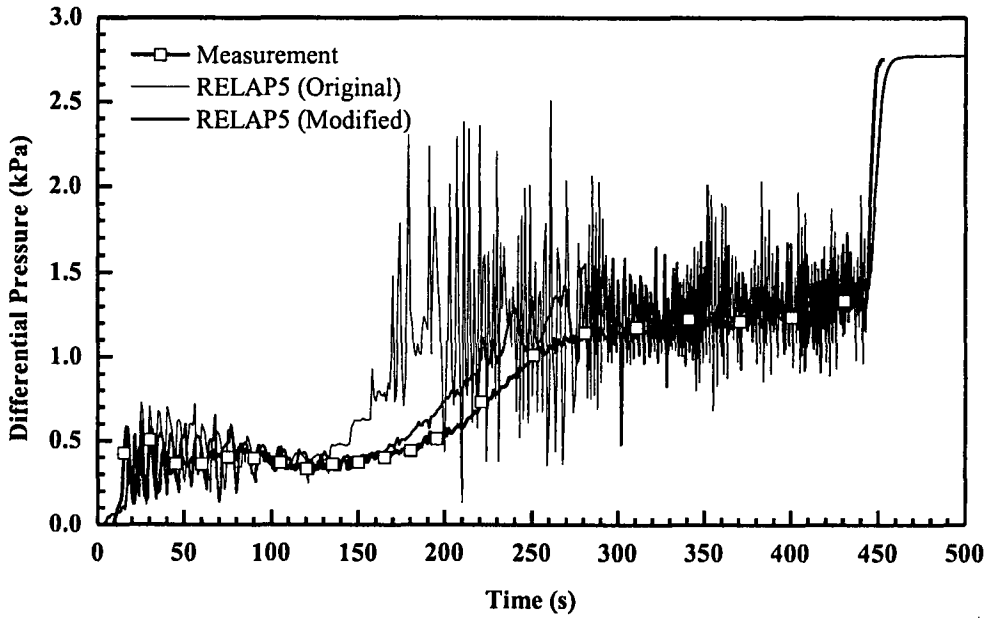

Figure 56. Differential Pressure at 6~7 ft Elevation for Test 31203

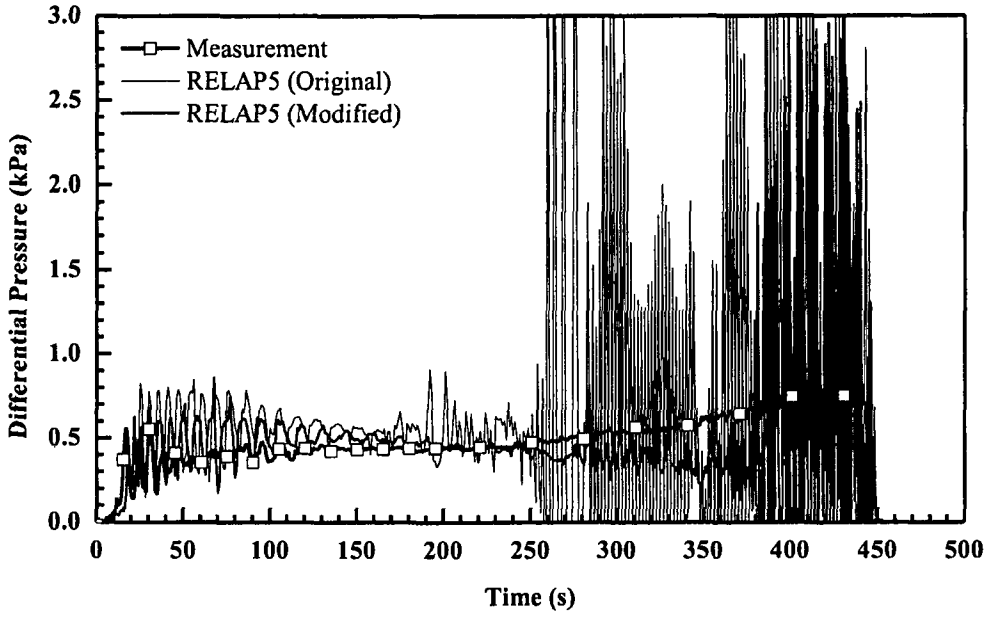

Figure 57. Differential Pressure at 10~11 ft Elevation for Test 31203

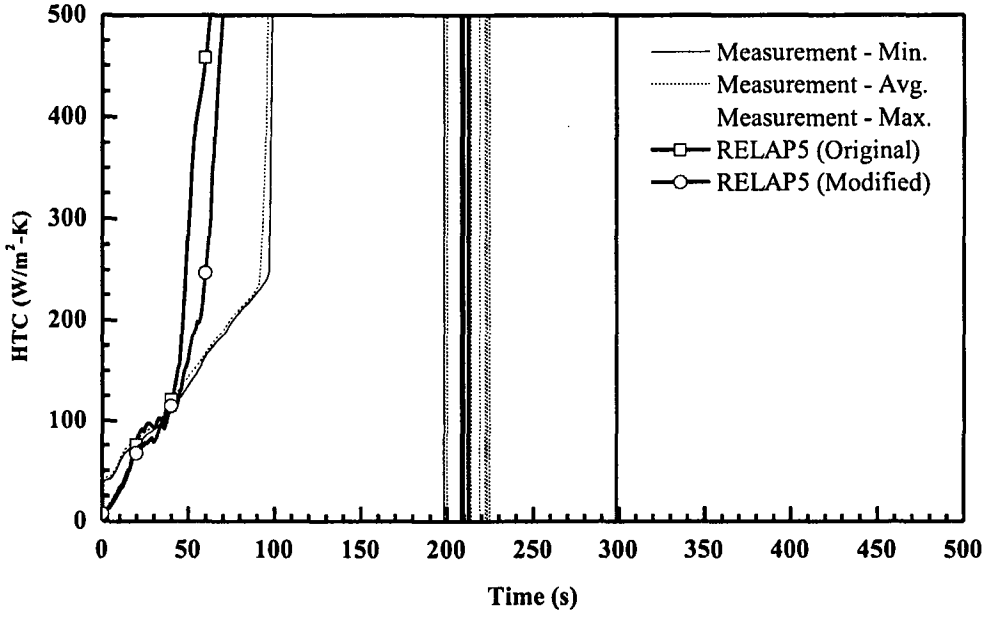

Figure 58. Heat Transfer Coefficient at 4 ft from Heated Bottom for Test 31203

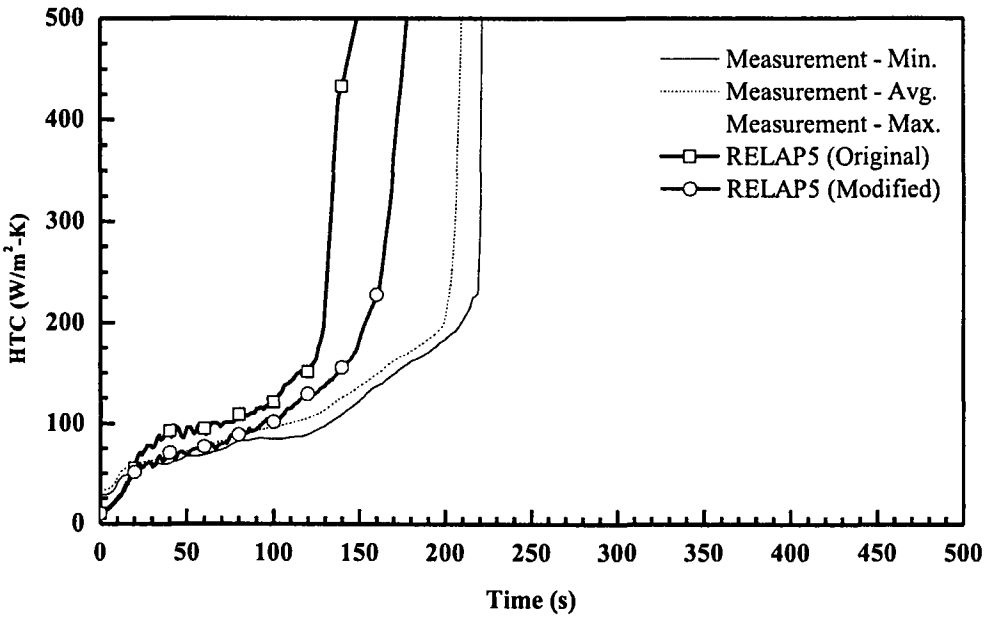

Figure 59. Heat Transfer Coefficient at 6 ft from Heated Bottom for Test 31203

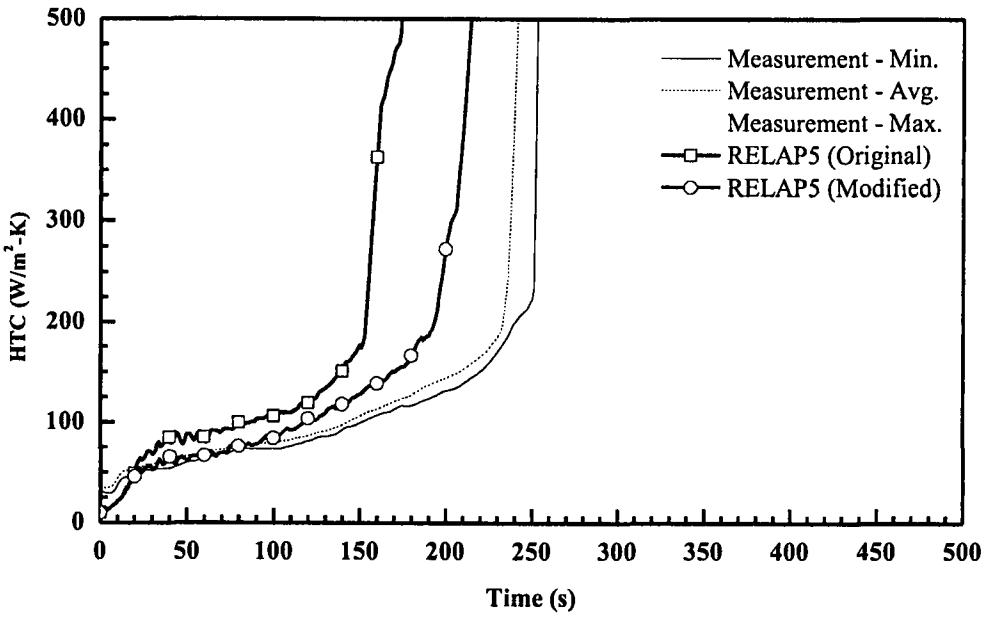

Figure 60. Heat Transfer Coefficient at 6.5 ft from Heated Bottom for Test 31203

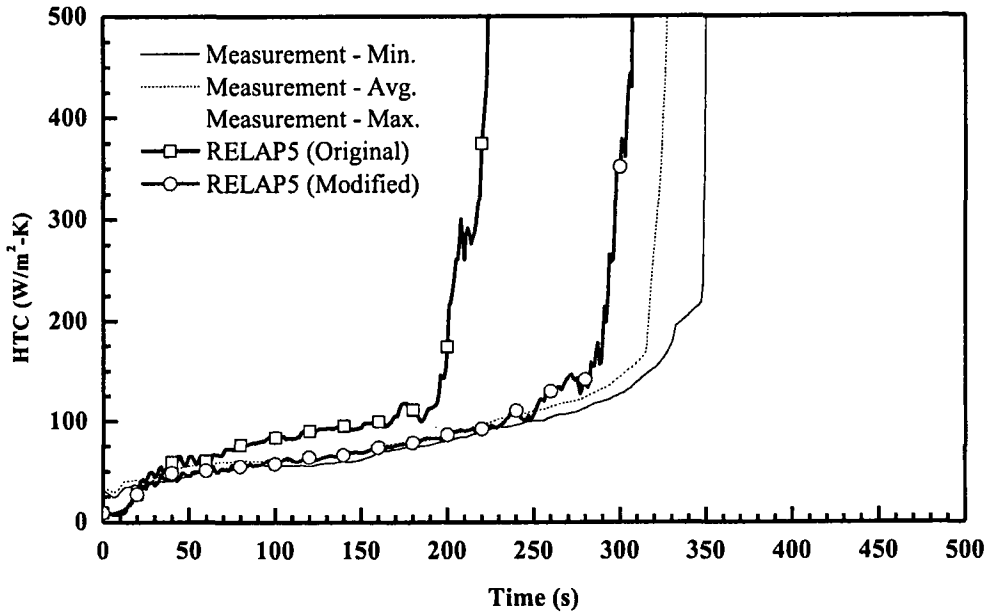

Figure 61. Heat Transfer Coefficient at 8 ft from Heated Bottom for Test 31203

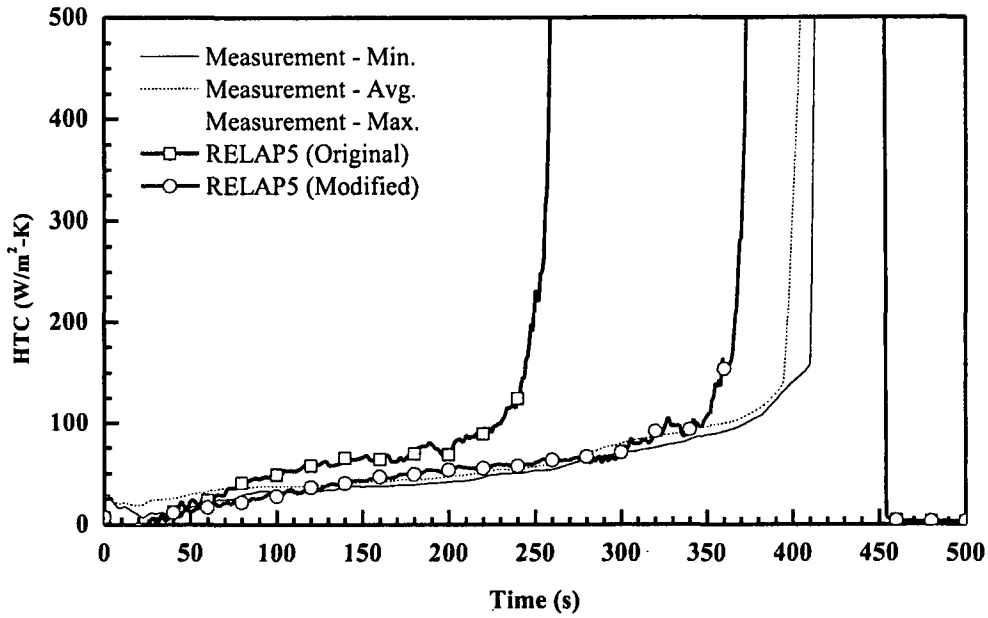

Figure 62. Heat Transfer Coefficient at 10 ft from Heated Bottom for Test 31203

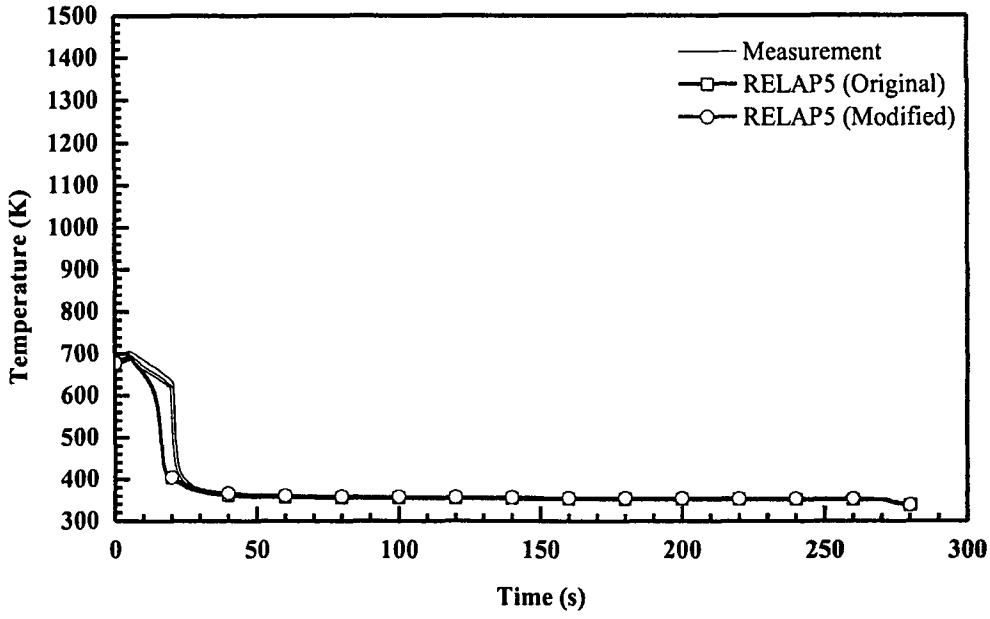

Figure 63. Rod Clad Temperatures at 2 ft from Heated Bottom for Test 31302

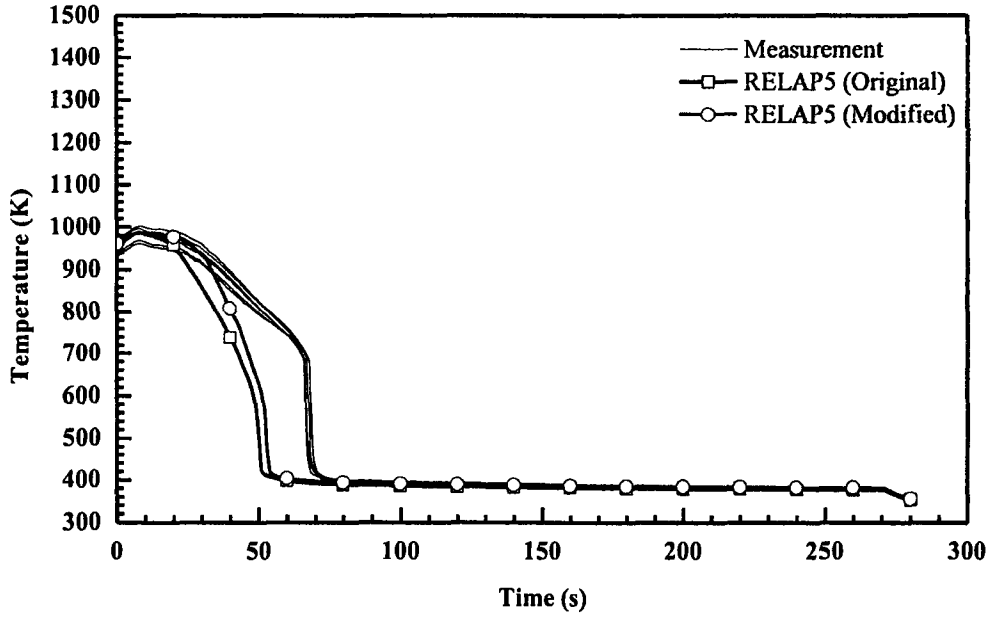

Figure 64. Rod Clad Temperatures at 4 ft from Heated Bottom for Test 31302

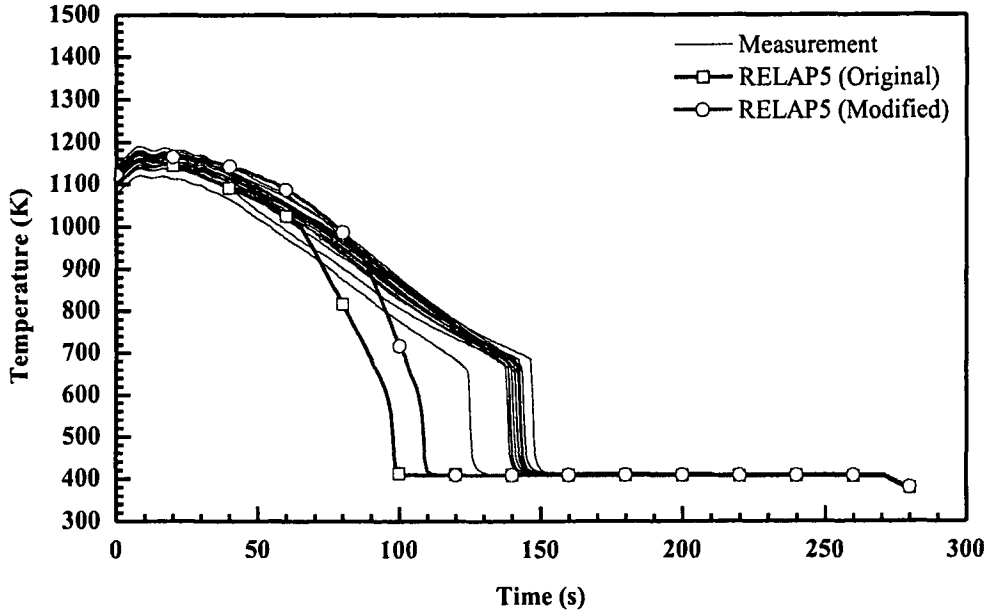

Figure 65. Rod Clad Temperatures at 6 ft from Heated Bottom for Test 31302

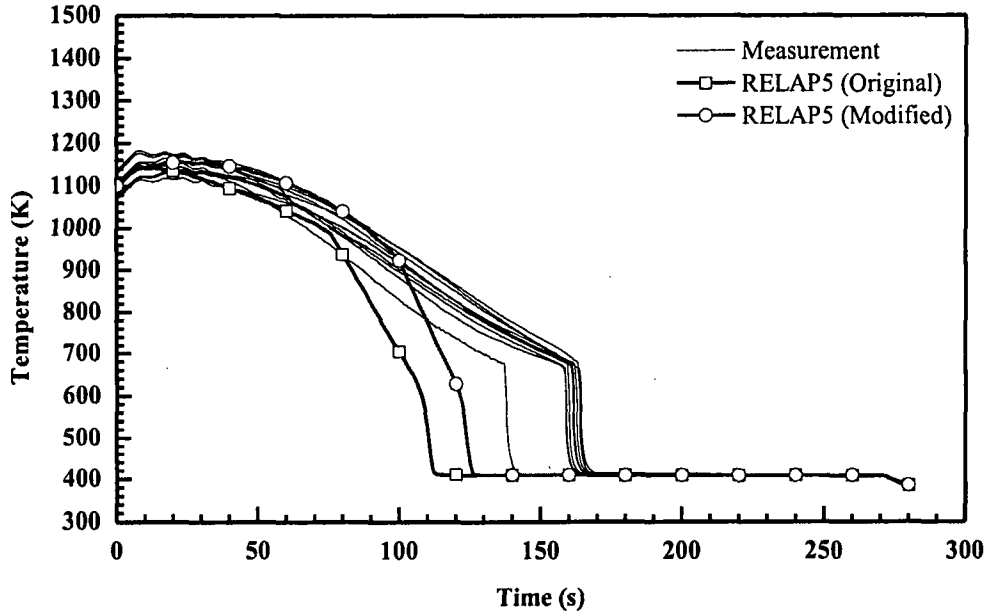

Figure 66. Rod Clad Temperatures at 6.5 ft from Heated Bottom for Test 31302

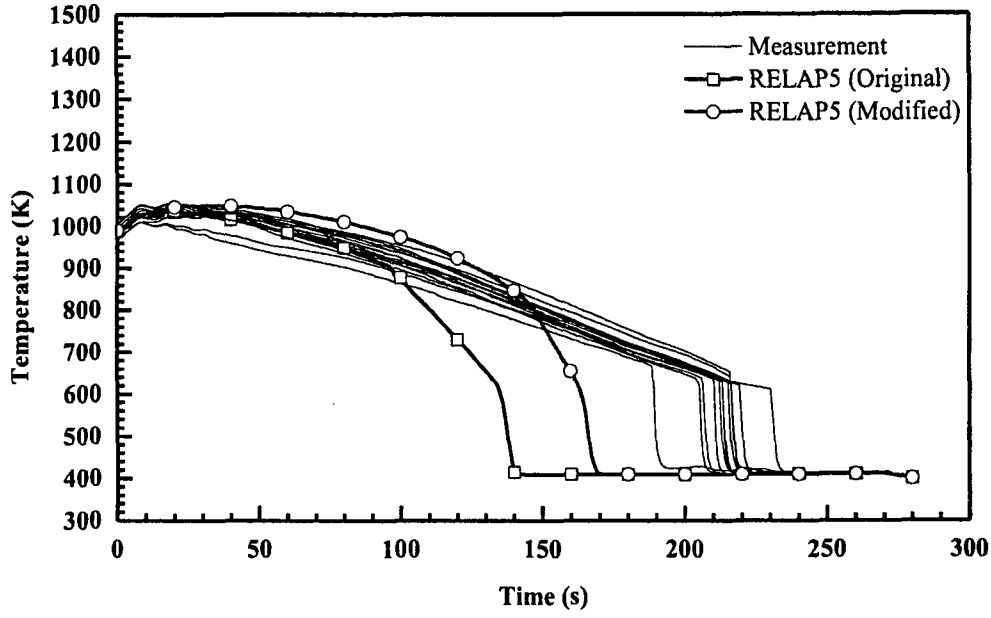

Figure 67. Rod Clad Temperatures at 8 ft from Heated Bottom for Test 31302

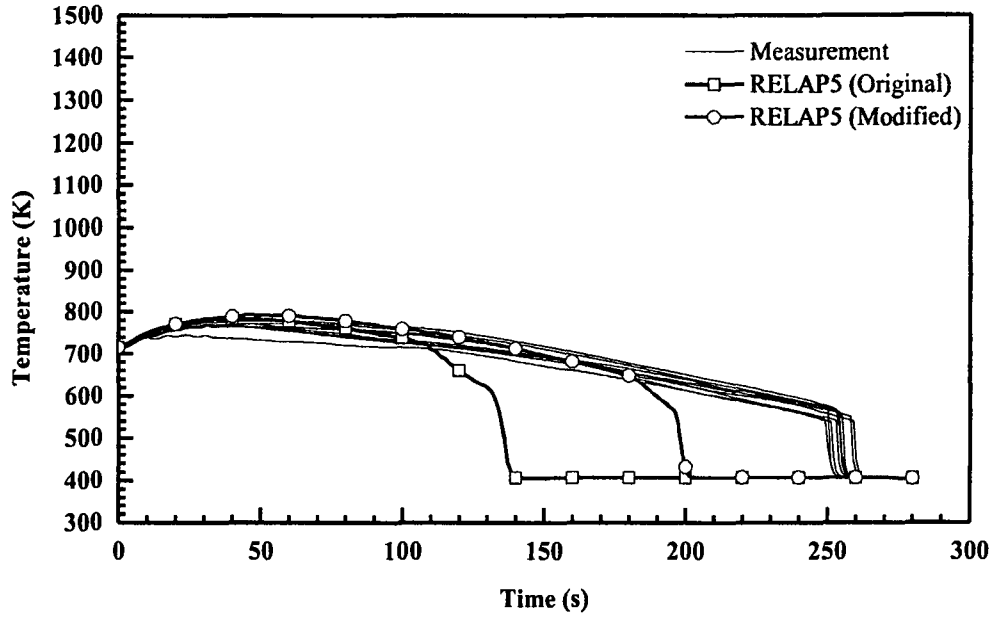

Figure 68. Rod Clad Temperatures at 10 ft from Heated Bottom for Test 31302

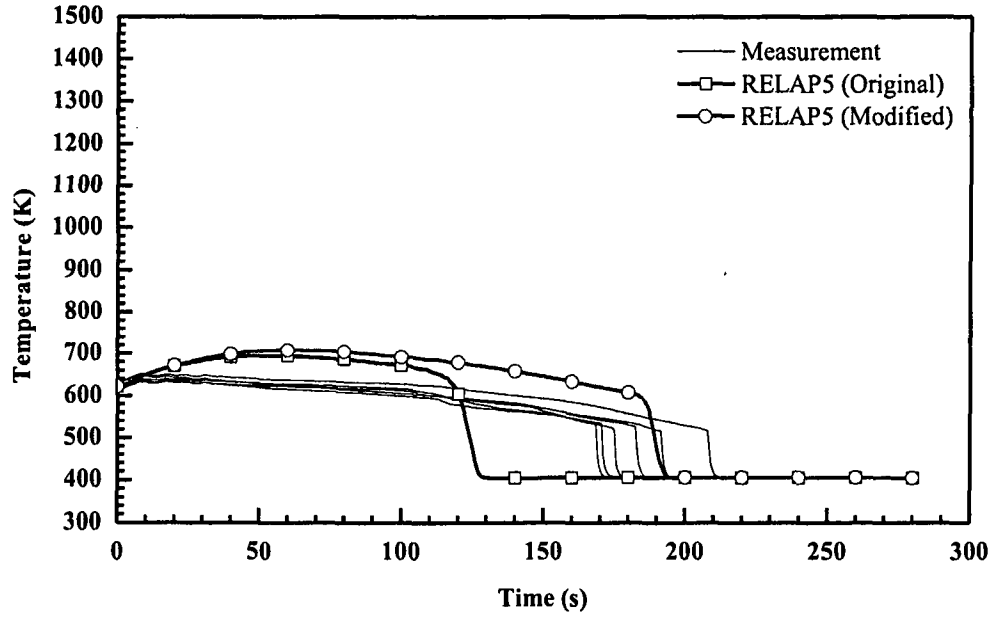

Figure 69. Rod Clad Temperatures at 11 ft from Heated Bottom for Test 31302

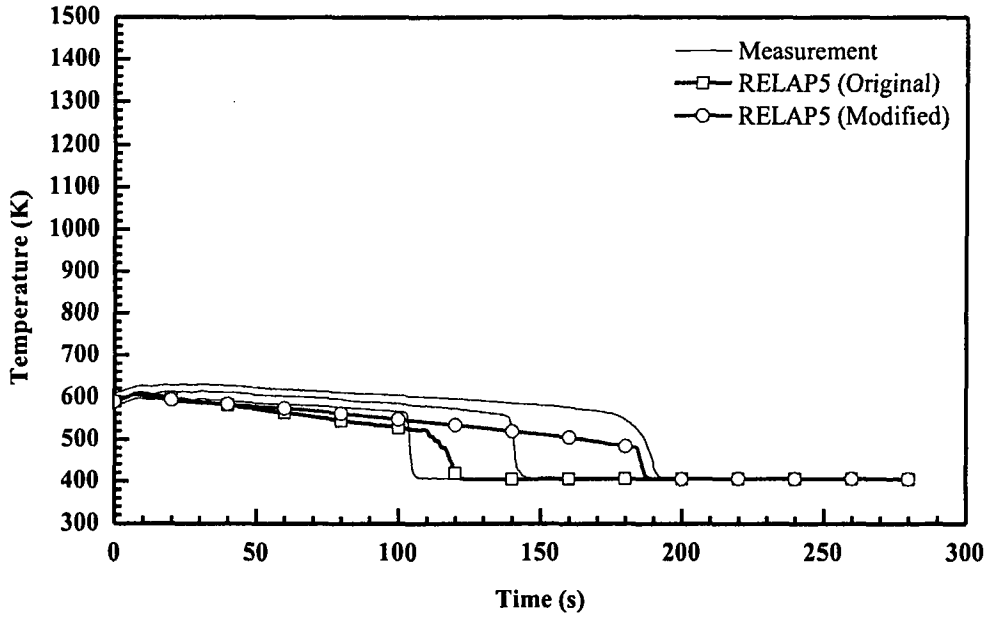

Figure 70. Rod Clad Temperatures at 11.5 ft from Heated Bottom for Test 31302

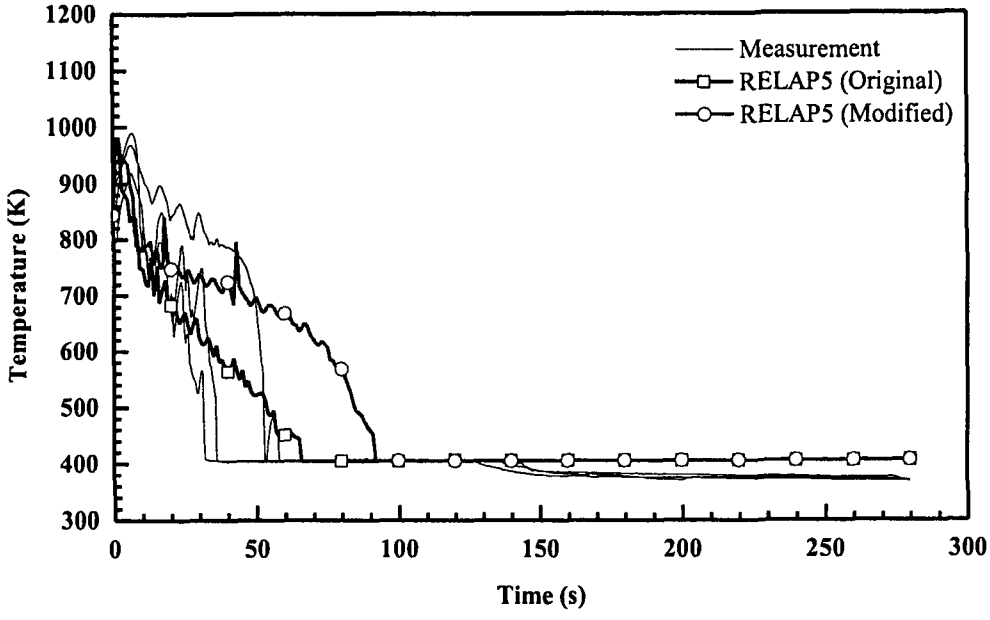

Figure 71. Vapor Temperatures at 6 ft from Heated Bottom for Test 31302

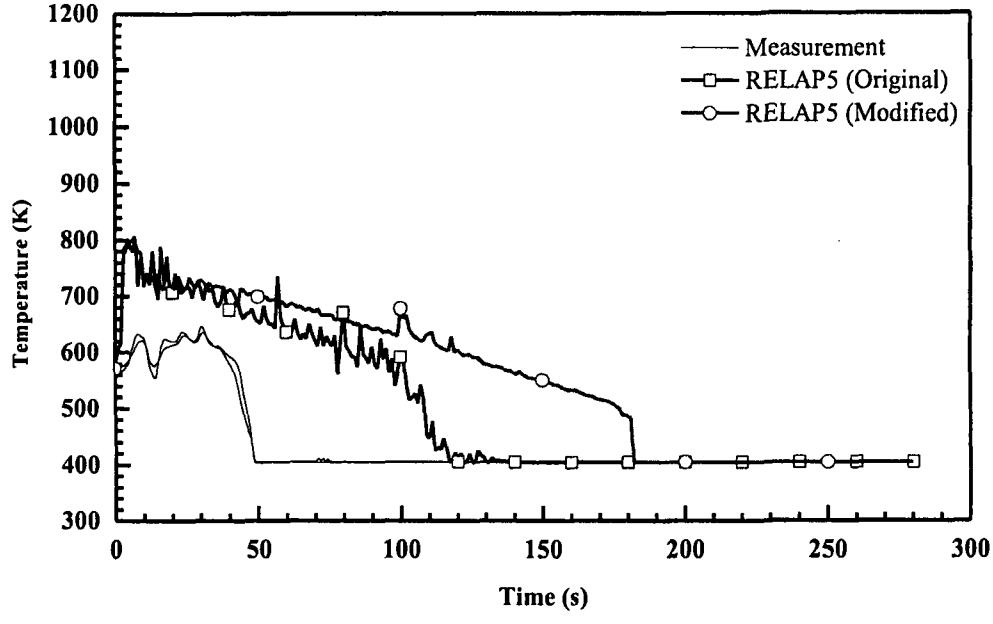

Figure 72. Vapor Temperatures at 10 ft from Heated Bottom for Test 31302

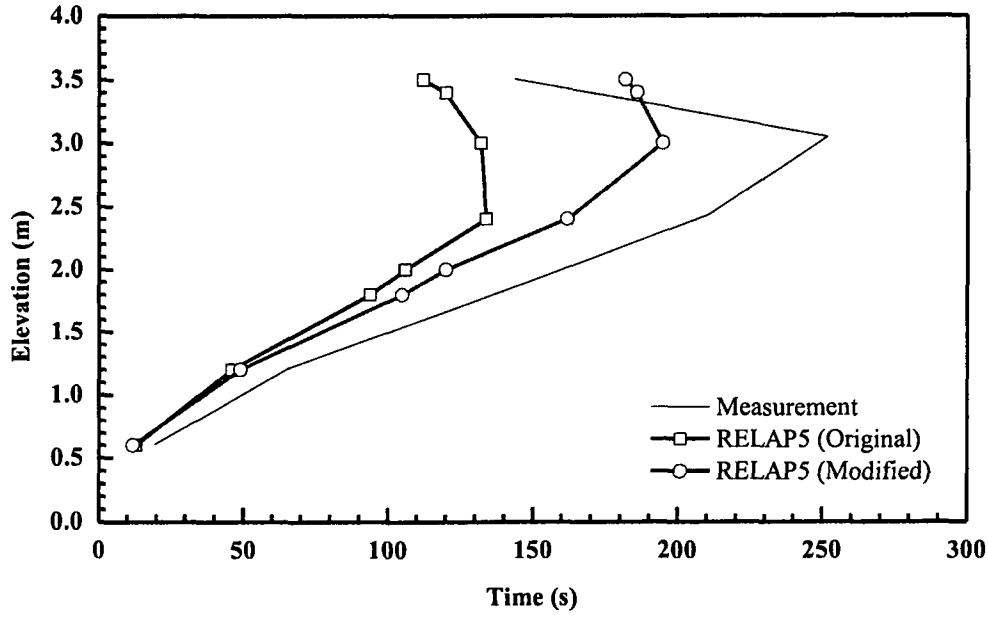

Figure 73. Quench Profile as a Function of Time for Test 31302

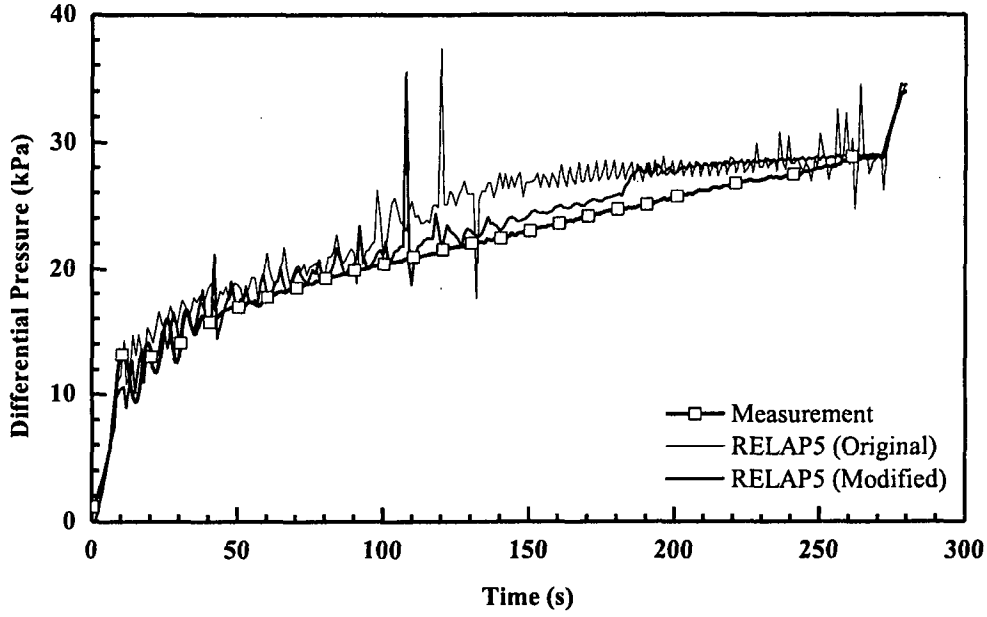

Figure 74. Differential Pressure for the Entire 12 ft Core for Test 31302

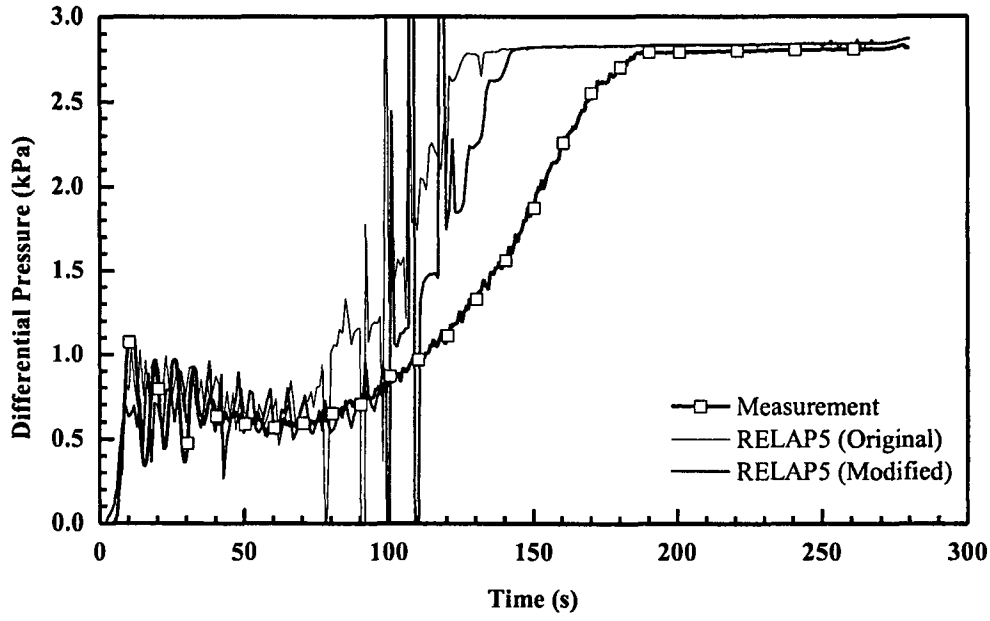

Figure 75. Differential Pressure at 6~7 ft Elevation for Test 31302

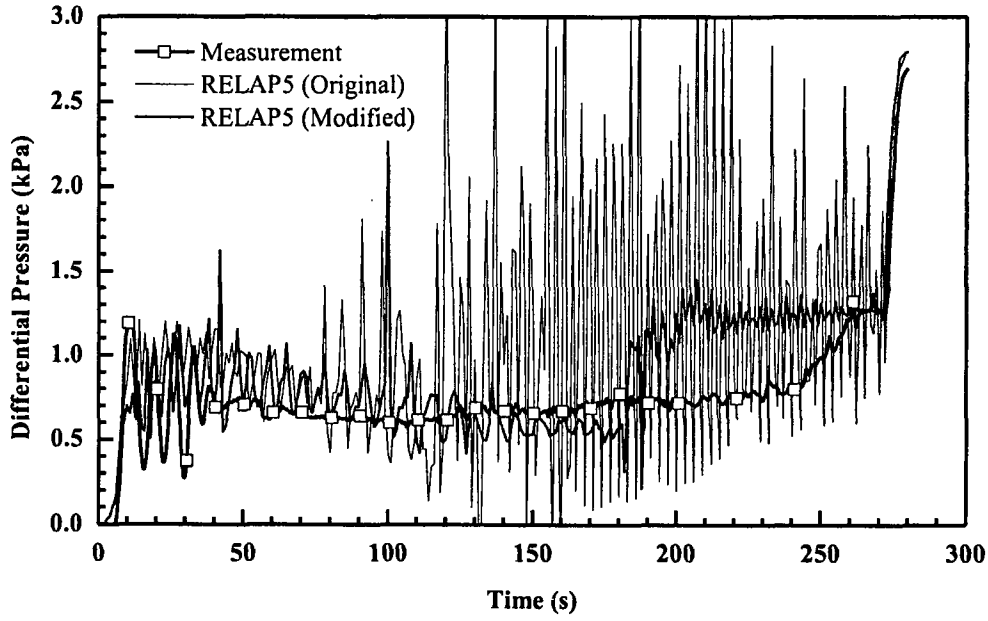

Figure 76. Differential Pressure at 10~11 ft Elevation for Test 31302

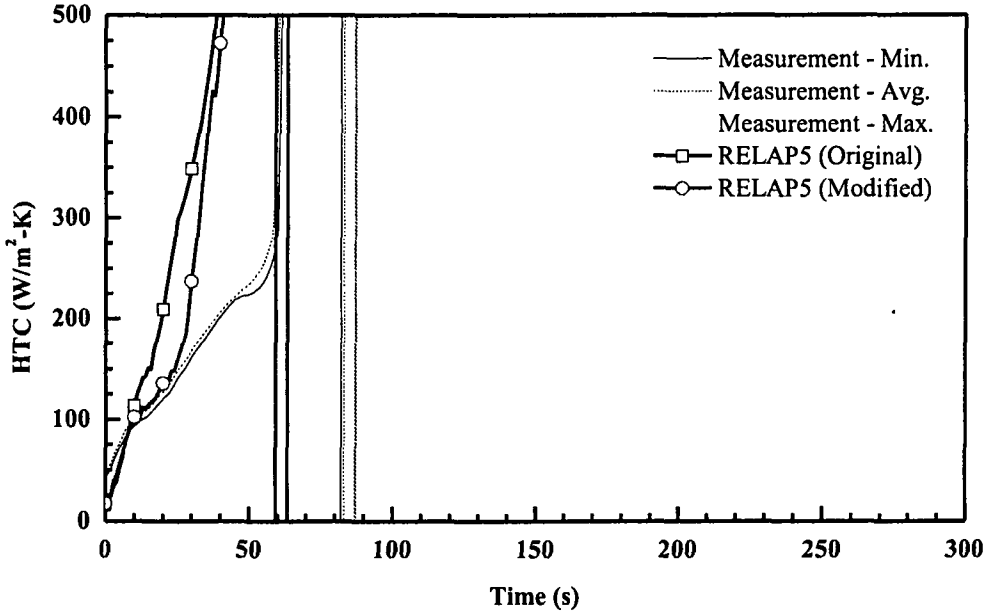

Figure 77. Heat Transfer Coefficient at 4 ft from Heated Bottom for Test 31302

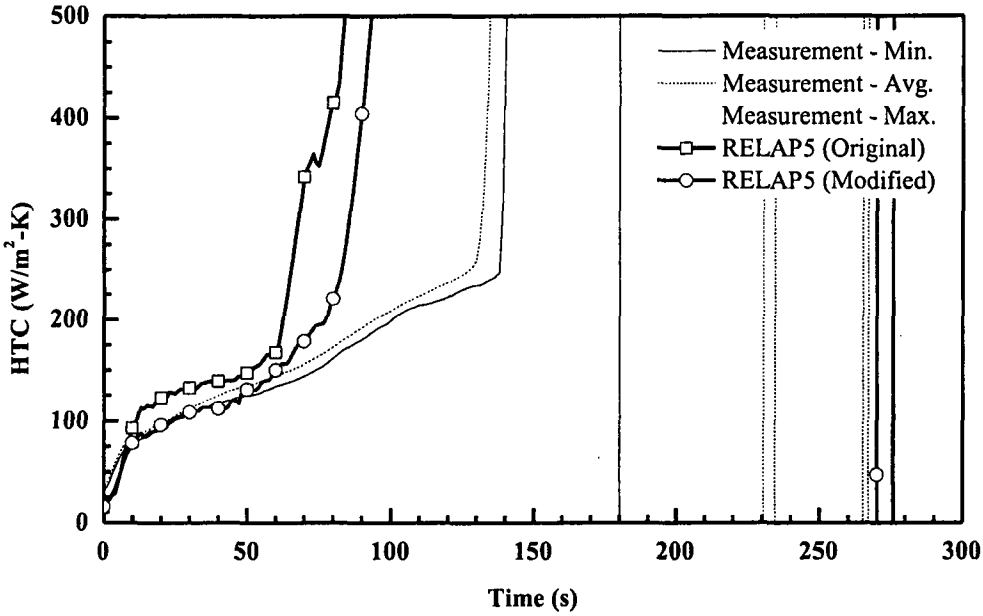

Figure 78. Heat Transfer Coefficient at 6 ft from Heated Bottom for Test 31302

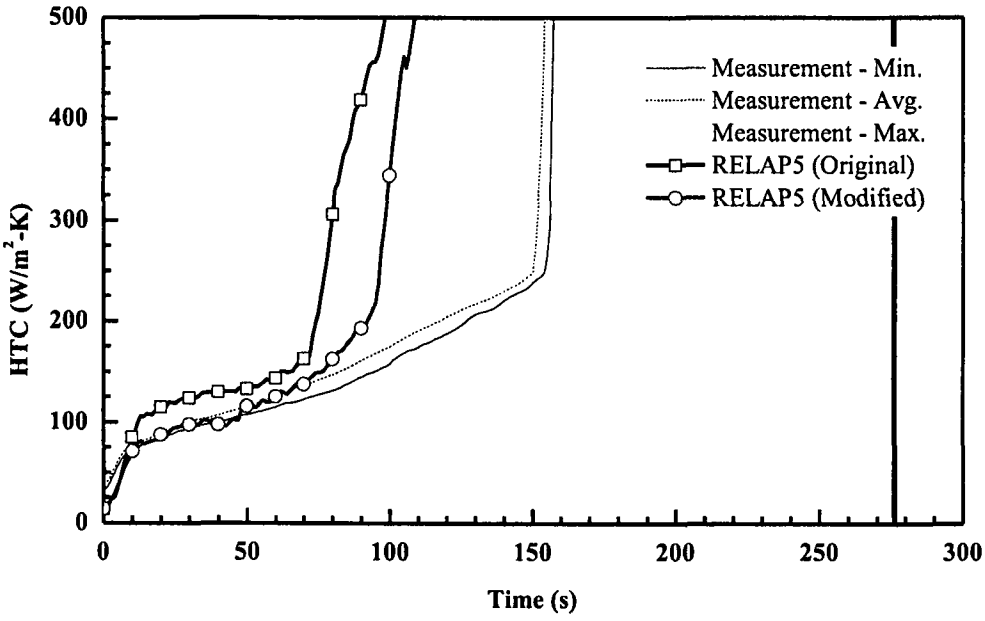

Figure 79. Heat Transfer Coefficient at 6.5 ft from Heated Bottom for Test 31302

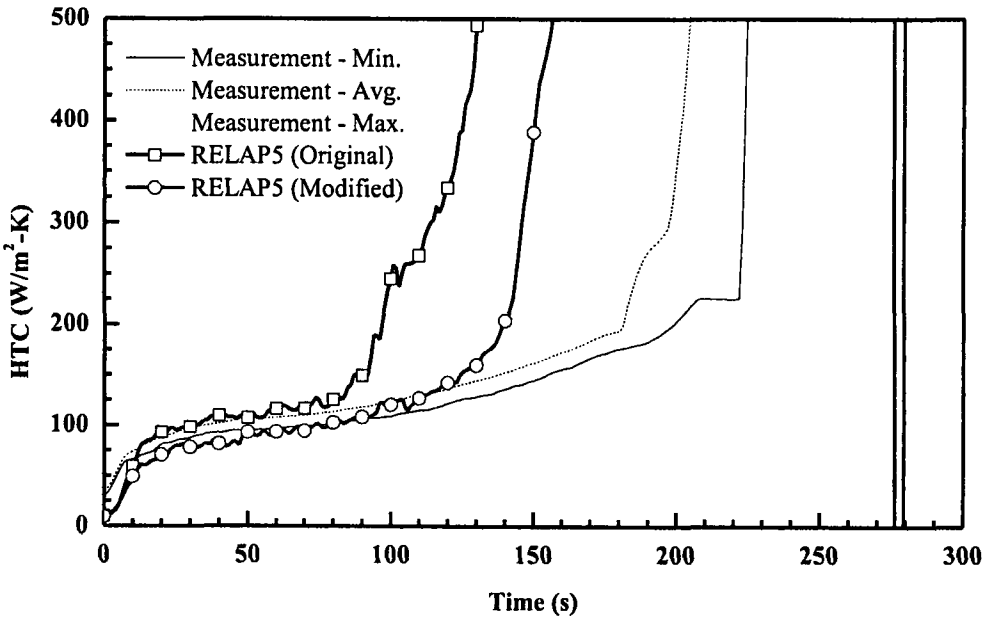

Figure 80. Heat Transfer Coefficient at 8 ft from Heated Bottom for Test 31302

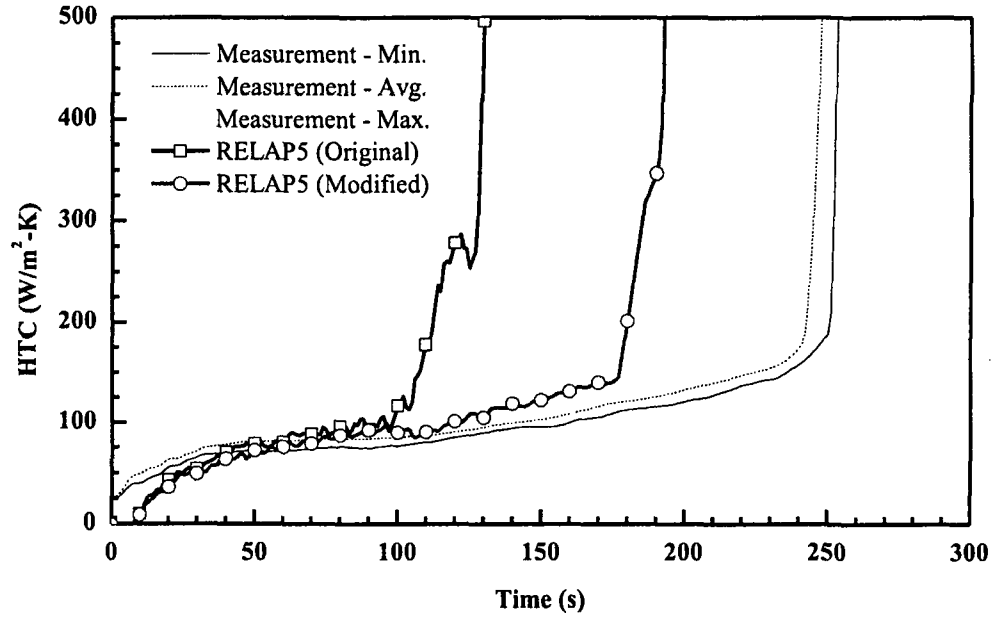

Figure 81. Heat Transfer Coefficient at 10 ft from Heated Bottom for Test 31302

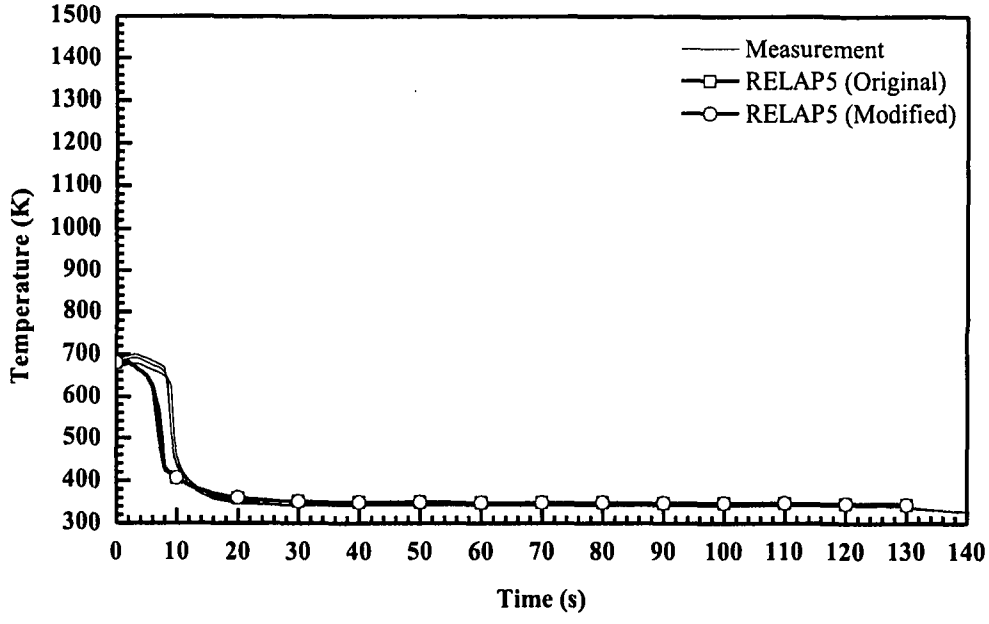

Figure 82. Rod Clad Temperatures at 2 ft from Heated Bottom for Test 31701

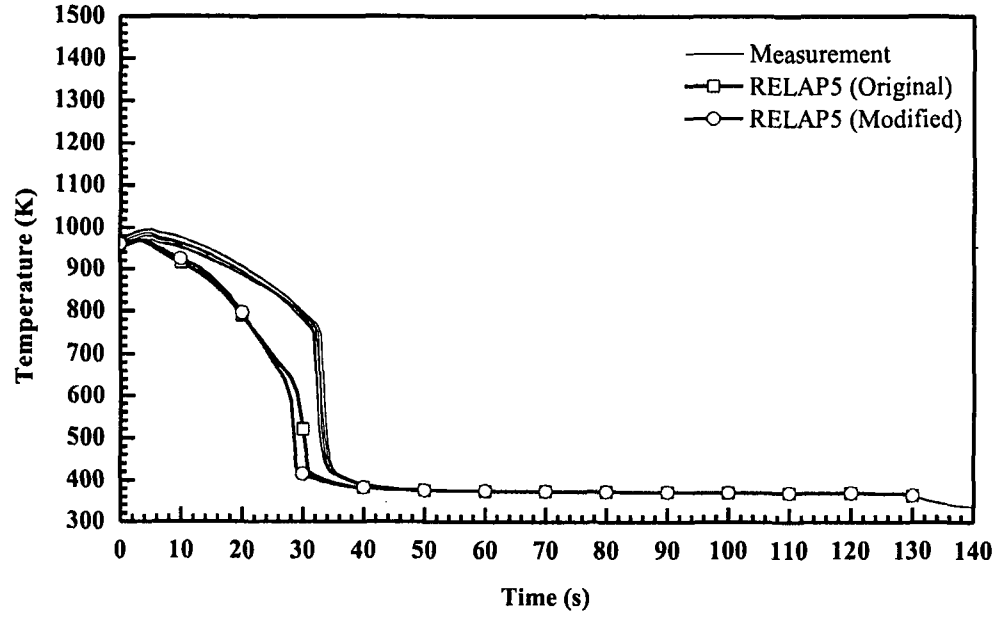

Figure 83. Rod Clad Temperatures at 4 ft from Heated Bottom for Test 31701

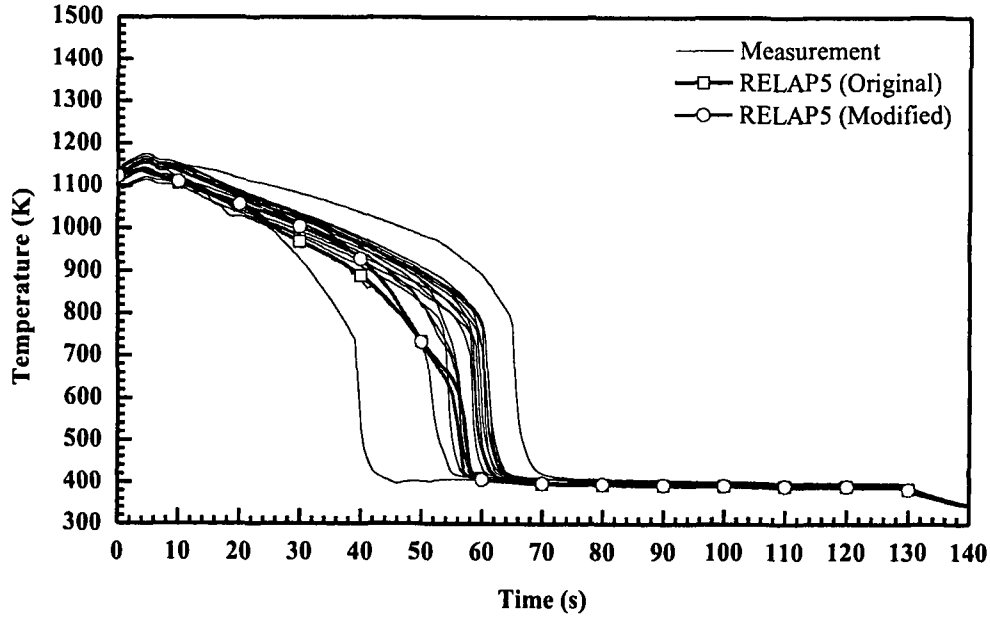

Figure 84. Rod Clad Temperatures at 6 ft from Heated Bottom for Test 31701

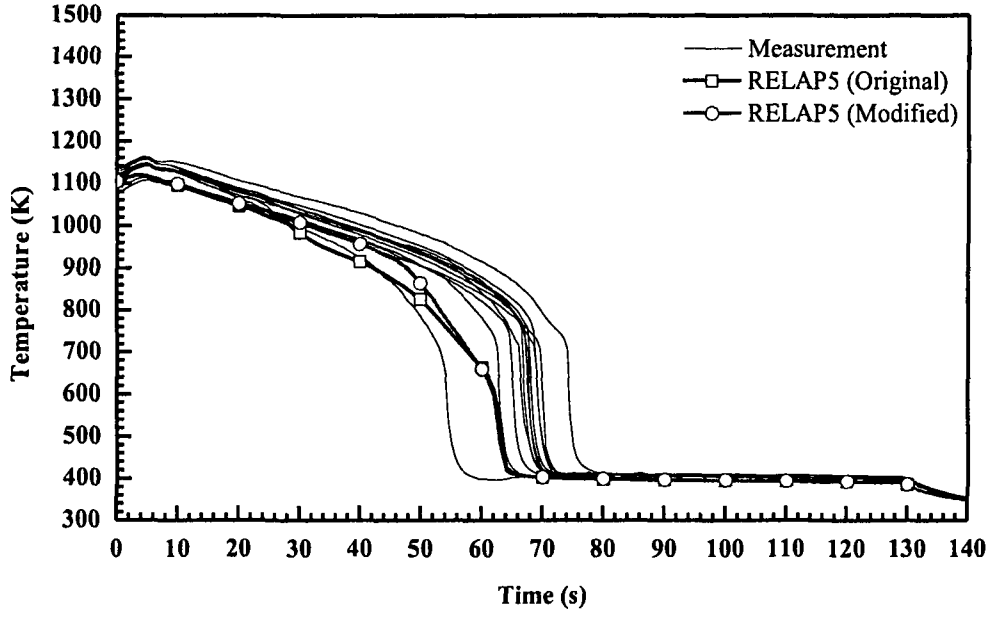

Figure 85. Rod Clad Temperatures at 6.5 ft from Heated Bottom for Test 31701

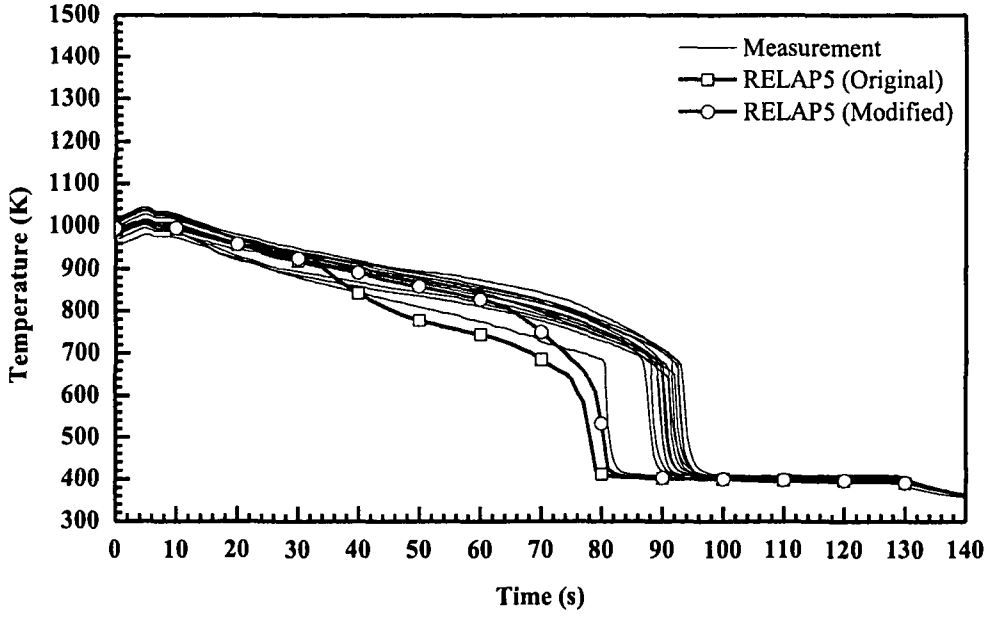

Figure 86. Rod Clad Temperatures at 8 ft from Heated Bottom for Test 31701

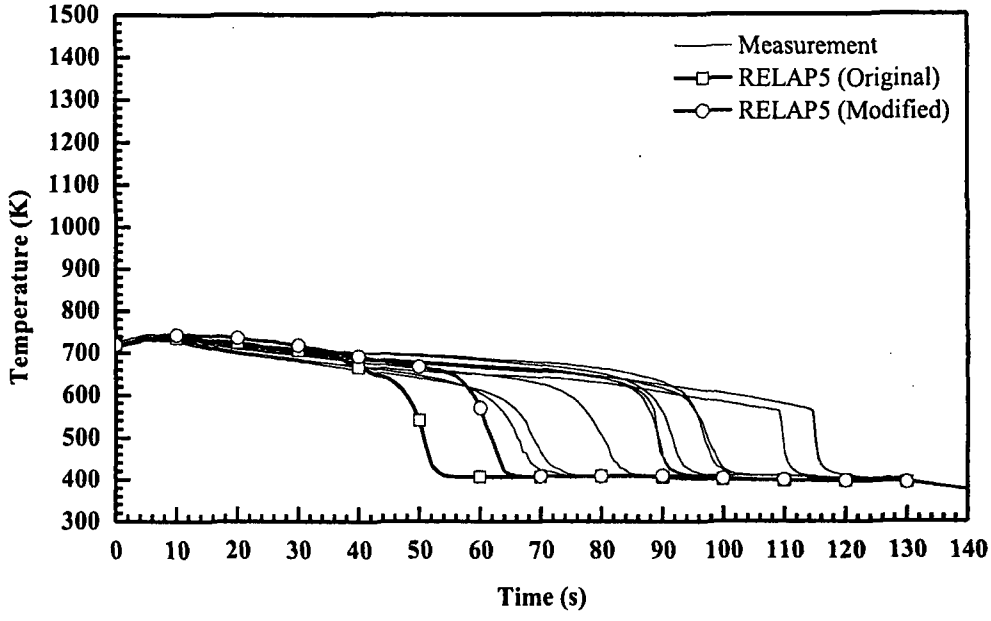

Figure 87. Rod Clad Temperatures at 10 ft from Heated Bottom for Test 31701

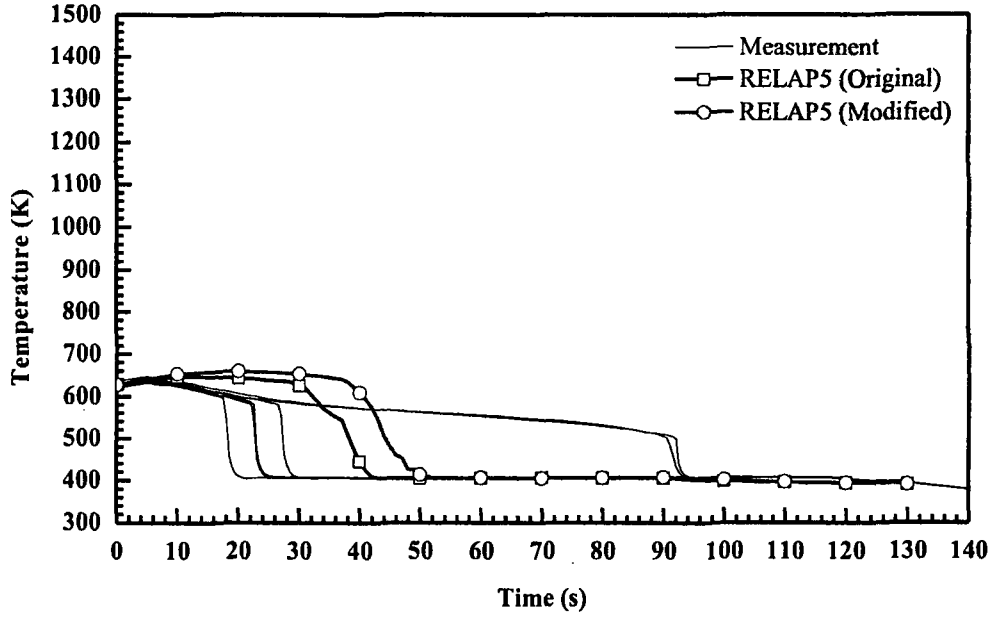

Figure 88. Rod Clad Temperatures at 11 ft from Heated Bottom for Test 31701

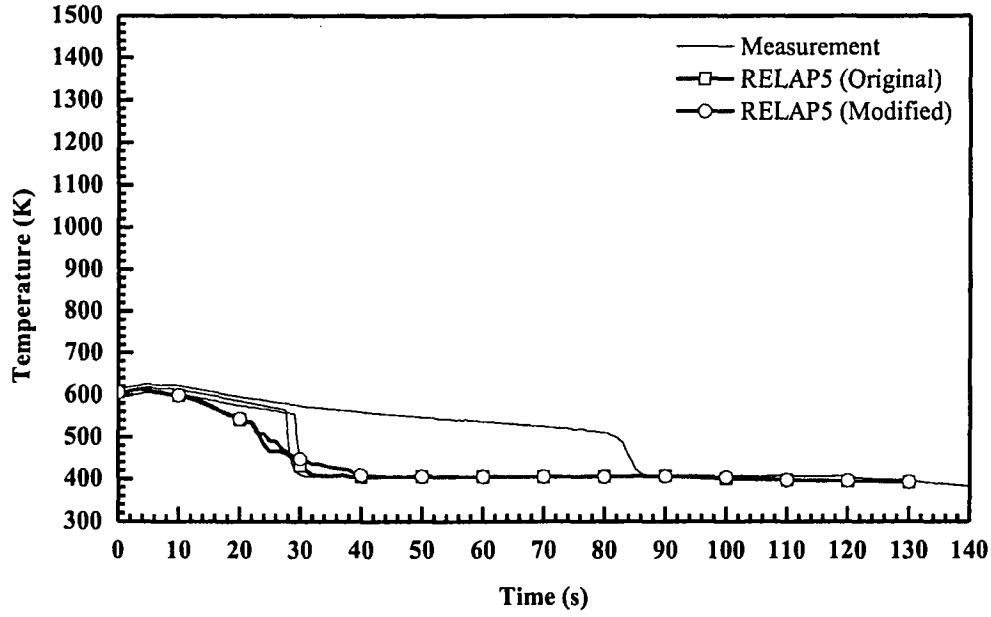

Figure 89. Rod Clad Temperatures at 11.5 ft from Heated Bottom for Test 31701

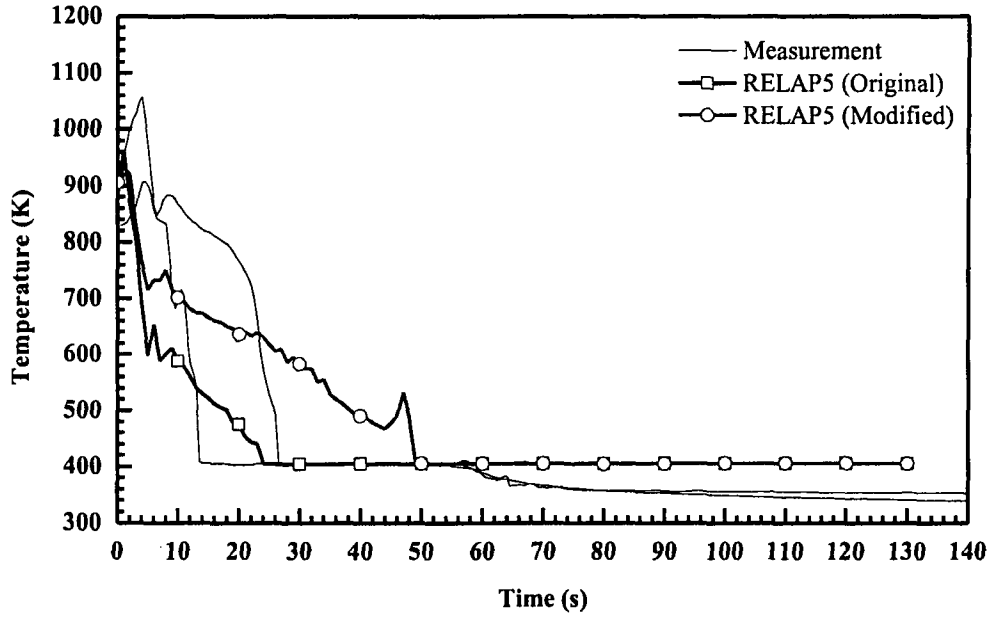

Figure 90. Vapor Temperatures at 6 ft from Heated Bottom for Test 31701

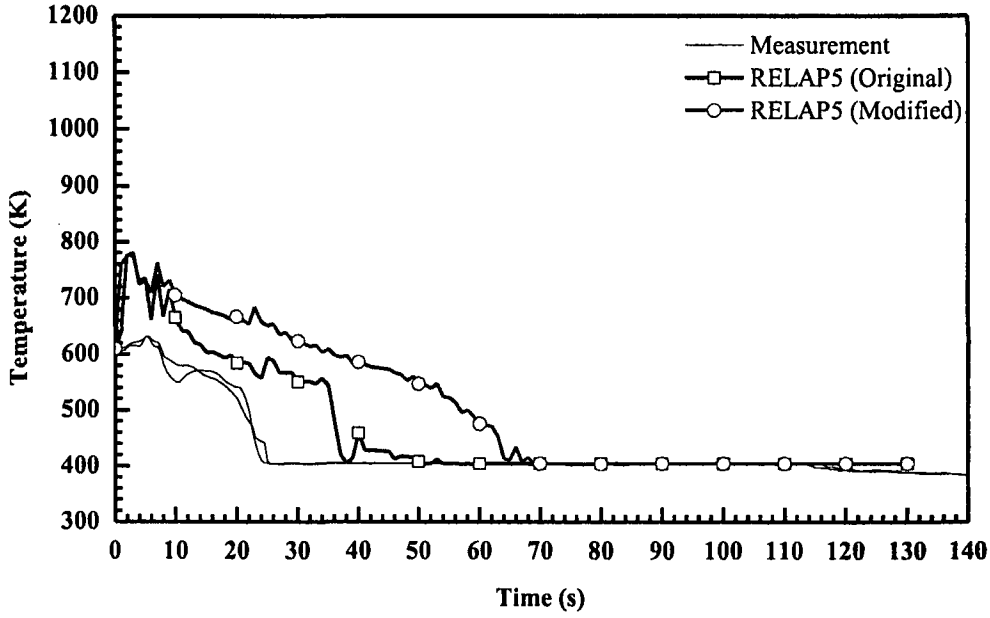

Figure 91. Vapor Temperatures at 10 ft from Heated Bottom for Test 31701

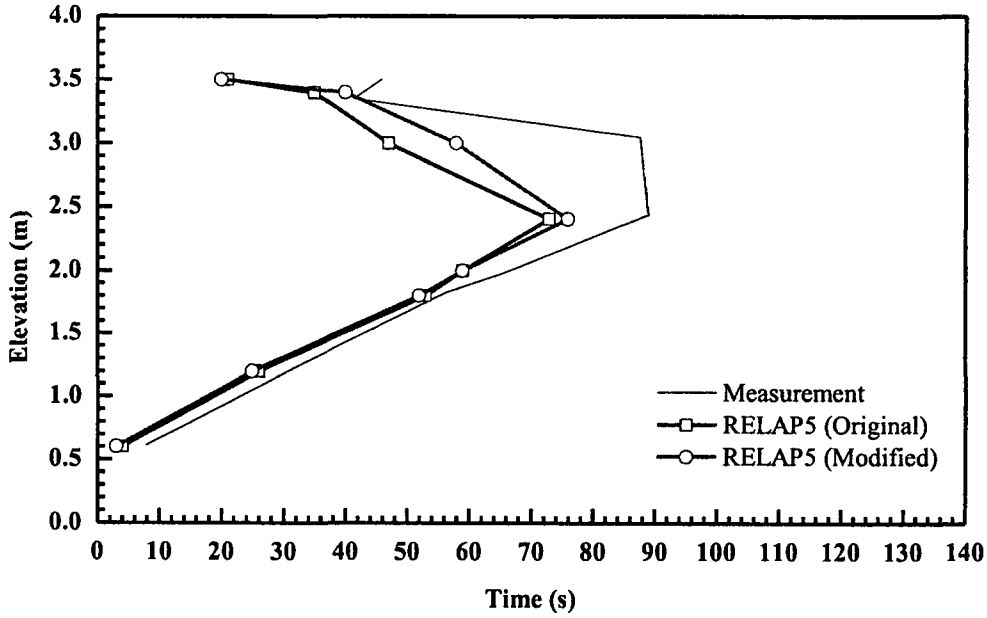

Figure 92. Quench Profile as a Function of Time for Test 31701

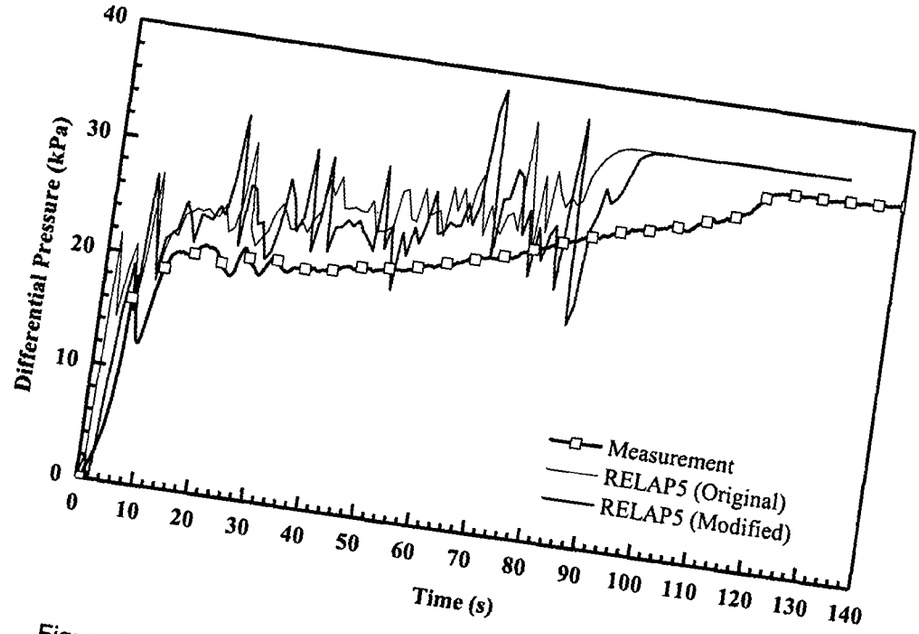

Figure 93. Differential Pressure for the Entire 12 ft Core for Test 31701

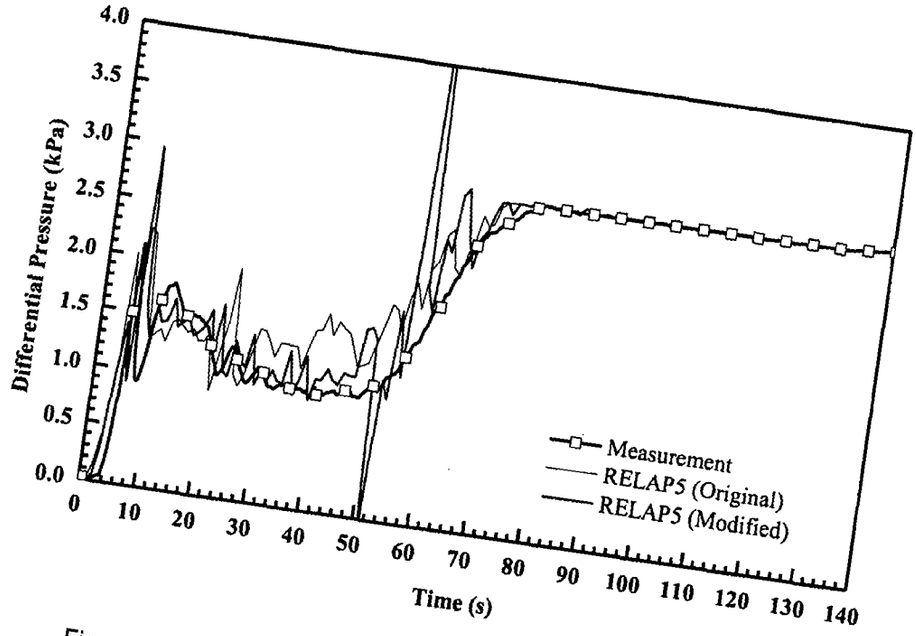

Figure 94. Differential Pressure at 6~7 ft Elevation for Test 31701

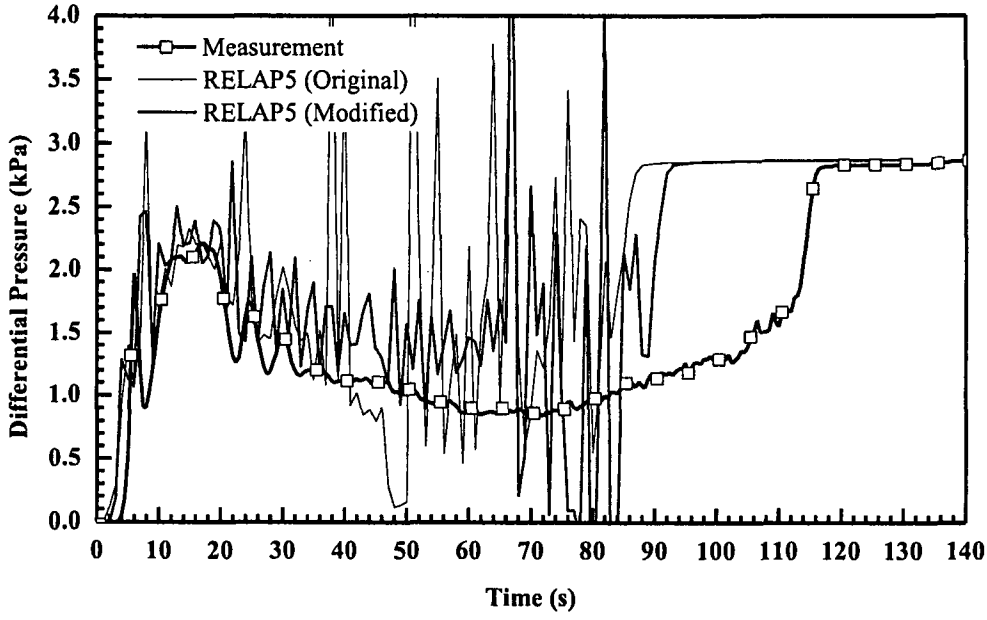

Figure 95. Differential Pressure at 10~11 ft Elevation for Test 31701

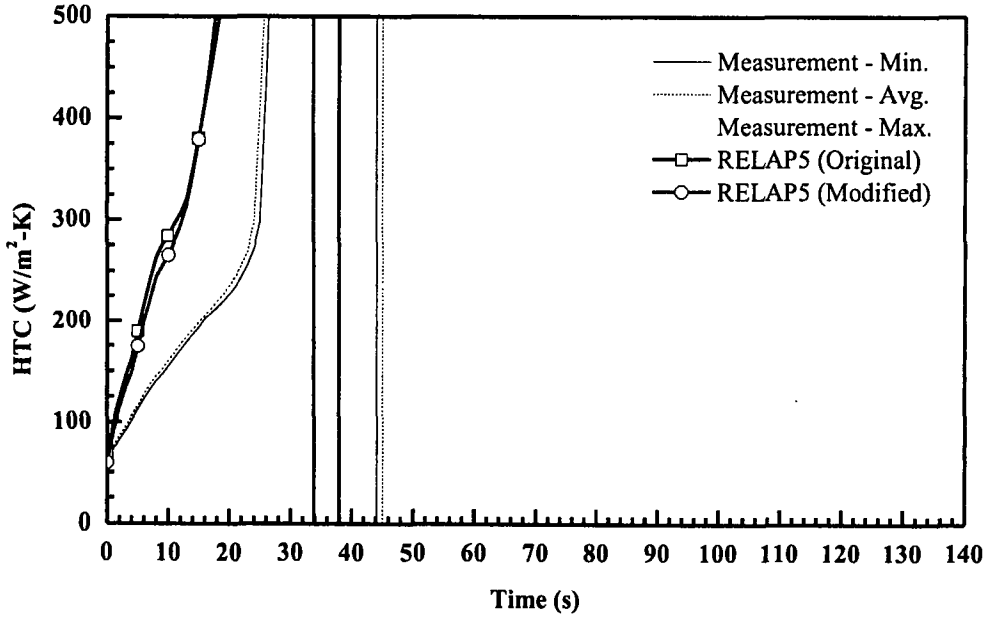

Figure 96. Heat Transfer Coefficient at 4 ft from Heated Bottom for Test 31701

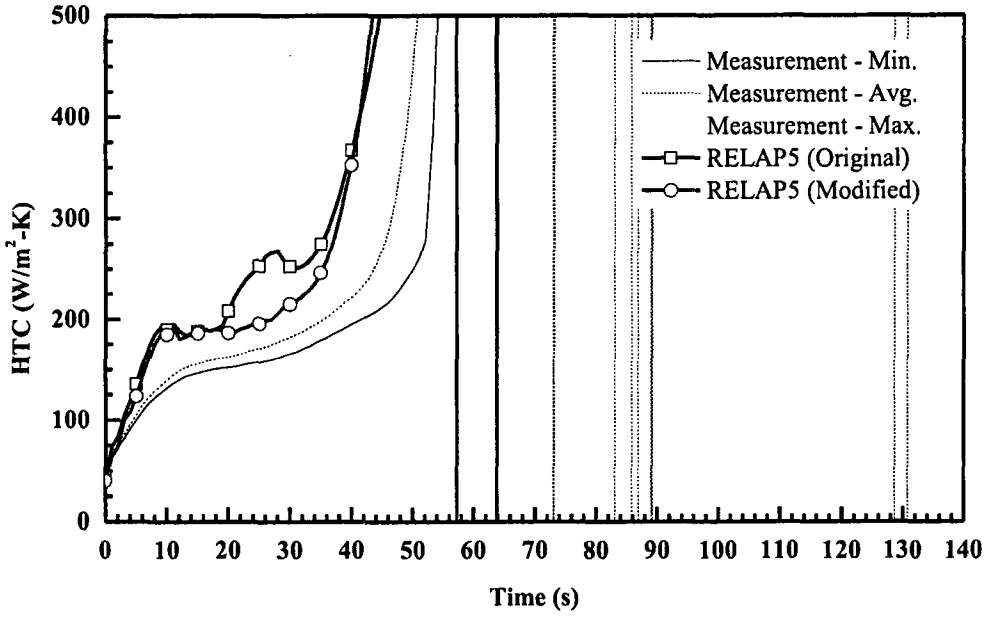

Figure 97. Heat Transfer Coefficient at 6 ft from Heated Bottom for Test 31701

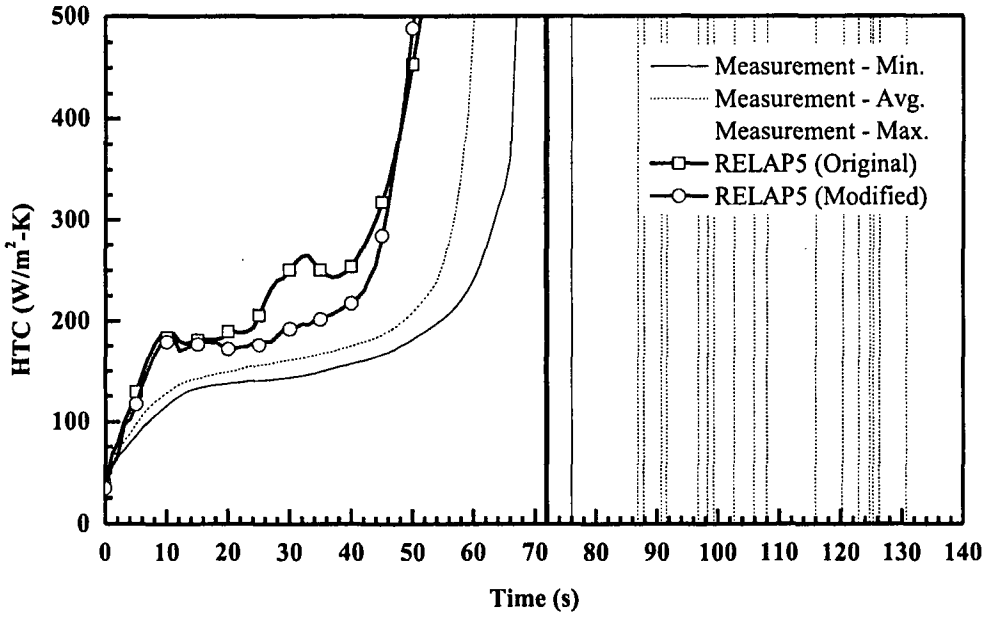

Figure 98. Heat Transfer Coefficient at 6.5 ft from Heated Bottom for Test 31701

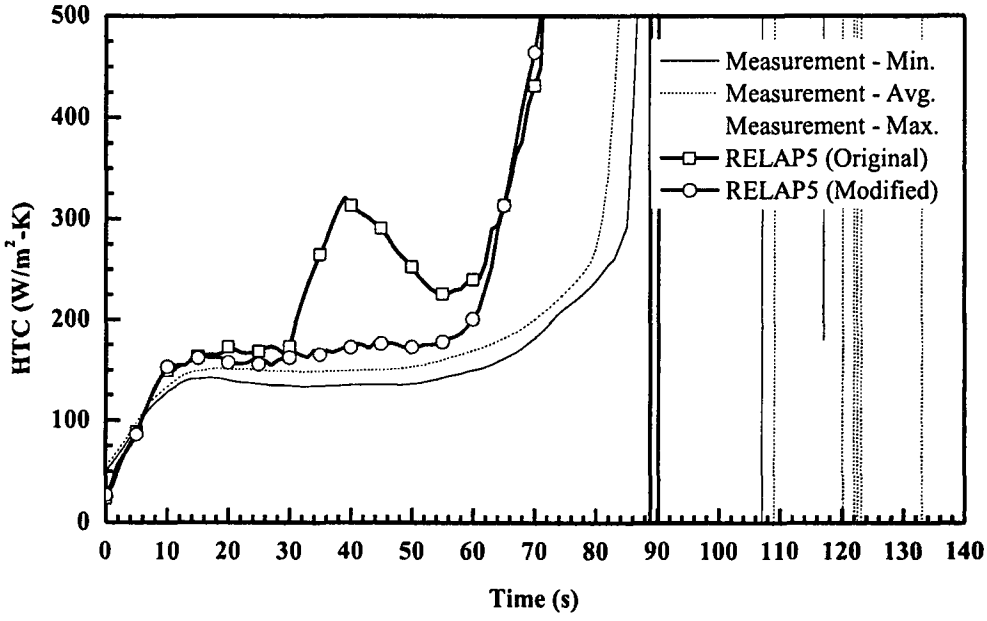

Figure 99. Heat Transfer Coefficient at 8 ft from Heated Bottom for Test 31701

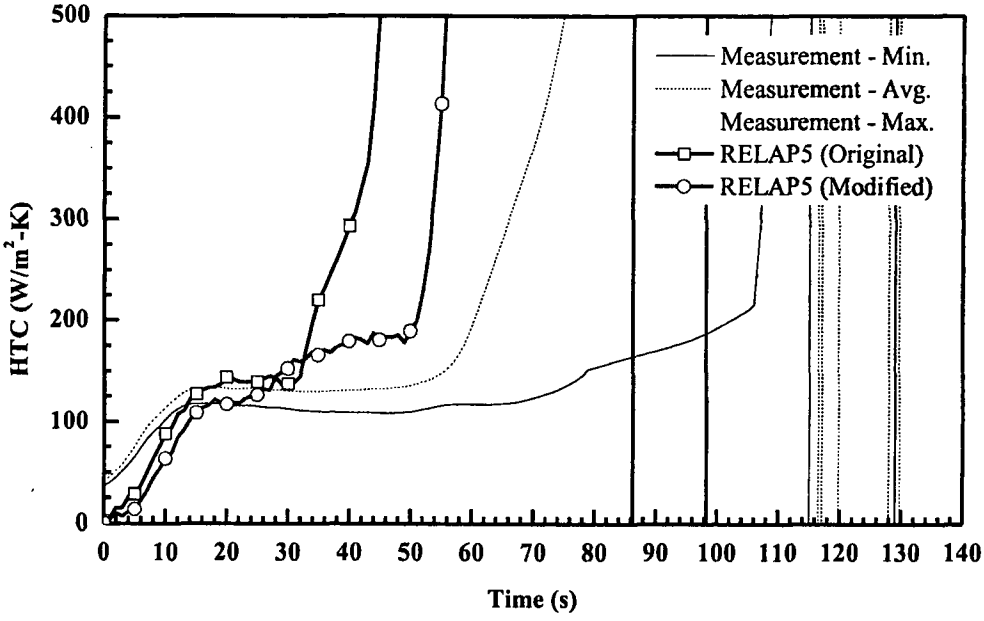

Figure 100. Heat Transfer Coefficient at 10 ft from Heated Bottom for Test 31701

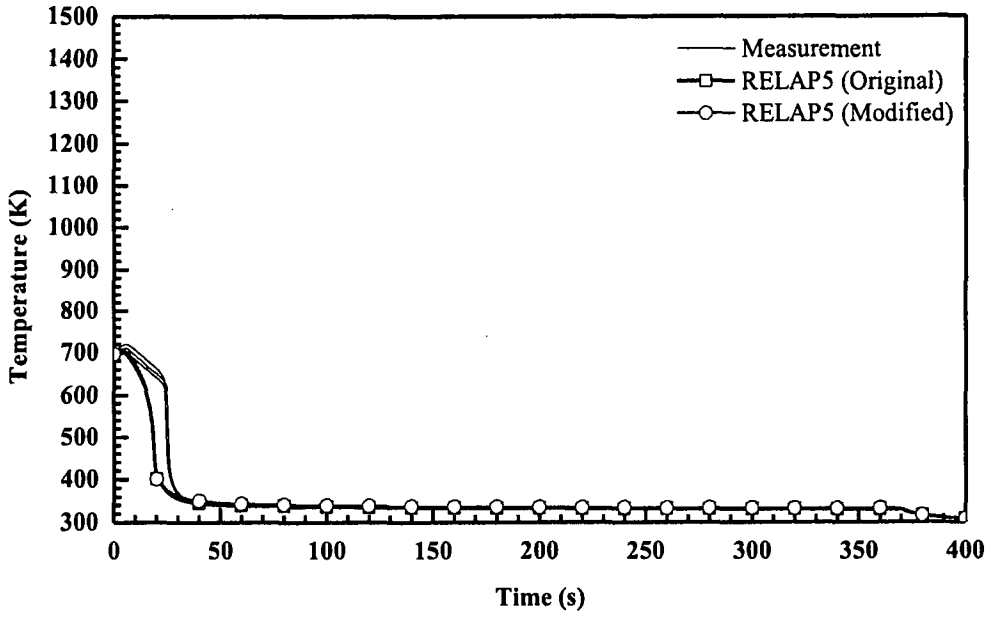

Figure 101. Rod Clad Temperatures at 2 ft from Heated Bottom for Test 31108

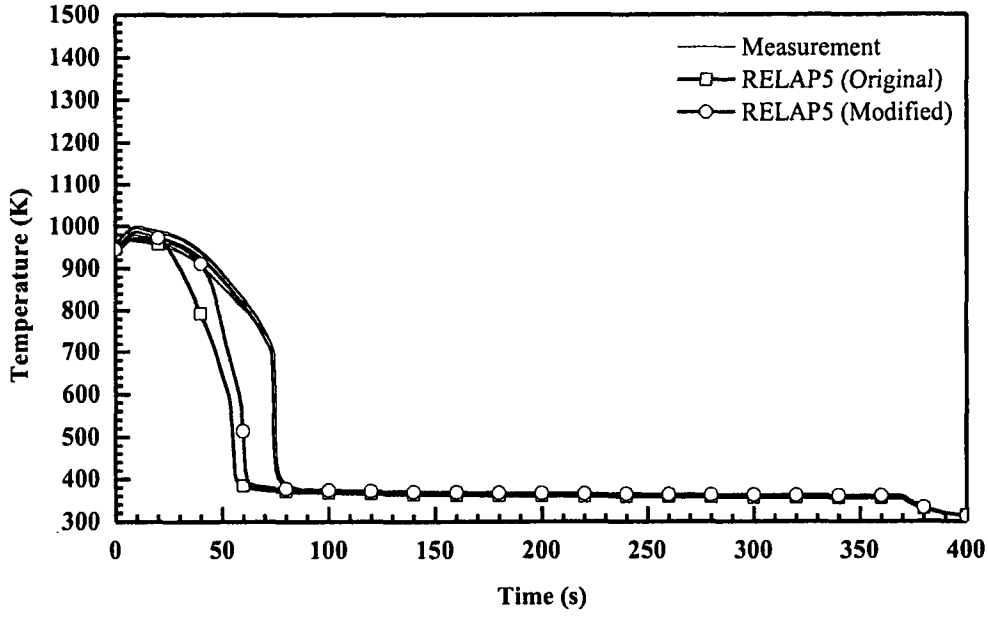

Figure 102. Rod Clad Temperatures at 4 ft from Heated Bottom for Test 31108

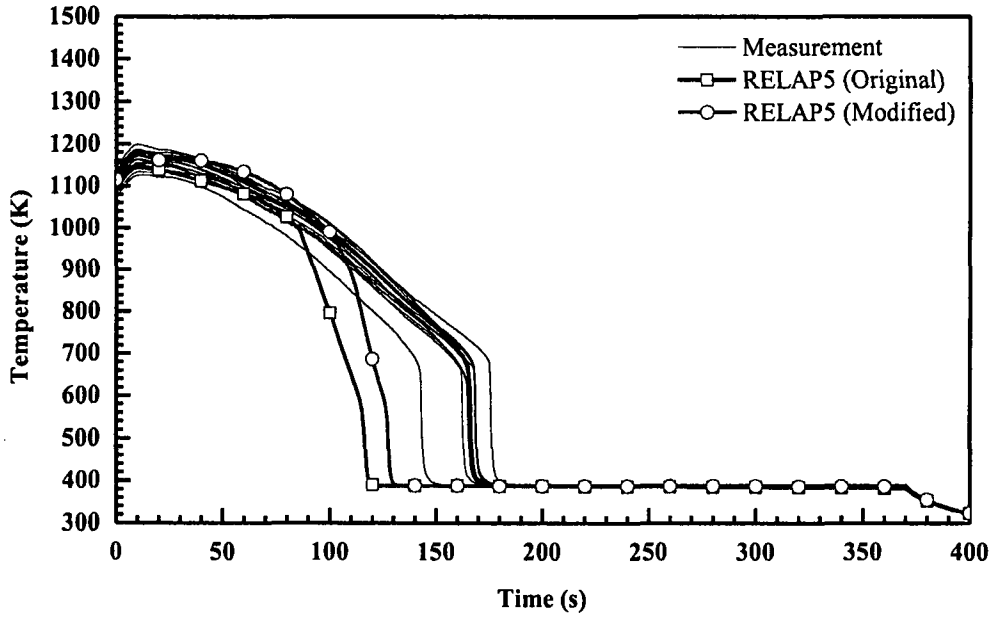

Figure 103. Rod Clad Temperatures at 6 ft from Heated Bottom for Test 31108

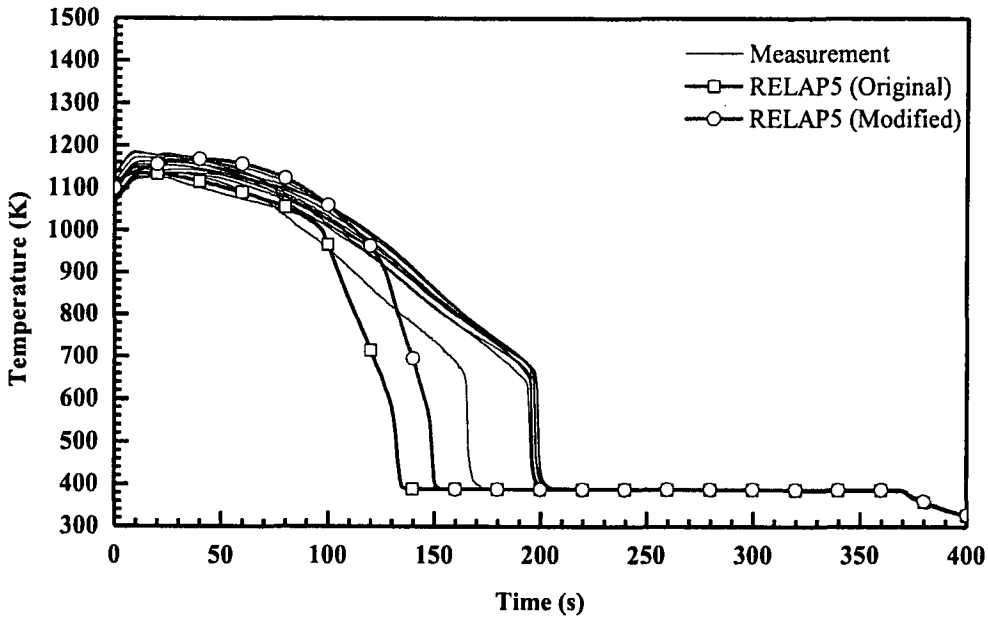

Figure 104. Rod Clad Temperatures at 6.5 ft from Heated Bottom for Test 31108

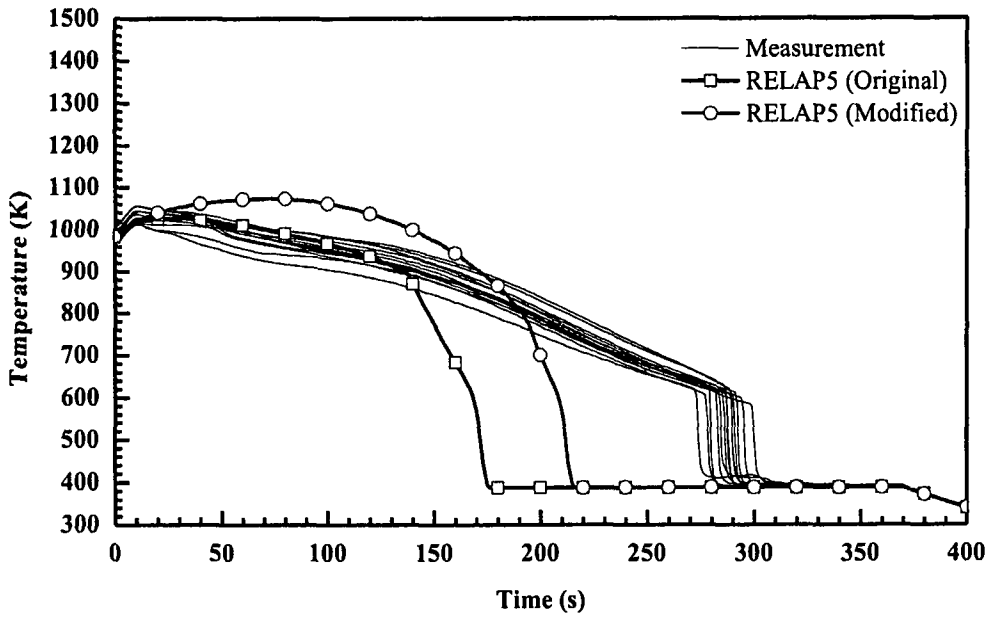

Figure 105. Rod Clad Temperatures at 8 ft from Heated Bottom for Test 31108

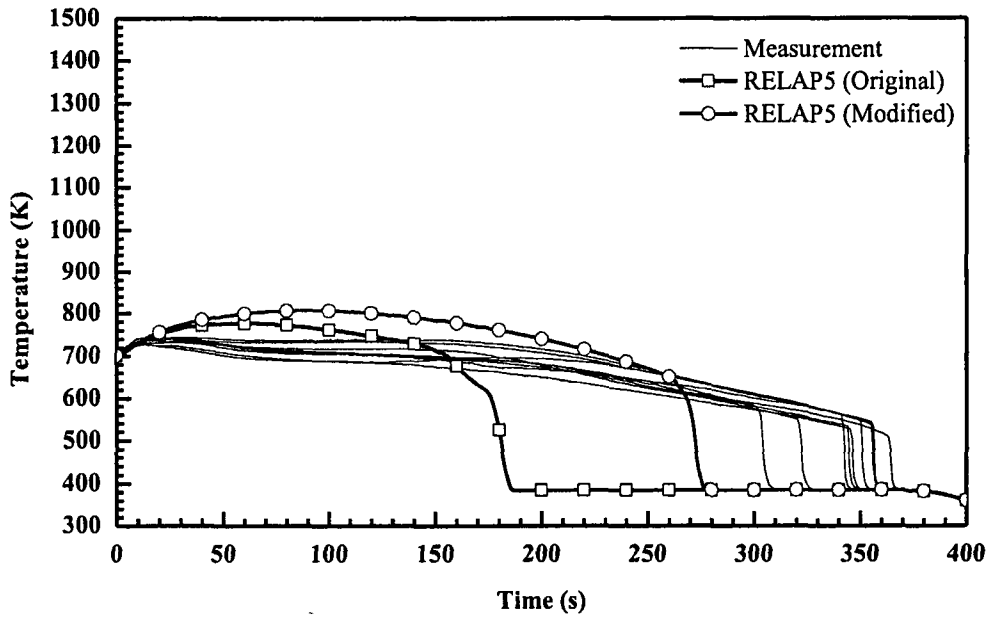

Figure 106. Rod Clad Temperatures at 10 ft from Heated Bottom for Test 31108

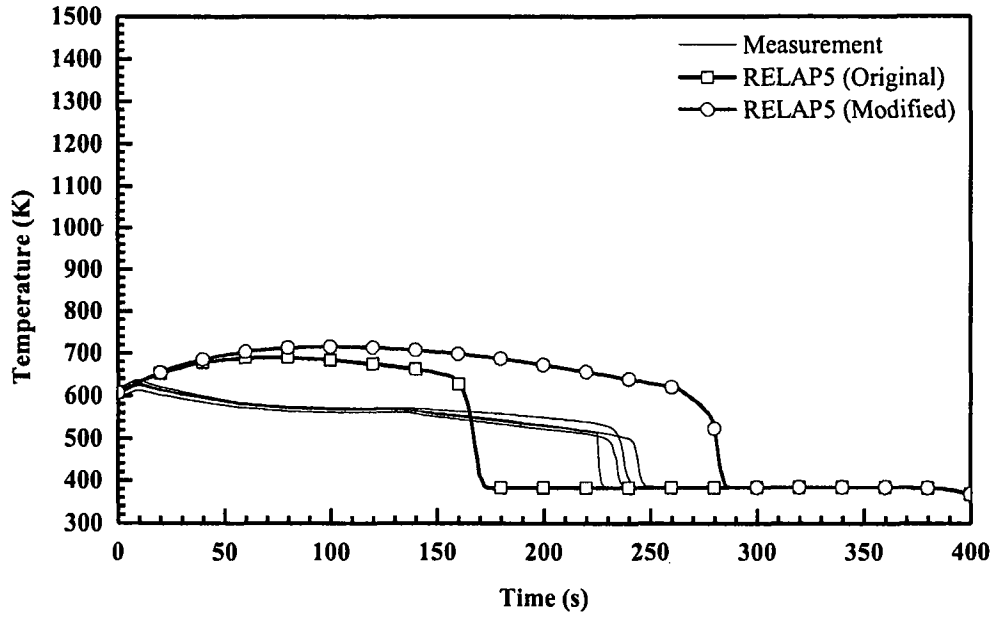

Figure 107. Rod Clad Temperatures at 11 ft from Heated Bottom for Test 31108

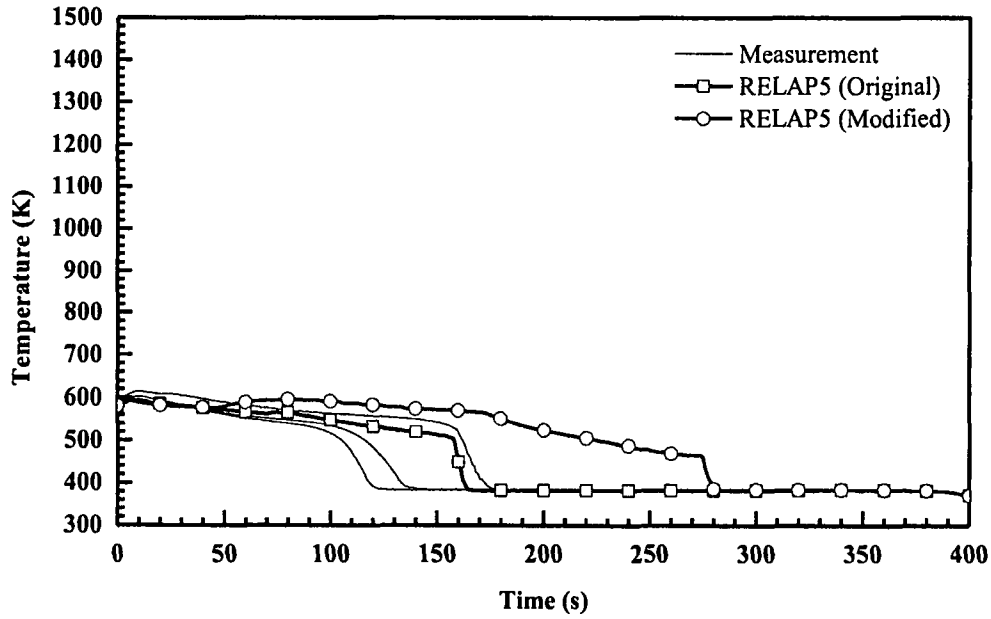

Figure 108. Rod Clad Temperatures at 11.5 ft from Heated Bottom for Test 31108

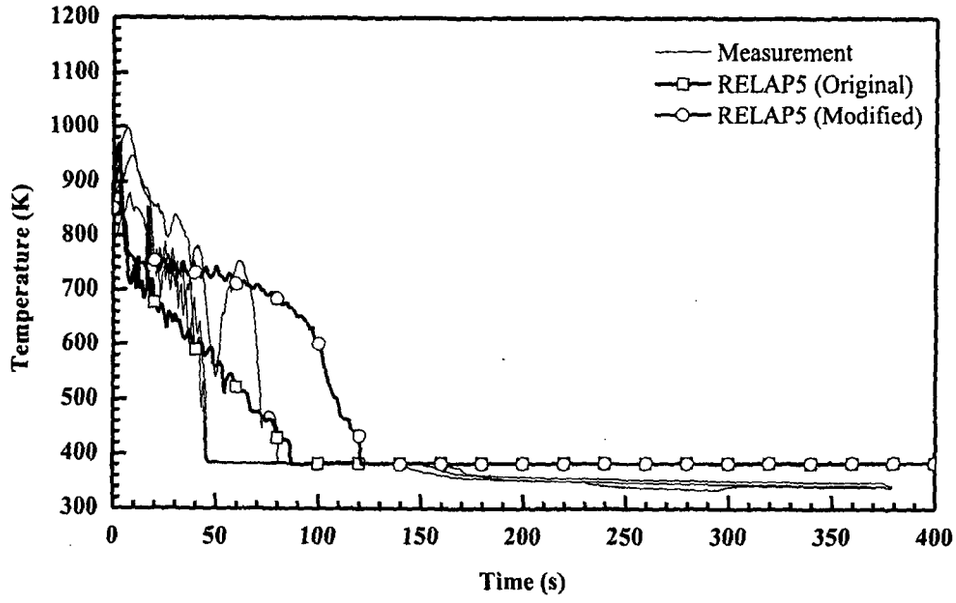

Figure 109. Vapor Temperatures at 6 ft from Heated Bottom for Test 31108

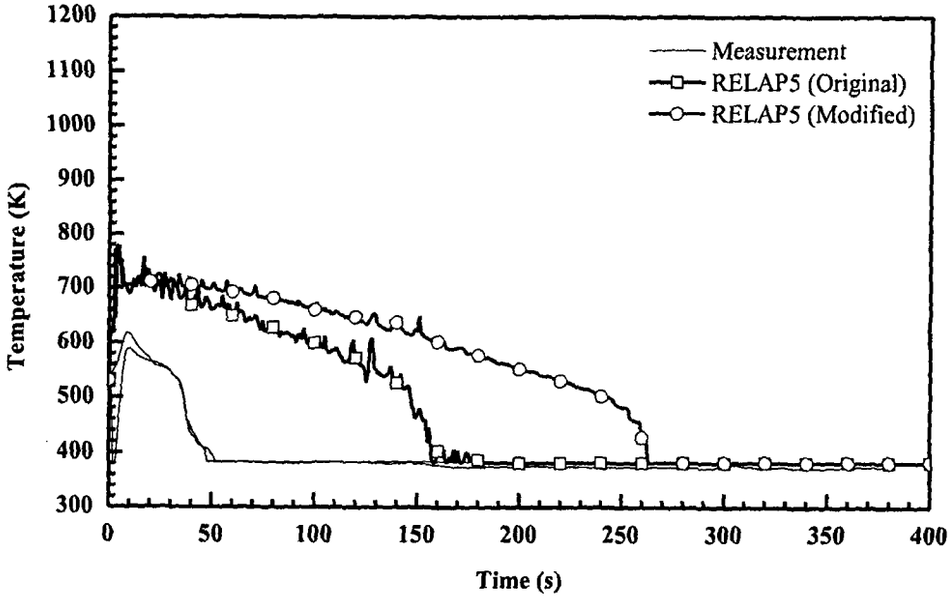

Figure 110. Vapor Temperatures at 10 ft from Heated Bottom for Test 31108

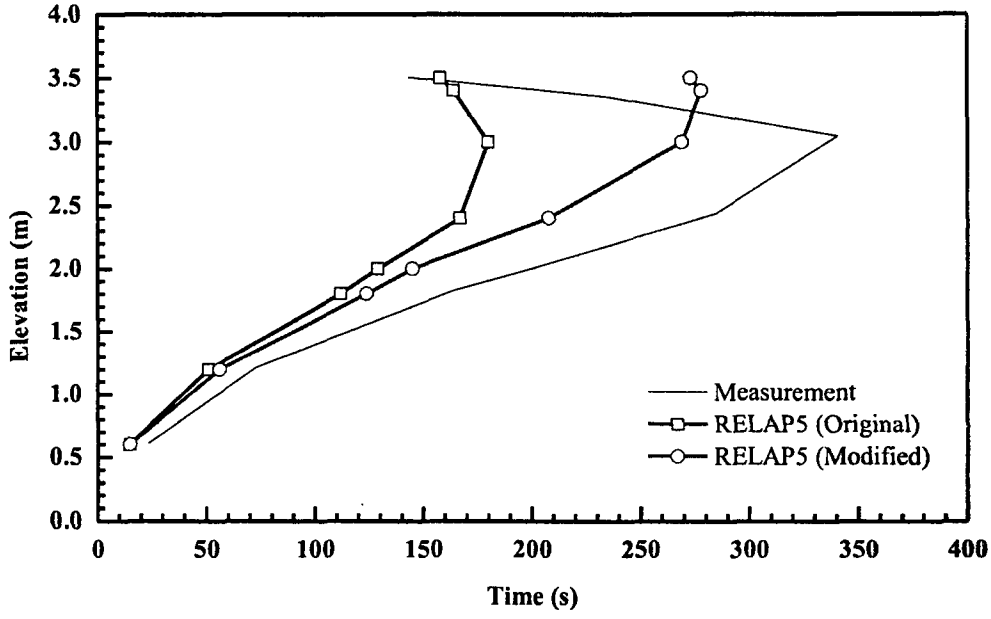

Figure 111. Quench Profile as a Function of Time for Test 31108

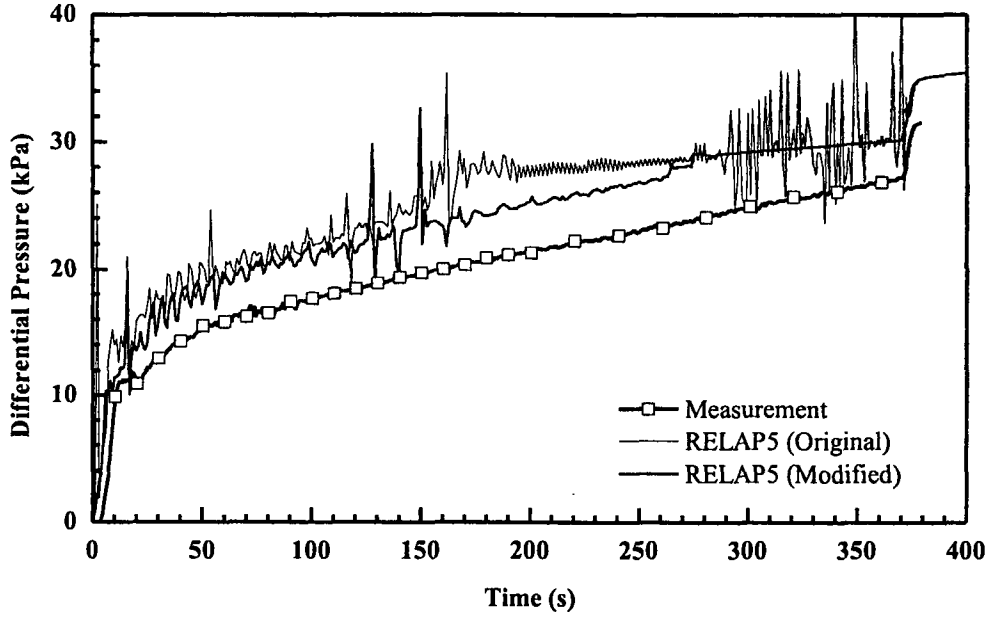

Figure 112. Differential Pressure for the Entire 12 ft Core for Test 31108

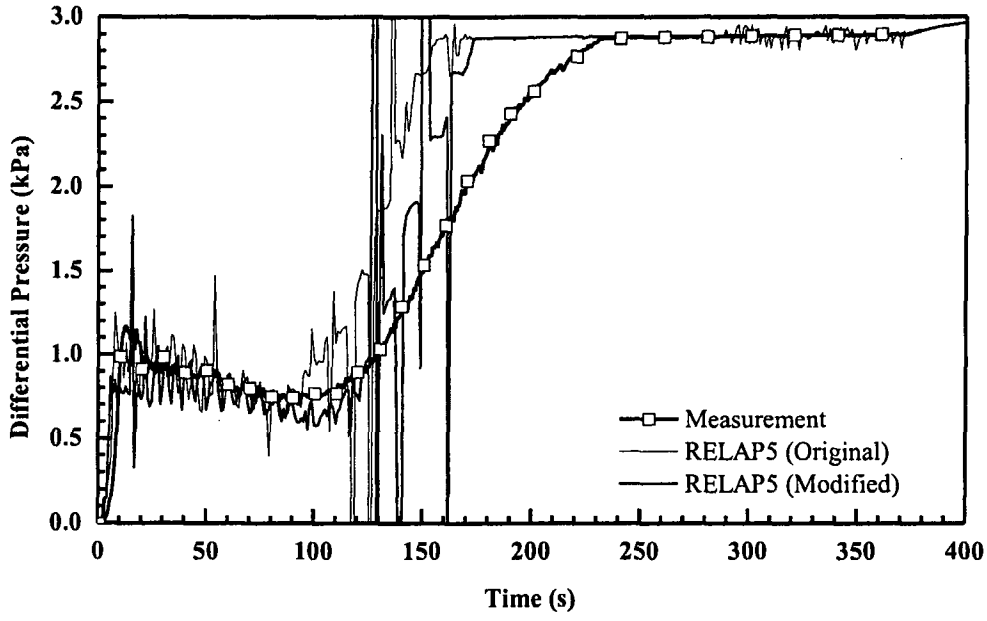

Figure 113. Differential Pressure at 6~7 ft Elevation for Test 31108

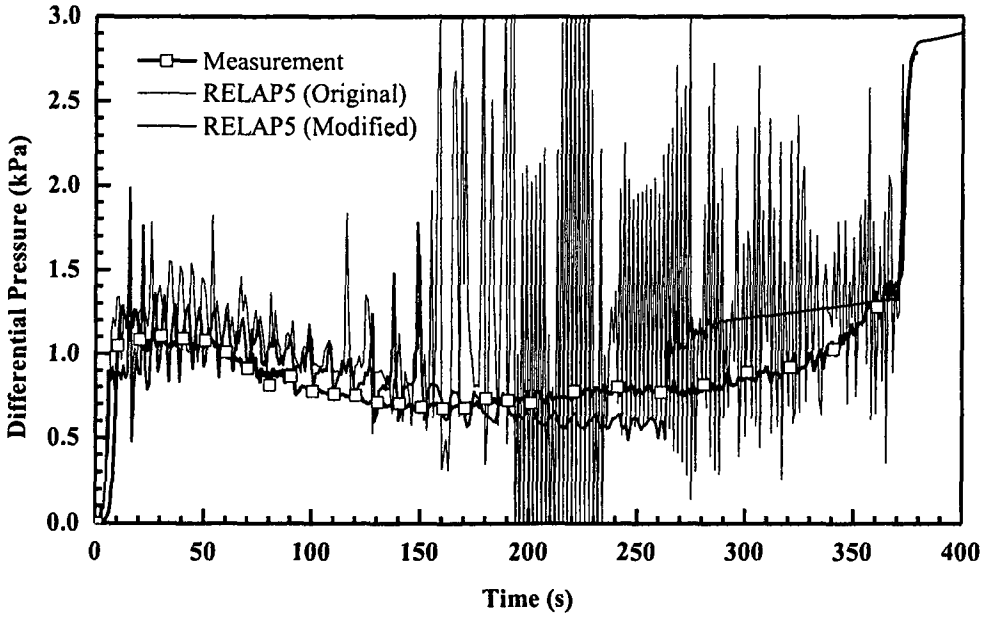

Figure 114. Differential Pressure at 10~11 ft Elevation for Test 31108

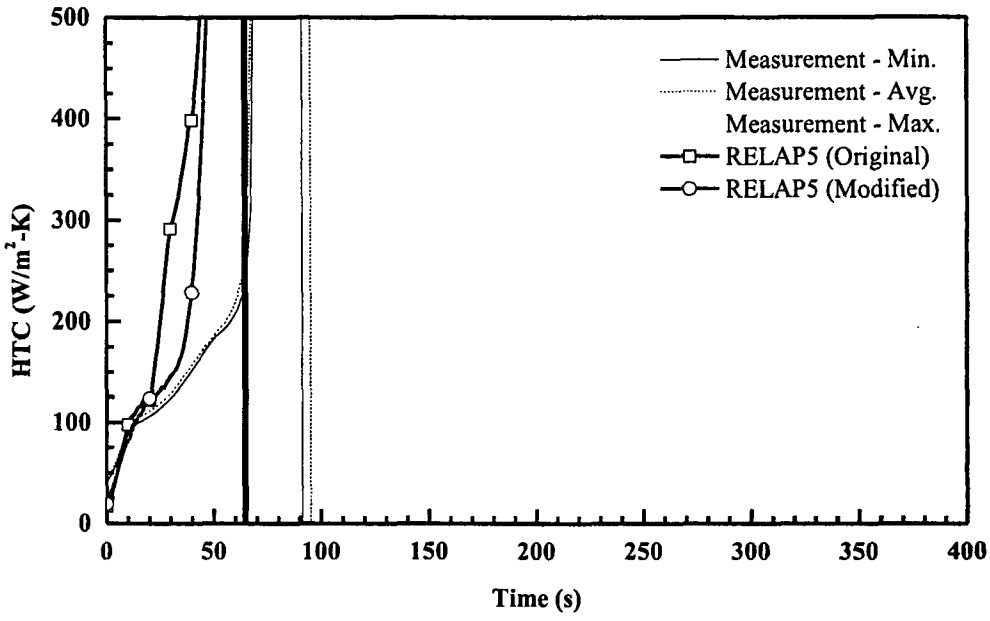

Figure 115. Heat Transfer Coefficient at 4 ft from Heated Bottom for Test 31108

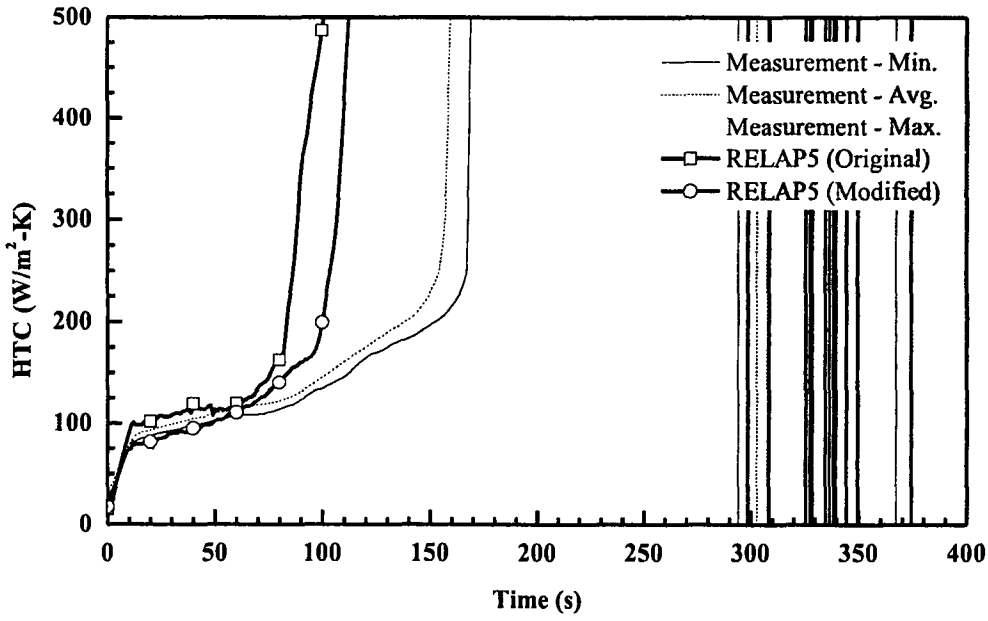

Figure 116. Heat Transfer Coefficient at 6 ft from Heated Bottom for Test 31108

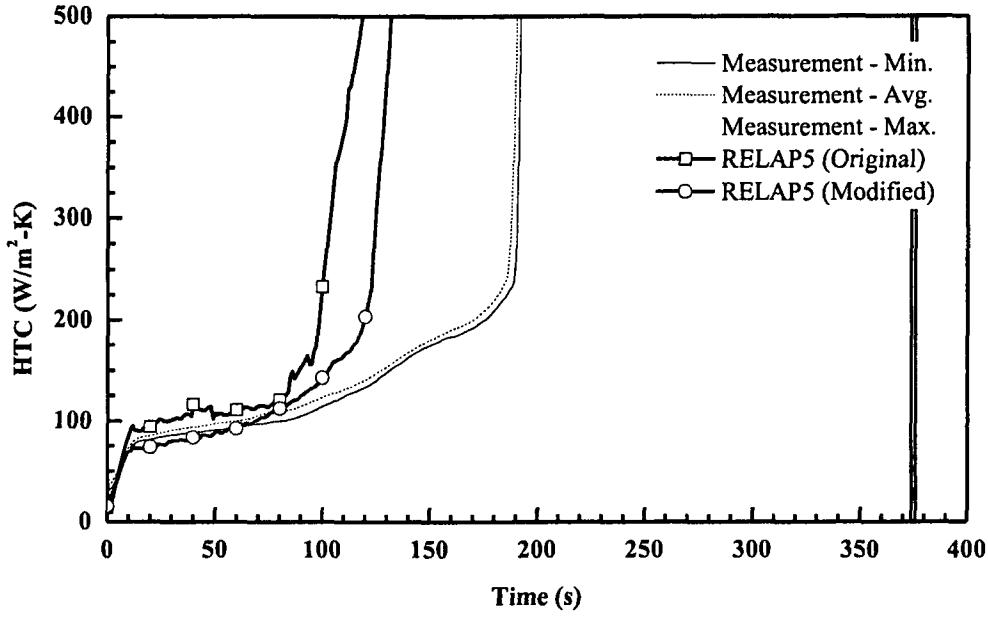

Figure 117. Heat Transfer Coefficient at 6.5 ft from Heated Bottom for Test 31108

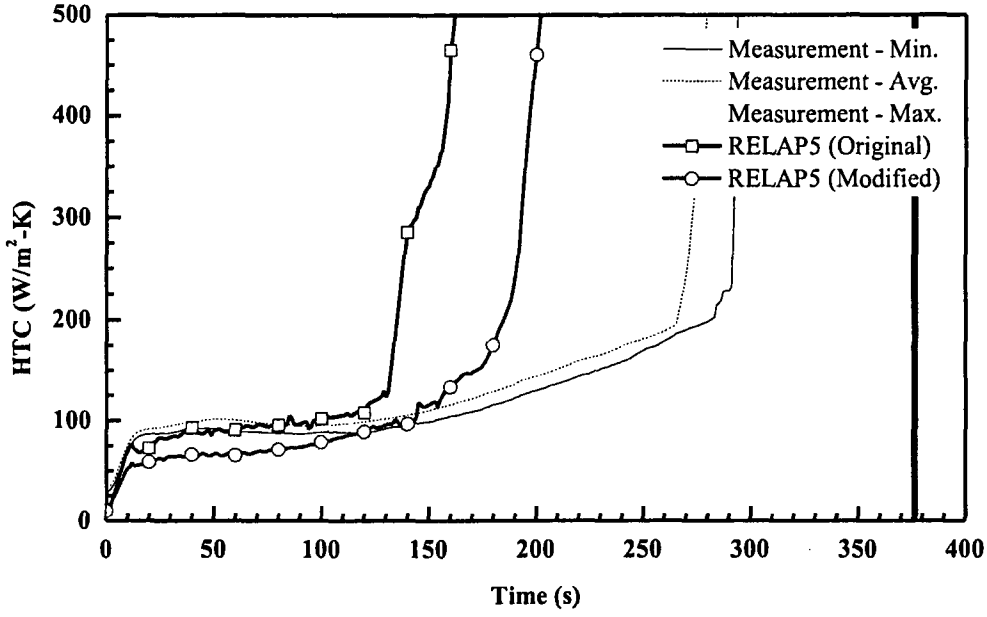

Figure 118. Heat Transfer Coefficient at 8 ft from Heated Bottom for Test 31108

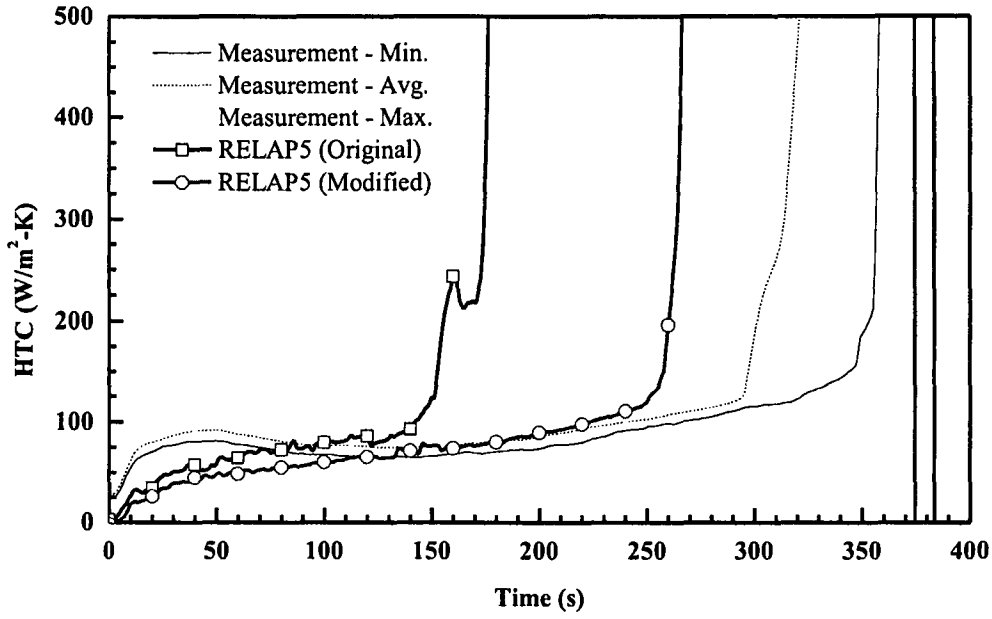

Figure 119. Heat Transfer Coefficient at 10 ft from Heated Bottom for Test 31108

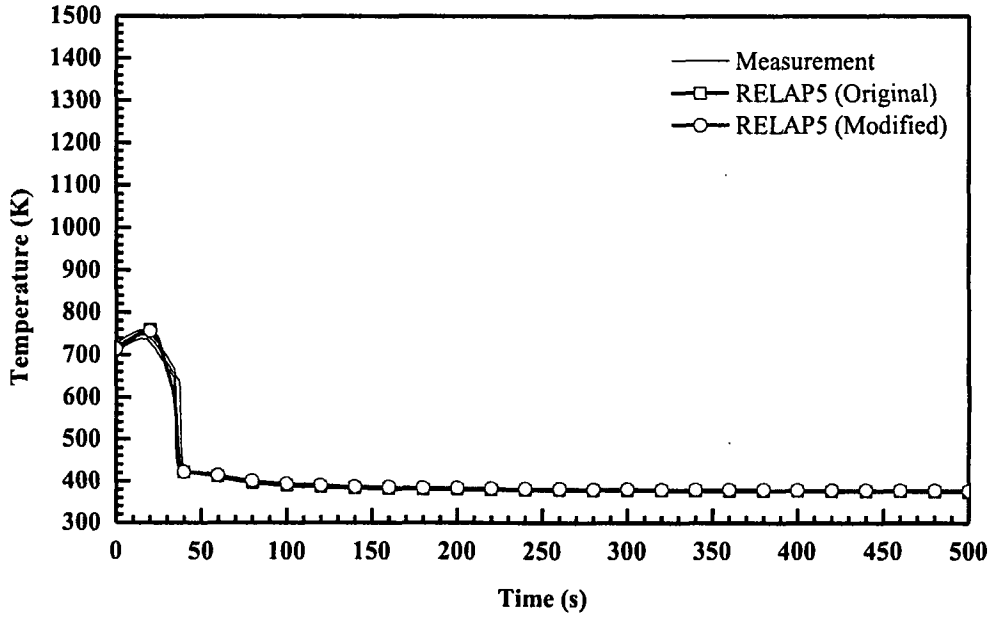

Figure 120. Rod Clad Temperatures at 2 ft from Heated Bottom for Test 32013

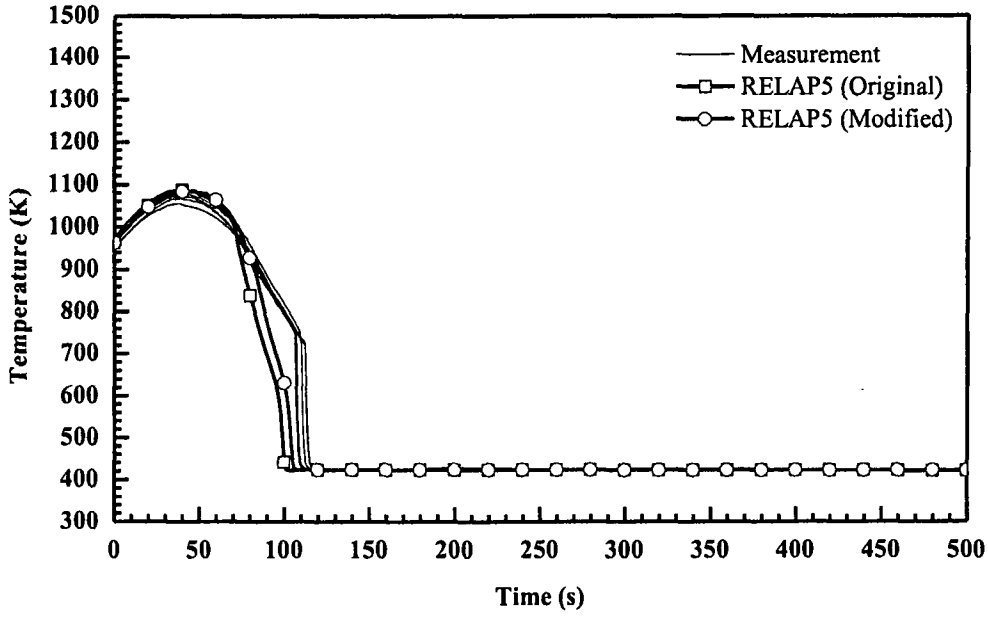

Figure 121. Rod Clad Temperatures at 4 ft from Heated Bottom for Test 32013

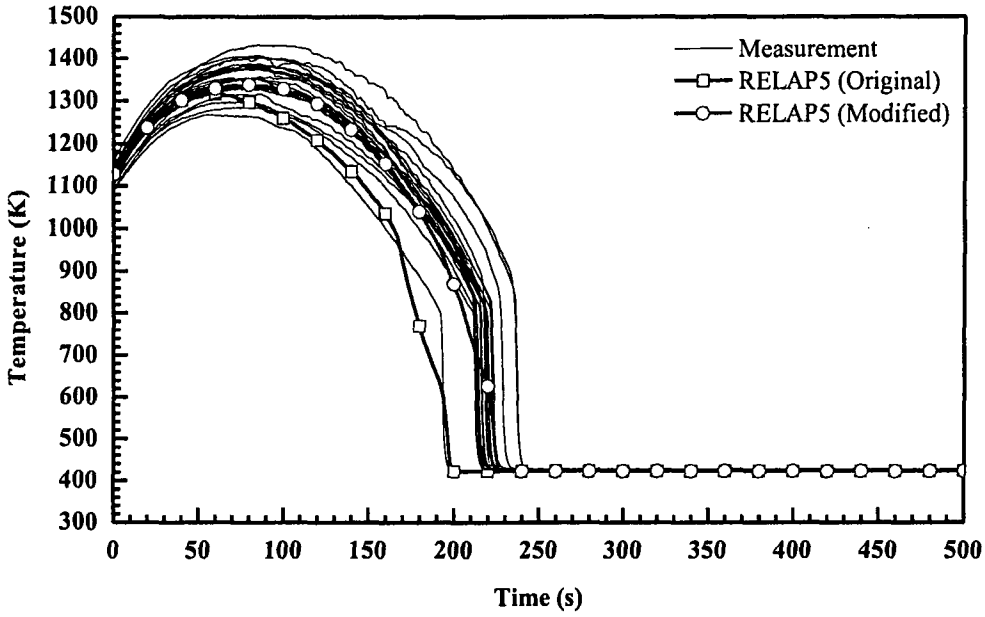

Figure 122. Rod Clad Temperatures at 6 ft from Heated Bottom for Test 32013

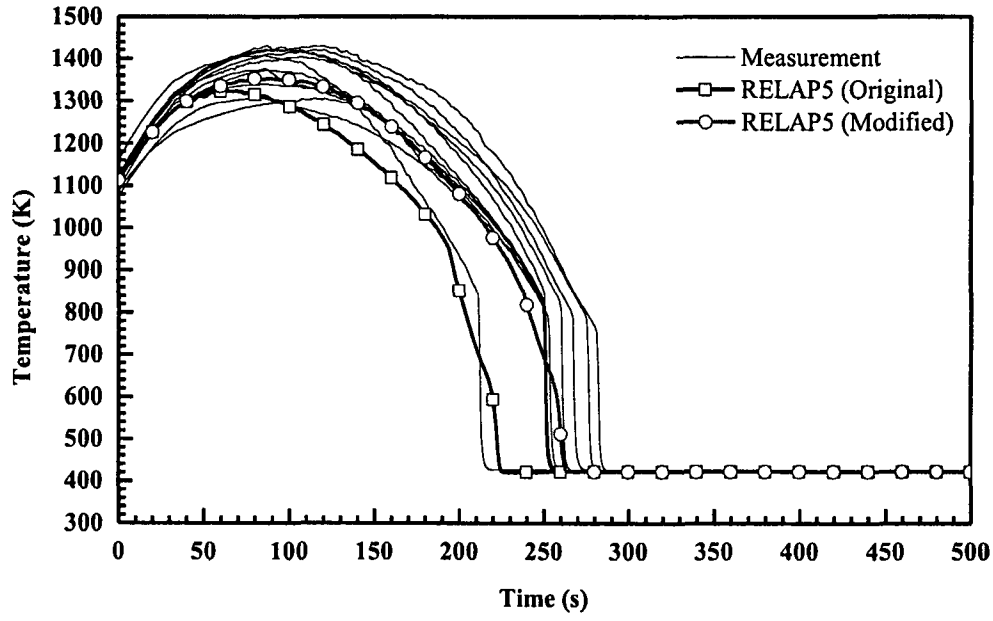

Figure 123. Rod Clad Temperatures at 6.5 ft from Heated Bottom for Test 32013

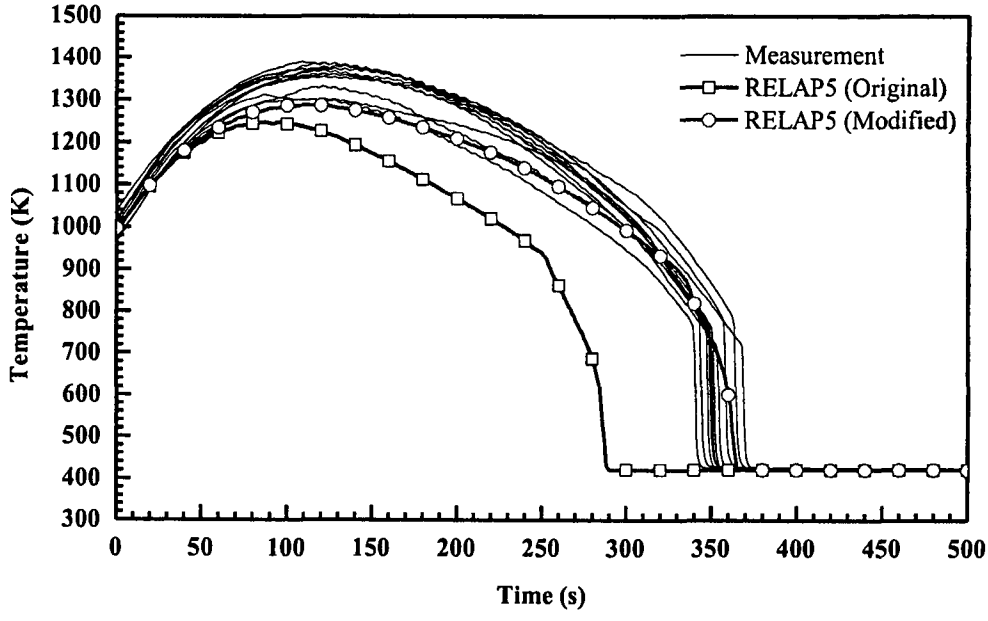

Figure 124. Rod Clad Temperatures at 8 ft from Heated Bottom for Test 32013

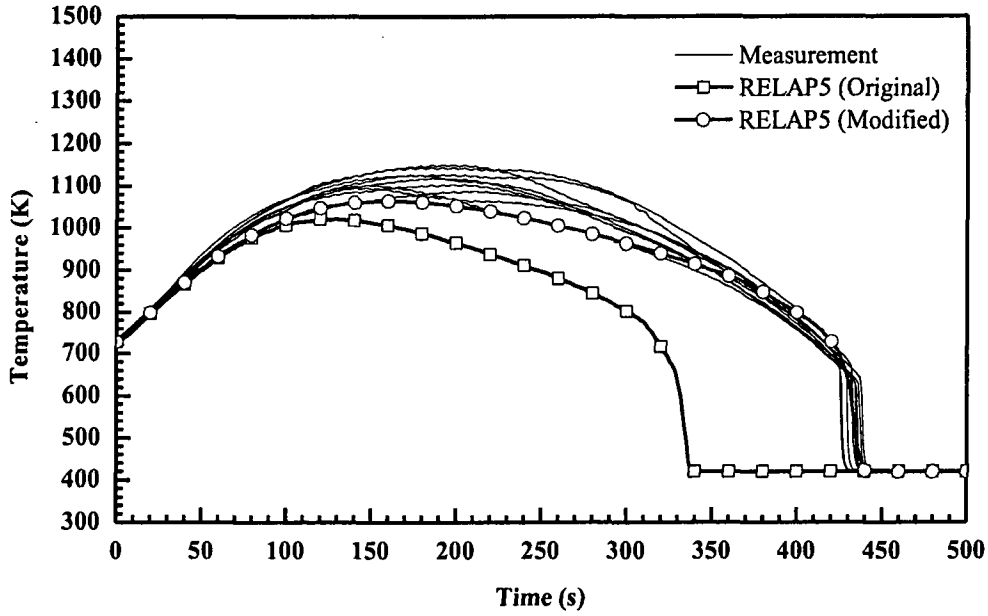

Figure 125. Rod Clad Temperatures at 10 ft from Heated Bottom for Test 32013

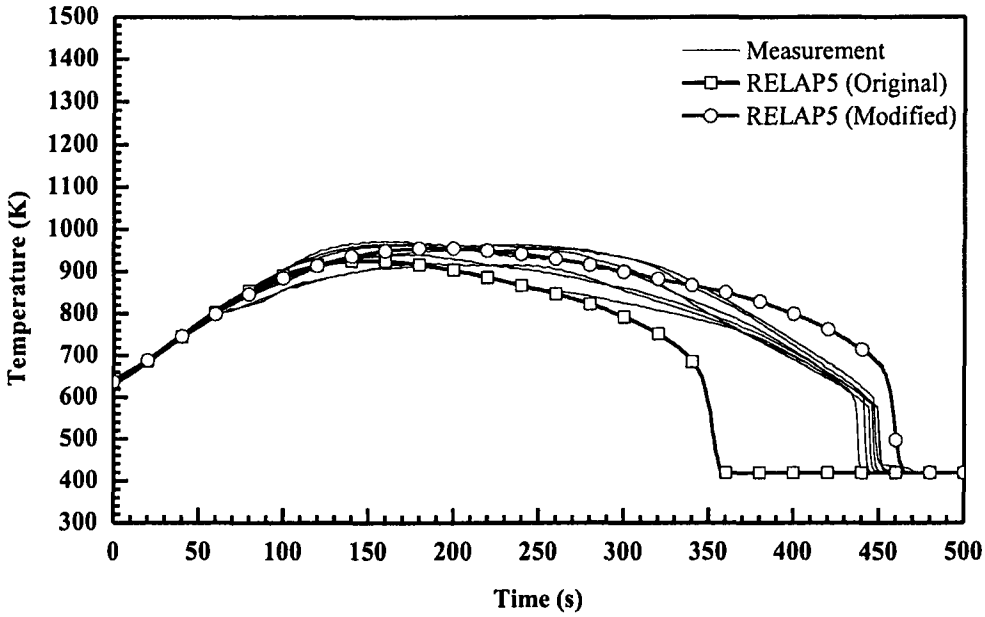

Figure 126. Rod Clad Temperatures at 11 ft from Heated Bottom for Test 32013

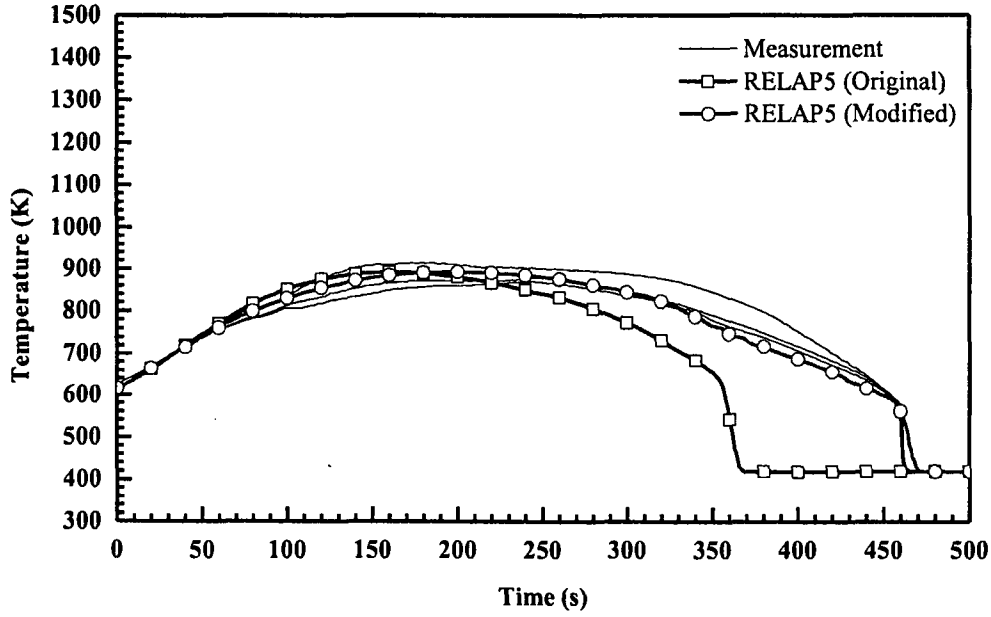

Figure 127. Rod Clad Temperatures at 11.5 ft from Heated Bottom for Test 32013

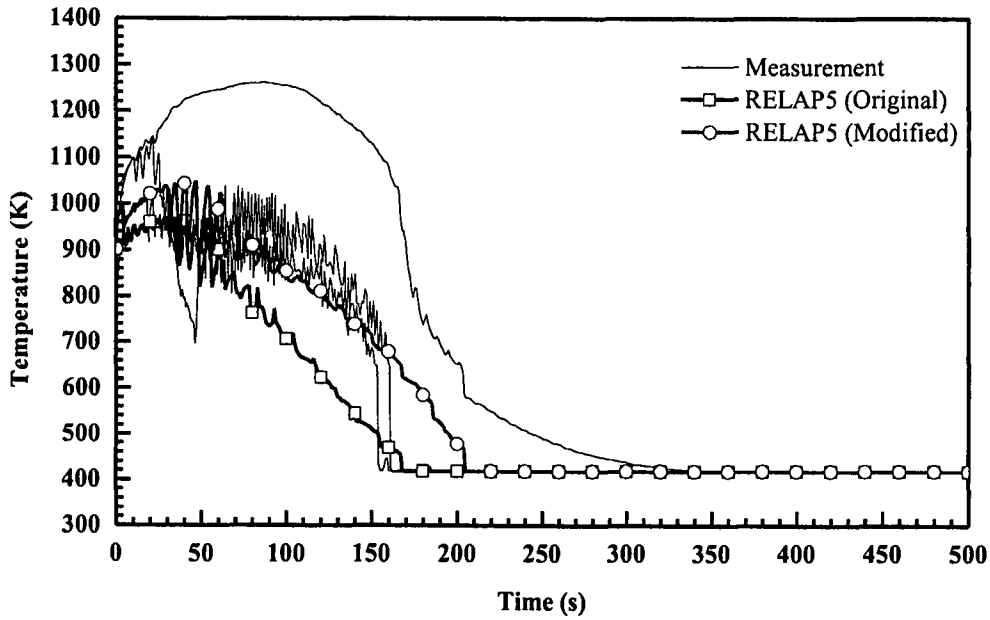

Figure 128. Vapor Temperatures at 6 ft from Heated Bottom for Test 32013

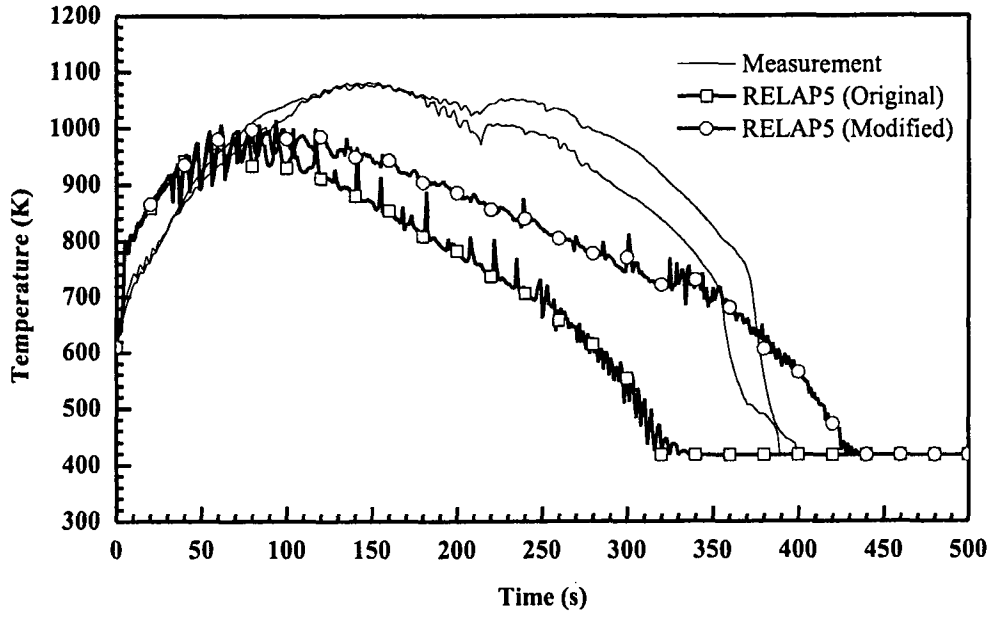

Figure 129. Vapor Temperatures at 10 ft from Heated Bottom for Test 32013

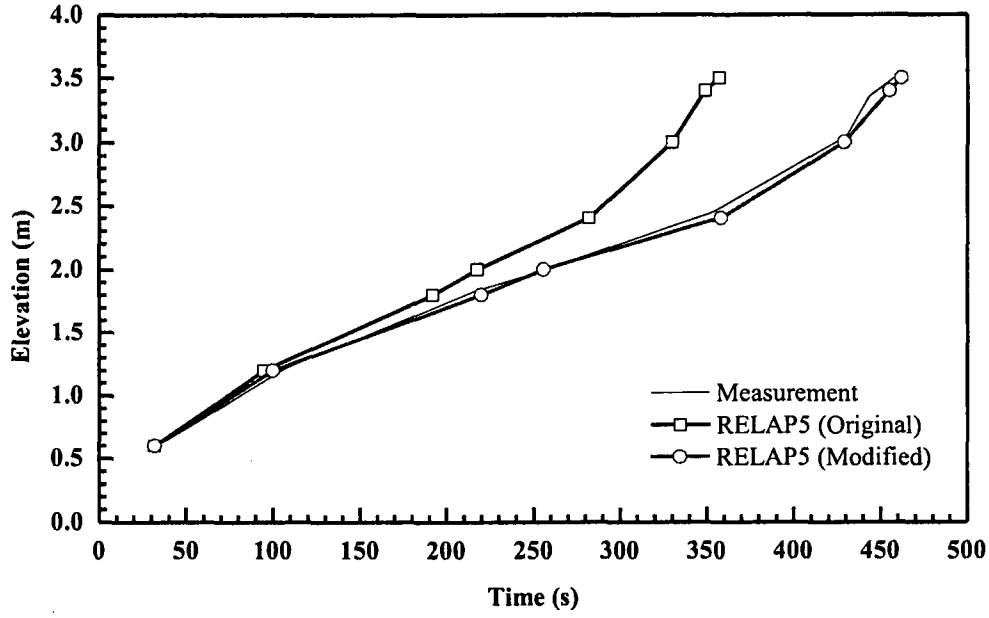

Figure 130. Quench Profile as a Function of Time for Test 32013

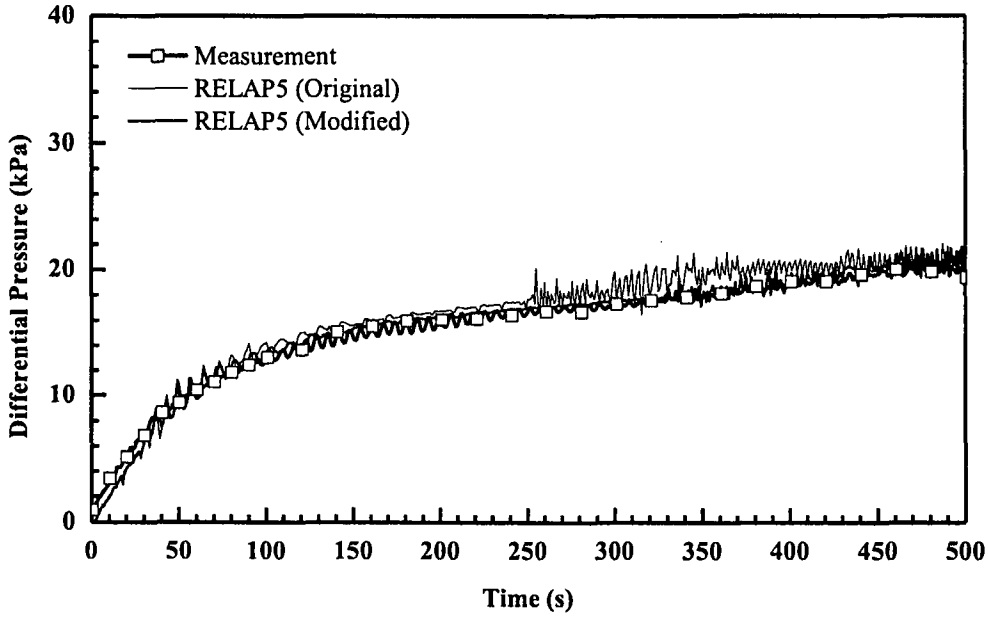

Figure 131. Differential Pressure for the Entire 12 ft Core for Test 32013

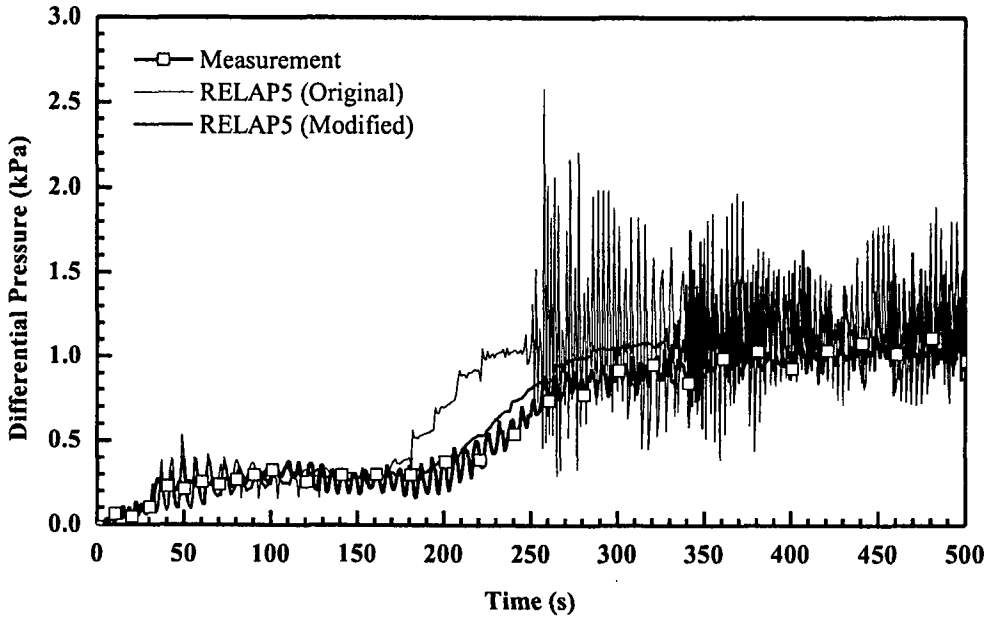

Figure 132. Differential Pressure at 6~7 ft Elevation for Test 32013

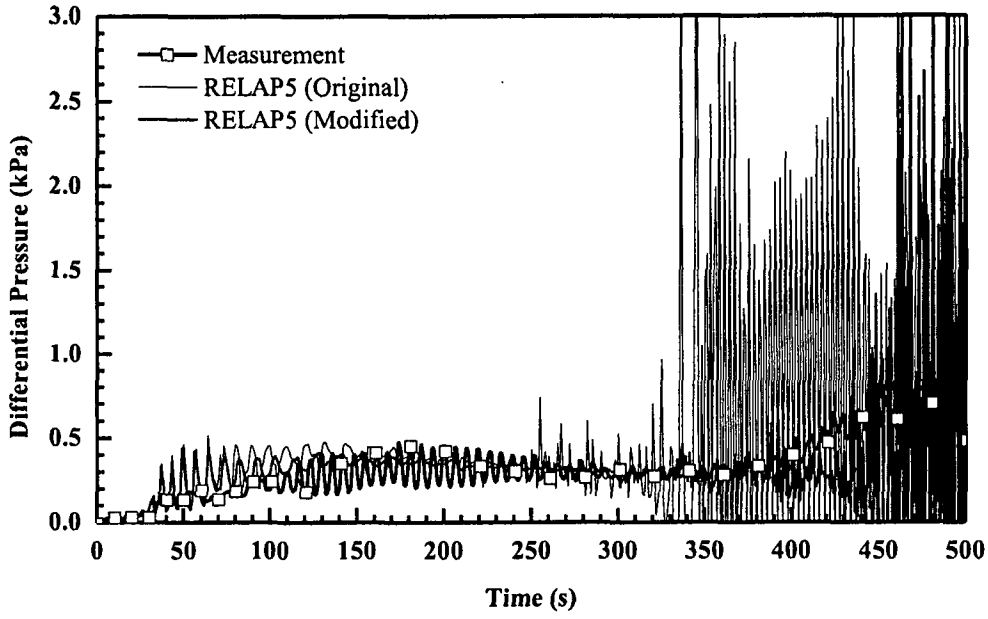

Figure 133. Differential Pressure at 10~11 ft Elevation for Test 32013

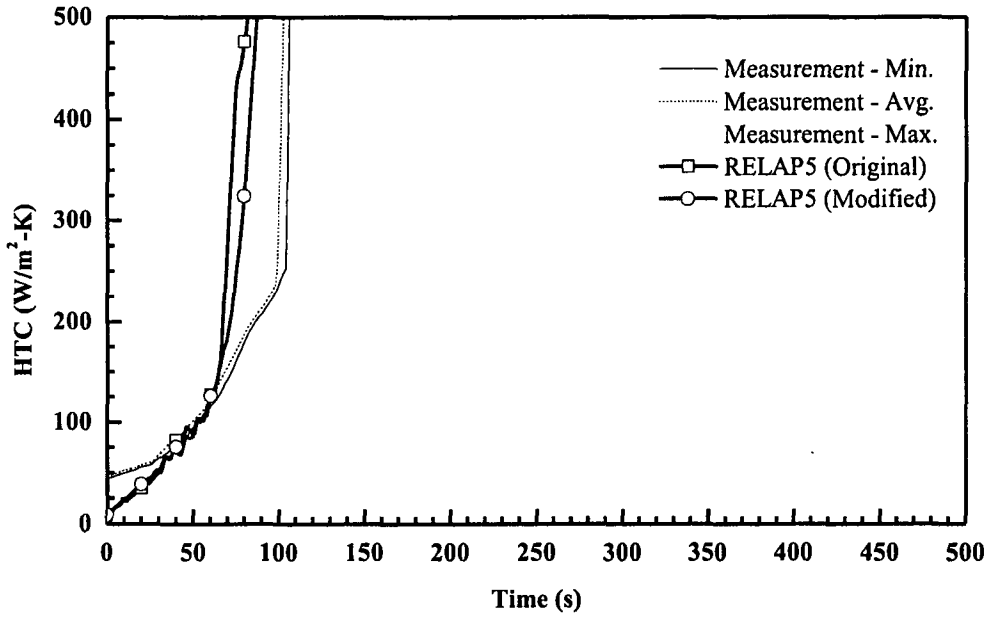

Figure 134. Heat Transfer Coefficient at 4 ft from Heated Bottom for Test 32013

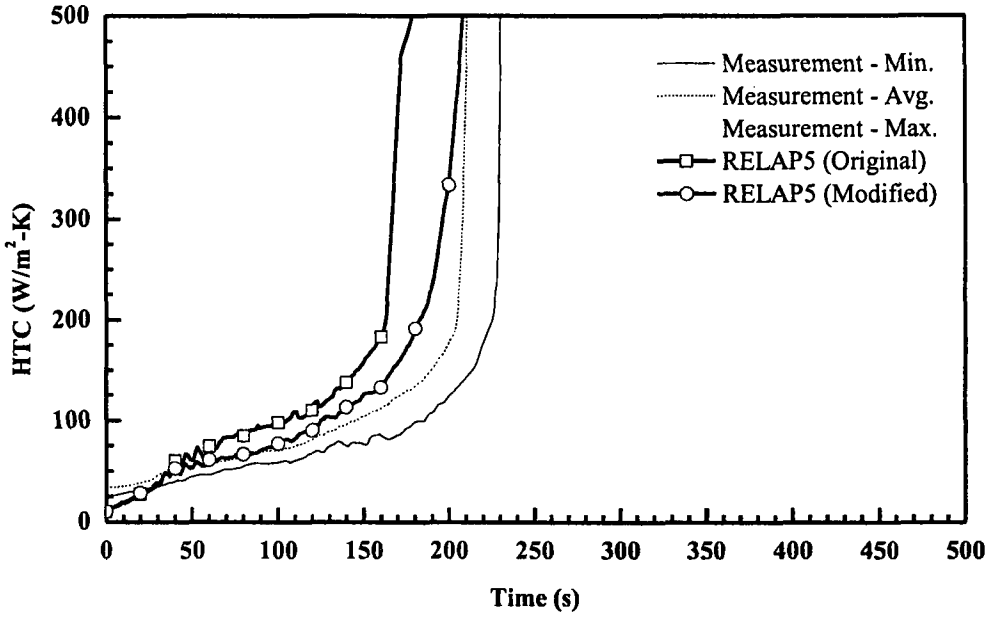

Figure 135. Heat Transfer Coefficient at 6 ft from Heated Bottom for Test 32013

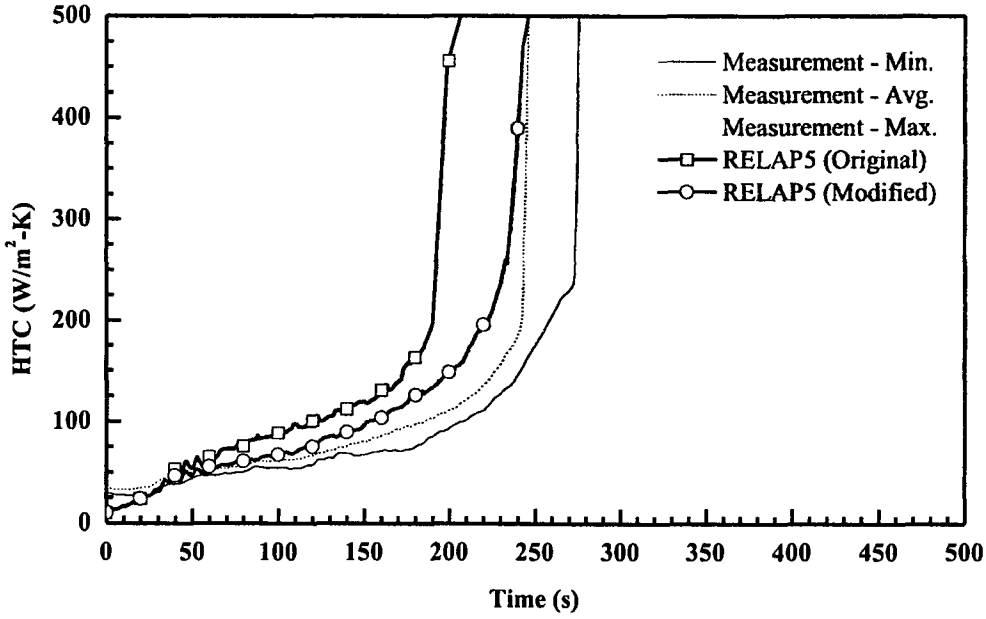

Figure 136. Heat Transfer Coefficient at 6.5 ft from Heated Bottom for Test 32013

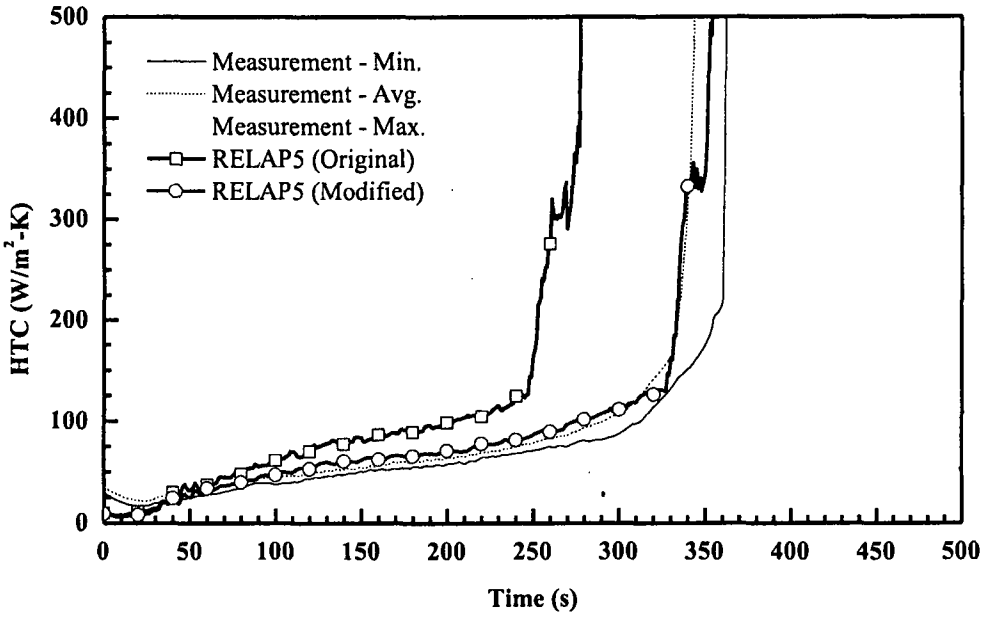

Figure 137. Heat Transfer Coefficient at 8 ft from Heated Bottom for Test 32013

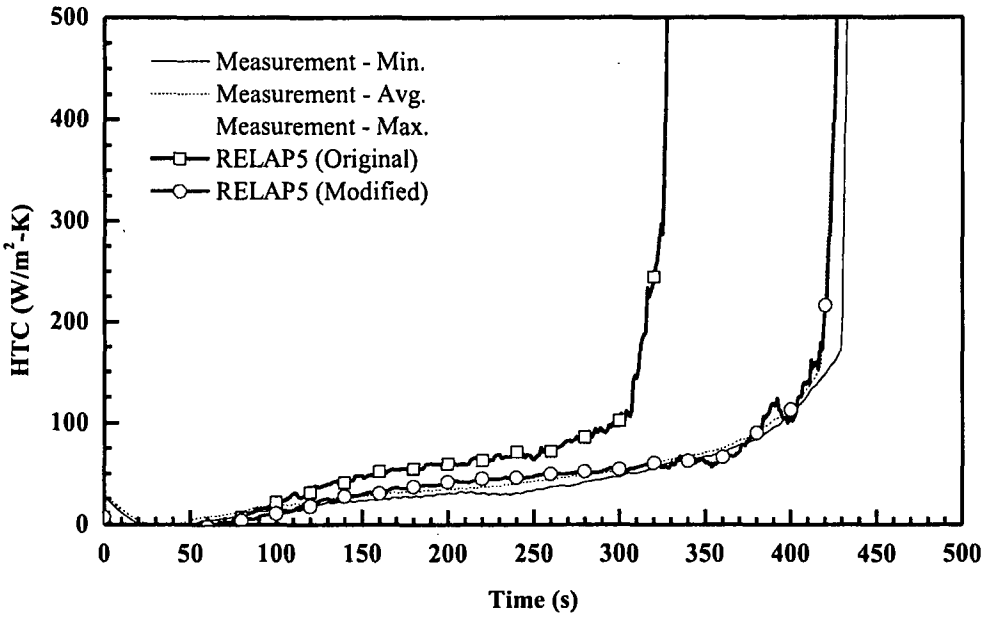

Figure 138. Heat Transfer Coefficient at 10 ft from Heated Bottom for Test 32013

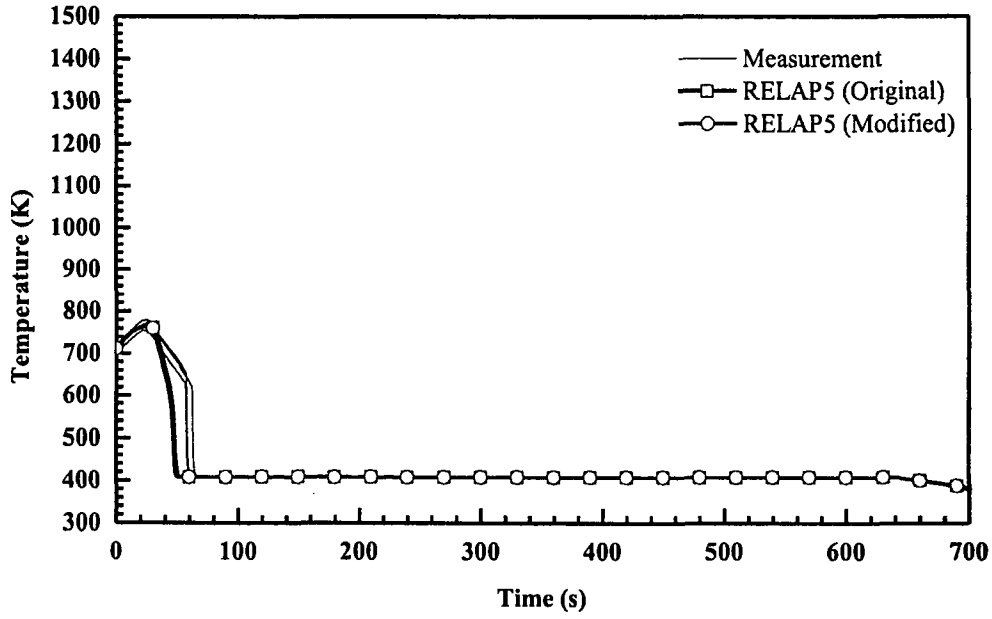

Figure 139. Rod Clad Temperatures at 2 ft from Heated Bottom for Test 32114

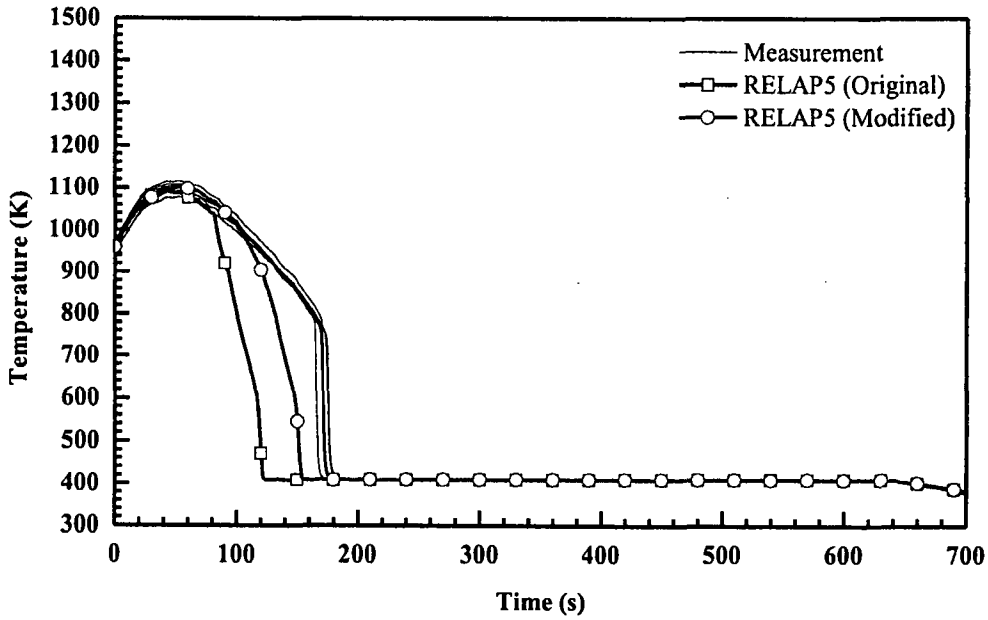

Figure 140. Rod Clad Temperatures at 4 ft from Heated Bottom for Test 32114

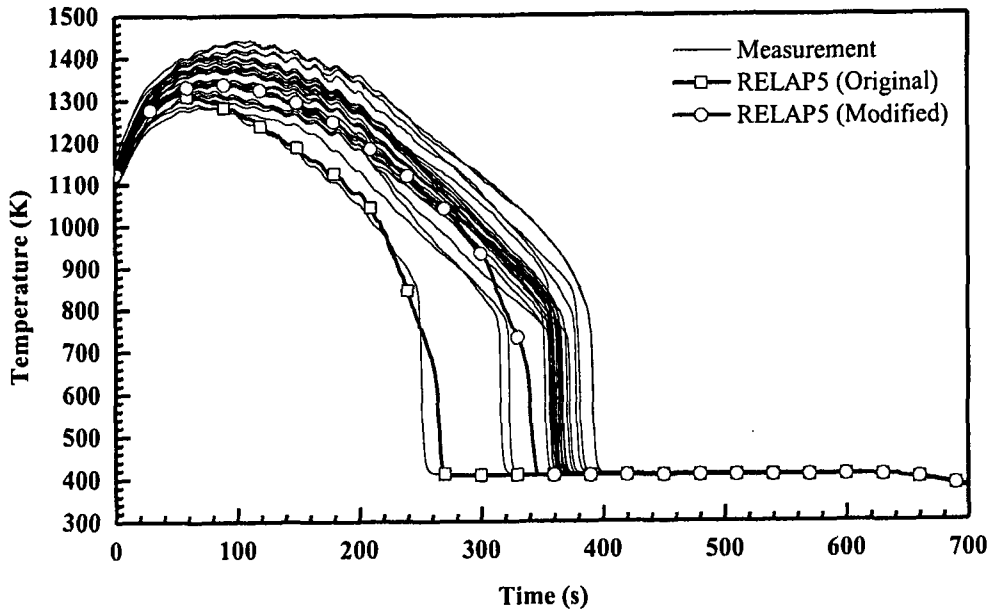

Figure 141. Rod Clad Temperatures at 6 ft from Heated Bottom for Test 32114

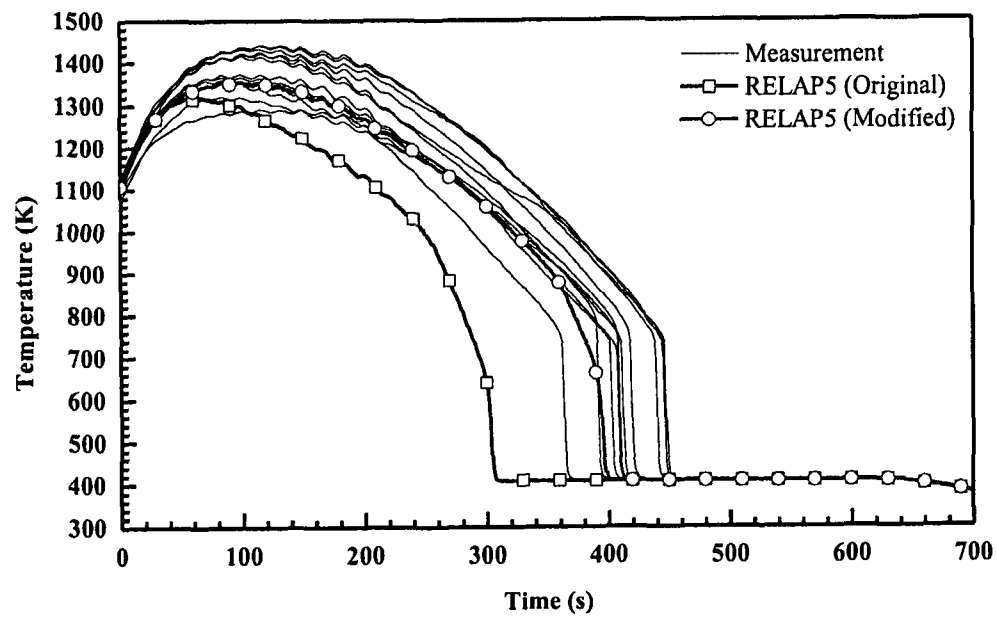

Figure 142. Rod Clad Temperatures at 6.5 ft from Heated Bottom for Test 32114

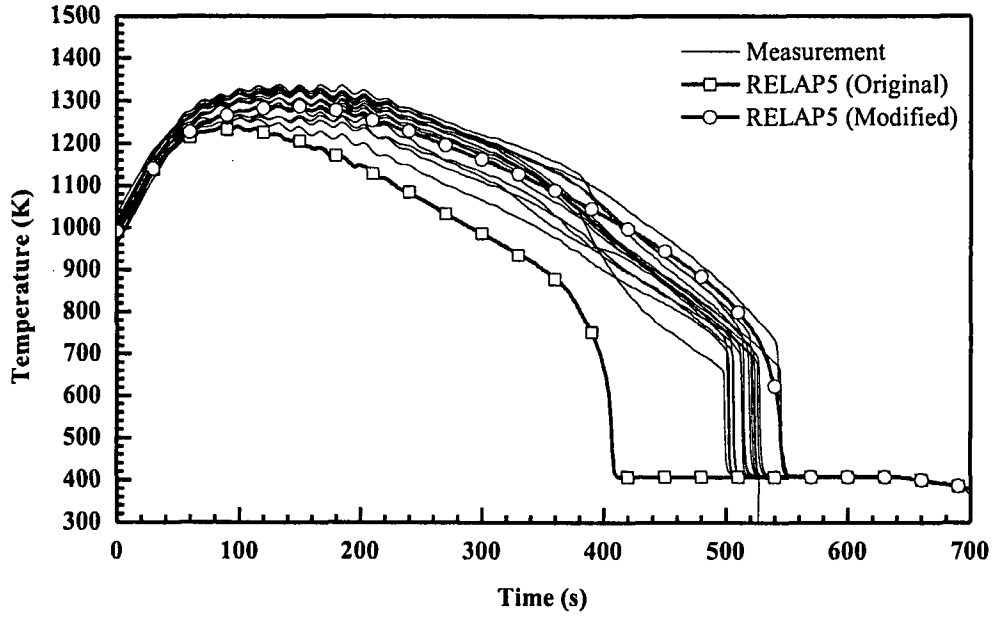

Figure 143. Rod Clad Temperatures at 8 ft from Heated Bottom for Test 32114

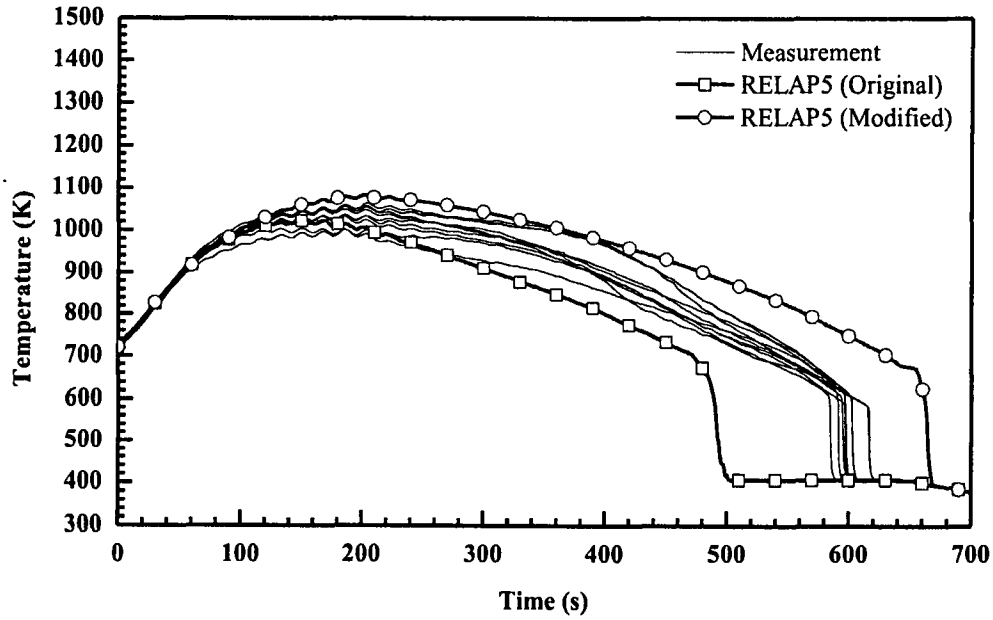

Figure 144. Rod Clad Temperatures at 10 ft from Heated Bottom for Test 32114

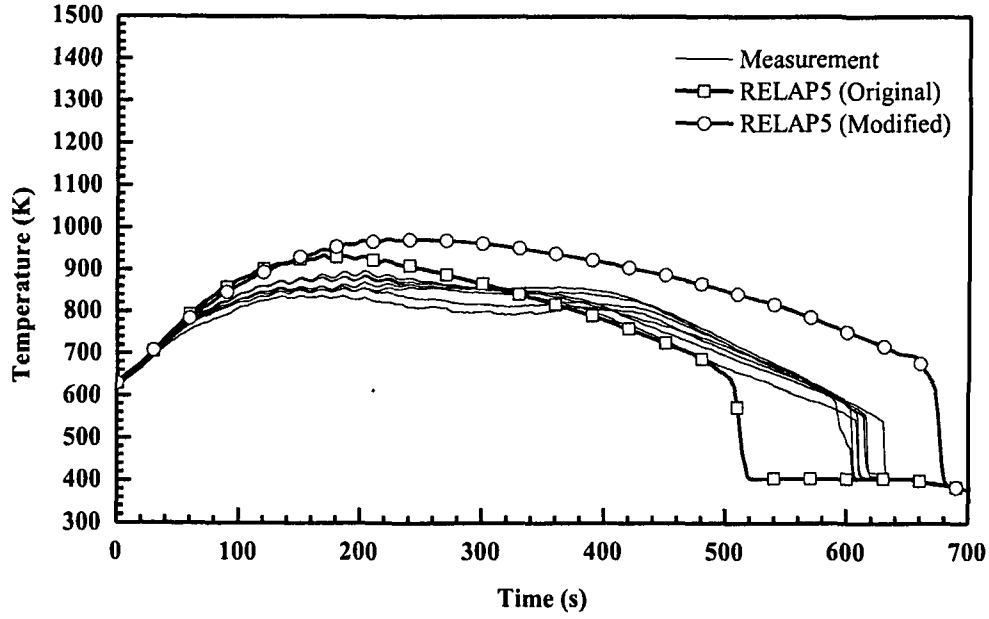

Figure 145. Rod Clad Temperatures at 11 ft from Heated Bottom for Test 32114

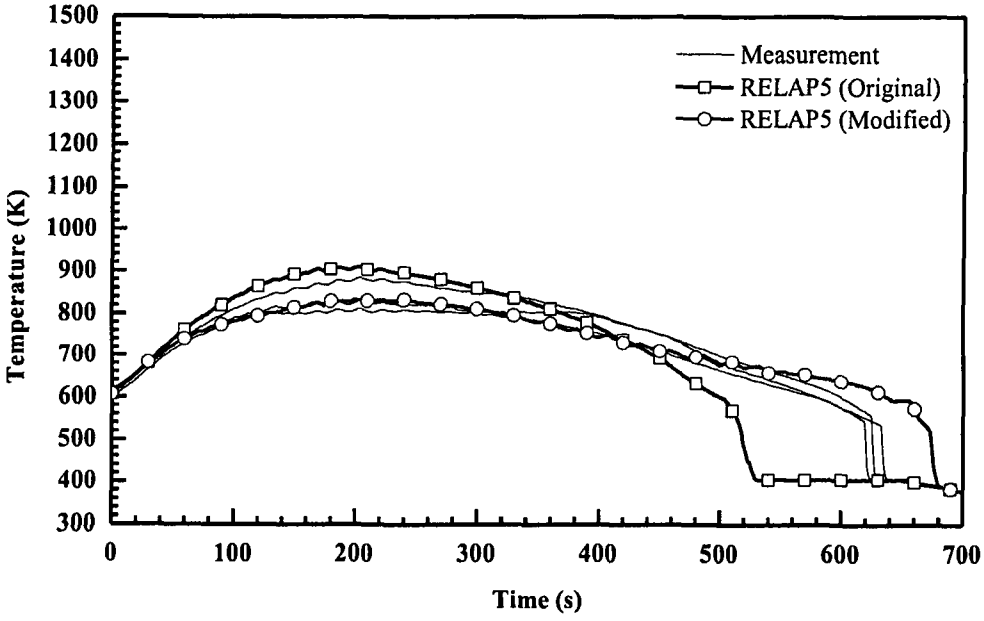

Figure 146. Rod Clad Temperatures at 11.5 ft from Heated Bottom for Test 32114

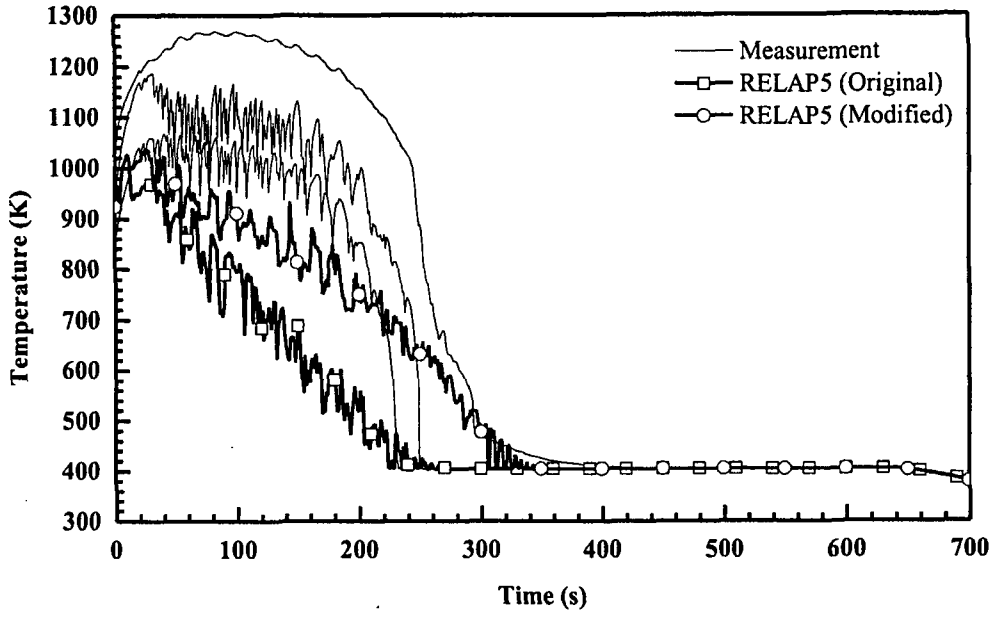

Figure 147. Vapor Temperatures at 6 ft from Heated Bottom for Test 32114

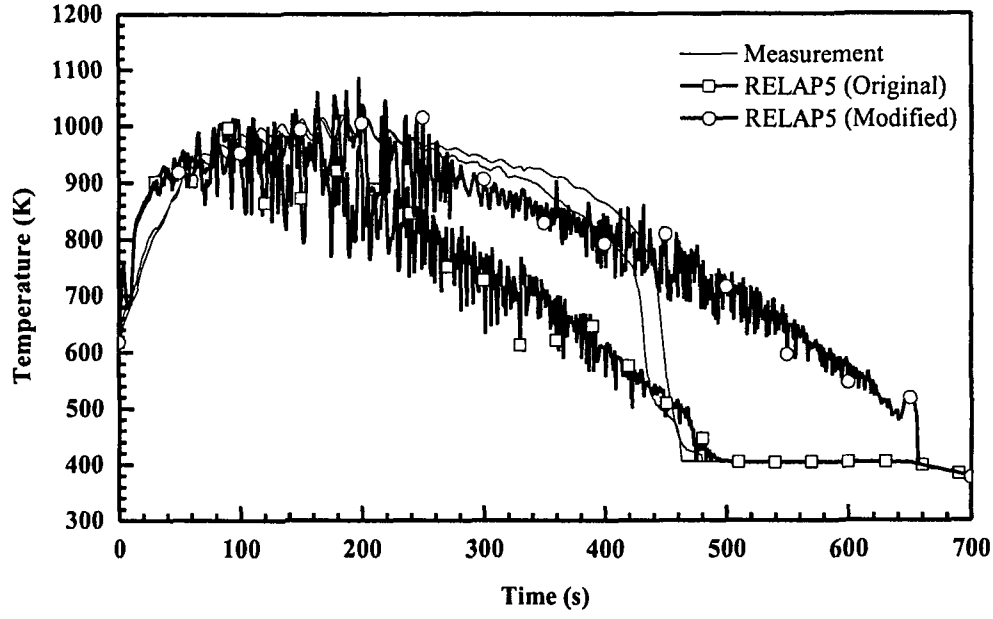

Figure 148. Vapor Temperatures at 10 ft from Heated Bottom for Test 32114

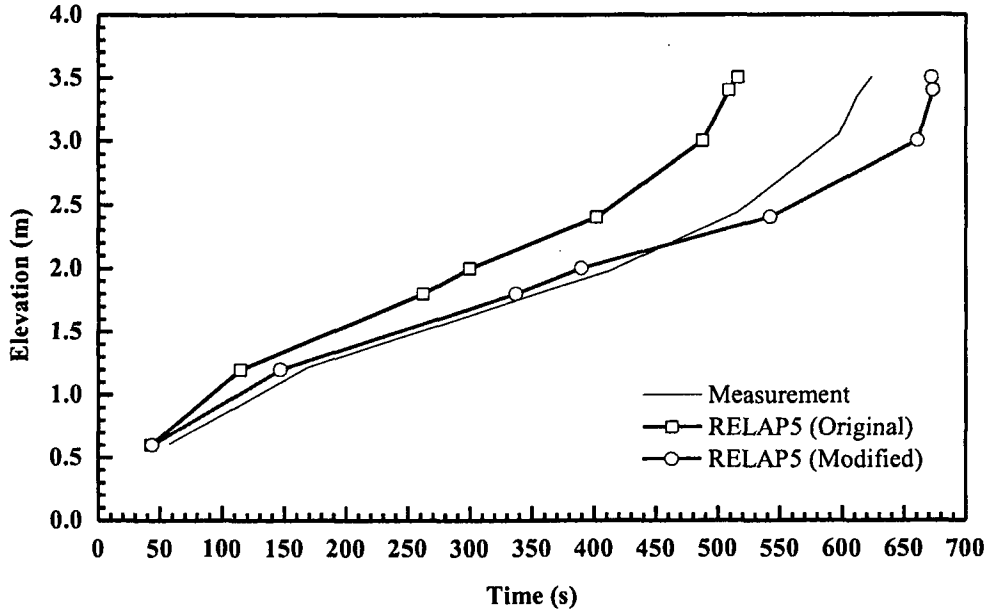

Figure 149. Quench Profile as a Function of Time for Test 32114

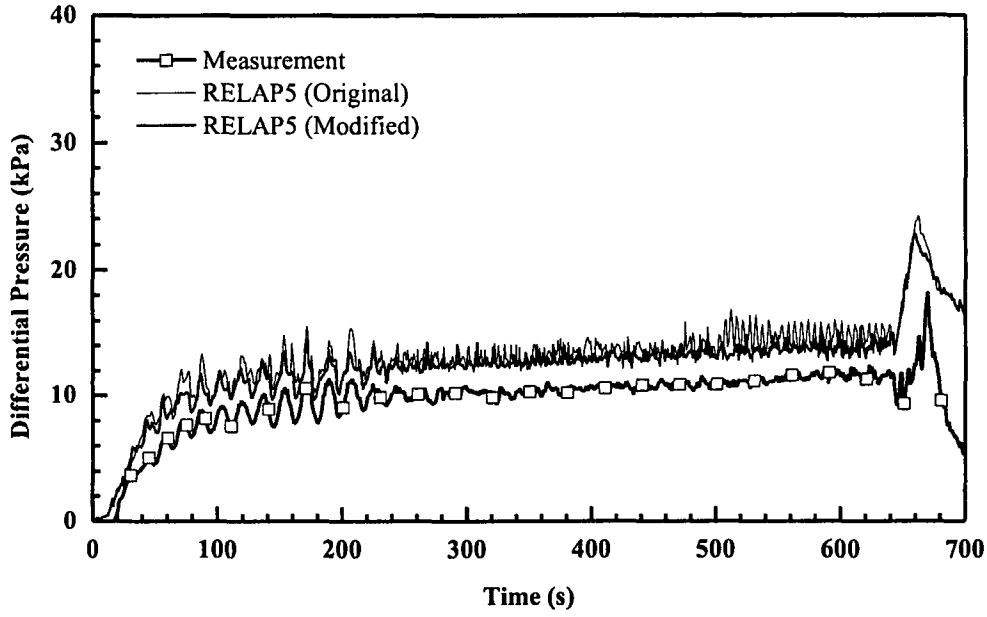

Figure 150. Differential Pressure for the Entire 12 ft Core for Test 32114

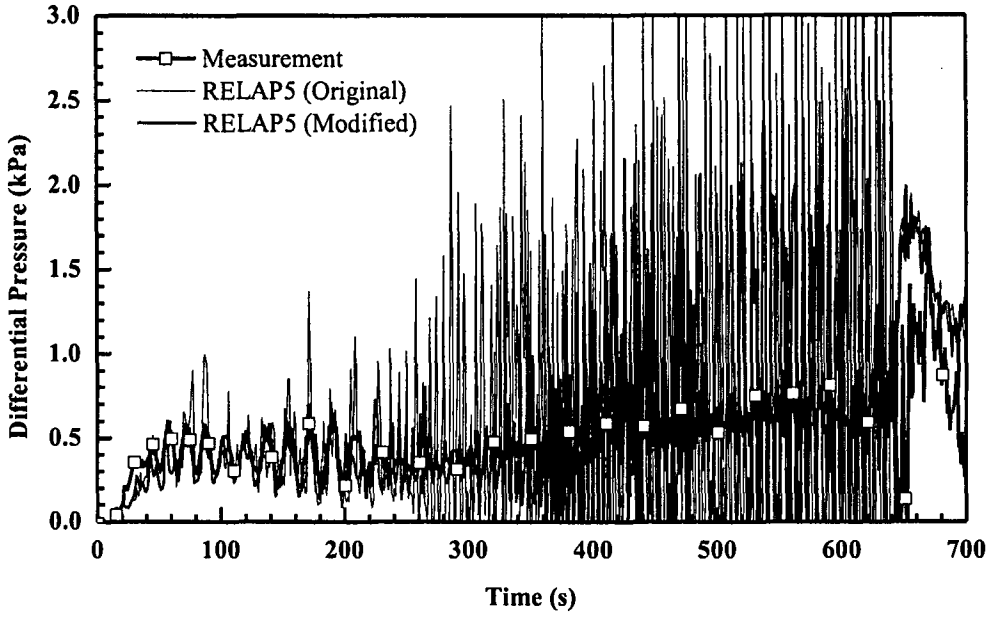

Figure 151. Differential Pressure at 6~7 ft Elevation for Test 32114

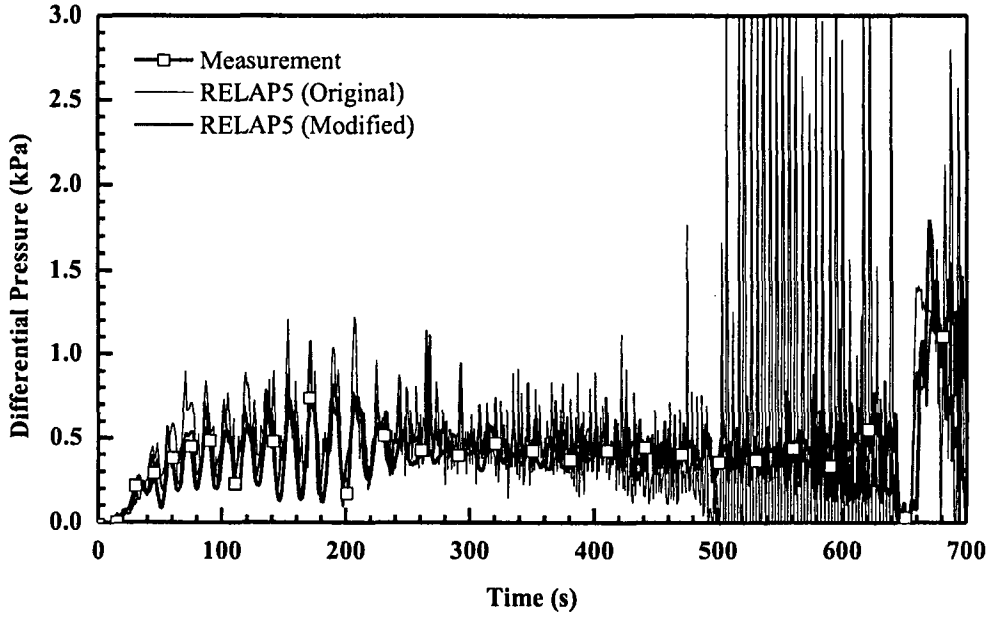

Figure 152. Differential Pressure at 10~11 ft Elevation for Test 32114

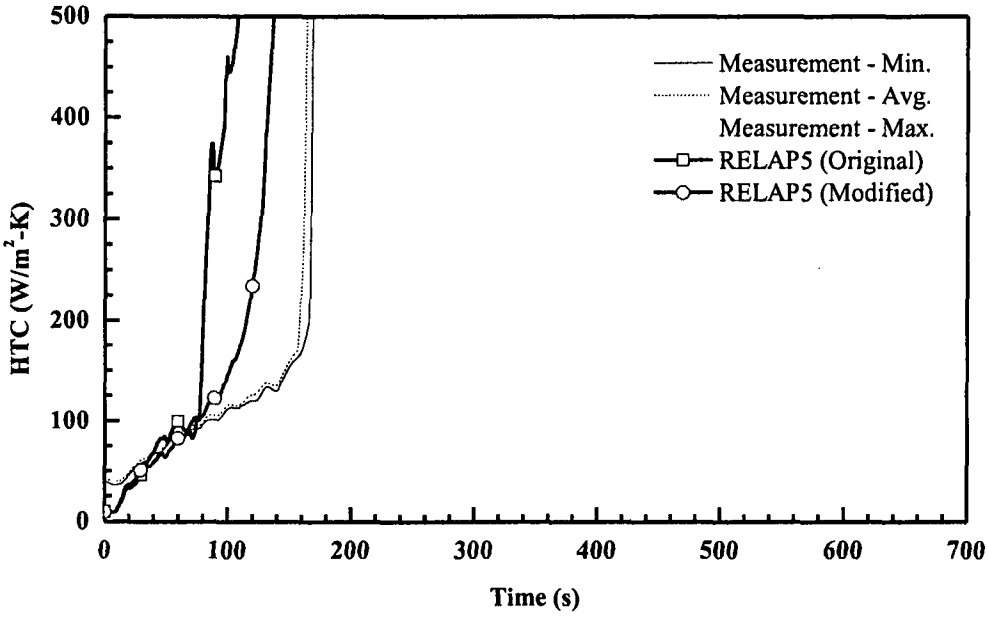

Figure 153. Heat Transfer Coefficient at 4 ft from Heated Bottom for Test 32114

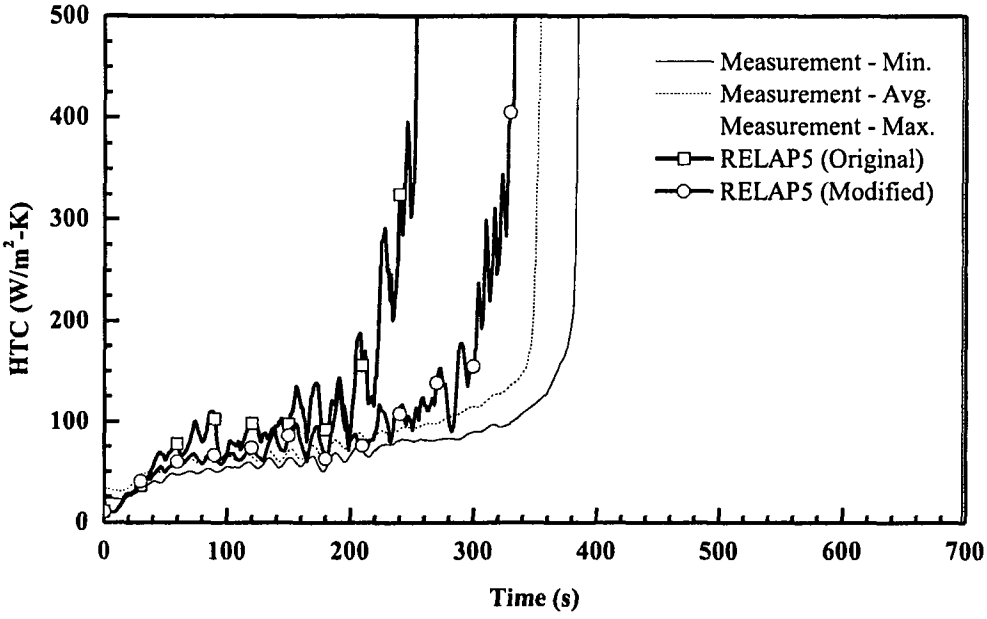

Figure 154. Heat Transfer Coefficient at 6 ft from Heated Bottom for Test 32114

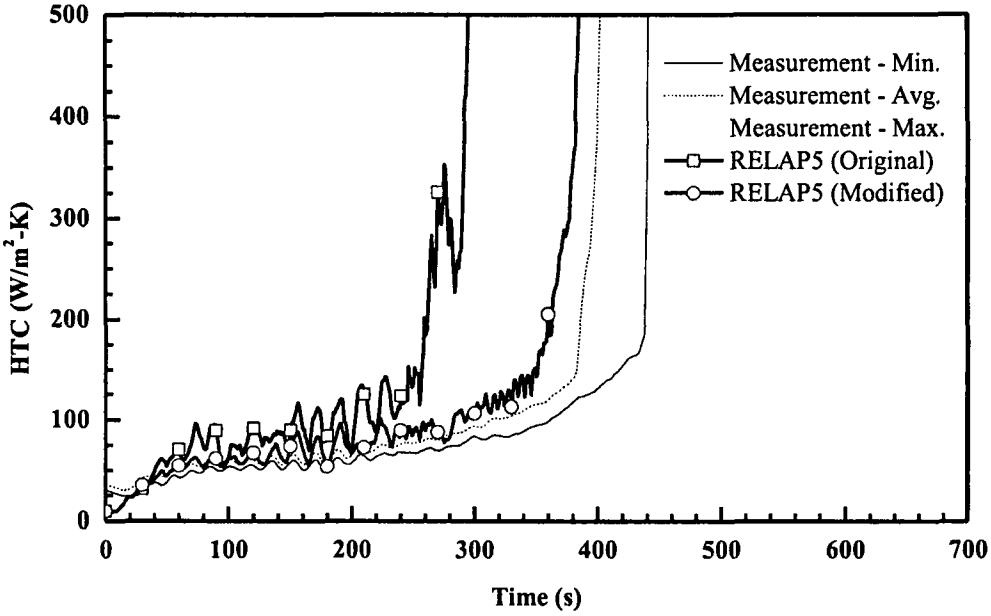

Figure 155. Heat Transfer Coefficient at 6.5 ft from Heated Bottom for Test 32114

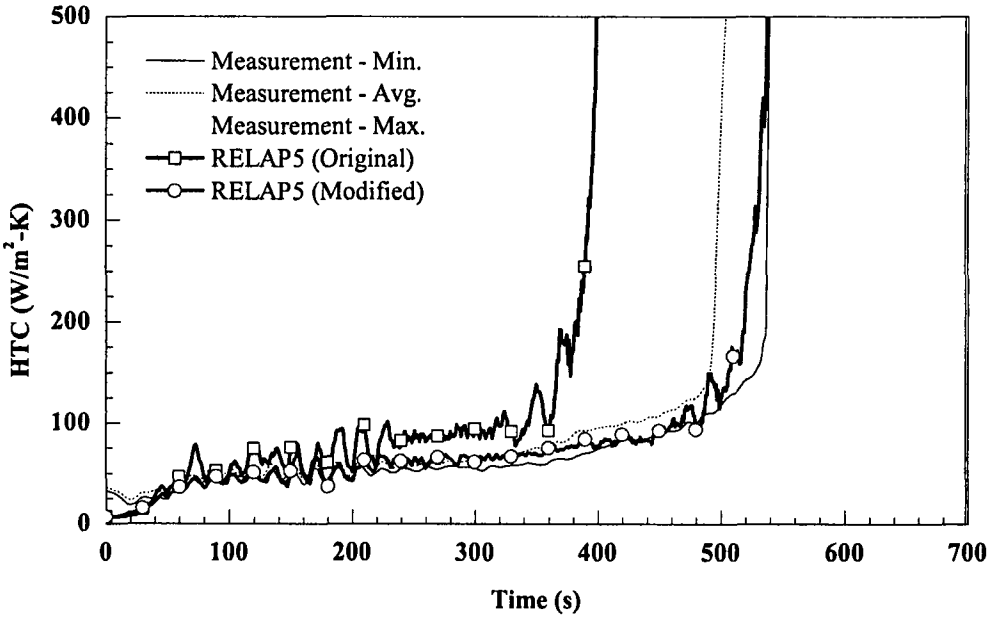

Figure 156. Heat Transfer Coefficient at 8 ft from Heated Bottom for Test 32114

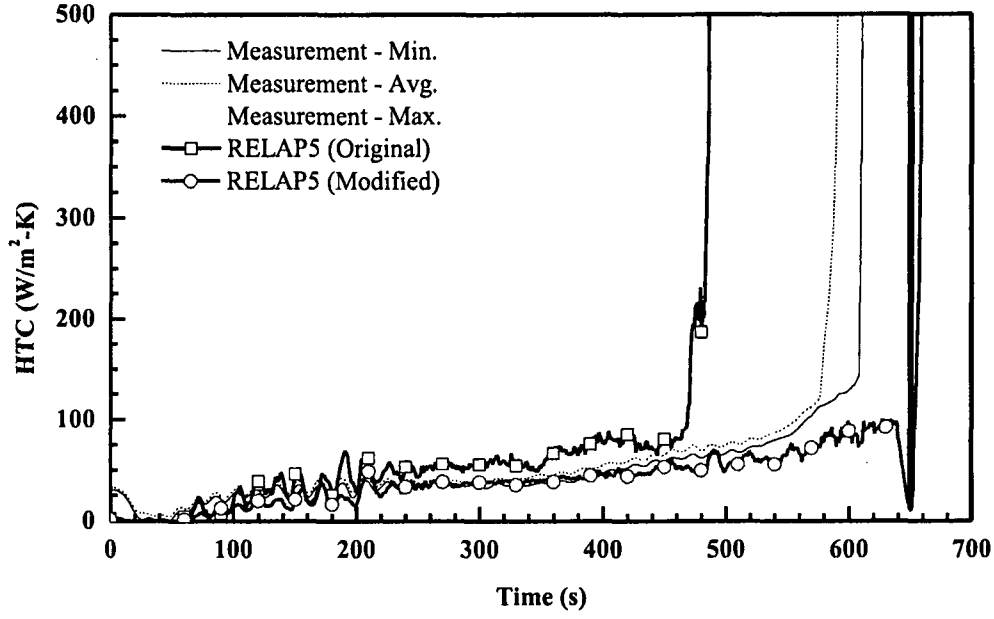

Figure 157. Heat Transfer Coefficient at 10 ft from Heated Bottom for Test 32114

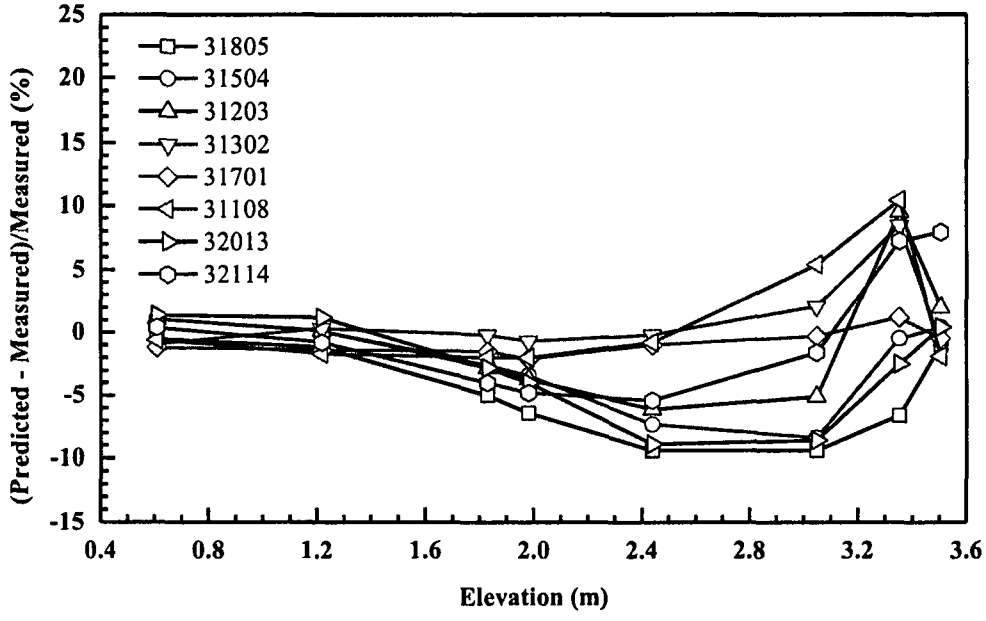

Figure 158. Percent Deviations of Predicted PCTs with Original Version

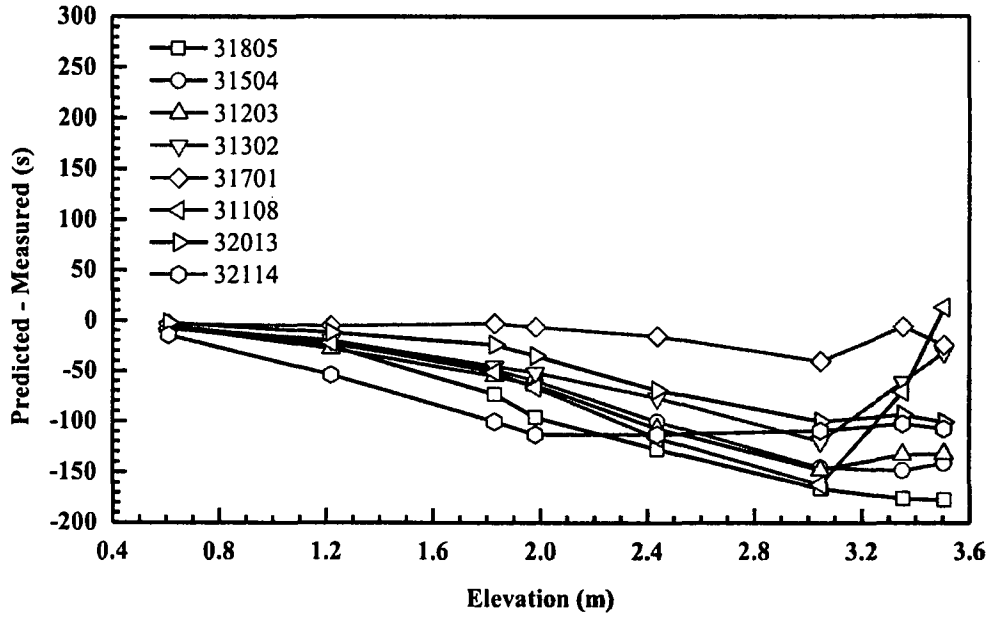

Figure 159. Differences in Quench Times with Original Version

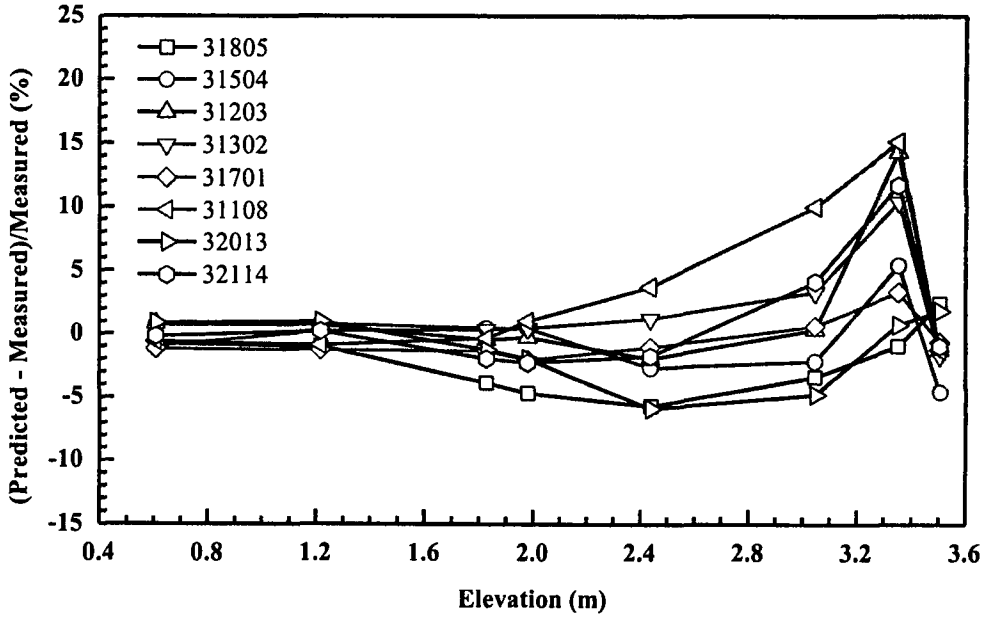

Figure 160. Percent Deviations of Predicted PCTs with Modified Version

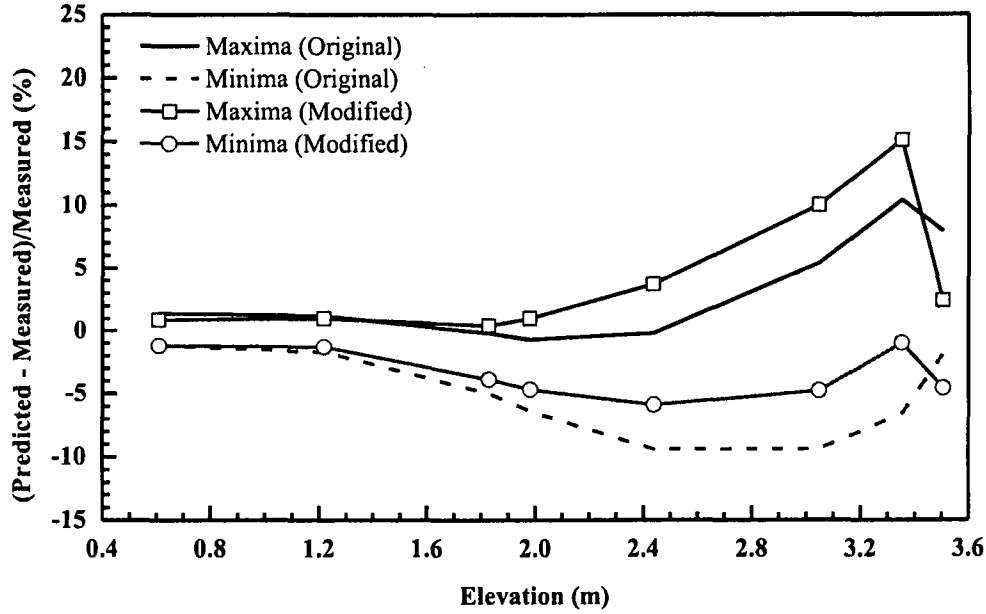

Figure 161. Effect of Modifications on PCT Predictions

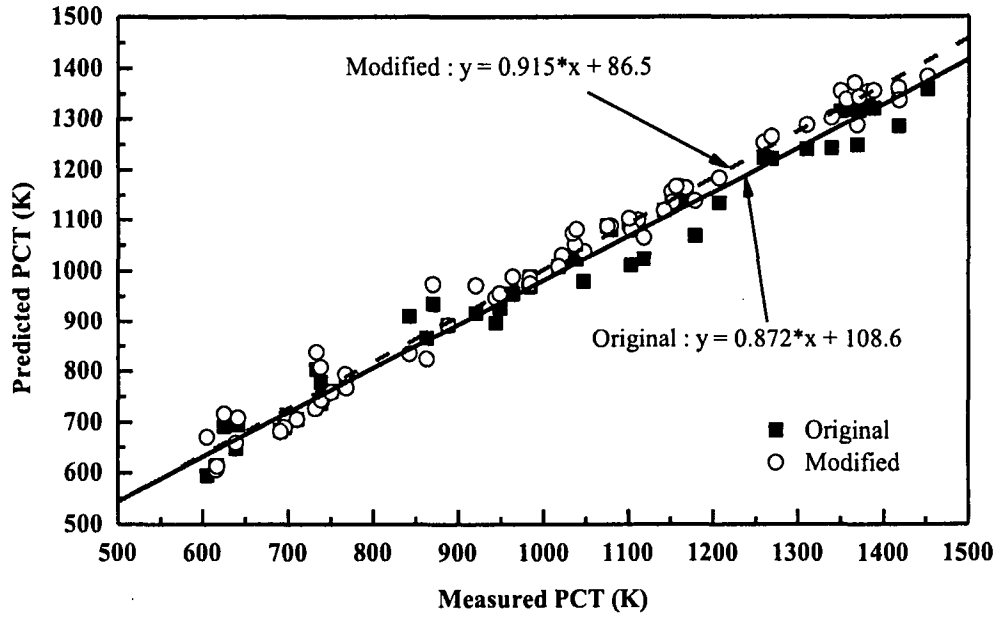

Figure 162. Comparison of Predictability for PCTs

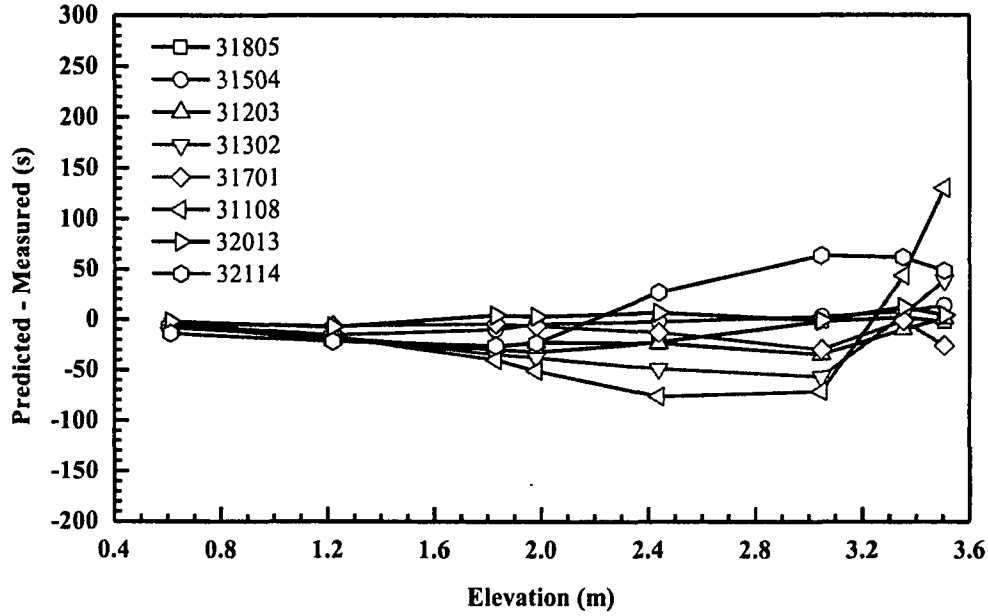

Figure 163. Differences in Quench Times with Modified Version

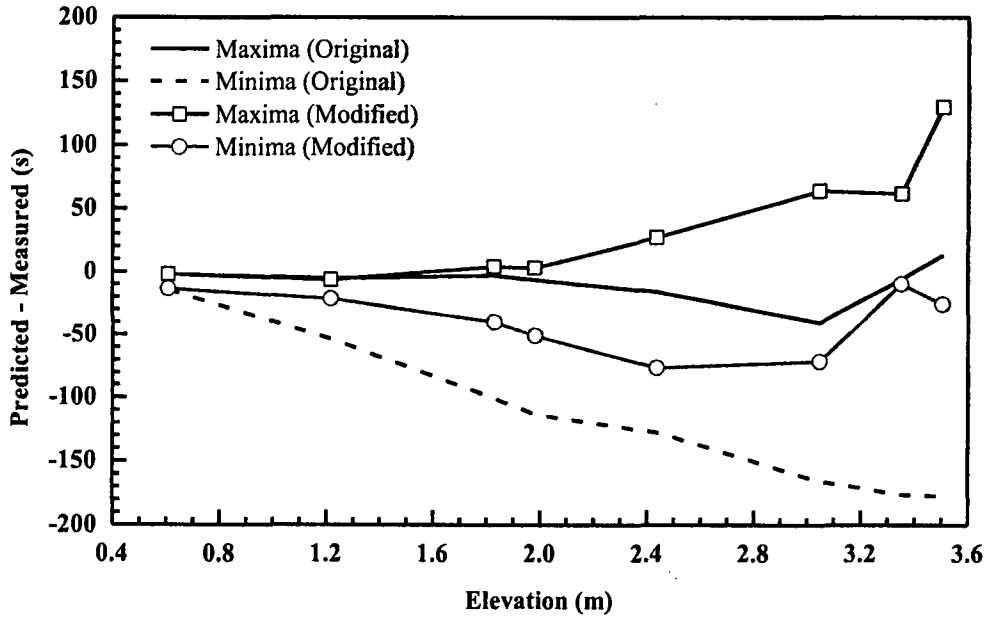

Figure 164. Effect of Modifications on Quench Time Predictions

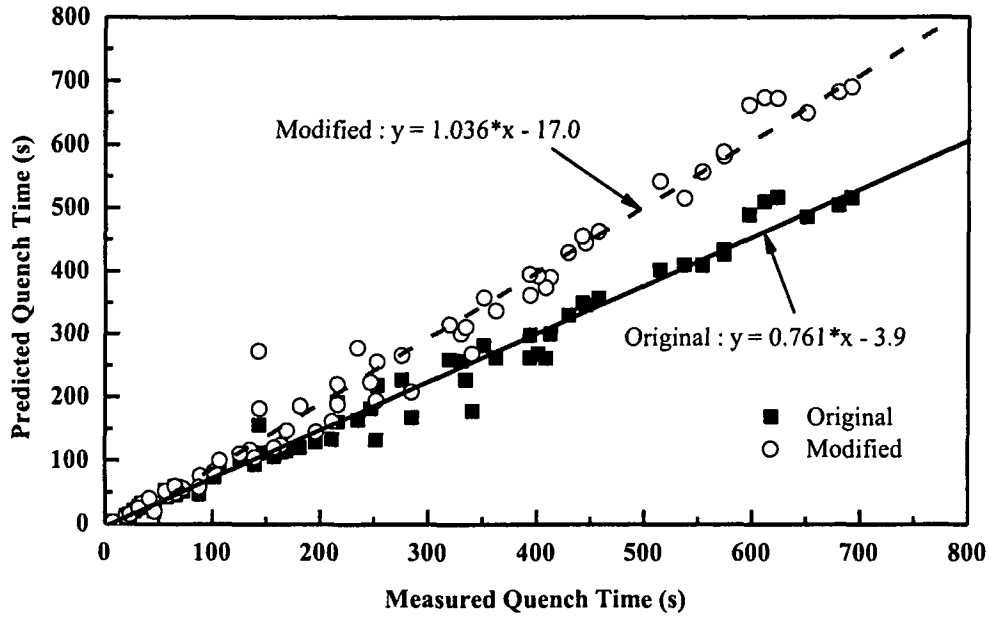

Figure 165. Comparison of Predictability for Quench Times

APPENDIX. RELAP5 BASE DECK FOR FLECHT-SEASET TEST 31805

```
=flecht seaset test no. 31805 using 49 nodes & 49 heat strs.
************************************************************************
* option 50: original critical flow model
1     50
100   new    transnt
101   run
102   si    si
105   10.0   20.0
************************************************************************
*
*    time step
*
************************************************************************
201   810.0   1.e-8   0.1   3   10  5000  5000
************************************************************************
*
*    mimor edits
*
************************************************************************
361   cntrlvar   005        *  core collapsed water level
362   cntrlvar   110        *  integrated water carry-over
363   cntrlvar   200        *  total power
20800001   fij   200010000
20800002   fij   200020000
20800003   fij   200030000
20800004   fij   200040000
20800005   fij   200050000
20800006   fij   200060000
20800007   fij   200070000
20800008   fij   200080000
20800009   fij   200090000
20800010   fij   200100000
20800011   fij   200110000
20800012   fij   200120000
20800013   fij   200130000
20800014   fij   200140000
20800015   fij   200150000
20800016   fij   200160000
20800017   fij   200170000
20800018   fij   200180000
20800019   fij   200190000
20800020   fij   200200000
20800021   fij   200210000
20800022   fij   200220000
20800023   fij   200230000
20800024   fij   200240000
20800025   fij   200250000
20800026   fij   200260000
20800027   fij   200270000
20800028   fij   200280000
20800029   fij   200290000
20800030   fij   200300000
20800031   fij   200310000
20800032   fij   200320000
```

```
20800033   fij   200330000
20800034   fij   200340000
20800035   fij   200350000
20800036   fij   200360000
20800037   fij   200370000
20800038   fij   200380000
20800039   fij   200390000
20800040   fij   200400000
20800041   fij   200410000
20800042   fij   200420000
20800043   fij   200430000
20800044   fij   200440000
20800045   fij   200450000
20800046   fij   200460000
20800047   fij   200470000
20800048   fij   200480000
*
20800051   htmode  200100101
20800052   htmode  200100201
20800053   htmode  200100301
20800054   htmode  200100401
20800055   htmode  200100501
20800056   htmode  200100601
20800057   htmode  200100701
20800058   htmode  200100801
20800059   htmode  200100901
20800060   htmode  200101001
20800061   htmode  200101101
20800062   htmode  200101201
20800063   htmode  200101301
20800064   htmode  200101401
20800065   htmode  200101501
20800066   htmode  200101601
20800067   htmode  200101701
20800068   htmode  200101801
20800069   htmode  200101901
20800070   htmode  200102001
20800071   htmode  200102101
20800072   htmode  200102201
20800073   htmode  200102301
20800074   htmode  200102401
20800075   htmode  200102501
20800076   htmode  200102601
20800077   htmode  200102701
20800078   htmode  200102801
20800079   htmode  200102901
20800080   htmode  200103001
20800081   htmode  200103101
20800082   htmode  200103201
20800083   htmode  200103301
20800084   htmode  200103401
20800085   htmode  200103501
20800086   htmode  200103601
20800087   htmode  200103701
20800088   htmode  200103801
20800089   htmode  200103901
20800090   htmode  200104001
```

```
20800091   htmode  200104101
20800092   htmode  200104201
20800093   htmode  200104301
20800094   htmode  200104401
20800095   htmode  200104501
20800096   htmode  200104601
20800097   htmode  200104701
20800098   htmode  200104801
20800099   htmode  200104901
20800101   dt      0
20800102   dtcrnt  0
20800111   fines   2001
20800112   tchfqf  2001
20800113   trewet  2001
20800114   zqbot   2001
*******************************************************************
*
*    TRIP LOGICS
*
*******************************************************************
500   time          0  gt  null  0     0.0  1  -1.0
*******************************************************************
*
*    hydraulic components
*
*******************************************************************
*    inlet boundary volume
*******************************************************************
1000000  lplenum   tmdpvol
1000101  1.0  1.0  0.0  0.0  0.0  0.0  0.0  0.0  00010
1000200  3    500
* test specific pressure and temperature
1000201  0.0   275790.0  326.2
1000202  5.0   275790.0  326.8
1000203  40.0  275790.0  323.8
1000204  77.0  275790.0  323.8
1000205  208.0   275790.0  325.6
1000206  357.0   275790.0  325.6
1000207  400.0   275790.0  326.2
1000208  700.0   275790.0  326.2
1000209  820.0   275790.0  326.2
*******************************************************************
*    inlet boundary junction
*******************************************************************
1500000  inlet    tmdpjun
1500101  100000000  160000000  0.0155565
1500200  0        500
* test specific inlet velocity
1500201 0.0   0.01964   0.0   0.0
1500202 12.4  0.02087   0.0   0.0
1500203 160.0   0.01982   0.0   0.0
1500204 228.0   0.01982   0.0   0.0
1500205 230.0   0.02139   0.0   0.0
1500206 280.0   0.02002   0.0   0.0
1500207 338.5   0.02002   0.0   0.0
1500208 349.5   0.02087   0.0   0.0
1500209 820.0   0.02087   0.0   0.0
```

```
*************************************************************************
*   inlet volume
*************************************************************************
1600000  inletv   snglvol
1600101  0.0155565 0.00381 0.0 0.0 90. 0.00381 1.e-6 0.0097 00
* test specific pressure and temperature
1600200  3        275790.0    326.2
*************************************************************************
*   inlet junction
*************************************************************************
1650000  inletj   sngljun
1650101   160010000    200000000  0.0      1.2     1.2    001000
1650110   0.0097  0.   1.         1.
1650201   1       0.0  0.0        0.0
*************************************************************************
*   core
*************************************************************************
2000000  core   pipe
2000001  49
2000101  0.0155565    49           * vol. flow area
2000201  0.0155565    48           * jun. flow area
2000301  0.0762       49           * vol. length
2000401  0.0          49           * vol. volume
2000601  90.0         49           * vol. vertical orientation
2000701  0.0762       49           * vol. elevation change
2000801  1.e-6        0.0097  49    * vol. friction data
* bottom most grid k --> junction to core inlet
2000901  0.0    0.0        6        * jun. loss coefficient
2000902  1.20   1.20       7
2000903  0.0    0.0       13
2000904  1.20   1.20      14
2000905  0.0    0.0       20
2000906  1.20   1.20      21
2000907  0.0    0.0       27
2000908  1.20   1.20      28
2000909  0.0    0.0       33
2000910  1.20   1.20      34
2000911  0.0    0.0       40
2000912  1.20   1.20      41
2000913  0.0    0.0       47
2000914  1.20   1.20      48
2001001  00100   49           * vol. control flag
2001101  000000  48           * jun. control flag
* test specific pressure and temperature
2001201 3 275790.0  403.8    0.0   0.0   0.0   1
2001202 3 275790.0  403.8    0.0   0.0   0.0   2
2001203 3 275790.0  415.5    0.0   0.0   0.0   3
2001204 3 275790.0  437.6    0.0   0.0   0.0   4
2001205 3 275790.0  459.6    0.0   0.0   0.0   5
2001206 3 275790.0  481.7    0.0   0.0   0.0   6
2001207 3 275790.0  503.8    0.0   0.0   0.0   7
2001208 3 275790.0  525.9    0.0   0.0   0.0   8
2001209 3 275790.0  548.0    0.0   0.0   0.0   9
2001210 3 275790.0  570.1    0.0   0.0   0.0   10
2001211 3 275790.0  592.1    0.0   0.0   0.0   11
2001212 3 275790.0  614.2    0.0   0.0   0.0   12
2001213 3 275790.0  636.3    0.0   0.0   0.0   13
```

```
2001214 3 275790.0  658.4    0.0   0.0   0.0   14
2001215 3 275790.0  680.5    0.0   0.0   0.0   15
2001216 3 275790.0  702.6    0.0   0.0   0.0   16
2001217 3 275790.0  724.6    0.0   0.0   0.0   17
2001218 3 275790.0  757.6    0.0   0.0   0.0   18
2001219 3 275790.0  790.5    0.0   0.0   0.0   19
2001220 3 275790.0  823.5    0.0   0.0   0.0   20
2001221 3 275790.0  856.4    0.0   0.0   0.0   21
2001222 3 275790.0  856.1    0.0   0.0   0.0   22
2001223 3 275790.0  855.9    0.0   0.0   0.0   23
2001224 3 275790.0  855.6    0.0   0.0   0.0   24
2001225 3 275790.0  855.3    0.0   0.0   0.0   25
2001226 3 275790.0  848.8    0.0   0.0   0.0   26
2001227 3 275790.0  842.4    0.0   0.0   0.0   27
2001228 3 275790.0  835.9    0.0   0.0   0.0   28
2001229 3 275790.0  829.4    0.0   0.0   0.0   29
2001230 3 275790.0  800.7    0.0   0.0   0.0   30
2001231 3 275790.0  772.0    0.0   0.0   0.0   31
2001232 3 275790.0  743.3    0.0   0.0   0.0   32
2001233 3 275790.0  714.6    0.0   0.0   0.0   33
2001234 3 275790.0  697.3    0.0   0.0   0.0   34
2001235 3 275790.0  680.1    0.0   0.0   0.0   35
2001236 3 275790.0  662.9    0.0   0.0   0.0   36
2001237 3 275790.0  645.7    0.0   0.0   0.0   37
2001238 3 275790.0  625.3    0.0   0.0   0.0   38
2001239 3 275790.0  604.9    0.0   0.0   0.0   39
2001240 3 275790.0  584.5    0.0   0.0   0.0   40
2001241 3 275790.0  564.1    0.0   0.0   0.0   41
2001242 3 275790.0  553.9    0.0   0.0   0.0   42
2001243 3 275790.0  543.8    0.0   0.0   0.0   43
2001244 3 275790.0  533.7    0.0   0.0   0.0   44
2001245 3 275790.0  523.6    0.0   0.0   0.0   45
2001246 3 275790.0  513.5    0.0   0.0   0.0   46
2001247 3 275790.0  503.4    0.0   0.0   0.0   47
2001248 3 275790.0  493.2    0.0   0.0   0.0   48
2001249 3 275790.0  483.1    0.0   0.0   0.0   49
2001300  0
2001301  0.0  0.0  0.0  48     * jun. initial condition
2001401  0.0097     0.0   1.0   1.0  48
*******************************************************************
*    outlet junction
*******************************************************************
2500000  outlet   sngljun
* ccfl on (f = 1)
* choking off (c = 1)
* reverse flow is restricted (kb = 1.e6)
2500101  200010000  300000000  0.0155565   0.0  1.e6    101000
2500102  1.0  1.0   1.0
2500201  0  0.0  0.0  0.0
*******************************************************************
*    upper plenum
*******************************************************************
3000000  uplenum   tmdpvol
3000101  1.0  1.0  0.0  0.0  0.0  0.0  0.0  0.0  00010
3000200  2
* test specific pressure
3000201   0.0     276550.0  1.0
```

```
3000202   820.0   276550.0  1.0
*************************************************************
*
*    heat structure
*
*************************************************************
*    fuel rod
*************************************************************
*
12001000  49  8  2  0  0.0  1  1   32
12001100  0   1
12001101  2  1.20650e-3
12001102  1  2.22250e-3
12001103  2  4.11480e-3
12001104  2  4.74980e-3
12001201  1   2             * boron nitride
12001202  2   3             * kanthal
12001203  1   5             * boron nitride
12001204  4   7             * ss 347
12001301  0.0   2
12001302  1.0   3
12001303  0.0   7
12001400  -1
* test specific initial wall temperature
12001401  491.9   491.9   491.9   491.9   491.9   491.9   491.9   491.9
12001402  515.3   515.3   515.3   515.3   515.3   515.3   515.3   515.3
12001403  538.8   538.8   538.8   538.8   538.8   538.8   538.8   538.8
12001404  562.2   562.2   562.2   562.2   562.2   562.2   562.2   562.2
12001405  585.6   585.6   585.6   585.6   585.6   585.6   585.6   585.6
12001406  609.1   609.1   609.1   609.1   609.1   609.1   609.1   609.1
12001407  632.5   632.5   632.5   632.5   632.5   632.5   632.5   632.5
12001408  655.9   655.9   655.9   655.9   655.9   655.9   655.9   655.9
12001409  679.4   679.4   679.4   679.4   679.4   679.4   679.4   679.4
12001410  727.4   727.4   727.4   727.4   727.4   727.4   727.4   727.4
12001411  775.6   775.6   775.6   775.6   775.6   775.6   775.6   775.6
12001412  823.8   823.8   823.8   823.8   823.8   823.8   823.8   823.8
12001413  872.0   872.0   872.0   872.0   872.0   872.0   872.0   872.0
12001414  920.1   920.1   920.1   920.1   920.1   920.1   920.1   920.1
12001415  933.9   933.9   933.9   933.9   933.9   933.9   933.9   933.9
12001416  947.5   947.5   947.5   947.5   947.5   947.5   947.5   947.5
12001417  961.2   961.2   961.2   961.2   961.2   961.2   961.2   961.2
12001418  989.6   989.6   989.6   989.6   989.6   989.6   989.6   989.6
12001419  1017.9  1017.9  1017.9  1017.9  1017.9  1017.9  1017.9  1017.9
12001420  1046.3  1046.3  1046.3  1046.3  1046.3  1046.3  1046.3  1046.3
12001421  1074.7  1074.7  1074.7  1074.7  1074.7  1074.7  1074.7  1074.7
12001422  1104.2  1104.2  1104.2  1104.2  1104.2  1104.2  1104.2  1104.2
12001423  1133.6  1133.6  1133.6  1133.6  1133.6  1133.6  1133.6  1133.6
12001424  1143.8  1143.8  1143.8  1143.8  1143.8  1143.8  1143.8  1143.8
12001425  1126.3  1126.3  1126.3  1126.3  1126.3  1126.3  1126.3  1126.3
12001426  1129.0  1129.0  1129.0  1129.0  1129.0  1129.0  1129.0  1129.0
12001427  1115.2  1115.2  1115.2  1115.2  1115.2  1115.2  1115.2  1115.2
12001428  1106.1  1106.1  1106.1  1106.1  1106.1  1106.1  1106.1  1106.1
12001429  1097.0  1097.0  1097.0  1097.0  1097.0  1097.0  1097.0  1097.0
12001430  1085.0  1085.0  1085.0  1085.0  1085.0  1085.0  1085.0  1085.0
12001431  1072.9  1072.9  1072.9  1072.9  1072.9  1072.9  1072.9  1072.9
12001432  1031.4  1031.4  1031.4  1031.4  1031.4  1031.4  1031.4  1031.4
12001433  989.8   989.8   989.8   989.8   989.8   989.8   989.8   989.8
```

```
12001434  933.5   933.5   933.5   933.5   933.5   933.5   933.5   933.5
12001435  877.1   877.1   877.1   877.1   877.1   877.1   877.1   877.1
12001436  862.2   862.2   862.2   862.2   862.2   862.2   862.2   862.2
12001437  847.4   847.4   847.4   847.4   847.4   847.4   847.4   847.4
12001438  832.4   832.4   832.4   832.4   832.4   832.4   832.4   832.4
12001439  795.4   795.4   795.4   795.4   795.4   795.4   795.4   795.4
12001440  758.4   758.4   758.4   758.4   758.4   758.4   758.4   758.4
12001441  721.4   721.4   721.4   721.4   721.4   721.4   721.4   721.4
12001442  698.3   698.3   698.3   698.3   698.3   698.3   698.3   698.3
12001443  675.2   675.2   675.2   675.2   675.2   675.2   675.2   675.2
12001444  652.1   652.1   652.1   652.1   652.1   652.1   652.1   652.1
12001445  629.0   629.0   629.0   629.0   629.0   629.0   629.0   629.0
12001446  614.8   614.8   614.8   614.8   614.8   614.8   614.8   614.8
12001447  600.6   600.6   600.6   600.6   600.6   600.6   600.6   600.6
12001448  586.4   586.4   586.4   586.4   586.4   586.4   586.4   586.4
12001449  572.2   572.2   572.2   572.2   572.2   572.2   572.2   572.2
* test specific length (159 rods)
12001501  0  0  0  1   6.05790  1
12001502  0  0  0  1  12.11580  48
12001503  0  0  0  1   6.05790  49
12001601  200010000  0      1  1  6.05790  1
12001602  200020000  10000  1  1 12.11580  48
12001603  200490000  0      1  1  6.05790  49
* test specific power fraction
12001701  200 0.00447   0.0   0.0   1
12001702  200 0.00895   0.0   0.0   2
12001703  200 0.00895   0.0   0.0   3
12001704  200 0.00895   0.0   0.0   4
12001705  200 0.00895   0.0   0.0   5
12001706  200 0.00895   0.0   0.0   6
12001707  200 0.00895   0.0   0.0   7
12001708  200 0.01051   0.0   0.0   8
12001709  200 0.01415   0.0   0.0   9
12001710  200 0.01415   0.0   0.0   10
12001711  200 0.01790   0.0   0.0   11
12001712  200 0.01832   0.0   0.0   12
12001713  200 0.02071   0.0   0.0   13
12001714  200 0.02310   0.0   0.0   14
12001715  200 0.02349   0.0   0.0   15
12001716  200 0.02706   0.0   0.0   16
12001717  200 0.02706   0.0   0.0   17
12001718  200 0.02981   0.0   0.0   18
12001719  200 0.03101   0.0   0.0   19
12001720  200 0.03172   0.0   0.0   20
12001721  200 0.03330   0.0   0.0   21
12001722  200 0.03330   0.0   0.0   22
12001723  200 0.03443   0.0   0.0   23
12001724  200 0.03455   0.0   0.0   24
12001725  200 0.03455   0.0   0.0   25
12001726  200 0.03455   0.0   0.0   26
12001727  200 0.03442   0.0   0.0   27
12001728  200 0.03330   0.0   0.0   28
12001729  200 0.03330   0.0   0.0   29
12001730  200 0.03168   0.0   0.0   30
12001731  200 0.03101   0.0   0.0   31
12001732  200 0.02984   0.0   0.0   32
12001733  200 0.02706   0.0   0.0   33
```

```
12001734  200 0.02706   0.0   0.0   34
12001735  200 0.02350   0.0   0.0   35
12001736  200 0.02310   0.0   0.0   36
12001737  200 0.02071   0.0   0.0   37
12001738  200 0.01832   0.0   0.0   38
12001739  200 0.01790   0.0   0.0   39
12001740  200 0.01415   0.0   0.0   40
12001741  200 0.01415   0.0   0.0   41
12001742  200 0.01051   0.0   0.0   42
12001743  200 0.00895   0.0   0.0   43
12001744  200 0.00895   0.0   0.0   44
12001745  200 0.00895   0.0   0.0   45
12001746  200 0.00895   0.0   0.0   46
12001747  200 0.00895   0.0   0.0   47
12001748  200 0.00895   0.0   0.0   48
12001749  200 0.00447   0.0   0.0   49
* additional left boundary
12001801  0.0094996  20.0  20.0  0.0  0.0  0.0  0.0  1.0  49
* additional right boundary
12001901 0.0094996 0.03810 3.65760 0.00000  0.48890 1.20 1.20 0.24250 1
12001902 0.0094996 0.07620 3.58140 0.07620  0.41270 1.20 1.20 0.29458 2
12001903 0.0094996 0.15240 3.50520 0.15240  0.33650 1.20 1.20 0.34667 3
12001904 0.0094996 0.22860 3.42900 0.22860  0.26030 1.20 1.20 0.39875 4
12001905 0.0094996 0.30480 3.35280 0.30480  0.18410 1.20 1.20 0.45083 5
12001906 0.0094996 0.38100 3.27660 0.38100  0.10790 1.20 1.20 0.50292 6
12001907 0.0094996 0.45720 3.20040 0.45720  0.03170 1.20 1.20 0.55500 7
12001908 0.0094996 0.53340 3.12420 0.00000  0.46360 1.20 1.20 0.60708 8
12001909 0.0094996 0.60960 3.04800 0.07620  0.38740 1.20 1.20 0.65917 9
12001910 0.0094996 0.68580 2.97180 0.15240  0.31120 1.20 1.20 0.73000 10
12001911 0.0094996 0.76200 2.89560 0.22860  0.23500 1.20 1.20 0.81333 11
12001912 0.0094996 0.83820 2.81940 0.30480  0.15880 1.20 1.20 0.89917 12
12001913 0.0094996 0.91440 2.74320 0.38100  0.08260 1.20 1.20 0.99500 13
12001914 0.0094996 0.99060 2.66700 0.45720  0.00640 1.20 1.20 1.09083 14
12001915 0.0094996 1.06680 2.59080 0.02530  0.46360 1.20 1.20 1.17333 15
12001916 0.0094996 1.14300 2.51460 0.10150  0.38740 1.20 1.20 1.25249 16
12001917 0.0094996 1.21920 2.43840 0.17770  0.31120 1.20 1.20 1.33166 17
12001918 0.0094996 1.29540 2.36220 0.25390  0.23500 1.20 1.20 1.41082 18
12001919 0.0094996 1.37160 2.28600 0.33010  0.15880 1.20 1.20 1.48998 19
12001920 0.0094996 1.44780 2.20980 0.40630  0.08260 1.20 1.20 1.53583 20
12001921 0.0094996 1.52400 2.13360 0.48250  0.00640 1.20 1.20 1.58168 21
12001922 0.0094996 1.60020 2.05740 0.02530  0.46360 1.20 1.20 1.61000 22
12001923 0.0094996 1.67640 1.98120 0.10150  0.38740 1.20 1.20 1.62667 23
12001924 0.0094996 1.75260 1.90500 0.17770  0.31120 1.20 1.20 1.64334 24
12001925 0.0094996 1.82880 1.82880 0.25390  0.23500 1.20 1.20 1.66000 25
12001926 0.0094996 1.90500 1.75260 0.33010  0.15880 1.20 1.20 1.64333 26
12001927 0.0094996 1.98120 1.67640 0.40630  0.08260 1.20 1.20 1.62667 27
12001928 0.0094996 2.05740 1.60020 0.48250  0.00640 1.20 1.20 1.61000 28
12001929 0.0094996 2.13360 1.52400 0.02530  0.43830 1.20 1.20 1.58167 29
12001930 0.0094996 2.20980 1.44780 0.10150  0.36210 1.20 1.20 1.53584 30
12001931 0.0094996 2.28600 1.37160 0.17770  0.28590 1.20 1.20 1.49001 31
12001932 0.0094996 2.36220 1.29540 0.25390  0.20970 1.20 1.20 1.41084 32
12001933 0.0094996 2.43840 1.21920 0.33010  0.13350 1.20 1.20 1.33165 33
12001934 0.0094996 2.51460 1.14300 0.40630  0.05730 1.20 1.20 1.25248 34
12001935 0.0094996 2.59080 1.06680 0.48250  0.51450 1.20 1.20 1.17332 35
12001936 0.0094996 2.66700 0.99060 0.05090  0.43830 1.20 1.20 1.09082 36
12001937 0.0094996 2.74320 0.91440 0.12710  0.36210 1.20 1.20 0.99499 37
12001938 0.0094996 2.81940 0.83820 0.20330  0.28590 1.20 1.20 0.89917 38
```

```
12001939 0.0094996 2.89560 0.76200 0.27950  0.20970 1.20 1.20 0.81334 39
12001940 0.0094996 2.97180 0.68580 0.35570  0.13350 1.20 1.20 0.73001 40
12001941 0.0094996 3.04800 0.60960 0.43190  0.05730 1.20 1.20 0.65917 41
12001942 0.0094996 3.12420 0.53340 0.50810  0.48890 1.20 1.20 0.60709 42
12001943 0.0094996 3.20040 0.45720 0.05090  0.41270 1.20 1.20 0.55501 43
12001944 0.0094996 3.27660 0.38100 0.12710  0.33650 1.20 1.20 0.50293 44
12001945 0.0094996 3.35280 0.30480 0.20330  0.26030 1.20 1.20 0.45085 45
12001946 0.0094996 3.42900 0.22860 0.27950  0.18410 1.20 1.20 0.39877 46
12001947 0.0094996 3.50520 0.15240 0.35570  0.10790 1.20 1.20 0.34668 47
12001948 0.0094996 3.58140 0.07620 0.43190  0.03170 1.20 1.20 0.29460 48
12001949 0.0094996 3.65760 0.03810 0.00000 20.0000 1.20 1.20 0.24252 49
*********************************************************************
*   housing
*********************************************************************
12002000  49  3  2  0  0.097   0   0
12002100  0   1
12002101  2  0.10208
12002201  3   2             * ss 304
12002301  0.  2
12002400  -1
* test specific initial wall temperature
12002401  368.2   368.2   368.2
12002402  372.2   372.2   372.2
12002403  376.2   376.2   376.2
12002404  380.2   380.2   380.2
12002405  384.2   384.2   384.2
12002406  388.2   388.2   388.2
12002407  392.2   392.2   392.2
12002408  396.2   396.2   396.2
12002409  400.2   400.2   400.2
12002410  404.2   404.2   404.2
12002411  408.2   408.2   408.2
12002412  412.2   412.2   412.2
12002413  416.2   416.2   416.2
12002414  420.2   420.2   420.2
12002415  424.2   424.2   424.2
12002416  428.2   428.2   428.2
12002417  432.2   432.2   432.2
12002418  435.8   435.8   435.8
12002419  439.4   439.4   439.4
12002420  443.0   443.0   443.0
12002421  446.7   446.7   446.7
12002422  450.3   450.3   450.3
12002423  453.9   453.9   453.9
12002424  457.5   457.5   457.5
12002425  461.2   461.2   461.2
12002426  458.4   458.4   458.4
12002427  455.7   455.7   455.7
12002428  452.9   452.9   452.9
12002429  450.2   450.2   450.2
12002430  447.4   447.4   447.4
12002431  444.7   444.7   444.7
12002432  441.9   441.9   441.9
12002433  439.2   439.2   439.2
12002434  436.9   436.9   436.9
12002435  434.7   434.7   434.7
12002436  432.4   432.4   432.4
```

```
12002437  430.2   430.2   430.2
12002438  425.9   425.9   425.9
12002439  421.7   421.7   421.7
12002440  417.4   417.4   417.4
12002441  413.2   413.2   413.2
12002442  411.9   411.9   411.9
12002443  410.7   410.7   410.7
12002444  409.4   409.4   409.4
12002445  408.2   408.2   408.2
12002446  406.9   406.9   406.9
12002447  405.7   405.7   405.7
12002448  404.4   404.4   404.4
12002449  403.2   403.2   403.2
12002501  200010000  0       1  1  0.0381  1
12002502  200020000  10000   1  1  0.0762  48
12002503  200490000  0       1  1  0.0381  49
12002601  0  0  0  1  0.0381  1
12002602  0  0  0  1  0.0762  48
12002603  0  0  0  1  0.0381  49
12002701  0  0.0  0.0  0.0  49
12002801  0.0  20.0  20.0  0.0  0.0  0.0  0.0  1.0  49
12002901  0.0  20.0  20.0  0.0  0.0  0.0  0.0  1.0  49
*********************************************************************
*    thimbles
*********************************************************************
12003000  49  3  2  0  0.005461   0   1
12003100  0   1
12003101  2  0.0060198
12003201  3   2                  * ss 304
12003301  0.0   2
12003400  -1
* test specific initial wall temp.
12003401  368.2   368.2   368.2
12003402  372.2   372.2   372.2
12003403  376.2   376.2   376.2
12003404  380.2   380.2   380.2
12003405  384.2   384.2   384.2
12003406  388.2   388.2   388.2
12003407  392.2   392.2   392.2
12003408  396.2   396.2   396.2
12003409  400.2   400.2   400.2
12003410  404.2   404.2   404.2
12003411  408.2   408.2   408.2
12003412  412.2   412.2   412.2
12003413  416.2   416.2   416.2
12003414  420.2   420.2   420.2
12003415  424.2   424.2   424.2
12003416  428.2   428.2   428.2
12003417  432.2   432.2   432.2
12003418  435.8   435.8   435.8
12003419  439.4   439.4   439.4
12003420  443.0   443.0   443.0
12003421  446.7   446.7   446.7
12003422  450.3   450.3   450.3
12003423  453.9   453.9   453.9
12003424  457.5   457.5   457.5
12003425  461.2   461.2   461.2
```

```
12003426  458.4   458.4   458.4
12003427  455.7   455.7   455.7
12003428  452.9   452.9   452.9
12003429  450.2   450.2   450.2
12003430  447.4   447.4   447.4
12003431  444.7   444.7   444.7
12003432  441.9   441.9   441.9
12003433  439.2   439.2   439.2
12003434  436.9   436.9   436.9
12003435  434.7   434.7   434.7
12003436  432.4   432.4   432.4
12003437  430.2   430.2   430.2
12003438  425.9   425.9   425.9
12003439  421.7   421.7   421.7
12003440  417.4   417.4   417.4
12003441  413.2   413.2   413.2
12003442  411.9   411.9   411.9
12003443  410.7   410.7   410.7
12003444  409.4   409.4   409.4
12003445  408.2   408.2   408.2
12003446  406.9   406.9   406.9
12003447  405.7   405.7   405.7
12003448  404.4   404.4   404.4
12003449  403.2   403.2   403.2
* 16 thimbles
12003501  0  0  0  1   0.6096  1
12003502  0  0  0  1   1.2192  48
12003503  0  0  0  1   0.6096  49
12003601  200010000  0      1  1  0.6096  1
12003602  200020000  10000  1  1  1.2192  48
12003603  200490000  0      1  1  0.6096  49
12003701  0  0.0  0.0  0.0  49
12003801  0.0  20.0  20.0  0.0  0.0  0.0  0.0  1.0  49
12003901  0.0  20.0  20.0  0.0  0.0  0.0  0.0  1.0  49
*********************************************************************
*   fillers
*********************************************************************
12004000  49  3  2  0  0.0    0    1
12004100  0   1
12004101  2  0.005022
12004201  3   2
12004301  0.0   2
12004400  -1
* test specific initial wall temp.
12004401  368.2   368.2   368.2
12004402  372.2   372.2   372.2
12004403  376.2   376.2   376.2
12004404  380.2   380.2   380.2
12004405  384.2   384.2   384.2
12004406  388.2   388.2   388.2
12004407  392.2   392.2   392.2
12004408  396.2   396.2   396.2
12004409  400.2   400.2   400.2
12004410  404.2   404.2   404.2
12004411  408.2   408.2   408.2
12004412  412.2   412.2   412.2
12004413  416.2   416.2   416.2
```

```
12004414  420.2   420.2   420.2
12004415  424.2   424.2   424.2
12004416  428.2   428.2   428.2
12004417  432.2   432.2   432.2
12004418  435.8   435.8   435.8
12004419  439.4   439.4   439.4
12004420  443.0   443.0   443.0
12004421  446.7   446.7   446.7
12004422  450.3   450.3   450.3
12004423  453.9   453.9   453.9
12004424  457.5   457.5   457.5
12004425  461.2   461.2   461.2
12004426  458.4   458.4   458.4
12004427  455.7   455.7   455.7
12004428  452.9   452.9   452.9
12004429  450.2   450.2   450.2
12004430  447.4   447.4   447.4
12004431  444.7   444.7   444.7
12004432  441.9   441.9   441.9
12004433  439.2   439.2   439.2
12004434  436.9   436.9   436.9
12004435  434.7   434.7   434.7
12004436  432.4   432.4   432.4
12004437  430.2   430.2   430.2
12004438  425.9   425.9   425.9
12004439  421.7   421.7   421.7
12004440  417.4   417.4   417.4
12004441  413.2   413.2   413.2
12004442  411.9   411.9   411.9
12004443  410.7   410.7   410.7
12004444  409.4   409.4   409.4
12004445  408.2   408.2   408.2
12004446  406.9   406.9   406.9
12004447  405.7   405.7   405.7
12004448  404.4   404.4   404.4
12004449  403.2   403.2   403.2
* 8 fillers
12004501  0  0  0  1   0.3048  1
12004502  0  0  0  1   0.6096  48
12004503  0  0  0  1   0.3048  49
12004601  200010000  0       1  1  0.3048  1
12004602  200020000  10000   1  1  0.6096  48
12004603  200490000  0       1  1  0.3048  49
12004701  0  0.0  0.0  0.0  49
12004801  0.0  20.0  20.0  0.0  0.0  0.0  0.0  1.0  49
12004901  0.0  20.0  20.0  0.0  0.0  0.0  0.0  1.0  49
*****************************************************************
*   failed rods
*****************************************************************
12005000  49  8  2  0  0.0   0    1
12005100  0   1
12005101  2  1.20650e-3
12005102  1  2.22250e-3
12005103  2  4.11480e-3
12005104  2  4.74980e-3
12005201  1   2             * boron nitride
12005202  2   3             * kanthal
```

```
12005203  1   5              * boron nitride
12005204  4   7              * ss 347
12005301  0.0   2
12005302  1.0   3
12005303  0.0   7
12005400  -1
* test specific initial wall temperature
12005401  368.2   368.2   368.2   368.2   368.2   368.2   368.2   368.2
12005402  372.2   372.2   372.2   372.2   372.2   372.2   372.2   372.2
12005403  376.2   376.2   376.2   376.2   376.2   376.2   376.2   376.2
12005404  380.2   380.2   380.2   380.2   380.2   380.2   380.2   380.2
12005405  384.2   384.2   384.2   384.2   384.2   384.2   384.2   384.2
12005406  388.2   388.2   388.2   388.2   388.2   388.2   388.2   388.2
12005407  392.2   392.2   392.2   392.2   392.2   392.2   392.2   392.2
12005408  396.2   396.2   396.2   396.2   396.2   396.2   396.2   396.2
12005409  400.2   400.2   400.2   400.2   400.2   400.2   400.2   400.2
12005410  404.2   404.2   404.2   404.2   404.2   404.2   404.2   404.2
12005411  408.2   408.2   408.2   408.2   408.2   408.2   408.2   408.2
12005412  412.2   412.2   412.2   412.2   412.2   412.2   412.2   412.2
12005413  416.2   416.2   416.2   416.2   416.2   416.2   416.2   416.2
12005414  420.2   420.2   420.2   420.2   420.2   420.2   420.2   420.2
12005415  424.2   424.2   424.2   424.2   424.2   424.2   424.2   424.2
12005416  428.2   428.2   428.2   428.2   428.2   428.2   428.2   428.2
12005417  432.2   432.2   432.2   432.2   432.2   432.2   432.2   432.2
12005418  435.8   435.8   435.8   435.8   435.8   435.8   435.8   435.8
12005419  439.4   439.4   439.4   439.4   439.4   439.4   439.4   439.4
12005420  443.0   443.0   443.0   443.0   443.0   443.0   443.0   443.0
12005421  446.7   446.7   446.7   446.7   446.7   446.7   446.7   446.7
12005422  450.3   450.3   450.3   450.3   450.3   450.3   450.3   450.3
12005423  453.9   453.9   453.9   453.9   453.9   453.9   453.9   453.9
12005424  457.5   457.5   457.5   457.5   457.5   457.5   457.5   457.5
12005425  461.2   461.2   461.2   461.2   461.2   461.2   461.2   461.2
12005426  458.4   458.4   458.4   458.4   458.4   458.4   458.4   458.4
12005427  455.7   455.7   455.7   455.7   455.7   455.7   455.7   455.7
12005428  452.9   452.9   452.9   452.9   452.9   452.9   452.9   452.9
12005429  450.2   450.2   450.2   450.2   450.2   450.2   450.2   450.2
12005430  447.4   447.4   447.4   447.4   447.4   447.4   447.4   447.4
12005431  444.7   444.7   444.7   444.7   444.7   444.7   444.7   444.7
12005432  441.9   441.9   441.9   441.9   441.9   441.9   441.9   441.9
12005433  439.2   439.2   439.2   439.2   439.2   439.2   439.2   439.2
12005434  436.9   436.9   436.9   436.9   436.9   436.9   436.9   436.9
12005435  434.7   434.7   434.7   434.7   434.7   434.7   434.7   434.7
12005436  432.4   432.4   432.4   432.4   432.4   432.4   432.4   432.4
12005437  430.2   430.2   430.2   430.2   430.2   430.2   430.2   430.2
12005438  425.9   425.9   425.9   425.9   425.9   425.9   425.9   425.9
12005439  421.7   421.7   421.7   421.7   421.7   421.7   421.7   421.7
12005440  417.4   417.4   417.4   417.4   417.4   417.4   417.4   417.4
12005441  413.2   413.2   413.2   413.2   413.2   413.2   413.2   413.2
12005442  411.9   411.9   411.9   411.9   411.9   411.9   411.9   411.9
12005443  410.7   410.7   410.7   410.7   410.7   410.7   410.7   410.7
12005444  409.4   409.4   409.4   409.4   409.4   409.4   409.4   409.4
12005445  408.2   408.2   408.2   408.2   408.2   408.2   408.2   408.2
12005446  406.9   406.9   406.9   406.9   406.9   406.9   406.9   406.9
12005447  405.7   405.7   405.7   405.7   405.7   405.7   405.7   405.7
12005448  404.4   404.4   404.4   404.4   404.4   404.4   404.4   404.4
12005449  403.2   403.2   403.2   403.2   403.2   403.2   403.2   403.2
* test specific length (2 rods)
```

```
12005501  0  0  0  1   0.0762  1
12005502  0  0  0  1   0.1524  48
12005503  0  0  0  1   0.0762  49
12005601  200010000  0       1  1  0.0762  1
12005602  200020000  10000   1  1  0.1524  48
12005603  200490000  0       1  1  0.0762  49
12005701  0    0.0   0.0   0.0   49
12005801  0.0  20.0  20.0  0.0  0.0  0.0  0.0  1.0  49
12005901  0.0  20.0  20.0  0.0  0.0  0.0  0.0  1.0  49
*********************************************************************
*
*    heat structure thermal properties
*
*********************************************************************
20100100  tbl/fctn  1  1   * boron nitride
20100200  tbl/fctn  1  1   * kanthal
20100300  tbl/fctn  1  1   * ss-304
20100400  tbl/fctn  1  1   * ss-347
*********************************************************************
*    conductivity
*********************************************************************
* boron nitride
20100101  300.0   25.16
20100102  400.0   24.91
20100103  500.0   24.67
20100104  600.0   24.42
20100105  700.0   24.18
20100106  800.0   23.93
20100107  900.0   23.69
20100108  1000.0  23.44
20100109  1100.0  23.19
20100110  1200.0  22.95
20100111  1300.0  22.70
20100112  1400.0  22.46
20100113  1500.0  22.21
20100114  1600.0  21.97
20100115  1700.0  21.72
* kanthal + boron nitride
20100201  300.0   29.13
20100202  400.0   29.61
20100203  500.0   30.09
20100204  600.0   30.58
20100205  700.0   31.06
20100206  800.0   31.54
20100207  900.0   32.02
20100208  1000.0  32.51
20100209  1100.0  32.99
20100210  1200.0  33.47
20100211  1300.0  33.96
20100212  1400.0  34.44
20100213  1500.0  34.92
20100214  1600.0  35.41
20100215  1700.0  35.89
* ss-304
20100301  300.0   12.97
20100302  400.0   14.59
20100303  500.0   16.21
```

```
20100304  600.0   17.82
20100305  700.0   19.44
20100306  800.0   21.06
20100307  900.0   22.68
20100308  1000.0  24.30
20100309  1100.0  25.91
20100310  1200.0  27.53
20100311  1300.0  29.15
20100312  1400.0  30.77
20100313  1500.0  32.39
20100314  1600.0  34.00
20100315  1700.0  35.62
*ss-347
20100401  300.0   16.37
20100402  400.0   17.10
20100403  500.0   17.83
20100404  600.0   18.55
20100405  700.0   19.28
20100406  800.0   20.01
20100407  900.0   20.73
20100408  1000.0  21.46
20100409  1100.0  22.19
20100410  1200.0  22.92
20100411  1300.0  23.64
20100412  1400.0  24.37
20100413  1500.0  25.10
20100414  1600.0  25.82
20100415  1700.0  26.55
**********************************************************************
*    volumetric heat capacity
**********************************************************************
*boron nitride
20100151  300.0   1.80040e6
20100152  400.0   2.34650e6
20100153  500.0   2.79610e6
20100154  600.0   3.16050e6
20100155  700.0   3.45090e6
20100156  800.0   3.67820e6
20100157  900.0   3.85370e6
20100158  1000.0  3.98860e6
20100159  1100.0  4.09380e6
20100160  1200.0  4.18070e6
20100161  1300.0  4.26020e6
20100162  1400.0  4.34360e6
20100163  1500.0  4.44200e6
20100164  1600.0  4.56650e6
20100165  1700.0  4.72820e6
* kanthal + boron nitride
20100251  300.0   2.29400e6
20100252  400.0   2.92790e6
20100253  500.0   3.26520e6
20100254  600.0   3.50590e6
20100255  700.0   3.69620e6
20100256  800.0   3.85510e6
20100257  900.0   3.99240e6
20100258  1000.0  4.11360e6
20100259  1100.0  4.22260e6
```

```
20100260  1200.0  4.32180e6
20100261  1300.0  4.41300e6
20100262  1400.0  4.49750e6
20100263  1500.0  4.57640e6
20100264  1600.0  4.65030e6
20100265  1700.0  4.72010e6
* ss-304
20100351  300.0   3.61140e6
20100352  400.0   3.96460e6
20100353  500.0   4.14360e6
20100354  600.0   4.23160e6
20100355  700.0   4.28970e6
20100356  800.0   4.35670e6
20100357  900.0   4.45010e6
20100358  1000.0  4.56620e6
20100359  1100.0  4.68090e6
20100360  1200.0  4.75070e6
20100361  1300.0  4.71290e6
20100362  1400.0  4.48710e6
20100363  1500.0  3.97600e6
20100364  1600.0  3.06650e6
20100365  1700.0  1.63060e6
* ss-347
20100451  300.0   3.8513e6
20100452  400.0   3.9914e6
20100453  500.0   4.1316e6
20100454  600.0   4.2718e6
20100455  700.0   4.4119e6
20100456  800.0   4.5521e6
20100457  900.0   4.6922e6
20100458  1000.0  4.8324e6
20100459  1100.0  4.9725e6
20100460  1200.0  5.1127e6
20100461  1300.0  5.2528e6
20100462  1400.0  5.3930e6
20100463  1500.0  5.5332e6
20100464  1600.0  5.6733e6
20100465  1700.0  5.8135e6
*************************************************************************
*
*    power table
*
*************************************************************************
* test specific power and decay curve
20220000  power   500   1.0   8.04952e5
20220001  0.0   1.00000
20220002  3.6   0.98320
20220003  8.1   0.95981
20220004  15.8  0.92975
20220005  23.6  0.90135
20220006  41.4  0.85792
20220007  55.8  0.82786
20220008  76.9  0.79111
20220009  98.1  0.76272
20220010  125.8   0.72764
20220011  162.5   0.69423
20220012  202.5   0.66417
```

```
20220013  244.7   0.63911
20220014  303.6   0.61072
20220015  339.2   0.59735
20220016  391.4   0.57898
20220017  451.4   0.56061
20220018  503.6   0.54557
20220019  546.9   0.53722
20220020  592.5   0.52553
20220021  636.9   0.51885
20220022  679.2   0.50883
20220023  729.2   0.50214
20220024  771.4   0.49379
20220025  798.1   0.49045
20220026  818.1   0.48711
20220027  819.2   0.35683
20220028  820.3   0.23823
20220029  821.4   0.12423
20220030  829.9   0.00000
*************************************************************************
*
*    control variables
*
*************************************************************************
*-----------------------------------------------------------------------
*   cntrlvar-005 : core collapsed water level
*-----------------------------------------------------------------------
20500100  wt-lvl1  sum  1.0  0.0  1
20500101  0.0  0.0381  voidf  200010000
20500102       0.0762  voidf  200020000
20500103       0.0762  voidf  200030000
20500104       0.0762  voidf  200040000
20500105       0.0762  voidf  200050000
20500106       0.0762  voidf  200060000
20500107       0.0762  voidf  200070000
20500108       0.0762  voidf  200080000
20500109       0.0762  voidf  200090000
20500110       0.0762  voidf  200100000
20500111       0.0762  voidf  200110000
20500112       0.0762  voidf  200120000
20500113       0.0762  voidf  200130000
20500114       0.0762  voidf  200140000
20500115       0.0762  voidf  200150000
20500116       0.0762  voidf  200160000
20500117       0.0762  voidf  200170000
20500118       0.0762  voidf  200180000
20500119       0.0762  voidf  200190000
20500120       0.0762  voidf  200200000
*
20500200  wt-lvl2  sum  1.0  0.0  1
20500201  0.0  0.0762  voidf  200210000
20500202       0.0762  voidf  200220000
20500203       0.0762  voidf  200230000
20500204       0.0762  voidf  200240000
20500205       0.0762  voidf  200250000
20500206       0.0762  voidf  200260000
20500207       0.0762  voidf  200270000
20500208       0.0762  voidf  200280000
```

```
20500209      0.0762  voidf  200290000
20500210      0.0762  voidf  200300000
20500211      0.0762  voidf  200310000
20500212      0.0762  voidf  200320000
20500213      0.0762  voidf  200330000
20500214      0.0762  voidf  200340000
20500215      0.0762  voidf  200350000
20500216      0.0762  voidf  200360000
20500217      0.0762  voidf  200370000
20500218      0.0762  voidf  200380000
20500219      0.0762  voidf  200390000
20500220      0.0762  voidf  200400000
*
20500300  wt-lvl3  sum  1.0  0.0  1
20500301 0.0   0.0762  voidf  200410000
20500302      0.0762  voidf  200420000
20500303      0.0762  voidf  200430000
20500304      0.0762  voidf  200440000
20500305      0.0762  voidf  200450000
20500306      0.0762  voidf  200460000
20500307      0.0762  voidf  200470000
20500308      0.0762  voidf  200480000
20500309      0.0381  voidf  200490000
*
20500500  wt-level  sum  1.0  0.0  1
20500501  0.0  1.0000  cntrlvar 001
20500502       1.0000  cntrlvar 002
20500503       1.0000  cntrlvar 003
*-------------------------------------------------------------------
*   cntrlvar-011~022 : void fraction at every 12 inches
*-------------------------------------------------------------------
* 0 ~ 1 ft
20501100  voidg1  sum  0.25  0.0  1
20501101  0.0  0.5  voidg  200010000
20501102       1.0  voidg  200020000
20501103       1.0  voidg  200030000
20501104       1.0  voidg  200040000
20501105       0.5  voidg  200050000
* 1 ~ 2 ft
20501200  voidg2  sum  0.25  0.0  1
20501201  0.0  0.5  voidg  200050000
20501202       1.0  voidg  200060000
20501203       1.0  voidg  200070000
20501204       1.0  voidg  200080000
20501205       0.5  voidg  200090000
* 2 ~ 3 ft
20501300  voidg3  sum  0.25  0.0  1
20501301  0.0  0.5  voidg  200090000
20501302       1.0  voidg  200100000
20501303       1.0  voidg  200110000
20501304       1.0  voidg  200120000
20501305       0.5  voidg  200130000
* 3 ~ 4 ft
20501400  voidg4  sum  0.25  0.0  1
20501401  0.0  0.5  voidg  200130000
20501402       1.0  voidg  200140000
20501403       1.0  voidg  200150000
```

```
20501404      1.0  voidg  200160000
20501405      0.5  voidg  200170000
* 4 ~ 5 ft
20501500  voidg5  sum  0.25  0.0  1
20501501  0.0  0.5  voidg  200170000
20501502      1.0  voidg  200180000
20501503      1.0  voidg  200190000
20501504      1.0  voidg  200200000
20501505      0.5  voidg  200210000
* 5 ~ 6 ft
20501600  voidg6  sum  0.25  0.0  1
20501601  0.0  0.5  voidg  200210000
20501602      1.0  voidg  200220000
20501603      1.0  voidg  200230000
20501604      1.0  voidg  200240000
20501605      0.5  voidg  200250000
* 6 ~ 7 ft
20501700  voidg7  sum  0.25  0.0  1
20501701  0.0  0.5  voidg  200250000
20501702      1.0  voidg  200260000
20501703      1.0  voidg  200270000
20501704      1.0  voidg  200280000
20501705      0.5  voidg  200290000
* 7 ~ 8 ft
20501800  voidg8  sum  0.25  0.0  1
20501801  0.0  0.5  voidg  200290000
20501802      1.0  voidg  200300000
20501803      1.0  voidg  200310000
20501804      1.0  voidg  200320000
20501805      0.5  voidg  200330000
* 8 ~ 9 ft
20501900  voidg9  sum  0.25  0.0  1
20501901  0.0  0.5  voidg  200330000
20501902      1.0  voidg  200340000
20501903      1.0  voidg  200350000
20501904      1.0  voidg  200360000
20501905      0.5  voidg  200370000
* 9 ~ 10 ft
20502000  voidg10  sum  0.25  0.0  1
20502001  0.0  0.5  voidg  200370000
20502002      1.0  voidg  200380000
20502003      1.0  voidg  200390000
20502004      1.0  voidg  200400000
20502005      0.5  voidg  200410000
* 10 ~ 11 ft
20502100  voidg11  sum  0.25  0.0  1
20502101  0.0  0.5  voidg  200410000
20502102      1.0  voidg  200420000
20502103      1.0  voidg  200430000
20502104      1.0  voidg  200440000
20502105      0.5  voidg  200450000
* 11 ~ 12 ft
20502200  voidg12  sum  0.25  0.0  1
20502201  0.0  0.5  voidg  200450000
20502202      1.0  voidg  200460000
20502203      1.0  voidg  200470000
20502204      1.0  voidg  200480000
```

```
20502205      0.5  voidg  200490000
*-----------------------------------------------------------------
*   cntrlvar-031~43 : wall temp - sat. temp
*                  at every measurement location
*-----------------------------------------------------------------
* 1 ft
20503100  dtemp1   sum  1.0  0.0  1
20503101  0.0  1.0  httemp  200100508
20503102     -1.0  sattemp 200050000
* 2 ft
20503200  dtemp2   sum  1.0  0.0  1
20503201  0.0  1.0  httemp  200100908
20503202     -1.0  sattemp 200090000
* 3 ft
20503300  dtemp3   sum  1.0  0.0  1
20503301  0.0  1.0  httemp  200101308
20503302     -1.0  sattemp 200130000
* 4 ft
20503400  dtemp4   sum  1.0  0.0  1
20503401  0.0  1.0  httemp  200101708
20503402     -1.0  sattemp 200170000
* 5 ft
20503500  dtemp5    sum  1.0  0.0  1
20503501  0.0  1.0  httemp  200102108
20503502     -1.0  sattemp 200210000
* 6 ft
20503600  dtemp6    sum  1.0  0.0  1
20503601  0.0  1.0  httemp  200102508
20503602     -1.0  sattemp 200250000
* 7 ft
20503700  dtemp7    sum  1.0  0.0  1
20503701  0.0  1.0  httemp  200102908
20503702     -1.0  sattemp 200290000
* 8 ft
20503800  dtemp8    sum  1.0  0.0  1
20503801  0.0  1.0  httemp  200103308
20503802     -1.0  sattemp 200330000
* 9 ft
20503900  dtemp9    sum  1.0  0.0  1
20503901  0.0  1.0  httemp  200103708
20503902     -1.0  sattemp 200370000
* 10 ft
20504000  dtemp10   sum  1.0  0.0  1
20504001  0.0  1.0  httemp  200104108
20504002     -1.0  sattemp 200410000
* 11 ft
20504100  dtemp11   sum  1.0  0.0  1
20504101  0.0  1.0  httemp  200104508
20504102     -1.0  sattemp 200450000
* 12 ft
20504200  dtemp12   sum  1.0  0.0  1
20504201  0.0  1.0  httemp  200104908
20504202     -1.0  sattemp 200490000
* 6.5 ft
20504300  dtemp65   sum  1.0  0.0  1
20504301  0.0  1.0  httemp  200102708
20504302     -1.0  sattemp 200270000
```

```
*-----------------------------------------------------------------
*   cntrlvar-051~62 : heat transfer coefficient
*                  at every measurement location
*-----------------------------------------------------------------
* 1 ft
20505100  htc1      div    1.0     1.0     1
20505101  cntrlvar  031    htrnr   200100501
* 2 ft
20505200  htc2      div    1.0     1.0     1
20505201  cntrlvar  032    htrnr   200100901
* 3 ft
20505300  htc3      div    1.0     1.0     1
20505301  cntrlvar  033    htrnr   200101301
* 4 ft
20505400  htc4      div    1.0     1.0     1
20505401  cntrlvar  034    htrnr   200101701
* 5 ft
20505500  htc5      div    1.0     1.0     1
20505501  cntrlvar  035    htrnr   200102101
* 6 ft
20505600  htc6      div    1.0     1.0     1
20505601  cntrlvar  036    htrnr   200102501
* 7 ft
20505700  htc7      div    1.0     1.0     1
20505701  cntrlvar  037    htrnr   200102901
* 8 ft
20505800  htc8      div    1.0     1.0     1
20505801  cntrlvar  038    htrnr   200103301
* 9 ft
20505900  htc9      div    1.0     1.0     1
20505901  cntrlvar  039    htrnr   200103701
* 10 ft
20506000  htc10     div    1.0     1.0     1
20506001  cntrlvar  040    htrnr   200104101
* 11 ft
20506100  htc11     div    1.0     1.0     1
20506101  cntrlvar  041    htrnr   200104501
* 12 ft
20506200  htc12     div    1.0     1.0     1
20506201  cntrlvar  042    htrnr   200104901
* 6.5 ft
20506300  htc65     div    1.0     1.0     1
20506301  cntrlvar  043    htrnr   200102701
*-----------------------------------------------------------------
*   cntrlvar-071~82 : differential pressure
*                  between every measurement location
*-----------------------------------------------------------------
* 0 ~ 1 ft
20507100  dp01   sum  1.0  0.0  1
20507101  0.0  1.0  p  200010000
20507102      -1.0  p  200050000
* 1 ~ 2 ft
20507200  dp12   sum  1.0  0.0  1
20507201  0.0  1.0  p  200050000
20507202      -1.0  p  200090000
* 2 ~ 3 ft
20507300  dp23   sum  1.0  0.0  1
```

```
20507301  0.0  1.0  p  200090000
20507302      -1.0  p  200130000
* 3 ~ 4 ft
20507400  dp34   sum  1.0  0.0  1
20507401  0.0  1.0  p  200130000
20507402      -1.0  p  200170000
* 4 ~ 5 ft
20507500  dp45   sum  1.0  0.0  1
20507501  0.0  1.0  p  200170000
20507502      -1.0  p  200210000
* 5 ~ 6 ft
20507600  dp56   sum  1.0  0.0  1
20507601  0.0  1.0  p  200210000
20507602      -1.0  p  200250000
* 6 ~ 7 ft
20507700  dp67   sum  1.0  0.0  1
20507701  0.0  1.0  p  200250000
20507702      -1.0  p  200290000
* 7 ~ 8 ft
20507800  dp78   sum  1.0  0.0  1
20507801  0.0  1.0  p  200290000
20507802      -1.0  p  200330000
* 8 ~ 9 ft
20507900  dp89   sum  1.0  0.0  1
20507901  0.0  1.0  p  200330000
20507902      -1.0  p  200370000
* 9 ~ 10 ft
20508000  dp910   sum  1.0  0.0  1
20508001  0.0  1.0  p  200370000
20508002      -1.0  p  200410000
* 10 ~ 11 ft
20508100  dp1011   sum  1.0  0.0  1
20508101  0.0  1.0  p  200410000
20508102      -1.0  p  200450000
* 11 ~ 12 ft
20508200  dp1112   sum  1.0  0.0  1
20508201  0.0  1.0  p  200450000
20508202      -1.0  p  200490000
* 0 ~ 12 ft
20508300  dp012   sum  1.0  0.0  1
20508301  0.0  1.0  p  200010000
20508302      -1.0  p  200490000
*-------------------------------------------------------------------
*   cntrlvar-110 : liquid carry-over fraction
*-------------------------------------------------------------------
20510100  flowin   mult  0.0155565   0.0  1
20510101  voidfj  165000000
20510102  rhofj   165000000
20510103  velfj   165000000
*
20510200  floin  integral  1.0  0.0  1
20510201  cntrlvar  101
* add small no. to avoid dividing by zero
20510300  floina    sum  1.0  0.0  1
20510301  1.e-20  1.0  cntrlvar 102
*
20510400  flowot   mult  0.0155565   0.0  1
```

```
20510401  voidfj  250000000
20510402  rhofj   250000000
20510403  velfj   250000000
*
20510500  floot  integral  1.0  0.0  1
20510501  cntrlvar  104
*
20511000  carryf    div    1.0     1.0     1
20511001  cntrlvar  103    cntrlvar 105
*-----------------------------------------------------------------
*   cntrlvar-200 : total power
*-----------------------------------------------------------------
20520000   power   function   1.0   0.0   1
20520001   time   0   200
*
.
```

NRC FORM 335 (9-2004) NRCMD 3.7

U.S. NUCLEAR REGULATORY COMMISSION

BIBLIOGRAPHIC DATA SHEET

(See instructions on the reverse)

1. REPORT NUMBER (Assigned by NRC, Add Vol., Supp., Rev., and Addendum Numbers, if any.)
NUREG/IA-0251

2. TITLE AND SUBTITLE
Improvement of RELAP5/MOD3.3 Reflood Model Based on the Assessments Against FLECHT-SEASET Tests

3. DATE REPORT PUBLISHED

MONTH	YEAR
February	2011

4. FIN OR GRANT NUMBER

5. AUTHOR(S)
Tong-Soo Choi, Chang-Hwan Ban
Dong-Gu Kang, Seung-Hoon Ahn

6. TYPE OF REPORT
Technical

7. PERIOD COVERED *(Inclusive Dates)*

8. PERFORMING ORGANIZATION - NAME AND ADDRESS *(If NRC, provide Division, Office or Region, U.S. Nuclear Regulatory Commission, and mailing address; if contractor, provide name and mailing address.)*
Korea Nuclear Fuel
Daejeon, Korea

Korea Institute of Nuclear Safety
Daejeon, Korea

9. SPONSORING ORGANIZATION - NAME AND ADDRESS *(If NRC, type "Same as above"; if contractor, provide NRC Division, Office or Region, U.S. Nuclear Regulatory Commission, and mailing address.)*
Division of Systems Analysis
Office of Nuclear Regulatory Research
U.S. Nuclear Regulatory Commission
Washington, DC 20555-0001

10. SUPPLEMENTARY NOTES
A. Calvo, NRC Project Manager

11. ABSTRACT *(200 words or less)*
The reflood model of RELAP5/MOD3.3 was assessed against eight selected FLECHT-SEASET tests. Comparisons of predicted and measured peak cladding temperatures and quench times indicated that the code predicts peak cladding temperatures relatively well. However, rod quenches were predicted to occur too early. To improve the predictability for quench times, we carefully reviewed and modified the wall-to-fluid heat transfer models for the film boiling regime. After the modifications, the same set of eight FLECHT-SEASET tests was simulated again to show that the modifications made in this study improve the code's predictability not only for quench times but also for peak clad temperatures. The modifications reduced the RMS error in the prediction of peak clad temperatures and quench times from 48.3 to 36.7 K and 85.9 to 32.1 seconds, respectively.

12. KEY WORDS/DESCRIPTORS *(List words or phrases that will assist researchers in locating the report.)*
RELAP5/MOD3.3
FLECHT-SEASET tests
Korea Atomic Energy Research Institute (KAERI)
Korea Electric Power Research Institute (KEPRI)
Korea Nuclear Fuel (KNF)
Code Application Maintenance Program (CAMP)
Pressurized Water Reactors (PWRs)
Large break loss-of-coolant accident (LBLOCA)
Ministry of Education, Science and Technology of the Rebublic of Korea
TRACE

13. AVAILABILITY STATEMENT
unlimited

14. SECURITY CLASSIFICATION
(This Page)
unclassified
(This Report)
unclassified

15. NUMBER OF PAGES

16. PRICE

Federal Recycling Program

UNITED STATES
NUCLEAR REGULATORY COMMISSION
WASHINGTON, DC 20555-0001

OFFICIAL BUSINESS